TECHNISCHE UNIVERSITÄT MÜNCHEN
Lehrstuhl für Bioverfahrenstechnik

Rapid Media Transition for Metabolic Control Analysis of Fed-Batch Fermentation Processes

Hannes Peter Link

Vollständiger Abdruck der von der Fakultät für Maschinenwesen der Technischen Universität München zur Erlangung des akademischen Grades eines

Doktor-Ingenieurs

genehmigten Dissertation.

Vorsitzender:	Univ.-Prof. Dr.-Ing. habil. Nikolaus A. Adams
Prüfer der Dissertation:	1. Univ.-Prof. Dr.-Ing. Dirk Weuster-Botz
	2. Prof. Dr. rer. nat. Uwe Sauer
	Eidgenössische Technische Hochschule Zürich/ Schweiz

Die Dissertation wurde am 01.07.2009 bei der Technischen Universität München eingereicht und durch die Fakultät für Maschinenwesen
am 18.09.2009 angenommen.

As far as the laws of mathematics refer to reality, they are not certain; and as far as they are certain, they do not refer to reality.

Albert Einstein
Physicist (1879-1955)

Preface

This thesis would not be realized without the help and support of many others.

My thank goes to Prof. Dr.-Ing. Dirk Weuster-Botz for an excellent supervision and the possibility to work under the great conditions at his institute. He always encouraged me to develop my own ideas and gave me substantial help at the right time.

I am also thankful to Prof. Dr. Uwe Sauer for his agreement to act as my co-examiner and to Prof. Dr.-Ing. Nikolaus Adams to act as chairman of my thesis.

I would like to thank the semester and diploma students Christoph Gürtner, Johannes Weinzierl, Li Sun and Bernd Anselment, as well as my succesor Michael Weiner for their assistance.

Thanks to Ezequiel Franco-Lara for all the things I learned from him when I was a student.

Thanks to my colleagues at the department for an excellent working atmosphere, their help and the good times we shared outside the laboratory.

I am grateful that I have good friends, they know who they are and I appreciate their support not only during the writing up part of my thesis.

Finally, I want to thank my parents Christa and Walter Link, they support me in everything I do and furthermore they are a great inspiration.

Contents

1. Introduction

Although industrial bioprocesses have been optimized for several decades, conversion of carbon source and productivity in fermentation is still considerably below a value that can be expected from theoretical calculations (Takors *et al.* 2007). Metabolic engineering thus aims to develop producer strains, in which entire cellular networks are optimized and fermentation and downstream processes are considered at early stages (Park *et al.* 2008). Metabolic engineering was developed in the previous decade to improve industrial strains using modern genetic tools, which are far more rational than random mutagenesis or screening approaches (Stephanopoulos 2002). In their textbook, Stephanopoulos *et al.* (1998) emphasize the significance of intracellular reaction rates (metabolic fluxes) and their control under *in vivo* conditions as the most significant contribution of metabolic engineering. The control of flux in cellular systems is the subject of the so-called Metabolic Control Analysis (MCA) developed from the landmark papers of Kacser and Burns (1973) and Heinrich and Rapoport (1974). Successful examples of the application of MCA are the glutamate synthetic pathway (Shimizu *et al.* 2002), the lysine biosynthetic network (Simpson *et al.* 1998) and the penicillin biosynthetic pathway (Nielsen 1997). However, rather a few experimental applications are reported, compared to the extensively covered theoretical framework of MCA.

Reasons for this are certainly the multiple challenging tasks when capturing experimental data of biological systems. There are several layers of biological information such as genes (described by the so-called Genome), the proteins and enzymes (Proteome), the small molecules and metabolites (Metabolome) and the conversion rates of metabolites and other building blocks (Fluxome). Measurements across these layers are usually combined in order to reveal interrelationships between them. However, effects of genetic modifications are hardly predictable, as metabolic fluxes are regulated in a complex manner, either by enzyme synthesis or by feedback from other parts of metabolism (allosteric regulation). Finally, the uncertainty associated with measurements in a biological system is perhaps the most striking difference between metabolic engineering and other engineering disciplines.

2. Thesis Motivation and Objective

Enzymes in a living cell have to meet demands at several levels. At the lowest level the function of an enzyme is to catalyze a reaction and at the level of a metabolic network its function may be to control the flux through a part of the pathway (Hofmeyr and Cornish-Bowden 2000). In order to understand the regulation of a biochemical pathway it is necessary to characterize functions and kinetics of its enzymes. Reaction kinetics are often studied with the purified enzyme in test tubes. Therefore, the reaction rate is determined for varying substrate and product concentrations. However, Teusink *et al.* (2000) have shown, that such *in vitro* studies do not sufficiently describe the function of enzymes *in vivo*. Complex regulatory mechanisms determine reaction rates in the cellular milieu and kinetic parameters differ from those determined in test tubes. Consequently, intracellular enzyme-catalyzed reactions in a biological system need to be studied *in vivo*, either under stationary or dynamic conditions.

Stimulus response experiments are widely applied to study the dynamic behavior of metabolic pathways (Theobald *et al.* 1997, Chassagnole *et al.* 2002, Visser *et al.* 2004a, Magnus *et al.* 2006). Commonly a pulse of carbon source is added to a continuous culture and intracellular metabolite concentrations are observed during several seconds up to minutes. It may be assumed that enzyme levels do not change over this short period and the responses can be attributed to the kinetic interactions at the metabolome level alone (Visser *et al.* 2004a). Nevertheless, stimulus response experiments can be laborious, time consuming and a single perturbation experiment may not generate enough information about the whole system. A further problem is that noise in the data is often indistinguishable from the highly non-linear dynamics.

In contrast to dynamic perturbations, steady state perturbations yield information about the metabolic system in multiple steady states (Nasution *et al.* 2008). Therefore, changes of metabolic fluxes are related to differences in enzyme levels and intracellular metabolite concentrations. Compared to stimulus response experiments, the experimental effort is low, as just a few metabolic states have to be analyzed. Chemostat cultures are preferred for steady state analysis, because external fluxes such as substrate uptake and growth rate are fixed at a constant level and the cells physiology is well defined (Mashego *et al.* 2007). However, continuous cultures are not essential for a metabolic steady state. Rather, it was shown that physiology and metabolism are highly diverse in chemostat-evolved bacteria (Ferenci 2008). Further, most industrial fermentation processes are operated in fed-batch mode under non-stationary conditions, which cannot be realized in a chemostat. As a

consequence, it was yet not possible to study metabolic pathways of a producer strain under conditions of a fed-batch process by means of steady state perturbations. This leads to the necessity to develop new cultivation strategies for perturbation experiments in large-scale processes.

Lab-scale bioreactors operating in parallel to a large-scale process were already successfully applied to monitor the metabolic state of cells in industrial bioprocesses (Massaoudi *et al.* 2003, Drysch *et al.* 2003). A parallel setup of bioreactors was developed and evaluated in this work for the purpose of perturbation experiments. Therefore, cells were separated from the production process and analyzed in a lab-scale bioreactor operating in parallel to the process. During cultivation in the lab-scale bioreactor, physiology and the intracellular state of the cells was observed by measurements of metabolite concentrations, fluxes and enzyme levels.

Kacser and Burns (1979) state in an early work: We consider a metabolic system as a whole and ask what operations on it yield information on the role of its parts? Similar questions were associated with the proposed experimental approach:

- Which measurements are theoretically required in order to identify rate controlling steps of a metabolic pathway using mathematical tools of MCA?
- Which measurements are practically feasible?
- Which assumptions and prerequisites are necessary in order to consider the physiological conditions of the relevant bioprocess?

Nielsen (1994) gave distinction to the term physiological engineering, comprising several different techniques: physiological studies, metabolic flux analysis, metabolic control analysis, thermodynamic analysis and kinetic modeling. In this sense, the following experimental tasks were considered and evaluated by means of central carbon metabolism of the model organism *Escherichia coli* under conditions of a fed-batch process:

- Physiological characterization of cells during the fed-batch process.
- Development of an experimental approach for steady state analysis in a lab-scale bioreactor operating in parallel to the fed-batch process.
- Studies about sampling procedures and analytical methods to quantify intracellular metabolites.
- Establishment of methods for metabolic flux analysis.

3. Theoretical Background

3.1. Bioreactor processes

Commonly, processes in a bioreactor are described by several time dependent state variables, such as concentrations of compounds in the cultivation medium, temperature and pH. Cellular metabolism and mass transport processes between cells and cultivation broth influence the state variables. In this section, methods are introduced to characterize these processes. A black box model is applied for biomass, which is only described by its concentration in the bioreactor. Dynamics of the most prevalent state variables are specified by coupling mass balances around the bioreactor with formal kinetics of uptake and production of substances in the cultivation broth.

3.1.1. Microbial growth

Growing heterotrophic microorganisms require organic carbon compounds, nitrogen, oxygen, mineral salts and eventually vitamins. These compounds are provided in the cultivation medium, where the cells can exchange material with their environment. The fluxes in and out of the cells are given relative to the biomass concentration, the so-called specific rates. The specific growth rate is defined as the increase of biomass concentration c_x relative to the actual biomass concentration.

$$\mu \equiv \frac{1}{c_x}\frac{dc_x}{dt} \tag{3.1}$$

Similarly, the specific uptake or production rate of a compound i is defined as the change of its concentration in the medium c_i divided by the biomass concentration.

$$q_i \equiv \frac{1}{c_x}\frac{dc_i}{dt} \tag{3.2}$$

In case all required nutrients are sufficiently supplied, except of only one limiting compound (e.g. the primary carbon source) the specific growth rate follows from Monod kinetics (Monod 1949).

$$\mu = \mu_{max}\frac{c_s}{c_s + K_s} \tag{3.3}$$

The growth rate in Eq.(3.3) approximates a maximal rate μ_{max} depending on the concentration of the limiting substrate c_s and a half saturation constant K_s. Yield coefficients

are defined as overall fluxes relative to a reference compound and relate biomass formation with substrate uptake. Using a double subscript, $Y_{i,j}$ describes the yield of compound i with regard to j. The biomass yield with regard to substrate takes the form of unit mass of biomass formed by unit mass of substrate consumed.

$$Y_{x,s} = \frac{\mu}{q_s} = \frac{dc_x}{dc_s} \tag{3.4}$$

With a constant biomass yield, substrate uptake merely follows from Eq.(3.4) and Eq.(3.3). Product formation is described similarly, if it is associated with growth. Otherwise, more detailed formal kinetic descriptions are employed.

3.1.2. Operation of bioreactors

Bioreactors are operated in three different modes: batch, continuous and fed-batch. In a batch process all nutrients required during cultivation, except for oxygen and chemicals for pH adjustment are initially added to the medium. In a continuos mode, nutrients are added continuously to the bioreactor and culture broth is removed at the same rate to maintain a constant culture volume. Beside these ideal modes, the fed-batch mode is most frequently applied for industrial biotechnological processes. During a fed-batch cultivation one or more nutrients are supplied to the bioreactor. For a fed-batch process with an inflow $\dot{V}_{in}$ and a reaction volume V_R the dynamic mass balance equation for a compound i in the medium of a bioreactor with homogenous concentrations (ideal stirred tank) is

$$\frac{dc_i}{dt} = \frac{\dot{V}_{in}}{V_R} \cdot (c_i^{in} - c_i) + c_x \cdot q_i \tag{3.5}$$

where c_i^{in} is the concentration of compound i in the feed. Commonly, there is no biomass in the feeding solution and the balance equation of biomass is

$$\frac{dc_x}{dt} = -\frac{\dot{V}_{in}}{V_R} \cdot c_x + c_x \cdot \mu \tag{3.6}$$

One major purpose of a fed-batch process is controlling the substrate concentration in the cultivation medium. Substrate-limited conditions are achieved by an appropriate feeding. In case of a constant residual substrate concentration in the bioreactor ($dc_s/dt = 0$) the required feeding rate for a desired q_s^{set} follows from Eq.(3.5).

$$\dot{V}_{in} = \frac{V_R \cdot c_x}{(c_s^{in} - c_s)} \cdot q_s^{set} \tag{3.7}$$

If the biomass yield is constant it is possible to express Eq.(3.7) by a predefined growth rate μ^{set}.

$$\dot{V}_{in} = \frac{V_R \cdot c_x}{Y_{x,s} \cdot (c_s^{in} - c_s)} \cdot \mu^{set} \tag{3.8}$$

Biomass concentration and reaction volume in Eq.(3.7) and Eq.(3.8) are not constant. The time dependency follows from exponential growth and results in the exponential feeding strategy in Eq.(3.9).

$$\dot{V}_{in}(t) = \frac{V_R^0 \cdot c_x^0}{Y_{x,s} \cdot (c_s^{in} - c_s)} \cdot \mu^{set} \cdot e^{(\mu^{set} \cdot t)} \tag{3.9}$$

An open-loop feeding strategy according to Eq.(3.9) ensures self-controlling of the specific rates as long as no other component becomes limiting or metabolic products inhibit growth (Jenzsch *et al.* 2006).

3.1.3. Estimation of specific rates in batch cultivations

Specific rates in a batch cultivation follow from measurements of biomass and concentrations of other compounds at different process times. Assuming a constant growth rate μ_{max} and integrating Eq.(3.1) allows to describe cellular growth depending on cultivation time and the initial biomass concentration c_x^0.

$$c_x(t) = c_x^0 \cdot e^{(\mu_{max} \cdot t)} \tag{3.10}$$

The constant specific growth rate is estimated by logarithmic regression of measured biomass concentrations at different process times to Eq.(3.10). Integration of Eq.(3.2) in combination with Eq.(3.10) describes the time dependency of a compound i.

$$c_i(t) = c_i^0 + \frac{q_i \cdot c_x^0}{\mu} \left(1 - e^{(\mu \cdot t)}\right) \tag{3.11}$$

Specific rates result from regression analysis of the measured time course of c_i. If biomass concentration is not significantly changing over the observed period, the time dependency of substrate concentration is approximated by Eq.(3.12), using an averaged biomass concentration $\bar{c}_x$.

$$c_i(t) = c_i^0 + q_i \cdot \bar{c}_x \cdot t \tag{3.12}$$

During a fed-batch process, time courses of biomass, products and substrates follow from Eq.(3.5) and Eq.(3.6). With the exception of an exponential feeding, dynamic modeling

is required to estimate specific rates.

Irrespective of the bioreactors operation mode, oxygen and carbon dioxide are continuously supplied and removed during a bioprocess. Oxygen uptake rate (OUR) and carbon dioxide production rate (CPR) are assessed by exhaust gas measurements. If the concentration of oxygen is constant in the medium, the oxygen transfer rate (OTR) follows from mass balancing in the gas phase.

$$\mathrm{OTR} = \frac{\dot{V}_{gas}^{in} \cdot x_{O_2}^{in} - \dot{V}_{gas}^{out} \cdot x_{O_2}^{out}}{V_R \cdot V_{mol}} \tag{3.13}$$

$\dot{V}_{gas}^{in}$ and $\dot{V}_{gas}^{out}$ are the in- and outlet airflow, $x_{O_2}^{in}$ and $x_{O_2}^{out}$ are the mole fractions of oxygen at the in- and outlet. V_{mol} is molar volume of an ideal gas, which is 22.414 L mol^{-1}. The outlet airflow is estimated from the inlet airflow using mass conservation of inertial compounds in the gas phase.

$$\dot{V}_{gas}^{in} \cdot x_{inertial}^{in} = \dot{V}_{gas}^{out} \cdot x_{inertial}^{out} \tag{3.14}$$

The sum of mole fractions of inertial compounds, O_2 and CO_2 equals one.

$$x_{inertial} + x_{CO_2} + x_{O_2} = 1 \tag{3.15}$$

Combining Eq.(3.15) with Eq.(3.14) and rearranging relates the outlet airflow to the inlet airflow.

$$\dot{V}_{gas}^{in} \cdot K = \dot{V}_{gas}^{out} \tag{3.16}$$

$$\text{where} \quad K = \frac{1 - x_{CO_2}^{in} - x_{O_2}^{in}}{1 - x_{CO_2}^{out} - x_{O_2}^{out}}$$

Assuming that OTR=OUR and inserting Eq.(3.16) into Eq.(3.13) gives

$$\mathrm{OUR} = \frac{\dot{V}_{gas}^{in}}{V_R \cdot V_{mol}} (x_{O_2}^{in} - K \cdot x_{O_2}^{out}) \tag{3.17}$$

CPR is estimated similarly.

$$\mathrm{CPR} = \frac{\dot{V}_{gas}^{in}}{V_R \cdot V_{mol}} (K \cdot x_{CO_2}^{out} - x_{CO_2}^{in}) \tag{3.18}$$

Dividing CPR and OUR by the actual biomass concentration gives the specific rates q_{O_2}

and q_{CO_2}. The maximum q_{O_2} of *E. coli* cells growing on a variety of carbon sources in aerobic cultures was reported to be approximately 20 mmol g_{DW}^{-1} h^{-1} (Andersen and Meyenburg 1980). For high biomass concentration OUR exceeds the maximal OTR, which depends on the performance of the bioreactor. Oxygen limitation causes formation of by-products, such as acetate, formate and ethanol, which exhibits a linear relationship with growth rate (Varma and Palsson 1994).

3.1.4. Elemental balances

Material that is flowing in and out of the cells is conserved and therefore the rates defined in Eq.(3.1) and Eq.(3.2) must satisfy several constraints. For example, carbon consumed by the cell in form of substrate is recovered in biomass, carbon dioxide and by-products. This relation is expressed by specific rates in form of a carbon balance.

$$\mu + \sum_{i=1}^{m} h_{p,i} \cdot q_{p,i} - \sum_{i=1}^{n} h_{s,i} \cdot q_{s,i} = 0 \tag{3.19}$$

The coefficients $h_{p,i}$ and $h_{s,i}$ represent the carbon content of m products and n substrates given as $mole_{carbon}$ $mole^{-1}$.

Balance equations have to be considered for other elements such as oxygen, hydrogen and nitrogen. The elemental composition of biomass, substrates, products and other compounds is collected in an elemental matrix $\mathbf{E}$, with rows corresponding to elements and columns to particular compounds. With the elemental matrix, balance equations are a system of linear equations:

$$\mathbf{Er} = \mathbf{0} \tag{3.20}$$

The vector $\mathbf{r}$ collects specific consumption and production rates, as well as μ. The degree of freedom is $F = m+n+1-i$, where i is the number of considered elements. The vector of specific rates $\mathbf{r}$ is partitioned into a vector of measured rates $\mathbf{r}_m$ and calculated rates $\mathbf{r}_c$ and Eq.(3.20) is rearranged.

$$\mathbf{E}_m\mathbf{r}_m + \mathbf{E}_c\mathbf{r}_c = \mathbf{0} \tag{3.21}$$

If $\mathbf{E}_c$ is square and has full rank the system is called observable, as there are enough measured rates to determine the non-measured rates.

$$\mathbf{r}_c = -\mathbf{E}_c^{-1}\mathbf{E}_m\mathbf{r}_m \tag{3.22}$$

If more measurements are available than the degrees of freedom F, the redundancy is

used to increase the accuracy of the measurements and to check the consistency of the data. A least square solution of the non-measured rates is estimated by

$$\mathbf{r}_c = -\mathbf{E}_c^{\#}\mathbf{E}_m\mathbf{r}_m \tag{3.23}$$

The matrix $\mathbf{E}_c^{\#}$ is the Penrose pseudo-inverse of $\mathbf{E}_c$. Stephanopoulos *et al.* (1998) show in detail how the best estimates $\hat{\mathbf{r}}_m$ follow from the redundancy of measured rates by

$$\hat{\mathbf{r}}_m = (\mathbf{I} - \mathbf{F}\mathbf{R}_r^T\mathbf{P}^{-1}\mathbf{R}_r)\mathbf{r}_m \tag{3.24}$$

where $\mathbf{I}$ is the identity matrix. The diagonal elements of the variance-covariance matrix $\mathbf{F}$ are the errors of measurements, which are supposed to be normally distributed with a mean value of zero. The variance-covariance matrix of the residuals is given as

$$\mathbf{P} = \mathbf{R}_r\mathbf{F}\mathbf{R}_r^T \tag{3.25}$$

The reduced redundancy matrix $\mathbf{R}_r$ are the independent rows of the redundancy matrix $\mathbf{R}$ given by

$$\mathbf{R} = \mathbf{E}_m - \mathbf{E}_c(\mathbf{E}_c^T\mathbf{E}_c)^{-1}\mathbf{E}_c^T\mathbf{E}_m \tag{3.26}$$

The best estimates $\hat{\mathbf{r}}_m$ are more reliable than the raw measurements and should be used to calculate the non-measured rates according to Eq.(3.23).

3.2. Metabolic processes

Similar to bioreactor processes, metabolic processes are described by variables of biochemical pathways which convert the feeding carbon source into biomass and products. Metabolic processes interact with the bioreactor processes by specific exchange rates introduced above.

3.2.1. Models of metabolic pathways

The genome annotation, along with biochemical information provides the information needed to reconstruct complete metabolic networks of a mircro-organism (Edwards *et al.* 2001). Additionally, data bases like EcoCyc provide structured symbolic descriptions of metabolic pathways, transport functions and gene regulation (Karp *et al.* 2002). Such

information is the basis for dynamic mass balances written for each metabolite x_i in the network:

$$\frac{dx_i}{dt} = \sum_j n_{i,j} v_j \tag{3.27}$$

where v_j corresponds to the jth metabolic flux, x_i represents the concentration of the metabolite, and the stoichiometric coefficient $n_{i,j}$ stands for the moles of metabolite i formed or consumed in reaction j (Schilling *et al.* 2000). The stoichiometric coefficients of $i = 1, 2, ..., m$ components and $j = 1, 2, ..., n$ reactions are collected in a $(m \times n)$ stoichiometric matrix $\mathbf{N}$. The reaction rates v, enzyme levels e, metabolite concentrations x, extracellular compounds c and other parameters p are collected in vectors given as

$$\mathbf{x} = (x_1, x_2, \ldots, x_m)^T \tag{3.28}$$

$$\mathbf{v} = (v_1, v_2, \ldots, v_n)^T \tag{3.29}$$

$$\mathbf{e} = (e_1, e_2, \ldots, e_n)^T \tag{3.30}$$

$$\mathbf{c} = (c_1, c_2, \ldots, c_l)^T \tag{3.31}$$

$$\mathbf{p} = (p_1, p_2, \ldots, p_k)^T \tag{3.32}$$

The dynamic mass balances of all metabolites are expressed in matrix notation by Eq.(3.33)

$$\frac{d\mathbf{x}}{dt} = \mathbf{N}\mathbf{v}(\mathbf{e}, \mathbf{x}, \mathbf{c}, \mathbf{p}) \tag{3.33}$$

Eq.(3.33) is a complete description of the metabolic system. The stoichiometric matrix accounts for structural properties of the system and the kinetic properties are considered by the functional relationship of reaction rates with regulatory effectors, enzyme levels and other parameters.

3.2.2. Structural analysis

Analysis of a biochemical system should at first consider the underlying structure and its invariants. The invariants of a system are properties that depend neither on the state of its environment nor on its internal state, but only on its structure (Reder 1988). The structure of a metabolic network is either given graphically as a reaction scheme or by the equivalent stoichiometric matrix. Structural analysis basically deals with matrix analysis and the rank of the stoichiometric matrix is an important characteristic. If the rank of $\mathbf{N}$ is m_0 (where m_0 is less than or equal to the number of rows m) there are $(m - m_0)$

dependent rows which can be expressed as linear combinations of the m_0 independent rows. This results in the following relationships of metabolites and metabolic fluxes.

Relationships between metabolites

Since each row of the stoichiometric matrix $\mathbf{N}$ corresponds to a metabolite there are m_0 independent metabolites $\mathbf{x}^{ind}$ and $(m-m_0)$ dependent metabolites $\mathbf{x}^{dep}$. The relationship between the independent and dependent metabolites is expressed as

$$\mathbf{N} = \mathbf{L}\mathbf{N}_R \tag{3.34}$$

where the $(m \times m_0)$ matrix $\mathbf{L}$ is the link matrix and $\mathbf{N}_R$ the reduced $(m_0 \times n)$ stoichiometric matrix of independent metabolites (Reder 1988). The dynamic mass balances of all metabolites in Eq.(3.33) can be expressed only by the independent metabolites $\mathbf{x}^{ind}$.

$$\frac{d\mathbf{x}}{dt} = \mathbf{L}\frac{d\mathbf{x}^{ind}}{dt} \tag{3.35}$$

Integration of Eq.(3.35) gives

$$\mathbf{x}(t) = \mathbf{L}\mathbf{x}^{ind}(t) + \mathbf{T} \tag{3.36}$$

Eq.(3.36) specifies the conservation relationships of metabolites (Reder 1988, Ehlde and Zacchi 1997). The sums of conserved moieties are collected in vector $\mathbf{T}$.

Relationships in the steady state

As a result of the high turnover of most metabolites a pseudo-steady state for the metabolites x_i is reasonable under most conditions, even after large perturbations in the environment (Stephanopoulos *et al.* 1998). With this assumption the differential equations in Eq.(3.33) reduces to a set of algebraic linear equations.

$$\mathbf{0} = \mathbf{N}\mathbf{v} \tag{3.37}$$

The relationship between steady state fluxes are defined by the kernel $\mathbf{K}$ of the reduced stoichiometric matrix (Reder 1988).

$$\mathbf{0} = \mathbf{N}_R\mathbf{K} \tag{3.38}$$

The $(n - m_0)$ columns of $\mathbf{K}$ are linearly independent and span the nullspace of $\mathbf{N}_R$. Each of the columns of $\mathbf{K}$ is a particular solution to Eq.(3.38). The n steady state fluxes (collected in a vector $\mathbf{J}$, indicating a steady state solution of $\mathbf{v}$) are now expressed as a linear combination of the $(n - m_0)$ independent fluxes in vector $\mathbf{J}^{ind}$:

$$\mathbf{J} = \mathbf{K}\mathbf{J}^{ind} \tag{3.39}$$

This equation is the basis for metabolic flux analysis, which provides a method to determine intracellular fluxes by measurements of (independent) extracellular fluxes (Ehlde and Zacchi 1997).

3.2.3. Metabolic flux analysis

Usually, there are more metabolites than reactions in a metabolic network and therefore Eq.(3.37) is underdetermined. Only in a few cases some reaction rates can be exactly determined by the analysis of $\mathbf{K}$ alone (Klamt *et al.* 2002). Estimation of intracellular fluxes is covered by the broad field of metabolic flux analysis (MFA). MFA comprises constrained-based approaches (Palsson 2000, Reed and Palsson 2003), isotopomer balancing (Wiechert and de Graaf 1996, Wiechert and de Graaf 1997) and stoichiometric metabolite balancing (Stephanopoulos *et al.* 1998).

Stoichiometric metabolite balancing

Stoichiometric metabolite balancing is based on the measurements of extracellular fluxes and also on assumptions that result in simplification of the network. According to Eq.(3.39) at least $n - m_0$ independent fluxes have to be measured in order to determine the remaining. In case that $\mathbf{J}^{ind}$ is exactly the subset of measured fluxes the steady state fluxes follow from Eq.(3.39). However, the nullspace is not unique and the measured fluxes will not equal the independent fluxes in Eq.(3.39) a priori.

According to Stephanopoulos *et al.* (1998) the flux vector $\mathbf{v}$ in Eq.(3.37) is partitioned into a vector of measured fluxes $\mathbf{v}_m$ and calculated fluxes $\mathbf{v}_c$. If the stoichiometric matrix is rearranged in the same way Eq.(3.37) reads:

$$\mathbf{0} = \mathbf{N}_m\mathbf{v}_m + \mathbf{N}_c\mathbf{v}_c \tag{3.40}$$

In the following it is assumed for simplicity that $\mathbf{N}$ has full rank and therefore $m = m_0$. If exactly $(n - m)$ fluxes were measured $\mathbf{N}_c$ is a square $(m \times m)$ matrix, which can be inverted, so that:

$$\mathbf{v}_c = -\mathbf{N}_c^{-1}\mathbf{N}_m\mathbf{v}_m \tag{3.41}$$

Unfortunately, $\mathbf{N}_c$ is only a square matrix if it has full rank and even if $\mathbf{N}$ has full rank as assumed above, the set of measurements might be chosen in such a way that the rank of $\mathbf{N}_c$ is less than m. In this case some of the measured rates are redundant. Also, $\mathbf{N}_c$ is non-square if the number of measured fluxes is greater than the degrees of freedom and the system is overdetermined. Then, a solution is obtained by the use of the Penrose pseudo-inverse $\mathbf{N}_c^{\#}$ (Stephanopoulos *et al.* 1998).

$$\mathbf{v}_c = -\mathbf{N}_c^{\#}\mathbf{N}_m\mathbf{v}_m \tag{3.42}$$

The pseudo-inverse exists for any matrix and allows computation of a least squares solution of Eq.(3.40), even if the system involves noncalculable rates (Klamt *et al.* 2002).

Constrained-based approaches

For metabolite balancing the measured fluxes are used to estimate the unknown fluxes of an underdetermined metabolic system. In case of a genome-scale model the set of linear equations $\mathbf{Nv} = \mathbf{0}$ is highly underdetermined and a constrained-based approach known as flux balance analysis (FBA) has been developed to estimate fluxes in such complex networks (Edwards and Palsson 1998). FBA is based on the fundamental law of mass conservation and the application of optimization principles to predict the optimal distribution of metabolic resources within a network (Schilling *et al.* 2000).

In Eq.(3.38) the steady state solutions of the metabolite mass balances were confined to the nullspace of the stoichiometric matrix $\mathbf{N}$. Within FBA additional constraints are imposed on the feasible steady state fluxes, such as lower and upper bounds of the fluxes,

$$\alpha_j \leq v_j \leq \beta_j \tag{3.43}$$

which enforce the reversibility/ irreversibility and maximal capacities of transport reactions (Edwards and Palsson 2000). The intersection of the nullspace and the region defined by the linear inequalities defines the feasible set of steady state fluxes, which can be further restricted by thermodynamic, kinetic or biochemical constraints. A particular flux distribution within the feasible set is found by linear programming. The linear

program maximizes a linear combination of fluxes, with the weights w_j,

$$\max Z = \sum_j w_j v_j = \mathbf{wv} \tag{3.44}$$

subject to the constraints in Eq.(3.37) and Eq.(3.43). Even if the most common objective function is maximization of cellular growth, other objectives such as a maximal ATP yield achieved better predictive accuracy during unlimited growth and also under nutrient scarcity (Schuetz *et al.* 2007).

3.3. Kinetics of enzyme-catalyzed reactions

In contrast to the structural properties the kinetic properties of a biochemical system depend on the environment as well as on its internal state, so they are not invariants of the system (Reder 1988). Generally, the reaction kinetics depend on metabolite concentrations $\mathbf{x}$, enzyme levels $\mathbf{e}$, and parameters collected in a vector $\mathbf{p}$. Exchange fluxes will additionally depend on concentrations of compounds in the cultivation medium $\mathbf{c}$.

$$\mathbf{v} = f(\mathbf{e}, \mathbf{x}, \mathbf{p}, \mathbf{c}) \tag{3.45}$$

The functional relation in Eq.(3.45) is usually highly non-linear and can be described by two classes of kinetic functions: mechanistic Michaelis-Menten type kinetics or alternative approximate formats, such as linear-logarithmic or power-law models. According to Heijnen (2005), approximative formats of *in vivo* kinetics should consider four properties:

- the rate is proportional to the enzyme level
- saturation kinetics at high metabolite concentrations
- small number of kinetic parameters
- an analytical steady state solution

Mechanistic functions mirror kinetics over the whole range of metabolite concentrations while non-mechanistic kinetics should be considered as approximations around a limited range. Such approximations are particularly suitable in living cells, with limits on physiological metabolite concentrations.

3.3.1. Mechanistic models

Enzyme-catalyzed reactions may appear as simple processes where a substrate S binds to an enzyme E and is released in form of the product P. However, in detail the reaction is more complex and composed of several elementary steps. The most simple case is an enzymatic reaction where one substrate is irreversible converted into a product.

$$S + E \rightleftharpoons ES \rightarrow E + P$$

With the assumptions, that the free enzyme and the enzyme complex are in a steady state ($dc_{ES}/dt = dc_E/dt = 0$) and the last step is rate limiting, the relation know as Michaelis-Menten equation is derived.

$$v = v_{max} \cdot \frac{c_S}{K_m + c_S} \tag{3.46}$$

The maximum reaction rate v_{max} depends on the initial enzyme concentration c_E^0. The Michaelis constant K_m expresses the affinity of the substrate. Mechanistic rate expressions become more complex in cases of reversible reactions, enzyme inhibition/activation and also for multi-substrate reactions. Further, enzymes with multiple binding sites exhibit sigmoidal kinetics, described by the Hill mechanism. Such cooperative and allosteric effects are typical for key regulatory enzymes of metabolism. However, kinetics of enzyme-catalyzed reactions are based on information obtained from *in vitro* kinetic studies on purified enzyme in test tubes. They are often not applicable under the *in vivo* conditions, which are present in the cellular milieu (Teusink *et al.* 2000, Heijnen 2005).

3.3.2. Thermokinetic models

A metabolic steady state may look similar to a thermodynamic equilibrium. However, as material is flowing through the metabolic network, concepts of non-equilibrium thermodynamics are required. Rather than balancing forward and backward fluxes of each elementary reaction as in thermodynamic equilibrium, the influxes and effluxes of the steady state metabolite pools are balanced (Heuett *et al.* 2008). In a non-equilibrium system the laws of thermodynamics give no information about the reaction rate. However, Onsager (1931) derived phenomenological equations, which linearly relate the reaction rate to the thermodynamic driving force in non-equilibrium systems. The thermodynamic driving force of the jth reaction is its affinity A_j which is equal to minus the Gibbs

free energy of reaction $\Delta_r G_j$.

$$A_j = -\Delta_r G_j = -\Delta_r G_j^0 - RT \ln \prod_{i=1}^{m} x_i^{n_{i,j}} \tag{3.47}$$

$\Delta_r G_j^0$ is the standard Gibbs energy of the jth reaction and $n_{i,j}$ are stoichiometric coefficients introduced above. As Onsager's equations are only valid close to equilibrium, they cannot be applied for cellular reactions operating far from equilibrium. It was shown, that for reversible enzyme-catalyzed reactions the relation of affinity and reaction rate is also linear far from equilibrium (Rottenberg 1973, van der Meer *et al.* 1980, Nielsen 1997). The linear relation of reaction rate and thermodynamic driving force is given as

$$v_j = L_j^{\#}(A_j - A_j^{\#}) \tag{3.48}$$

The parameters $A_j^{\#}$ and $L_j^{\#}$ are related to kinetic parameters of the forward and backward reaction rate. Nielsen (1997) derives the following kinetic description from Eq.(3.48)

$$v_j = a_j \sum_{i=1}^{m} k_{j,i} \ln x_i + b_j \tag{3.49}$$

Basically, this expression results from Eq.(3.48) and Eq.(3.47) and the kinetic parameters $k_{j,i}$ are recognized as stoichiometric coefficients of substrates and products. In case of regulatory effectors Nielsen (1997) proposed to use empirical coefficients.

3.3.3. Linear-logarithmic (lin-log) models

Non mechanistic formats such as linear-logarithmic (lin-log) models showed the capacity to adequately approximate mechanistic models (Visser and Heijnen 2003, Visser *et al.* 2004b). Lin-log models have their origin in the thermokinetic expression given in Eq.(3.49) and their general form for the jth reaction rate is given as

$$v_j = e_j(a_j + p_{j,1} \ln x_1 + p_{j,2} \ln x_2 + \cdots + p_{j,m} \ln x_m) \tag{3.50}$$

The rate is proportional to the concentration of the enzyme e catalyzing the reaction j and a linear combination of logarithms of the metabolite concentrations x_i (if required external compounds are included in the linear combination). Normalizing the reaction rate, the enzyme level and metabolite concentrations in Eq.(3.50) to a reference state

gives

$$\frac{v_j}{v_j^0} = \frac{e}{e^0}(1 + \varepsilon_{x_1}^{v_j} \ln \frac{x_1}{x_1^0} + \varepsilon_{x_2}^{v_j} \ln \frac{x_2}{x_2^0} + \cdots + \varepsilon_{x_m}^{v_j} \ln \frac{x_m}{x_m^0}) \tag{3.51}$$

In this form the model parameters are elasticity coefficients, which are scaled local sensitivity coefficients.

$$\varepsilon_{x_i}^{v_j} \equiv \frac{x_i}{v_j}\frac{\partial v_j}{\partial x_i} = \frac{\partial \ln v_j}{\partial \ln x_i} \tag{3.52}$$

Alternatively, elasticity coefficients can be interpreted as kinetic orders g_i of a power-law model.

3.3.4. The power-law formalism

The power-law formalism is the core element of the Biochemical Systems Theory (BST) developed by Savageau (1969a,b) and is derived from a first order Taylor series approximation of the kinetic rate law. Similar to chemical reactions, the rate law consists of a rate constant α and the particular components raised to a real-valued exponent (the exponent of the enzyme level is normally 1).

$$v_j = \alpha_j e_j \sum_{i=1}^{m} x_i^{g_{j,i}} \tag{3.53}$$

The kinetic orders $g_{i,j}$ are elasticity coefficients defined in Eq.(3.52), as recognized by partial derivation of Eq.(3.53).

3.4. Metabolic Control Analysis (MCA)

MCA was developed from the landmark papers of Kacser and Burns (1973) and Heinrich and Rapoport (1974) and is a well established framework, quantifying the control of flux in a metabolic network. MCA explains how the steady state variables of a biochemical pathway (fluxes and metabolite concentrations) are determined by systems parameters without knowing the detailed kinetic rate laws. Therefore, only local properties of kinetic rate laws are required, which are described by elasticity coefficients introduced in Eq.(3.52). These local parameters are related to the systems sensitivities, the flux control coefficients:

$$C_{e_j}^{J_i} = \frac{e_j}{J_i}\frac{dJ_i}{de_j} = \frac{d \ln J_i}{d \ln e_i} \tag{3.54}$$

and the concentration control coefficients:

$$C_{e_j}^{x_i} = \frac{e_j}{x_i}\frac{dx_i}{de_j} = \frac{d\ln x_i}{d\ln e_i} \tag{3.55}$$

Control coefficients are a measure of how a change of an enzyme level affects a particular steady state flux or metabolite pool. Heinrich *et al.* (1977) gave a more general definition of control control coefficients in terms of any parameter that acts exclusively on an enzyme. There have been further objections both the name and concept of control coefficients, which are discussed by Fell (1992).

3.4.1. Estimation of elasticity coefficients

Elasticity coefficients are estimated from mechanistic models by partial derivation of the rate laws (Chassagnole *et al.* 2002). In case of power-law and lin-log models elasticity coefficients are model parameters (Alvarez-Vasquez *et al.* 2005, Magnus *et al.* 2006). Kinetic rate laws and their parameters are commonly identified by means of dynamic modeling, describing time courses of intracellular metabolite concentrations. Nikerel *et al.* (2006) have shown, that elasticity coefficients can be potentially unidentifiable from dynamic data only and steady state experiments are required.

Estimation of elasticities from steady state data can be considered as an inverse problem, determining rate laws from what they produce: fluxes and metabolite pools (Giersch 1994). The first experimental method is described by Kacser and Burns (1979) who propose arbitrary changes anywhere in the *in vivo* system to obtain small deviations in concentrations and fluxes from which elasticity coefficients can be estimated. Their approach was later termed the double modulation method (Fell 1992). Since then, several extensions of the double modulation method were developed, that apply modulations, effecting specifically one enzyme (Hofmeyr *et al.* 1993, Giersch 1994). Matrix formulation allows applying these methods to metabolic systems of any structure and size (Acerenza and Cornish-Bowden 1997). Giersch and Cornish-Bowden (1996) define precisely which sets of reactions have to be modulated in order to calculate a particular elasticity. Co-response analysis accounts for fractional changes of steady state variables avoiding knowledge about the percentage modulation of a parameter, but still requires specific effectors of an enzyme (Hofmeyr and Cornish-Bowden 1996). A draw-back of these methods is the perturbation of a single enzyme, because in practice there will be always more than one enzyme changed. Further, the linearization around a reference state causes difficulties if experimental data is evaluated. On the one hand, changes in the metabolic pathway

must be small so that the linearization is valid. On the other hand, feasible experimental approaches require large changes. The recently developed lin-log approach avoids this problem since it provides a procedure for estimation of elasticities from large perturbation experiments (Wu *et al.* 2004). The lin-log approach and the double modulation method are further detailed in section 5.2.

As a convenient alternative, Nielsen (1997) derived elasticty coefficients of thermokinetic models from Eq.(3.48)

$$\varepsilon_{x_i}^{v_j} = -\frac{n_{i,j}RT}{A_j - A_j^{\#}} \tag{3.56}$$

For reversible reactions near equilibrium the parameter $A_j^{\#}$ is zero and the elasticity coefficient follows directly from the affinity, that is minus the Gibbs free energy.

3.4.2. Estimation of control coefficients

Control coefficients are estimated either directly by manipulation of enzyme activity or indirectly by their relationships with elasticity coefficients. Kacser and Burns (1973) describe these relationships of control and elasticity coefficients with the connectivity and summation theorems. The theorems were derived using a rather intuitive approach and do not include branched pathways or conserved moieties. A general applicability of MCA theorems was possible using the structural relations derived from the pathways stoichiometry explained above (Reder 1988, Small and Fell 1989, Ehlde and Zacchi 1997). The different theorems of MCA are reviewed by Visser and Heijnen (2002). They distinguish the structural approach of Reder (1988), the systematic approach of Ehlde and Zacchi (1997) and a third approach proposed by Giersch (1988a,b). Additionally, the authors present a novel engineering approach, which is based on the linearization of the steady state mass balance equation of independent metabolites:

$$\frac{d\mathbf{x}^{ind}}{dt} = \mathbf{N}_R\mathbf{v}(\mathbf{x}^{ind}, \mathbf{x}^{dep}(\mathbf{x}^{ind}, \mathbf{T}), \mathbf{e}) \tag{3.57}$$

Eq.(3.57) is similar to Eq.(3.33), with the difference that the reduced stoichiometric matrix introduced in Eq.(3.34) is applied. The reaction rates depend on independent and dependent metabolites, as well as on enzyme levels (external compounds and parameters are excluded for clarity). The dependent variables however depend on independent variables and the conserved sum in vector $\mathbf{T}$, which was introduced in Eq.(3.36). The basic problem of MCA theorems is the nested relationship of dependent and independent metabolites, their conserved sum and the kinetic rate laws. Therefore, linearization

requires differentiation of implicit functions with vector variables. Visser and Heijnen (2002) derive the following linearization of Eq.(3.57):

$$\mathbf{0} = \mathbf{N}_R \cdot \mathbf{J}_0 \cdot \left(\frac{\mathbf{e}}{\mathbf{e}_0} + \mathbf{E}^{\mathbf{x}_0} \cdot \mathbf{L}_0 \cdot \left(\frac{\mathbf{x}^{ind}}{\mathbf{x}_0^{ind}} - \mathbf{i} \right) \right) \tag{3.58}$$

The vector $\mathbf{J}_0$ contains steady state fluxes in the references state. Similarly metabolite concentrations in the reference state are indexed by 0. The vector $\mathbf{i}$ is the unit vector and elasticity coefficients are collected in matrix $\mathbf{E}$ (with rows referring to reactions and columns to metabolites).

Dependencies of conserved moieties are considered by a link matrix for the normalized variables $\mathbf{L}_0$, which is different from the link matrix $\mathbf{L}$ in Eq.(3.34).

$$\left(\frac{\mathbf{x}}{\mathbf{x}_0} - \mathbf{i} \right) = \mathbf{L}_0 \cdot \left(\frac{\mathbf{x}^{ind}}{\mathbf{x}_0^{ind}} - \mathbf{i} \right) \tag{3.59}$$

The link matrix for normalized variables follows from:

$$\mathbf{L}_0 = (\mathbf{X}_0)^{-1} \cdot \mathbf{N} \cdot (\mathbf{N}_R)^{\#} \cdot \mathbf{X}_0^{ind} \tag{3.60}$$

The concentration control coefficients are derived from Eq.(3.58) with standard matrix algebra.

$$\mathbf{C}^{\mathbf{x}} = -\mathbf{L}_0 \cdot (\mathbf{N}_R \cdot \mathbf{J}_0 \cdot \mathbf{E} \cdot \mathbf{L}_0)^{-1} \cdot \mathbf{N}_R \cdot \mathbf{L}_0 \tag{3.61}$$

The flux control coefficients follow from substitution of the steady state metabolite levels in the linearized rate equation (a more detailed description is given by Visser and Heijnen (2002)).

$$\mathbf{C}^{\mathbf{J}_0} = (\mathbf{E}^{\mathbf{x}_0} \cdot \mathbf{C}^{\mathbf{x}} + \mathbf{i}) \tag{3.62}$$

Linearization of Eq.(3.57) is also the basis for the (Log)linear approach of Hatzimanikatis and Bailey (1996). They derive similar equations as given in Eq.(3.61) and Eq.(3.62) and derive relative weights of conserved moieties, which are related to Eq.(3.60).

3.5. Thermodynamic analysis

Beside kinetic and stoichiometric analysis thermodynamic principles are increasingly applied in systems biology approaches. Kümmel *et al.* (2006) couple informations about directions of metabolic fluxes and ranges of metabolite concentrations via the second

law of thermodynamics in order to estimate feasible ranges of Gibbs energy of reaction. Similarly, Henry *et al.* (2007) apply thermodynamic constraints in addition to the mass balance constraints for metabolic flux analysis.

According to the second law of thermodynamics reactions only occur in direction of negative Gibbs energy of reaction $\Delta_r G$, which is calculated for a reaction j from the Gibbs energy of formation of the participating components.

$$\Delta_r G_j = \sum_i n_{i,j} \Delta_f G_i \tag{3.63}$$

The stoichiometric coefficients $n_{i,j}$ were defined in Eq.(3.27). The Gibbs energy of formation is calculated from the standard Gibbs energy of formation $\Delta_f G^0$ and the thermodynamic activity, which is often replaced by the molar concentration.

$$\Delta_f G_i = \Delta_f G_i^0 + RT \ln(c_i) \tag{3.64}$$

The standard Gibbs energy of formation of biochemical reactions in the cellular milieu is estimated by the group contribution method (Mavrovouniotis 1991) and values are available for most of the compounds of the genome scale model *E. coli* K-12 (*i*JR904 GSM/GPR) of Reed *et al.* (2003).

Network embedded thermodynamic (NET) analysis as proposed by Kümmel *et al.* (2006) applies the following optimization procedure to estimate the feasible range of Gibbs free energy of a particular reaction k:

$$\begin{aligned} \min / \max \quad & \Delta_r G_k \\ \text{subject to} \quad & \Delta_r G_j < 0 \ \forall v_j > 0 \\ & \Delta_r G_j > 0 \ \forall v_j < 0 \\ & c_i^{min} \leq c_i \leq c_i^{max} \end{aligned} \tag{3.65}$$

With this procedure, the feasible range of Gibbs free energy is not only considered in view of the kth reaction, rather the thermodynamic interdependencies of all reactions in the network are included. Therefore, NET analysis significantly limits ranges of Gibbs free energy and additionally concentration ranges of non-measured metabolites.

3.6. Central metabolism of *Escherichia coli*

Escherichia coli is a gram negative bacterium classified as part of the Enterobacteriaceae family. It was discovered in 1885 by German pediatrician and bacteriologist Theodor Escherich. *E. coli* is one of the best studied prokaryotic model organisms, and an important species in biotechnology. The cells grow on synthetic media with an optimal temperature of 37°C and a pH between 6.5 and 7.3. Metabolism of *E. coli* is facultative anaerobe, this means energy is generated by respiration or mixed acid fermentation. Commonly, metabolic processes are grouped into catabolism and anabolism. The fueling reactions of catabolism break down a substrate into precursors which are needed for biosynthesis. Additionally the process yields energy and redox cofactors. Anabolism is responsible for the biosynthesis of the building blocks of the cells including protein, amino acids, DNA and RNA nucleotides, lipids, different monomers, polyamines etc. (Wang and Hatzimanikatis 2006a). Even if biosynthetic pathways are complex all of them originate from a set of 12 precursors supplied by the central metabolic pathways (Ingraham *et al.* 1983). Anabolic and catabolic processes are connected by energy carrying metabolites like the adenylates ATP, ADP and AMP, as well as redox cofactors NADH and NADPH (Stephanopoulos *et al.* 1998). Central metabolism can be grouped into glycolysis and gluconeogenesis, pentose phosphate pathway, tricarboxylic acid cycle, pyruvate metabolism and oxidative phosphorylation. The network of central metabolism shown in Figure (3.1) was constructed from the EcoCyc Database (Karp *et al.* 2002) and the genome-scale model *E. coli* *i*JR904 GSM/GPR (Reed *et al.* 2003).

Glycolysis and Gluconeogenesis

The glycoltic pathway in *E. coli* converts glucose into pyruvate. Glucose enters the cell via the phosphotransferase system (pts), where a high energy phosphate group is translocated from phosphoenolpyruvate (PEP) to the incoming glucose. The phosphorylated glucose-6-phosphate (G6P) is interconverted by phosphoglucose isomerase (pgi) into fructose-6-phosphate (F6P). Normally pgi is present in excess and therefore G6P and F6P are at equilibrium constituting a single metabolite pool (Stephanopoulos *et al.* 1998).

In the Embden-Meyerhof-Parnas pathway F6P is further phosphorylated by phosphofructokinase (pfk) to fructose-1,6-bisphosphate (FBP) under the consumption of free energy in form of ATP. FBP is metabolized to dihydroxy-acetone phosphate (DHAP) and glyceraldehyde-3-phosphate (GAP) by FBP-aldolase (fba). The triosephosphates GAP and DHAP are interconvertible by triosephosphate isomerase (tpi). GAP dehydrogenase

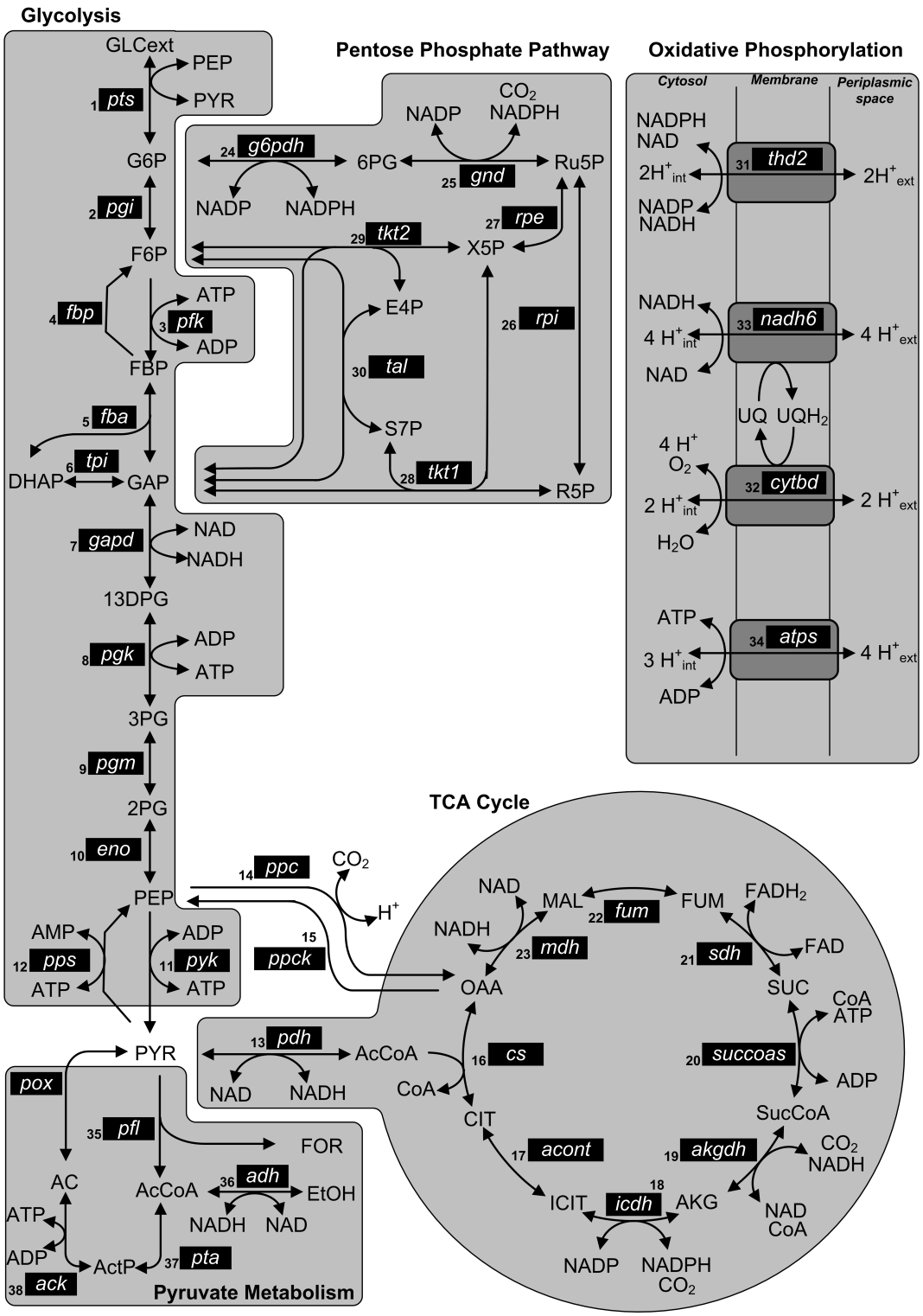

Figure 3.1.: Central metabolism of *Escherichia coli*. Reactions are further detailed in Table (A.9).

(gapd) catalyzes oxidation of GAP to 1,3-diphosphoglycerate (13DPG) producing NADH. The first step of glycolysis gaining free energy in form of ATP is the reaction of 13DPG to 3-phosphoglycerate (3PG) catalyzed by phosphoglycerate kinase (pgk). 3PG is interconverted by phosphoglycerate mutase (pgm) to 2-phosphoglycerate (2PG). Enolase (eno) catalyzes dehydration of 2PG into PEP. The high energy phosphate group of PEP is transfered to ADP in the last step of glycolysis, pyruvat kinase (pyk) forming ATP and pyruvate.

Gluconeogenesis is basically a glycolytic flux in reverse direction, which is necessary for growth on other carbon sources like pyruvate. Compared to glycolysis only two different enzymes are involved. The reaction of pyruvate to PEP is catalyzed by PEP synthase (pps) under consumption of ATP. An important role in regulation of gluconeogenic flux plays fructose-bisphosphatase (fbp), which converts FBP into F6P.

Pentose Phosphate Pathway (PPP)

In the pentose phosphate pathway (PPP) G6P is oxidized to 6-phosphogluconate (6PG) by glucose-6-phosphate dehydrogenase (g6pdh). The enzyme 6-phosphogluconate dehydogenase (gnd) coverts 6PG to ribulose-5-phosphate (Ru5P) and CO_2. Each reaction produces 1 mol of NADPH per mole of G6P entering the pathway. In the non-oxidative branch of the pathway Ru5P is converted into ribose-5-phosphate (R5P) or xylose-5-phosphate (X5P) by ribulose-5-phosphate isomerase (rpi) and epimerase (rpe). R5P and X5P can react to GAP and sedoheptulose-7-phosphate (S7P) by a transketolase (tkt1). Transaldolase (tala) converts S7P and GAP into erythrose-4-phosphate (E4P) and F6P. A second transketolase (tkt2) catalyzes the reaction of E4P and X5P to GAP and F6P. The metabolites GAP and F6P are also part of glycolysis and therefore the overall stoichiometry of PPP depends on the extend of which carbon is recycled back into glycolysis.

Tricarboxylic Acid Cycle

Depending on the energetic and redox state of the cell, pyruvate formed in glycolysis is further converted in several pathways. The tricarboxylic acid cycle (TCA) comprises reaction steps for the complete oxidation of pyruvate. The first step is an oxidative decarboxylation catalyzed by the enzyme complex pyruvate dehydrogenase (pdh) which is forming acetyl-Coenzyme A (AcCoA). AcCoA enters the TCA cycle in a reaction catalyzed by citrate synthase (cs) and reacts with oxaloacetate (OAA) to form citrate (CIT). In the subsequent reactions two of the six carbon atoms of citrate are oxidized to CO_2

and oxaloacetate, which is recycled at the end of the pathway. Citrate is isomerized to isocitrate (ICIT) by the enzyme aconitase (acont). The intermediate metabolite of this reaction cis-aconitate has no other function in metabolism and is disregarded in the consideration of the TCA cycle (Stephanopoulos *et al.* 1998). ICIT is converted to α-ketoglutarate (AKG) by isocitratedehydrogenase (icdh). In a similar step as the reaction of pyruvate to AcCoA, the enzyme complex AKG-dehydrogenase (akgdh) converts AKG to succinyl-CoA (SucCoA), which is hydrolyzed to succinic acid by SucCoA synthetase (sucoas). The dehydrogenation of succinate (SUC) to fumarate (FUM) by succinate dehydrogenase (sucd) requires FAD as reducing cofactor. FUM is metabolized to malate (MAL) by fumarase (fum). Malate dehydrogenase (mdh) recycles MAL to the initially used OAA producing NADH.

The TCA cycle yields three biosynthetic precursors, AKG, SucCoA and OAA. Additionally, oxidation of C-H- and C-C-bonds of citrate yields free energy which is conserved by generation of ATP in the reaction catalyzed by sucoas. Further, energy is conserved in the reduced cofactors NADH (formed by icdh, akgdh and mdh) and $FADH_2$ (formed by sucd). This energy is recovered by the last stage of catabolism, oxidative phosphorylation.

Oxidative Phosphorylation

The aerobic respiratory chain of *E. coli* consists of a set of membrane-bound dehydrogenases that feed electrons into the quinone pool in the cytoplasmic membrane and two ubiquinol oxidases that oxidize ubiquinol and reduce molecular oxygen to water (Calhoun *et al.* 1993). NADH ubiquinone oxidoreductase (nadh6) and cytochrome terminal oxidase (cytbd) work together to transfer electrons from NADH to oxygen, using the energy from those electrons to pump protons across the cytoplasmic membrane and generate the proton-motive force. This proton motive force is essential for ATP synthesis (atps) and proton-driven symportes (Karp *et al.* 2002). As one of very few microbes, *E. coli* contains two transhydrogenase isoforms with unknown physiological function that could potentially transfer electrons directly from NADH to NADP and vice versa (Sauer *et al.* 2004). A membrane bound, proton-translocating transhydrogenase (thd) is shown in Figure (3.1).

Pyruvate Metabolism

Oxidation of pyruvate by the reactions of TCA cycle occurs only under aerobic conditions, when NADH and $FADH_2$ are reoxidized by the respiratory chain. Under oxygen-limited

conditions pyruvate is oxidized to metabolic by-products of mixed acid fermentation. A key reaction of anaerobic glucose fermentation is the pyruvate formate-lyase (pfl). Similar as pdh which bridges TCA and glycolysis, AcCoA is formed by pyruvate and CoA, but instead of CO_2 and NADH this reaction produces one molecule of formate. In contrast to pdh and pfl which are essential for *E. coli* the pyruvate oxidase (pox) which converts pyruvate directly to acetate is of uncertain physiological function (Abdel-Hamid *et al.* 2001). In subsequent reactions AcCoA is converted into acetate or ethanol. Acetat is produced from AcCoA by phosphate acetyltransferase (pta) and acetate kinase (ack) yielding energy in form of ATP. Ethanol production from AcCoA by acetaldehyde dehydrogenase and alcohol dehydrogenase yields two mole of NAD per mole of formed ethanol.

3.7. Metabolomics

Strategies for analyzing metabolites exist since the early days of biochemistry, but capturing metabolomic changes in the cellular milieu are only beginning to be appreciated (Vaidyanathan 2005). Developments in microbial metabolomics were currently reviewed by Mashego *et al.* (2007) as well as Oldiges *et al.* (2007). Takors *et al.* (2007) demonstrate the importance of metabolome data in the context of systems biology as it is applied in modern biotechnology. There are two possibilities to measure intracellular metabolite concentrations: metabolites can be extracted from the whole culture broth or the cells are separated from the extracellular medium before the extraction procedure. The following unit operations are common to all protocols for microbial metabolome analysis:

- sampling from the bioreactor
- inactivation of metabolism
- quantitative extraction of metabolites
- selective and sensitive detection of metabolites

3.7.1. Sampling and inactivation of metabolism

Due to high turn over rates of many intracellular metabolite pools, rapid sampling techniques with simultaneous inactivation of metabolic activity were developed: a sampling tube device (Weuster-Botz 1997); an automated sampling devive for pulse experiments

(Schaefer *et al.* 1999); the stopped-flow sampling device (Buziol *et al.* 2002); a mini plug-flow reactor, the BioScope (Visser *et al.* 2002); a single tube heat exchanger (Schaub *et al.* 2006) and a low pressure *in situ* sampling device (Hiller *et al.* 2007a). A detailed overview of rapid sampling devices for metabolic engineering applications is given by Schädel and Franco-Lara (2009).

Simultaneously to sampling a quenching step should halt metabolism as rapidly as possible, this means intracellular enzymes are inactivated so that the metabolite pools are "frozen" (Winder *et al.* 2008). Rapid inactivation of metabolic activity is commonly achieved by quenching the sample into aqueous 60% (v/v) methanol at -50°C (Jensen *et al.* 1999, Buchholz *et al.* 2001, Al Zaid Siddiquee *et al.* 2004, Wittmann *et al.* 2004, Hoque *et al.* 2005, Magnus *et al.* 2006). After a centrifugation step the supernatant is discarded and cells are prepared for metabolite extraction. Several authors noticed leakage of intracellular metabolites into the quenching fluid during sampling (Wittmann *et al.* 2004, Faijes *et al.* 2007, Mashego *et al.* 2007, Bolten *et al.* 2007). Bolten *et al.* (2007) investigated leakage of amino acids and several intermediate metabolites for a variety of organisms. They conclude that a cold shock phenomenon during the phase of rapid cooling is responsible for a major loss of metabolites into the quenching fluid and methanol quenching is not a suitable method. Recently, Villas-Bôas and Bruheim (2007) proposed a glycerol-saline quenching fluid and showed, that most metabolites are detected at significantly higher levels when compared to methanol/water. Mashego *et al.* (2007) concluded that in case metabolite leakage occurs, leaked metabolites should be quantifiable. Compared to the amount of sample, the quenching fluid is in excess to assure mixing temperatures below -20°C, therefore already low concentrated intracellular metabolites leaking into the quenching fluid get further diluted. Depending on the biomass concentration in the sample and the percentage of lost metabolites, concentrations in the quenching fluid are expected to be below 1 μM and highly sensitive analytical methods are required to quantify leaked metabolites. Nasution *et al.* (2006) proposed to use ATP as indicator metabolite for cell leakage. Bolten *et al.* (2007) and Faijes *et al.* (2007) proposed to check metabolome data by means of the adenylates energy charge.

Alternative methods include simultaneous quenching and extraction of the whole culture broth. Within the differential method proposed by Taymaz-Nikerel *et al.* (2009) the cells are not separated from the quenched sample, but directly extracted with boiling ethanol. Schaub *et al.* (2006) integrated sampling, quenching and extraction in one unit operation using a heat exchanger. However, these approaches require correction for metabolites in the cultivation medium.

3.7.2. Extraction

After sampling and inactivation of metabolism, the intracellular metabolites have to be extracted from the cells. The aim here is not only to release the metabolites from the cell interior but also to permanently deactivate enzymes. During extraction, the target metabolites should not undergo any physical or chemical modification, and degradation should be minimized (Winder *et al.* 2008). Freeze-thaw cycles, boiling or extreme pH are commonly applied in extraction protocols. Six different extraction methods for metabolite measurements in *E. coli* were compared by Maharjan and Ferenci (2003). They conclude that the extraction methodology has a significant influence on the results of metablome analysis and propose cold methanol extraction for global metabolome analysis. However, with cold extraction an efficient deactivation of enzymes is not always assured. Hiller *et al.* (2007b) compared three extraction methods for *E. coli*: Perchloric acid, boiling ethanol and hot water. They could show that extraction with buffered hot water (30 mM triethanolamine, pH = 7.5, 95°C) is a reliable method.

3.7.3. Analytical platforms

Several analytical techniques were applied for the quantification of metabolites in cell extracts, e.g. enzymatic assays, gas chromatography-mass spectrometry (GC-MS), nuclear magnetic resonance (NMR) and liquid chromatography-mass spectrometry (LC-MS). LC-MS, GC-MS and most recently capillary electrophoresis-mass spectrometry (CE-MS) are highly sensitive techniques for simultaneous quantification of various metabolites in a small amount of sample. Mass spectrometry has become important in biosience with the development of soft ionization techniques, such as electrospray ionization (ESI) (Mashego *et al.* 2007). The LC-ESI-MS technique was successfully used to estimate metabolites in central metabolism (Buchholz *et al.* 2001, Luo *et al.* 2007). However, there are problems with high salt content in the samples or the eluent, which can interfere with the electro spray source by suppressing ionization. Luo *et al.* (2007) use an eluent with the volatile ion pair reagent tributylamine (TBA) to avoid problems with ionization. In case of a high salt content in the sample, isotope dilution mass spectrometry (IDMS) was proposed to account for ion suppression by an U-^{13}C labeled internal standard (Wu *et al.* 2005).

3.8. Proteomics

Proteomics covers methods to examine the levels of proteins in a cellular system and their changes in response to different genotypes or environmental conditions. The exploration of the *E. coli* proteome can be divided into three phases (Han and Lee 2006):

- the gel-based approaches like two-dimensional gel electrophoresis (2-DE) for the separation of proteins
- non-gel approaches for the identification of proteins resolved by 2-DE
- predictive approaches using bioinformatic tools

Global proteome analysis has brought a new way of how the physiology of cells is studied and two discoveries greatly contribute to understanding of biological systems. First, the physiological behavior of cells can be diagnosed by changes in proteine expression. Second, there is evidence that biological systems can be described by a small number of "physiological modules" (VanBogelen 2003). In this sense, the term stimulon was introduced by Gottesman and Neidhardt (1983) to decribe a set of proteins whose expression changes in a stimulus-response experiment.

Several proteom studies revealed that such changes of expression levels in response to changing conditions are hardly predictable. Hua *et al.* (2004) show that differences of proteome profiles in glucose-limited and nitrogen-limited *E. coli* cells are mainly caused by the reduced growth rate, rather than by the kind of limiting substrate. Smith and Neidhardt (1983) found more drastic changes in metabolome pools than in protein levels when changing from aerobic to anaerobic growth conditions of *E. coli*.

Proteomics becomes increasingly important in biotechnological applications as several proteomic signatures can be used to monitor cellular states (Han and Lee 2006). During a fed-batch process, substrate-limitation is the major purpose for changes in the proteom of *E. coli*, where the expression of enzymes of TCA cycle and energy metabolism was found to be highly up-regulated (Yoon *et al.* 2003, Raman *et al.* 2005, Wang *et al.* 2005).

Studying kinetics of protein synthesis in response to the changes in environmental conditions is a further challenging step for proteome analysis. Enzyme induction is a slow process compared to metabolism, but there is only little information about how fast a whole stimulon reacts to changed conditions. It is known that RNA polymerase works with 30 nucleotides per second and a RNA chain with 5000 nucleotides is synthesized in approximately 3 minutes (Alberts *et al.* 1995). The rate of protein synthesis depends on

the growth rate and the amount of ribosomes in the cell (Farewell und Neidhardt 1998). A possibility to study the *in vivo* protein synthesis is the dual channel method (Bernhardt *et al.* 1999). In *Bacillus subtilis*, synthesis of the acetoine dehydrogenase complex as response to exhaustion of glucose is induced after 10 minutes and reaches a balance between synthesis and accumulation after 30 minutes (Bernhardt *et al.* 2003).

4. Material and Methods

4.1. Micro-organism

All cultivations described in this work were performed with *Escherichia coli* K12 DSM 498 (DSMZ, German Resource Center for Biological Material). The dried culture obtained from the DSMZ was rehydrated and cultivated in 100 mL complex media (Table 4.1) in a 1000 mL shake flask (37°C, 250 rpm) until a optical density of 4 was reached. The cell suspension was mixed with sterile glycerol to give a final concentration of 20% (v/v). The glycerol stock was aliquoted and stored at -20°C.

Table 4.1.: Complex medium for *E. coli* stocks.

Compound	Concentration	
Peptone	5	g L^{-1}
NaCl	5	g L^{-1}
Yeast extract	10	g L^{-1}
Glucose	6	g L^{-1}

4.2. Cultivation media

All cultivations were performed with a defined medium given in Table (4.2). The medium was adjusted with 2 molar NaOH to pH 7.

Table 4.2.: Composition of the mineral salt media.

Compound	Concentration	
NH_4Cl	0.2	g L^{-1}
$(NH_4)SO_4$	2	g L^{-1}
KH_2PO_4	3.25	g L^{-1}
K_2HPO_4	2.5	g L^{-1}
$NaH_2PO_4 \cdot H_2O$	1.5	g L^{-1}
$MgSO_4$ solution (500 g L^{-1} $MgSO_4 \cdot$ 7 H_2O)	2	mL L^{-1}
trace-element solution	2	mL L^{-1}

Table 4.3.: Composition of the trace-element solution.

Compound	Concentration	
$CaCl_2 \cdot 2\ H_2O$	5	g L^{-1}
$ZnSO_4 \cdot 7\ H_2O$	0.25	g L^{-1}
$CuCl_2 \cdot 2\ H_2O$	0.125	g L^{-1}
$MnSO_4 \cdot H_2O$	1.25	g L^{-1}
$CoCl_2 \cdot 6\ H_2O$	0.875	g L^{-1}
H_3BO_3	0.0625	g L^{-1}
$AlCl_3 \cdot 6\ H_2O$	1.25	g L^{-1}
$Na_2MoO_4 \cdot 2\ H_2O$	0.25	g L^{-1}
$Fe_2SO_4 \cdot 7\ H_2O$	9.15	g L^{-1}

The mineral medium was sterilized in an autoclave for 20 min at 120°C. Trace-element solution and $MgSO_4$ solution were added after sterilization via a sterile filter.

4.3. Cultivation

4.3.1. Pre-cultures

Pre-cultures were grown overnight in 1000 mL shake-flasks filled with 100 mL minimal medium (37°C, 250 rpm). All shake-flasks were inoculated by addition of 500 μL culture from a glycerol stock. Subsequently, 1.2 mL from a sterile glucose solution with 500 g L^{-1} glucose was added to achieve a concentration of 6 g L^{-1} in the cultivation medium.

4.3.2. Fed-batch cultivation

A 42 L stirred tank bioreactor (Techfors, Infors AG, Switzerland) with 22 L minimal medium was utilized for fed-batch cultivation with an open-loop control of biomass formation according to Jenzsch *et al.* (2006). Dissolved O_2 (DO) was maintained above 40% by controlling aeration and stirrer speed. The pH was adjusted with 25% (v/v) NH_4OH to a constant value of 7.0.

As shown in Figure (4.1), the fed-batch process was subdivided into an initial lag-phase and two exponential feeding phases.

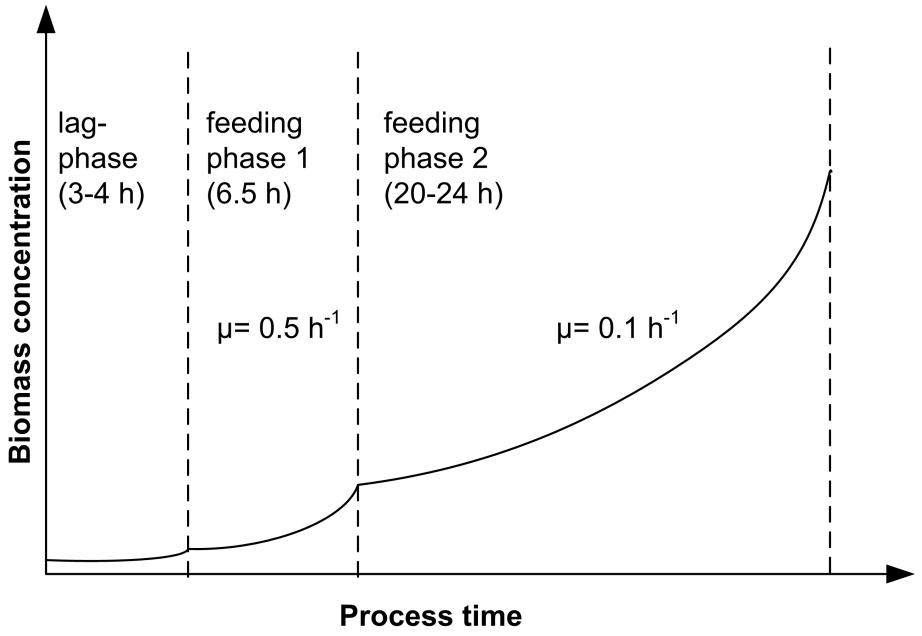

Figure 4.1.: Schematic description of the three phases in the fed-batch process.

After inoculation with 500 mL pre-culture 20 mL of a sterile glucose solution (100 g L^{-1}) was added to the bioreactor, so that glucose concentration in the cultivation medium was approximately 0.1 g L^{-1}. The exponential glucose feeding profile given in Eq.(3.9) was applied when the increasing DO signal indicated depletion of glucose. Sterile glucose solution was fed to the bioreactor by a peristaltic pump, which was controlled by a sequence implemented in the process control software (Iris, Infors AG, Bottmingen, Switzerland). For the first feeding phase 2 L of a 100 g L^{-1} glucose solution was prepared and the specific growth rate was μ^{set} =0.5 h^{-1}. After 6.5 h biomass concentration reached approximately 3 g_{DW} L^{-1} and 8 L of a 300 g L^{-1} glucose solution was prepared for feeding phase two, where the growth rate was reduced to 0.1 h^{-1}. The parameters of the two feeding phases are summarized in Table (4.4).

Table 4.4.: Parameters of the exponential feeding profile according to Eq.(3.9).

Parameter	Feeding phase 1	Feeding phase 2
c_x^0	0.1 g_{DW} L^{-1}	3 g_{DW} L^{-1}
$Y_{x,s}$	0.45 g_{DW} g^{-1}	0.45 g_{DW} g^{-1}
V_0	22 L	23 L
c_s^0	100 g L^{-1}	300 g L^{-1}
c_s	0 g L^{-1}	0 g L^{-1}
μ^{set}	0.5 h^{-1}	0.1 h^{-1}

A dynamic model of the process according to Eq.(3.5) was implemented in a MATLAB/ Simulink model. Formal monod kinetics of cellular growth ($\mu_{max} = 0.7$ h^{-1}; $K_s = 0.001$ g L^{-1}) and substrate uptake ($Y_{x,s} = 0.45$ g_{DW} g^{-1}) were combined with the mass balances of substrate, biomass and reaction volume.

4.4. Rapid Media Transition (RMT)

Steady state experiments were performed in a lab-scale bioreactor in parallel to the fed-batch process during feeding phase 2. The reaction of cells from the fed-batch process was observed when they where rapidly exposed to a new carbon source. This approach of Rapid Media Transition (RMT) is shown in Figure (4.2).

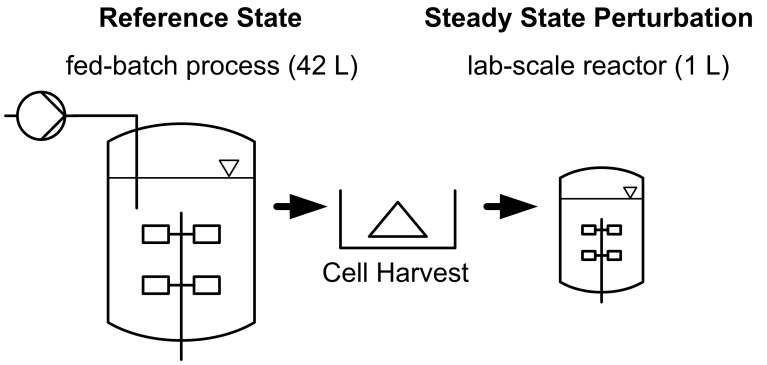

Figure 4.2.: Experimental set up applied for rapid media transition. Biomass from the production process is repeatedly transferred to a lab-scale stirred-tank bioreactor. Cells are separated by a centrifuge.

Culture broth from the fed-batch process was withdrawn by the ground valve of the bioreactor before each RMT experiment. Cells were separated by centrifugation (4000 g, 37°C, 5 min). The supernatant was discarded and cells were resuspended in 200 mL minimal media (37°C). The total volume of resuspended cells was determined prior to inoculation of the perturbation reactor, which was a 1.5 L stirred-tank bioreactor (Labfors, Infors AG, Bottmingen, Switzerland) prepared with 750 mL minimal medium. Oxygen and CO_2 were monitored in the off-gas (Easy Line, ABB Automation, Zurich Switzerland). The pH was controlled at a constant value of 7.0 using 5% NH_4OH and 1 molar H_2SO_4 . Dissolved oxygen was monitored with a DO sensor (Mettler Toledo, Giessen, Germany). The cells were cultivated for 16-18 minutes in batch an fed-batch operation mode with different substrates.

4.4.1. RMT experiments in batch mode

Glucose, pyruvate, succinate and acetate were utilized in four RMT experiments in batch operation mode. From the fed-batch process 1.5 L culture broth was withdrawn before each perturbation experiment. The cells were cultivated for 16 minutes after addition of carbon source. Samples of extracellular metabolites and biomass were taken 5 times during the short-term cultivation (0, 4, 8, 12 and 16 min). Sampling of intracellular metabolites was performed after 6, 10 and 14 min. Table (4.5) summarizes cultivation conditions of the four RMT experiments.

Table 4.5.: Conditions of four rapid media transition experiments in batch mode.

RMT Experiment	1	2	3	4
Substrate	Glucose	Pyruvate	Succinate	Acetate
c_s^0	100 g L^{-1}	100 g L^{-1}	60 g L^{-1}	100 g L^{-1}
aeration	air 8 L min^{-1}	air 8 L min^{-1}	air 8 L min^{-1}	air 8 L min^{-1}
V_R	1.015 L	1.040 L	1.020 L	1.020 L

4.4.2. RMT experiments in fed-batch mode

In four RMT experiments substrate was supplied with a constant feeding rate, which was changed in three intervals of 6 minutes. The feeding profile and moments of sampling are shown in Figure (4.3). Feeding was started one minute after inoculation of the

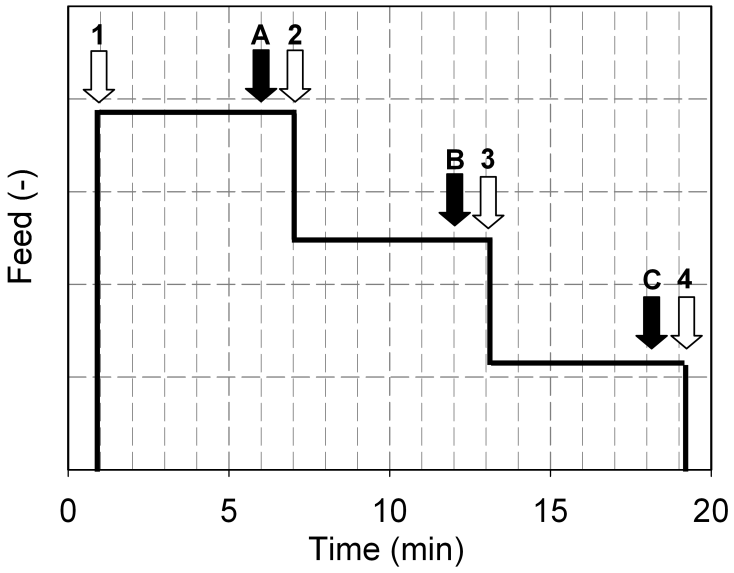

Figure 4.3.: Feeding profile during rapid media transition experiments in fed-batch mode. Moments of sampling are indicated by the arrows (white: biomass and extracellular metabolites; black: intracellular metabolites).

perturbation reactor. Each time the feeding rate was reduced, the amount of supplied substrate was determined by an analytical balance and samples of extracellular metabolites and biomass were withdrawn (white arrows in Figure 4.3). Sampling of intracellular metabolites was performed after 6, 12 and 18 min (black arrows in Figure 4.3). The three intervals with constant feeding are labeled A, B and C in the following. In four RMT experiments cells were cultivated with glucose under aerobic and anaerobic conditions, and with pyruvate and succinate as carbon source. The conditions of the four RMT experiments are summarized in Table (4.6).

Table 4.6.: Conditions of four rapid media transition experiments in fed-batch mode.

RMT Experiment	1	2	3	4
Substrate	Glucose	Pyruvate	Succinate	Glucose
c_s^0	100 g L^{-1}	100 g L^{-1}	60 g L^{-1}	100 g L^{-1}
aeration	air 10 L min^{-1}	air 10 L min^{-1}	air 10 L min^{-1}	N_2 2 L min^{-1}
V_R	1.005 L	1.01 L	1.01 L	1.015 L
Feeding rate A	2.3 mL min^{-1}	2.3 mL min^{-1}	1.9 mL min^{-1}	2.3 mL min^{-1}
Feeding rate B	1.5 mL min^{-1}	1.3 mL min^{-1}	1.3 mL min^{-1}	1.5 mL min^{-1}
Feeding rate C	0.8 mL min^{-1}	0.8 mL min^{-1}	0.6 mL min^{-1}	0.8 mL min^{-1}

4.5. Preparation of U-^{13}C labeled cell extracts

For preparation of U-^{13}C labeled cell extracts *E. coli* was cultivated on U-^{13}C labeled glucose (Eurisotop, Saint-Aubin Cedex, France). As U-^{13}C glucose is quite expensive it is preferable to harvest the whole culture broth in order to achieve a maximum yield of labeled cell extract. Therefore, cultivation was performed in an automated milliliter setup to reduce experimental effort during cell harvest. Pre-cultures were grown overnight in 200 mL shake-flasks filled with 20 mL minimal medium (37°C, 250 rpm). All shake-flasks were inoculated by addition of 100 μL culture from a glycerol stock and 240 μL from a sterile U-^{13}C glucose solution with a concentration of 500 g L^{-1}. Cells of the pre-culture were separated by centrifugation (4000 g, 4°C, 5 min) and resuspended in 90 mL minimal medium, containing 4 mL anti foam reagent (Clerol FBA 265, Cognis, Germany) and 32 g L^{-1} U-^{13}C labeled glucose. The resuspended cells were aliquoted in 8 sterile single-use stirred-tank bioreactors. Individual DO and pH were monitored online by measuring the fluorescence decay time of two chemical sensors immobilized at the bottom of each single-use bioreactor. The pH was controlled by the process control software (fedbatch-XP, DASGIP, Jülich, Germany) with addition of 5% NH_4OH at a constant value of 7.0. CO_2 in the air supply was was completely removed by passing the air through a bottle containing 1 L of 4 molar KOH solution.

All bioreactors were harvested when DO signal increased in the first bioreactor, indicating depletion of glucose. Culture broth of one bioreactor (app. 11 mL) was manually transfered into a test tube with 20 mL hot buffered water (95°C, 30 mM TEA, pH= 7.5), in order to simultaneously stop metabolism and extract metabolites from the cells. The quenched samples were incubated 5 min at 95°C in a thermostat and mixed manually meanwhile. Subsequently, the test tubes were cooled down on ice and then centrifuged for 10 min at 4500 g and 4°C. The supernatant was transferred into a new test tube and cooled to -80°C. The frozen supernatant was lyophilised for 48 h. The dried supernatant was re-suspended in 16 mL 50% (v/v) methanol/water. The U-^{13}C labeled cell extract was mixed 1:1 with standard solution of unlabeled metabolites in different concentrations (0, 5, 30, 50, 100, 200, 300, 500 μM). The mixture was analyzed by LC-MS and the ratio of unlabeled and U-^{13}C labeled metabolites was determined by the peak areas of masses $M+0$ and $M+N$ (where M is the molecular mass of the metabolite or its fragment and N the number of carbon atoms of the metabolite or its fragment).

4.6. Analytical methods

4.6.1. Sampling of biomass and extracellular metabolites

Extracellular metabolites and biomass were measured five-fold. Therefore, 10 mL of culture broth was withdrawn and rapidly chilled on pre-cooled glass envelopes, filled with glass beads (4°C). The sample was subdivided into 5 pre-weighted sample containers. Cells were separated (10,000 g, 10 min, 4°C) and the supernatant was stored at -20°C until analysis. The cell pellet was washed and dried at 80°C to measure cell dry weight (DW). Optical density (OD) was determined at 660 nm. The correlation factor between OD_{660} and DW was 0.6 g_{DW} L^{-1}.

4.6.2. HPLC analysis of culture supernatant

Separation of substrates and by-products in the culture supernatant was achieved on an Aminex HPX-87H 300 mm × 7.8 mm I.D. cation-exchange column (Bio-Rad, Germany). The mobile phase was 5 mM H_2SO_4 and flow rate was 0.7 mL min^{-1} (Smartline 5000 HPLC pump, Knauer, Germany) running 30 minutes. The injection volume was 20 μL. Column temperature was set to 50°C. Glucose, acetate, formate, succinate, pyruvate, and fumarate were detected using a RI-detector detector (Smartline 2300, Knauer). AKG was detected with an UV-VIS detector at 210 nm (LC295, Perkin Elmer)

4.6.3. Sampling of intracellular metabolites

Rapid sampling was performed with the sampling device described by Hiller *et al.* (2007). Before sampling, sample containers were filled with 25 mL quenching fluid, pressure was reduced to 200 mbar and the container was cooled down to -50°C. The quenching fluids used in this work were either 60% (v/v) methanol/water (MW) or 60% (v/v) methanol/glycerol (MG), both buffered with 30 mM triethanolamine (TEA) at pH = 7. After sampling, three different protocols for sample preparation and extraction were applied. The cells were either separated from the quenching fluid (sampling protocols SP1 and SP2) or the quenched sample was extracted directly (sampling protocol SP3).

Sampling protocol 1 (SP1): Extraction with standard addition

The protocol is shown in Figure (4.4). The quenched cell suspension (MW or MG) was

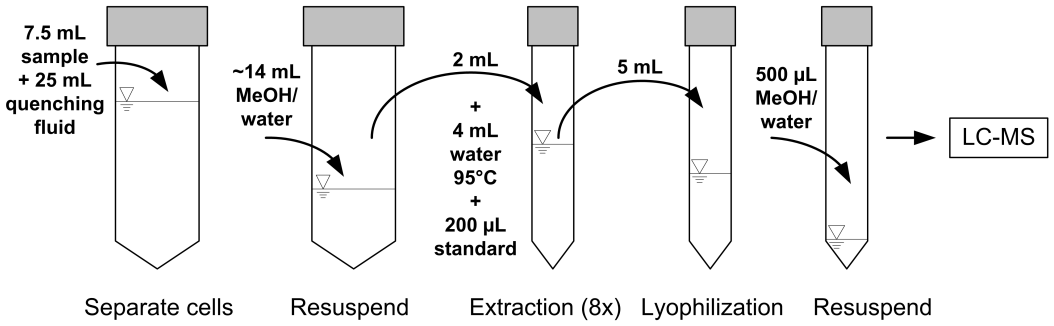

Figure 4.4.: Sampling protocol 1 (SP1).

transferred into a test tube and centrifuged for 6 min at 6,000 g and -19°C to separate cells. The supernatant was sterile filtered and stored at -20°C, in order to measure metabolites, which leaked into the quenching fluid. The cell pellet was resuspended in 60% (v/v) methanol/water (-20°C). OD_{660} and cell volume of the cell suspension was determined before metabolite extraction. 2 mL of cell suspension and 200 μL standard solution were added to 4 mL de-ionised water (30 mM TEA, pH = 7.5) in pre-heated test tubes and shaken for 5 min at 95°C on a thermomixer (Comfort, Eppendorf, Hamburg, Germany). The test tubes were cooled down on ice and then centrifuged for 10 min at 4500 g and 4°C. 5 mL of the supernatant was transferred into a new test tube and cooled to -80°C. The frozen supernatant was lyophilized and stored at -20°C until analysis. For analysis the sample was re-suspended with 500 μL 50% (v/v) methanol/water.

Influences of the extraction procedure on the stability of metabolites and effects of the sample matrix were considered by standard addition. Eight extracts of one sample were produced, each with a standard mixture of metabolites in different concentrations (0 μM, 100 μM, 200 μM, 300 μM, 400 μM, 500 μM, 600 μM, 700 μM). Concentrations of metabolites were calculated via linear regression of the calibration curve (MATLAB R2006b, The MathWorks Inc). The size of the 95% confidence interval is calculated according to the method of standard addition in DIN 32633 (German Institute for Standardization). Since standard addition is an extrapolation method, confidence intervals are higher compared to an external calibration.

Sampling protocol 2 (SP2): Extraction without standard addition

Sampling protocol 2 (SP2) is shown in Figure (4.5). The quenched cell suspension (MG)

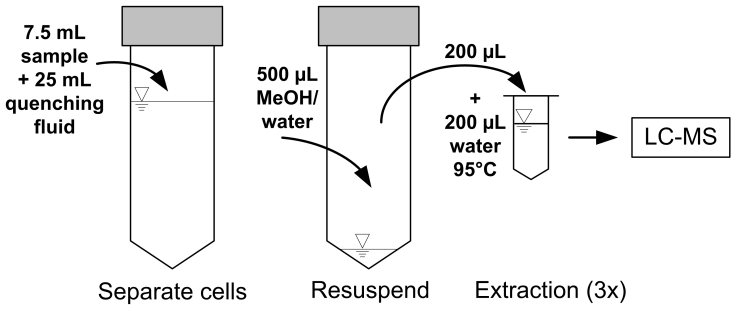

Figure 4.5.: Sampling protocol 2 (SP2).

was transferred into a test tube and centrifuged for 6 min at 6,000 g and -19°C to separate cells. In case a washing step was applied cells were resuspended in 25 mL quenching fluid (-20°C, MG) and centrifuged again. The cell pellet was resuspended in 500 μL of 60% (v/v) methanol/water (-20°C). OD_{660} of the cell suspension was determined before metabolite extraction. Intracellular metabolites were measured in three cell extracts of one sample. For extraction 200 μL of cell suspension was added to 200 μL aqueous buffer (30 mM TEA, pH = 7.5) in pre-heated test tubes and shaken for 3 min at 95°C on a thermomixer (Comfort, Eppendorf, Hamburg, Germany). The test tubes were cooled down on ice and then centrifuged for 10 min at 10,000 g and -19°C. 300 μL of the supernatant was transferred into a new test tube and stored at -80°C until analysis. External calibration curves were obtained from extraction of a sample with standard addition. Therefore, 100 μL cell suspension was mixed with 100 μL standard solution of metabolites in six different concentrations (0 μM, 10 μM, 25 μM, 50 μM, 100 μM, 150 μM) and subsequently processed as described above.

Sampling protocol 3 (SP3): Extraction of the whole culture broth

Sampling protocol 3 (SP3) is shown in Figure (4.6). The quenched cell suspension (MW) was transferred into a test tube and OD_{660} of the sample was determined. 2 mL of the quenched sample were added to 4 mL water (30 mM TEA, pH= 7) in pre-heated test

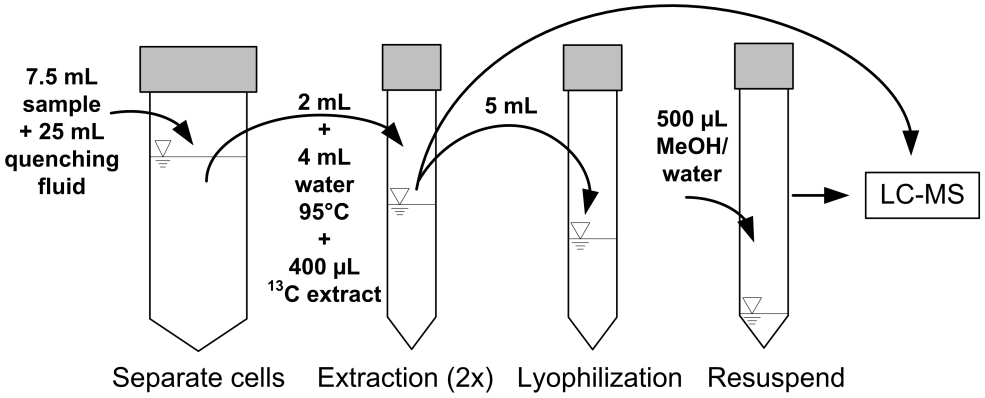

Figure 4.6.: Sampling protocol 3 (SP3).

tubes and shaken for 5 min at 95°C on a thermomixer (Comfort, Eppendorf, Hamburg, Germany). Optionally, isotope dilution mass spectrometry (IDMS) was applied, by addition of 400 μL of U-^{13}C-labeled cell extract before extraction. The test tubes were cooled down on ice and then centrifuged for 10 min at 4500 g and 4°C. 5 mL of the supernatant was transferred into a new test tube and cooled to -80°C. 1 mL of the remaining supernatant was stored at -20°C until analysis. The frozen supernatant was lyophilzed and stored at -20°C until analysis. For analysis the sample was re-suspended with 500 μL 50% (v/v) methanol/water. Metabolites were quantified directly in the cell extract and also in the concentrated sample. Metabolites were quantified by IDMS or external calibration.

4.6.4. LC-MS analysis of cell extracts

Quantification of metabolites in the cell extracts was performed by an LC-MS method adopted from Luo *et al.* (2007). A Synergi Hydro-RP (C18) 150 mm × 2.1 mm I.D., 4 μm 80 Å particles column (Phenomenex, Aschaffenburg, Germany) with eluent A (10 mM tributylamine aqueous solution adjusted to pH 4.95 with 15 mM acetic acid) and eluent B (methanol) was applied for chromatography. A degassed binary gradient at 0.2 mL min^{-1} was achieved with a P 1100 HPLC pump (Thermo Finnigan, Dreieich, Germany). The injection volume was 20 μL. Sample temperature was 4°C and column temperature was set to 35°C. HPLC flow was transferred directly to the mass spectrometer via the electro-spray ionisation (ESI) interface. ESI-MS analysis was performed using an LCQ advantage iontrap mass spectrometer (Thermo Finnigan, Dreieich, Germany). N_2 was

used as sheath gas and helium served as damping gas. Data acquisition and analysis were conducted using the Xcalibur software (Thermo Finnigan, Dreieich, Germany). Optimal ESI parameters were determined either with the LCQtune software (Thermo Finnigan, Dreieich, Germany) or with the optimization software GAME.opt (Link and Weuster-Botz 2006) as shown in Table (A.6). Selected ion monitoring was applied for detection of negative ions.

4.7. Computational methods

4.7.1. Estimation of extracellular fluxes

In case of RMT experiments in batch mode, external fluxes were estimated from the time courses of biomass, substrates and by-products during the perturbation experiments. Assuming exponential growth, the specific growth rate is estimated from logarithmic regression of the DW measurements to Eq.(3.10). Slope and Y-axis intercept of the regression analysis give an estimate for specific growth rate μ and initial biomass concentration c_x^0 . The specific substrate uptake rate follows from Eq.(3.12) and the biomass concentration measured after 8 minutes. Deviations between estimates from the exact Eq.(3.11) and the approximation are negligible for the observed time interval of 16 minutes. Specific production rates of by-products were estimated in the same way.

External fluxes of the fed-batch process and the fed-batch RMT experiments require estimation of time derivatives in order to solve Eq.(3.5) for the specific rates. In the case that no substrate is present in the cultivation medium, the time derivative is zero and substrate uptake is determined analytically from mass balances.

During all experiments OUR and CPR were determined from exhaust gas measurements and mass balancing in the gas phase according to Eq.(3.17) and Eq.(3.18).

4.7.2. Elemental balances

Elemental balances of carbon (C), hydrogen (H), oxygen (O) and nitrogen (N) are used to increase the accuracy of the measured rates through a least squares calculation and to identify gross measurement errors. Therefore, specific OUR and CPR, as well as the

specific production and consumption rates of biomass, substrates, by-products, ammonia and water are collected in vector $\mathbf{r}_m$.

$$\mathbf{r}_m = (q_{O_2}, q_{CO_2}, q_{gluc}, q_{pyr}, q_{suc}, q_{ac}, q_{for}, q_{etoh}, \mu, q_{nh_3}, q_{h_2o})^T \tag{4.1}$$

The elemental composition of biomass was assumed to be $CH_{1.93}O_{0.55}N_{0.26}$ (Stephanopoulos *et al.* 1998). With an elementary matrix $\mathbf{E}$ (given in Table (A.7)) the four elemental balances result in a system of linear equations given in Eq.(3.20). Except of NH_3 and H_2O all specific rates were experimentally determined and the system of linear equations was overdetermined. The redundancy of measurements was used to increase accuracy of the measurements by least squares calculation of best estimates $\hat{\mathbf{r}}_m$.

4.7.3. Stoichiometric metabolite balancing (MFA)

Stoichiometric metabolic flux analysis (MFA) was performed by metabolite balancing using best estimates of extracellular fluxes. A simplified stoichiometric model of central carbon metabolism of *E. coli* was adopted from Holms (2001) and Wiback *et al.* (2004). The model with 27 intracellular metabolites and 36 reactions is listed in Table (A.9). The growth flux was considered as a drain of 12 metabolites given in Table (A.12). The reactions are separated into 9 measured transport reactions (pts and exchange fluxes) and 27 intracellular reactions. The stoichiometric matrix of non-measured fluxes $\mathbf{N}_c$ is square and has full rank. The vector $\mathbf{v}_m$ of measured reaction rates is given in mmol g_{DW}^{-1} h^{-1}.

$$\mathbf{v}_m = (q_{CO_2}, q_{gluc}, q_{ac}, q_{suc}, q_{for}, q_{pyr}, q_{fum}, q_{akg}, q_{etoh})^T \tag{4.2}$$

Cellular growth is considered as a non-measured flux and the predictions of MFA were compared with the measured growth rate. Redox cofactors NADH and NADPH are lumped into one compound NAD(P)H. OUR is not included in the model, because energy metabolism is only considered by generation of 2 moles ATP from one mole NAD(P)H (similar stoichiometry as in the genome scale model *E. coli* K-12 *i*JR904), without any assumption about the P/O ratio. A further simplification is that the second transketolase reaction (tkt2) is not considered.

4.7.4. Flux Balance Analysis (FBA)

Compared to stoichiometric metabolite balancing Flux Balance Analysis (FBA) allows a more detailed analysis of cellular metabolism. The COBRA Toolbox for MATLAB (Becker *et al.* 2007) and the genome scale model *E. coli* K-12 (*i*JR904 GSM/GPR) of Reed *et al.* (2003) were employed for FBA. The objective function was cellular growth and substrate uptake was constrained to measured values (in mmol $g_{DW}^{-1}h^{-1}$). Predictions of cellular growth and respiratory rates ($\mathbf{r}_{FBA}$) were compared with the experiments. The reactions of central metabolism are compared to the simplified MFA model in Table (A.9). Biosynthetic demand according to *i*JR904 GSM/GPR is listed in Table (A.11).

4.7.5. Network-embedded thermodynamic (NET) analysis

The anNET tool for MATLAB (Zamboni *et al.* 2008) and the genome scale model *E. coli* *i*JR904 GSM/GPR (Reed *et al.* 2003) were employed for NET analysis. Measured metabolites were limited to 10% of the experimentally determined concentration. Minimal and maximal concentration limits of non-measured metabolites were set to 1 μM and 10 mM respectively. The energy charge was restricted to a range of 0.5-1 and the ratios NADH/NAD as well as NADPH/NADP were both limited to 0.001-0.2. Intracellular conditions were considered with a pH of 7.6 and an ionic strength of 0.15 M (Kümmel *et al.* 2007). Thermodynamic data was provided with the aNET software.

5. Results and Discussion

This section is subdivided into four principal parts. The first part describes findings associated with the measurement of intracellular metabolites. Subsequently, theoretical considerations clarify the requirements from steady state experiments. The new experimental strategy of rapid media transition is evaluated in the third section. Finally, the results of the metabolic control analysis of central carbon metabolism of *E. coli* in a fed-batch process are presented in the last part.

5.1. Measurements of intracellular metabolites

A critical evaluation of sampling protocols for metabolome analysis is necessary, because they are not standardized and errors may occur during each unit operation resulting in under- or overestimation of the true concentration *in vivo*. Whilst statistical errors are considered by methods like standard addition or isotope dilution mass spectrometry (IDMS), the influence of systematic errors is hardly quantified.

In the following, the focus is on leakage of ATP, ADP and AMP during quenching of *E. coli* cultures. Concentrations of adenylates are determined *in vivo*, in the quenching fluid and in the culture supernatant in order to quantify cellular leakage. Effects of buffers used with cold methanol quenching are investigated and the commonly applied methanol/water solution is compared with a methanol/glycerol mixture.

5.1.1. Screening of quenching fluids

Leakage of ATP was investigated in three kinds of quenching fluids:

- 60% (v/v) methanol/water
- 60% (v/v) methanol/water buffered with TEA or HEPES in two concentrations (10 mM and 70 mM)
- 60% (v/v) methanol/glycerol

Samples from an *E. coli* batch culture were quenched into the different quenching fluids. After centrifugation and sterile filtration of the quenching fluid supernatant, ATP was determined enzymaticaly (ATP determination kit, sensitive assay, Biaffin GmbH & Co

KG, Germany). In order to reduce effects of methanol on the enzymatic activity each sample was diluted 1:10 with de-ionized water. It is assumed that each sample contains the same amount of culture broth and the level of intracellular ATP was constant during time of sampling. The first assumption was verified by checking the total sample volume, that was 25 mL quenching fluid and 7.5 mL culture broth. The assumption of a constant intracellular ATP level is applicable, since all samples were taken in a short time interval during exponential growth. Figure (5.1) shows the concentration of ATP in the quenching fluid supernatant related to the amount of biomass in the sample. Error bars indicate the standard deviation of three enzymatic tests of the same sample.

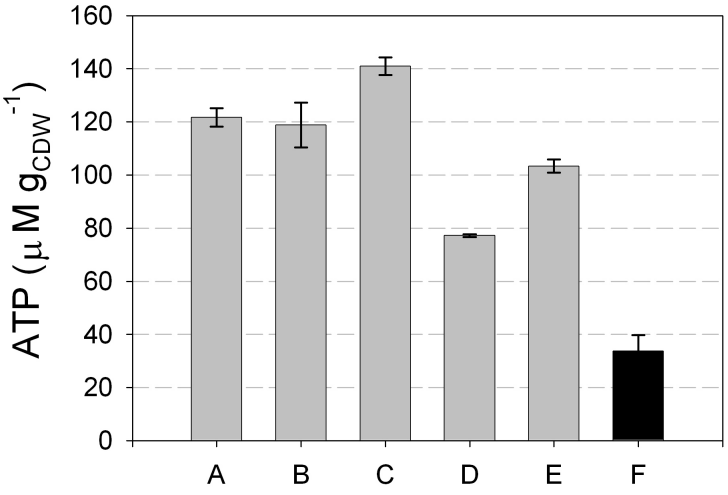

Figure 5.1.: Concentration of ATP in the supernatant of different quenching fluids after sampling, centrifugation and sterile filtration. (A) 60% (v/v) methanol/ water, (B) 60% (v/v) methanol/ water 10 mM TEA, (C) 60% (v/v) methanol/ water 10 mM HEPES, (D) 60% (v/v) methanol/ water 70 mM TEA, (E) 60% (v/v) methanol/ water 70 mM HEPES, (F) 60% (v/v) methanol/ glycerol.

ATP was present in the supernatant of all quenching fluids, whereas no ATP was detected in the culture supernatant (data not shown). Therefore, ATP in the quenching fluid is a result of leakage during sampling. Equal concentrations of ATP were present in the methanol solution (A) and the quenching fluids buffered with 10 mM of TEA (B) and HEPES (C). Lower concentrations of ATP are determined in the quenching fluids buffered with 70 mM TEA and HEPES (D and E). Taymaz-Nickerel *et al.* (2009) also noticed no significant reduction of cellular leakage if the quenching fluid was buffered (in their studies with 70 mM HEPES and 10 mM tricine). A considerable reduction of ATP leakage is observed in case of the methanol/glycerol buffer (F). As glycerol is known as protecting

agent also used for cryostocks it might have a stabilizing effect during quenching.

5.1.2. Leakage of adenylates in a glycerol based quenching fluid

Cellular leakage using a methanol/glycerol quenching fluid was quantified and compared to a methanol/water solution. The adenylates ATP, ADP and AMP were measured in the cell extract, the supernatant of the quenching fluid and of the culture broth during a fed-batch cultivation of *E. coli* using LC-MS. Sampling for metabolome analysis was performed two times during feeding phase 2 (20.75 h and 23.75 h, see Figure 4.1). Each time three types of samples were withdrawn:

1. 7.5 mL culture broth quenched into 25 mL of quenching fluid G: 60% (v/v) methanol/ water with 30 mM TEA
2. 7.5 mL culture broth quenched into 25 mL of quenching fluid H: 60% (v/v) methanol/ glycerol with 30 mM TEA
3. 15 mL culture broth (without quenching) for analysis of extracellular metabolites and biomass.

Samples at each process time are taken within less than one minute. Due to the controlled conditions in the bioreactor a metabolic steady state can be assumed and the biological variation between samples G and H can be neglected. Samples with quenching fluid G and quenching fluid H were prepared for analysis in parallel. For this reason differences between sample G and H resulting from sample processing can be excluded. OD_{660} and the size of cells was measured in triplicate for each sample. Figure (5.2) shows the specific cell volume, following from these measurements. Error bars result from error propagation of measured OD_{660} and size of cells.

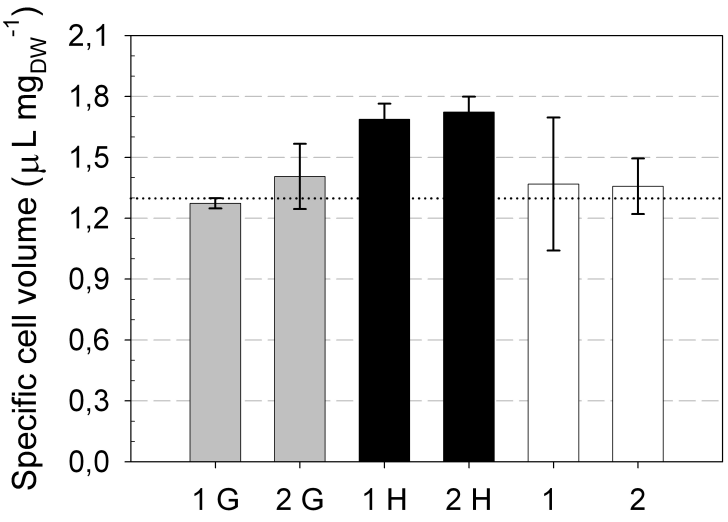

Figure 5.2.: Specific cell volume determined in the two direct samples (1, 2) and in the quenched samples using quenching fluid G and quenching fluid H (1 G, 2 G, 1 H and 2 H).

The specific cell volume is consistent for samples taken directly from the culture broth and the quenched samples using quenching fluids G (about 1.3 μL mg_{DW}^{-1}). The size of the cells determined in the glycerol based quenching fluid H is higher in both cases. This might be a result of glycerol interacting with the cell wall. In the following, intracellular concentrations are computed with a specific cell volume of 1.3 μL mg_{DW}^{-1}.

Intracellular concentrations of adenylates

In Figure (5.3) intracellular concentrations of adenylates are shown for sample 1 and 2. Results obtained with quenching fluid G (1G and 2G) are opposed to those of quenching fluid H (1H and 2H). Error bars indicate the 95% confidence interval obtained from the linear regression analysis of standard addition to one sample.

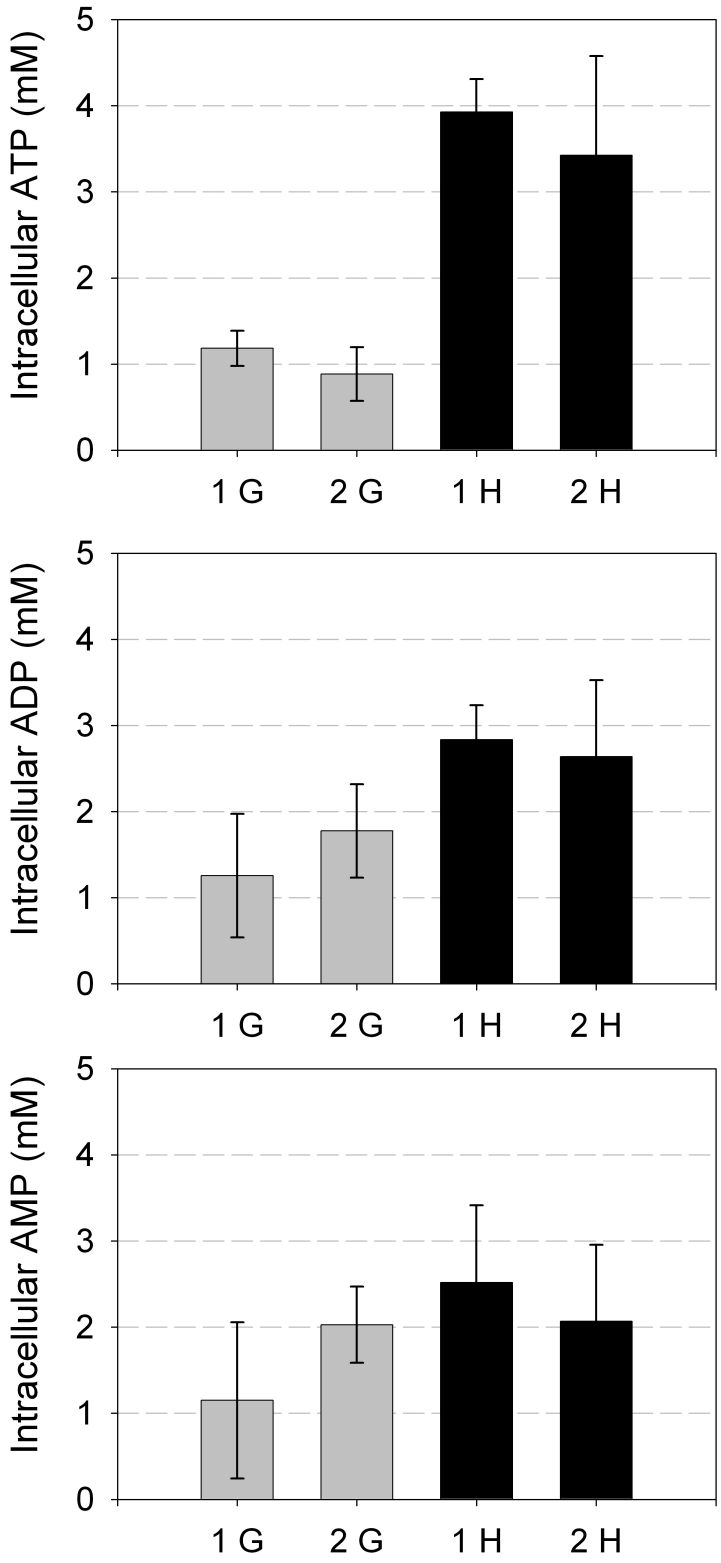

Figure 5.3.: Intracellular concentrations of adenylates. Samples were taken two times (1 and 2). Two different quenching fluids were used: 60% (v/v) methanol/ water with 30 mM TEA (G) and 60% (v/v) methanol/ glycerol with 30 mM TEA (H). Error bars indicate the 95% confidence interval obtained from the linear regression analysis of standard addition.

In all cases intracellular concentrations were higher if quenching fluid H was applied. Differences are most apparent for ATP and still significant for ADP, whereas almost equal concentrations of AMP are detected in the four samples. A metabolic steady state between the two sampling times can be assumed from a theoretical point of view (pseudo-steady-state hypothesis, Vallino and Stephanopoulos 1993). This assumption is clearly reflected in the constant concentrations of adenylates obtained with each method. Hence, the described sampling procedure proved to be robust against statistical errors. This is also reflected by the coefficient of correlation (R^2) of the linear regression obtained from standard addition, which was higher than 0.95 in all cases. However, the tremendous impact of systematic errors resulting from cellular leakage becomes obvious when the concentrations of ATP are compared for both quenching fluids.

Quantification of cellular leakage

Concentrations of ATP, ADP and AMP were also measured in the cultivation medium and the supernatant of the quenching fluid, in order to quantify the percentage of leaked metabolites. All concentrations in the supernatant of quenching fluid G were higher compared to quenching fluid H. In accordance with the results of measurements in the cell extracts, differences were most significant in case of ATP. Approximately 2 μM ATP was detected in both samples of the culture supernatant, coming very likely from cell lysis during cultivation. ADP and AMP were not detected in the culture supernatant.

Concentrations in the quenching fluid supernatant were first corrected for the amount in the culture supernatant and then related to the intracellular volume in the quenched sample (gray filled bars in Figure (5.4)). Together with intracellular concentrations determined from cell extracts the real intracellular pools were estimated, which are shown in Figure (5.4). Considering that the balances in Figure (5.4) involve several measurements, which are all subject to errors, the total values are in good agreement. The error bars are estimated from propagation of errors of concentrations in cell extracts, quenching fluid and medium. The error is highest in case of AMP in sample 1 G (approximately 75%) and smallest for ATP in sample 1 H (8%). Despite experimental error, it is remarkable that the percentage of leaked adenylates is almost constant for each metabolite using quenching fluid H. In general, leakage seems to be more specific than supposed so far (Bolten *et al.* 2007). In all cases, leakage is more apparent for ATP than for ADP and AMP. This might be an explanation why intracellular adenylates obtained by methanol quenching in other studies result in values of the energy charge (EC) which are not within physiological

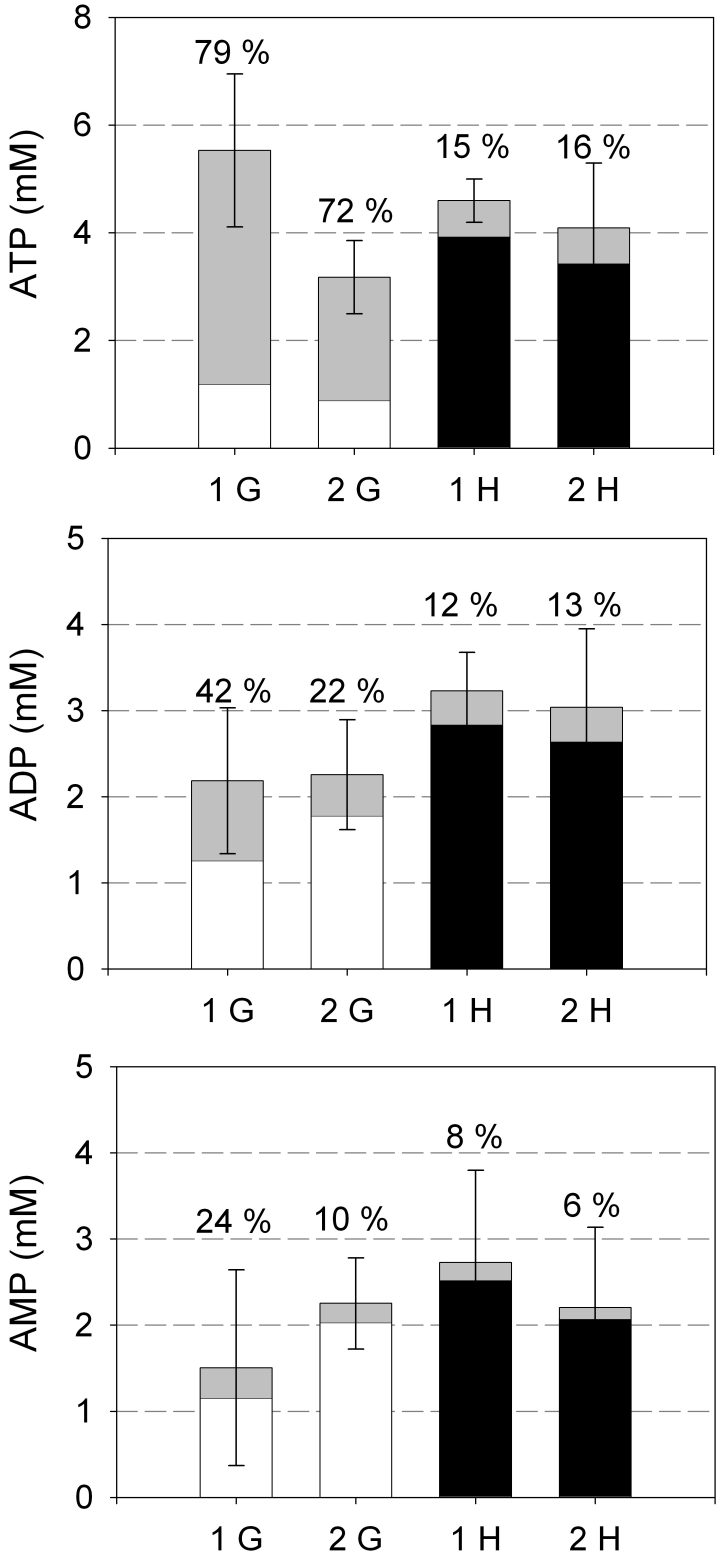

Figure 5.4.: Concentrations of adenylates in cell extract (blank and black bars) and in the supernatant of quenching fluid G and H (grey bars) are shown related to the intracellular volume. The percentage of leaked adenylates is additionally given.

meaningful ranges (e.g., Buchholz *et al.* 2001). The adenylates energy charge is defined as

$$\mathrm{EC} = \frac{(c_{ATP} + 0.5 \cdot c_{ADP})}{(c_{ATP} + c_{ADP} + c_{AMP})} \tag{5.1}$$

There would be no influence on the EC in case of unspecific leakage (e.g., 70 % loss of ATP, ADP and AMP). Using the corrected values of adenylates found in this study the EC is between 0.72 (quenching fluid H) and 0.59 (quenching fluid G).

5.1.3. Measurements with different sampling protocols

Currently there is no standardized method to quantify intracellular metabolite concentrations. Rather there are divers methods of sampling and extraction, each with its own advantages and draw-backs. The results above and other studies have demonstrated, that the applied sampling protocol has tremendous impact on the metabolome data. As a consequence, several sampling protocols were tested and applied in this work. Pure methanol quenching was less effective for *E. coli*, although the method prevents leakage in case of yeast (Canelas *et al.* 2008). Further, cold metabolite extraction with freeze-thaw cycles was applied in addition to hot extraction. With this method unstable metabolites like DHAP were detected in significant amounts. However, enzymes were not effectively deactivated with this approach. To keep track of the protocols, the results presented here were exclusively obtained with three protocols SP1, SP2 and SP3 as introduced above. General findings associated with the protocols are given in the following.

The method of standard addition (SP1)

Results obtained with protocol SP1 using standard addition are exemplified by means of the samples 1G, 2G, 1H and 2H of the previous section. Figure (5.5) shows the calibration curves for ATP and malate. The concentration of standard in the analyzed sample is plotted against the LS-MS signal. In case of ATP the calibration curves are linear and the regression analysis results in a high coefficient of correlation. The unknown concentration in the sample is estimated by the negative x-axis intercept of the regression line. This extrapolation is very sensitive to noise in the measurements. An order of magnitude estimate for the relative error of standard addition is 100%, given in the remarks of DIN 32633 (German Institute for Standardization). In case of malate the calibration curve is non-linear and the concentration in the sample is much lower than the applied

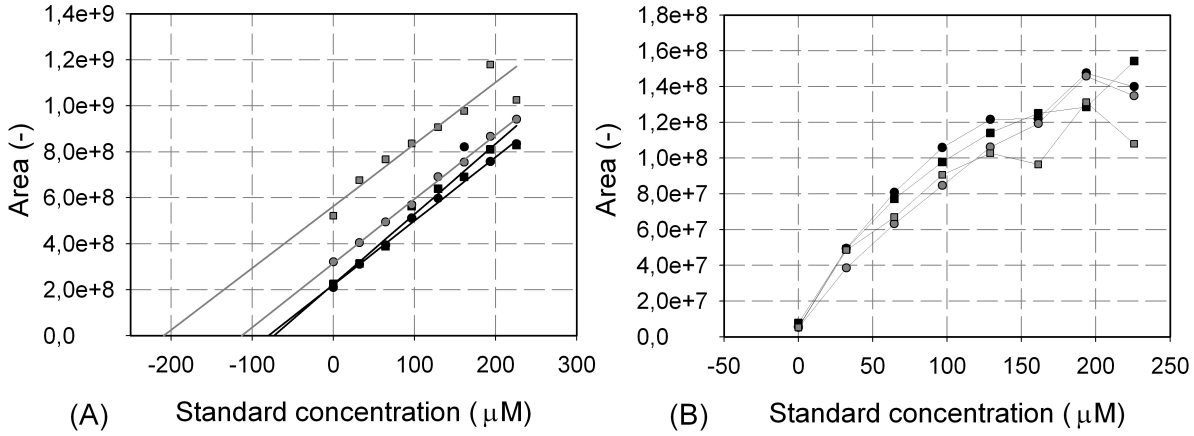

Figure 5.5.: Calibration with standard addition of ATP (A) and Malate (B). The LC-MS signal (peak area) is plotted against the concentration of standard in the samples.

standards. It is not possible to estimate the unknown concentration with sufficient accuracy in such cases. For other metabolites like PEP and pyruvate there was much noise, which additionally complicated evaluation of the standard addition (data not shown). In case of adenylates there was little noise and the applied standards were in appropriate concentration ranges. For this reason it was possible to estimate concentrations with the small 95% confidence intervals as shown in Figure (5.3). Hence, standard addition proved to be an adequate method for a targeted analysis, aiming for quantification of only a few metabolites. For global metabolome analysis the method is less appropriate.

External Calibration (SP2)

As a consequence of the high experimental error associated with the method of standard addition, a simplified protocol for extraction and analysis should reduce experimental error. Within sampling protocol SP2 lyophilization was omitted, smaller volumes were processed and an external calibration was applied. The reduced experimental effort minimized possible sources of error. Statistical errors were considered by three independent cell extracts of one sample. In order to account for thermal degradation and matrix effects the standard solution was mixed with culture broth and was processed according to sampling protocol SP2. The calibration curves obtained with this approach are shown in Figure (A.1) and (A.2). For most metabolites the LC-MS signal linearly correlates with the standard concentration in the lower ranges. However, with increasing concentration most calibration curves become non-linear. Nevertheless, with a few exceptions there is little noise in the calibration curves. Additionally, the results of measured intracellular

concentrations proved that SP2 is robust against statistical errors, as the standard deviation of three extracts of one sample was below 10% for most metabolites (data shown in section 5.3). In summary, measurements with SP2 have small statistical errors and therefore allow comparative studies of metabolite profiles. However, there are high systematic errors caused by non-linear calibration curves, cellular leakage and thermal degradation, which detract from conclusions about absolute metabolite concentrations.

The differential method and isotope dilution mass spectrometry (SP3)

The differential method proposed by Taymaz-Nickerel *et al.* (2009) requires measurements of metabolites in total culture broth and the cultivation supernatant. Accordingly, with sampling protocol SP3 the quenched sample is directly extracted without separating cells and thus avoids cellular leakage. In all cases metabolite concentrations were significantly higher compared to the other sampling protocols. The preferences of avoiding cellular leakage clearly exceeded the drawback of external metabolites interfering with the measurements. Metabolites were quantified with external calibration and also with IDMS.

IDMS considers thermal degradation of metabolites during extraction, matrix effects and ion supression during LC-MS analysis. A U-^{13}C labeled cell extract was prepared from *E.coli* cultivated in a mL system. LC-MS analysis showed that U-^{13}C enrichment was close to 1, as almost no signal of unlabeled metabolites was detected in cell extracts and the signal of U-^{13}C labeled metabolites was intense for all metabolites. The cell extract was calibrated as described by Wu *et al.* (2005) with an unlabeled standard solution. The calibration curves are shown in Figure (A.3). The concentration of unlabeled standard in the sample is plotted against the ratio of the signal of unlabeled and U-^{13}C labeled metabolites. The slope of each internal standard based calibration line equals the reciprocal of U-^{13}C labeled metabolite in labeled cell extract. Compared to external calibration the IDMS calibration curves are linear even for high concentrations of standards. Just in case of AcCoA the calibration curve is flattening and only the low concentration range was applied for calibration.

5.2. Theoretical aspects of steady state analysis

A steady state is typical for a metabolic pathway due to the concept of homoeostasis, where metabolite pools are kept at constant levels even though material is flowing through the system. MCA relates steady state properties of metabolic pathways to properties of its parts, the enzymatic reactions. The required operations and measurements for metabolic steady state analysis are discussed in the following.

5.2.1. Comparing the lin-log approach and the double modulation method

Giersch and Cornish-Bowden (1996) distinguish between a metabolite concentration x_i in context of a local rate law and the same metabolite concentration as a system variable (S_i), but they also point out the synonymy. The steady state flux J through an enzyme-catalyzed reaction embedded in a complex system must obey the kinetic rate law in Eq.(3.45), evaluated for the steady state concentrations $\mathbf{S}$. This relation is given by

$$J = v(e, \mathbf{x}, \mathbf{p})\big|_{\mathbf{x}=\mathbf{S}} \tag{5.2}$$

For this reason, a synonymous treatment of steady state flux J and the local rate v (as well as for x_i and S_i) is feasible in the following consideration. Differences between two metabolic states, resulting from changes in the *in vivo* system are explained by the total derivative of Eq.(5.2)

$$dv = \frac{\partial v}{\partial e}de + \sum_{i=1}^{n}\frac{\partial v}{\partial x_i}dx_i + \sum_{\ell=1}^{o}\frac{\partial v}{\partial p_\ell}dp_\ell \tag{5.3}$$

Assuming constant kinetic parameters ($dp_\ell = 0$) and rearranging Eq.(5.3) results in:

$$\frac{dv}{v} = \frac{\partial v}{\partial e}\frac{e}{v}\frac{de}{e} + \sum_{i=1}^{n}\frac{\partial v}{\partial x_i}\frac{x_i}{v}\frac{dx_i}{x_i} \tag{5.4}$$

Including the definition of elasticity coefficients in Eq.(3.52), the changes in fluxes are related to changes in metabolite concentrations by:

$$d\ln v = \varepsilon_e^v d\ln e + \varepsilon_{x_1}^v d\ln x_1 + \varepsilon_{x_2}^v d\ln x_2 + \cdots + \varepsilon_{x_n}^v d\ln x_n \tag{5.5}$$

Under the assumption that the reaction rate is linearly dependent on the enzyme level, the elasticity with respect to the enzyme level equals one ($\varepsilon_e^v = 1$). Rearranging Eq.(5.5) and approximating infinitesimal changes by measurable differences results in

$$\Delta \ln v - \Delta \ln e = \varepsilon_{x_1}^v \Delta \ln x_1 + \varepsilon_{x_2}^v \Delta \ln x_2 + \cdots + \varepsilon_{x_n}^v \Delta \ln x_n \tag{5.6}$$

In order to solve Eq.(5.6) for the n unknown elasticity coefficients, $k = n$ independent changes of fluxes and metabolite concentrations have to be measured:

$$\begin{aligned}
\Delta \ln v^1 - \Delta \ln e^1 &= \varepsilon_{x_1}^v \Delta \ln x_1^1 + \varepsilon_{x_2}^v \Delta \ln x_2^1 + \cdots + \varepsilon_{x_n}^v \Delta \ln x_n^1 \\
\Delta \ln v^2 - \Delta \ln e^2 &= \varepsilon_{x_1}^v \Delta \ln x_1^2 + \varepsilon_{x_2}^v \Delta \ln x_2^2 + \cdots + \varepsilon_{x_n}^v \Delta \ln x_n^2 \\
&\cdots \\
\Delta \ln v^k - \Delta \ln e^k &= \varepsilon_{x_1}^v \Delta \ln x_1^k + \varepsilon_{x_2}^v \Delta \ln x_2^k + \cdots + \varepsilon_{x_n}^v \Delta \ln x_n^k
\end{aligned} \tag{5.7}$$

The system of linear equations is written in matrix notation:

$$[\Delta \mathbf{ln}\ \mathbf{v}\ ] - [\Delta \mathbf{ln}\ \mathbf{e}\ ] = [\Delta \mathbf{ln}\ \mathbf{x}\ ][\boldsymbol{\varepsilon}_{\mathbf{x}}^v] \tag{5.8}$$

The changes of metabolite concentrations are collected in a $k \times n$ matrix [Δ**ln x**] , the k changes of fluxes in vector [Δ**ln v**], the k changes in enzyme levels in vector [Δ**ln e**] and the n unknown elasticity coefficients in vector $[\boldsymbol{\varepsilon}_{\mathbf{x}}^v]$.

In case of a constant enzyme level and $n = 2$ unknown elasticities, Eq.(5.8) corresponds to the double modulation method (Kacser and Burns 1979). For the case that $k > n$, a least squares solution of the system of linear equations is estimated by multiple linear regression as it is already proposed within the lin-log approach of Wu *et al.* (2004). Due to the similarities of the double modulation method and the multiple linear regression to Eq.(5.8), these terms are used equally in the following.

The measurable differences in Eq.(5.8) are estimated with regard to one reference state ($\Delta \ln x_i = \ln x_i - \ln x_{i,0} = \ln x_i / x_{i,0}$) and from Eq.(5.8) it follows

$$\left[\mathbf{ln}\frac{\mathbf{ve}_0}{\mathbf{ev}_0}\right] = \left[\mathbf{ln}\frac{\mathbf{x}}{\mathbf{x}_0}\right][\boldsymbol{\varepsilon}_x^v] \tag{5.9}$$

Eq.(5.9) implies a power-law format with constant elasticities (kinetic orders), whereas in a data set covering large concentration ranges elasticities depend on the particular reference state. The lin-log approach of Wu *et al.* (2004) considers the problem of variable elasticities. For this purpose, the lin-log rate law in Eq.(3.51) is rearranged

$$\left(\frac{v}{v_0}\frac{e_0}{e}\right) - 1 = [\boldsymbol{\varepsilon}_{\mathbf{x}}^{v}] \ln\left(\frac{\mathbf{x}}{\mathbf{x}_0}\right) \tag{5.10}$$

A data set of different metabolic states, comprising enzyme levels, fluxes, and metabolite concentrations leads to a system of linear equations similar to Eq.(5.9)

$$\left[\frac{\mathbf{v}\mathbf{e}_0}{\mathbf{e}\mathbf{v}_0}\right] - \mathbf{i} = \left[\mathbf{ln}\frac{\mathbf{x}}{\mathbf{x}_0}\right] [\boldsymbol{\varepsilon}_{x}^{v}] \tag{5.11}$$

with the unit vector $\mathbf{i}$ and the $k \times n$ matrix $[\mathbf{ln}\ \mathbf{x}/\mathbf{x}_0]$, derived from m metabolic states from which one is chosen as reference ($k = m - 1$). Within the lin-log approach the metabolic state with highest coefficient of correlation (R^2) of the linear regression is chosen as reference. Only the left-hand side of Eq.(5.9) and Eq.(5.11) is different (the dependent variables of the regression analysis), whereas the unknown parameters and the independent variables on the right-hand side are the same for the lin-log approach and the double modulation method.

5.2.2. Case study: Kinetic rate law of phosphoglucose isomerase (PGI)

This example considers an enzymatic reaction catalyzed by phosphoglucose isomerase (PGI) using a reversible Michaelis-Menten rate law and parameters described by Teusink *et al.* (2000).

$$v_{PGI} = v_{max} \cdot \frac{\dfrac{x_{G6P}}{K_{G6P}}\left(1 - \dfrac{\Gamma}{K_{eq}}\right)}{1 + \dfrac{x_{G6P}}{K_{G6P}} + \dfrac{x_{F6P}}{K_{F6P}}} \tag{5.12}$$

With v_{max} = 1.26 U mg protein^{-1}, K_{eq} = 0.314, K_{G6P} =1.4 mM, K_{F6P} = 0.3 mM and the mass action ratio $\Gamma = x_{F6P}/x_{G6P}$. Two metabolites, glucose-6-phosphate (G6P) and fructose-6-phosphate (F6P), influence the rate law in Eq.(5.12). Elasticities are derived by partial derivation.

$$\varepsilon_{G6P}^{PGI} = \frac{x_{G6P}}{v_{PGI}} \frac{\partial v_{PGI}}{\partial x_{G6P}} = 1 + \frac{x_{F6P}}{x_{G6P} K_{eq} \left(1 - \frac{\Gamma}{K_{eq}}\right)} - \frac{x_{G6P}}{K_{G6P} \left(1 + \frac{x_{G6P}}{K_{G6P}} + \frac{x_{F6P}}{K_{F6P}}\right)} \tag{5.13}$$

$$\varepsilon_{F6P}^{PGI} = \frac{x_{F6P}}{v_{PGI}} \frac{\partial v_{PGI}}{\partial x_{F6P}} = -\frac{x_{F6P}}{x_{G6P} K_{eq} \left(1 - \frac{\Gamma}{K_{eq}}\right)} - \frac{x_{F6P}}{K_{F6P} \left(1 + \frac{x_{G6P}}{K_{G6P}} + \frac{x_{F6P}}{K_{F6P}}\right)} \tag{5.14}$$

In order to obtain a data set concentrations of G6P and F6P are sampled from a small and a large concentration range as listed in Table (5.1). One data set comprises 10 randomly

Table 5.1.: Concentration ranges of G6P and F6P which are used to simulate data sets for the PGI case study.

Small concentration range	x_{G6P} (mM)	1.45 - 1.55
	x_{F6P} (mM)	1.45 - 1.55
Large concentration range	x_{G6P} (mM)	1 - 3
	x_{F6P} (mM)	1 - 3

sampled metabolite concentrations (x_{G6P}, x_{F6P}) and the PGI rate according to Eq.(5.12). White noise is simulated by adding normal distributed random numbers (standard deviation Δx_i=relative error $\cdot x_i$ and mean zero) to concentrations and fluxes. The elasticities ε_{G6P}^{PGI} and ε_{F6P}^{PGI} are estimated from the data set by multiple linear regression to Eq.(5.9) and Eq.(5.11) (MATLAB R2006b, Statistics Toolbox, The MathWorks Inc.). According to the lin-log approach the metabolic state with highest R^2 is chosen as reference state. For a performance evaluation of both approaches, elasticities are estimated 500 times from different data sets. In Figure (5.6) the results are opposed to the exact values (according to Eq.(5.13) and Eq.(5.14)) at the reference state of a particular data set.

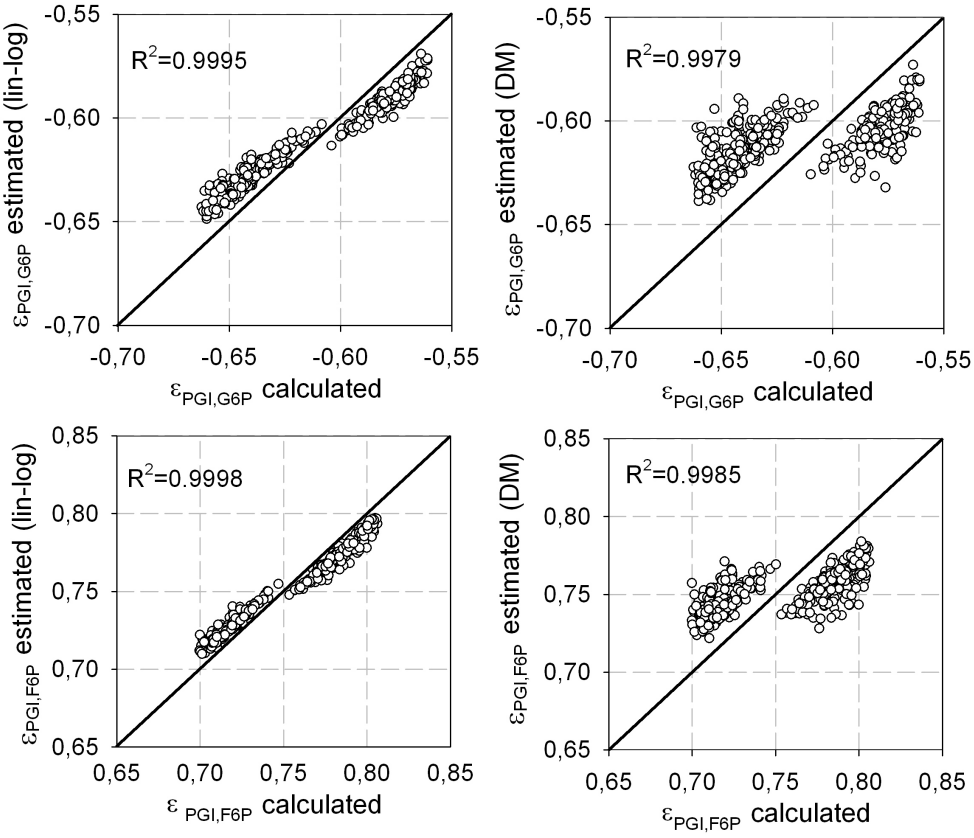

Figure 5.6.: Parity plots of elasticity coefficients computed from Eq.(5.13)/ Eq.(5.14) and estimated values from data sets comprising 10 metabolic states sampled from the small concentration range in Table (5.1). From each data set the metabolic state with highest R^2 is chosen as reference state. (lin-log) lin-log approach, (DM) double modulation method.

The parity plots in Figure (5.6) demonstrate the ability of the lin-log approach to account for changing metabolite levels and both elasticities are estimated with high accuracy. In case of the double modulation method the estimates deviate to a greater extend from the exact values. The 500 data sets, which are used to estimate elasticities in Figure (5.6), are sampled from the small concentration range in Table (5.1). In presence of already 5% relative error both methods fail to estimate elasticties with sufficient accuracy (results not shown). If the data is sampled from a larger concentration range the regression to Eq.(5.9) and Eq.(5.11) is less sensitive to experimental error. Figure (5.7) depicts the results in the case data is sampled from the large concentration range in Table (5.1).

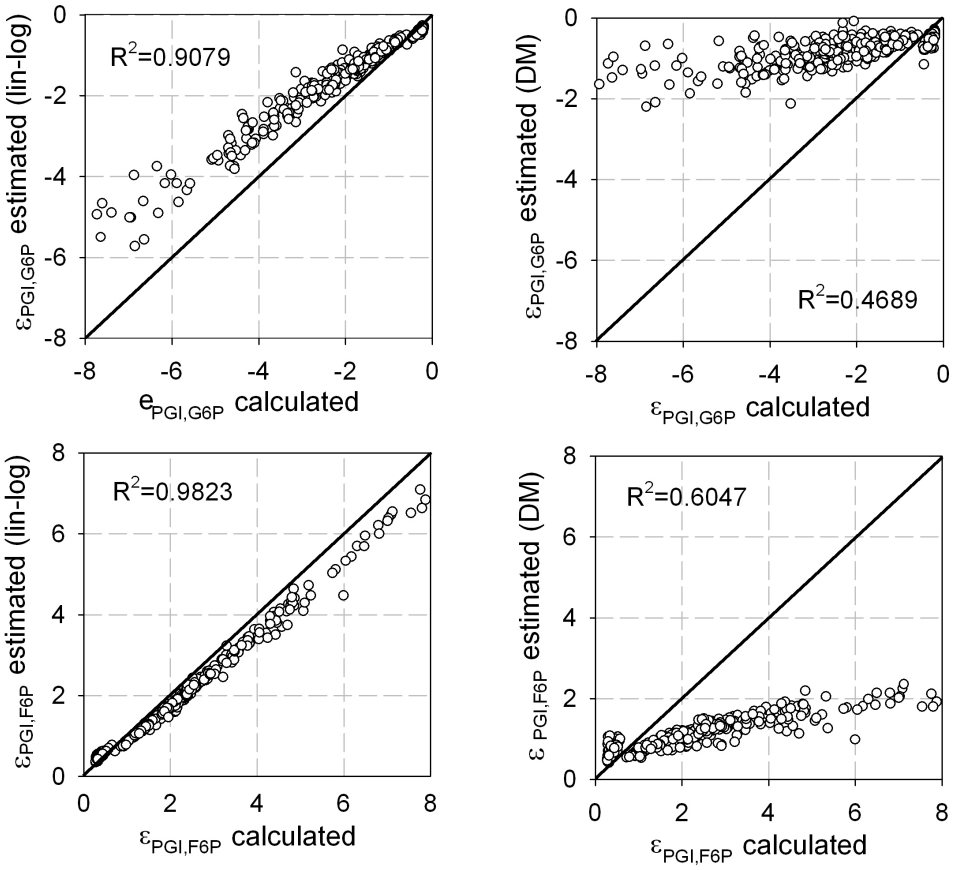

Figure 5.7.: Parity plots of elasticity coefficients computed from Eq.(5.13)/ Eq.(5.14) and estimated values from data sets comprising 10 metabolic states sampled from the large concentration range in Table (5.1). From each data set the metabolic state with highest R^2 is chosen as reference state. (lin-log) lin-log approach, (DM) double modulation method.

Elasticities in Figure (5.7) are distributed over a large interval and the results clarify that the lin-log approach even accounts for these large changes. As the double modulation method implies a power-law format elasticities are assumed to be constant over the whole concentration range. Therefore, estimated elasticities are restricted to a small area and do not correlate with the exact values. Although the correlation is much higher for the lin-log approach, the estimates deviate more from the exact values in case of larger elasticities. As this bias might be caused by the reference state, a new criterion for the selection of an optimal reference state is tested: the metabolic state with a minimal euclidian distance to the mean value of metabolite levels in the data set. In Figure (5.8) the results are shown for this criterion and data from the large concentration range.

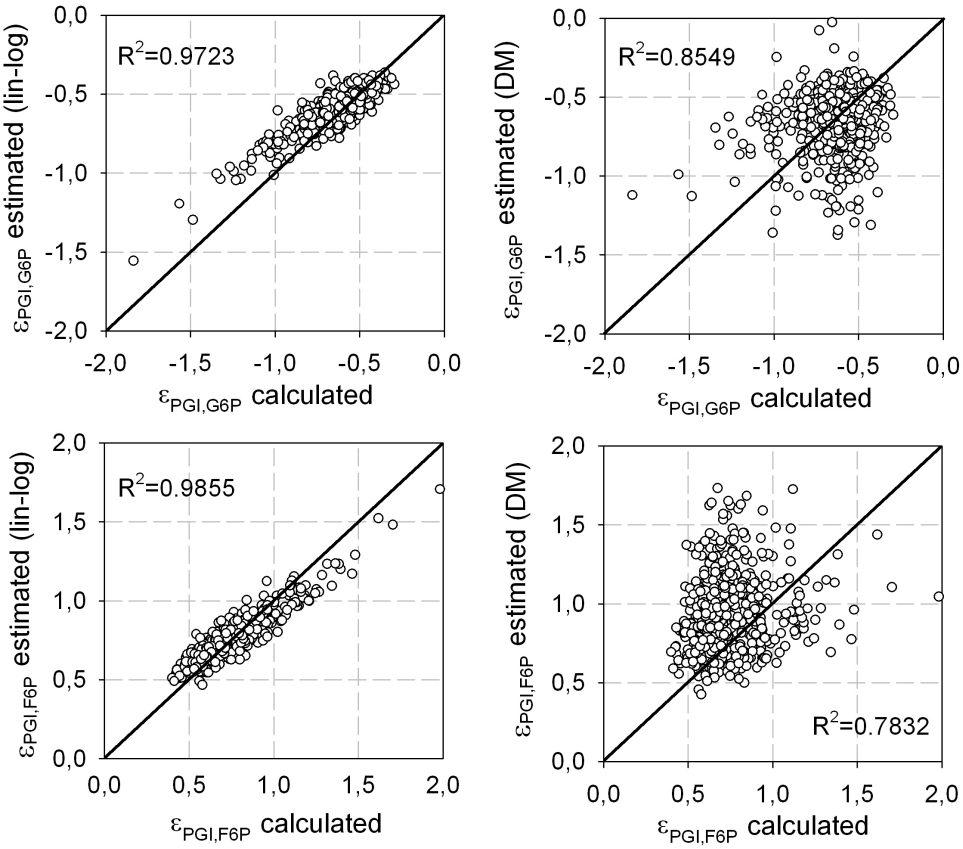

Figure 5.8.: Parity plot of elasticity coefficients computed from Eq.(5.13)/ Eq.(5.14) and estimated values from data sets comprising 10 metabolic states sampled from the large concentration range in Table (5.1). From each data set the metabolic state with central metabolite level is chosen as reference state. (lin-log) lin-log approach, (DM) double modulation method.

The effect of the new criterion is obvious when Figure (5.8) is compared to Figure (5.7). In all cases, the correlation between estimated and exact elasticity coefficients improves. Although the double modulation method benefits from the choice of reference the lin-log approach is obviously superior. The results of this case study demonstrate the misconception of assuming constant elasticities in a power-law format. Elasticities depend on the metabolite level. This must be considered in particular if large perturbation data is evaluated.

5.2.3. Case study: Reconstituted pathway of Giersch (1995)

Giersch (1995) applies the multiple modulation method to experimental data of an *in vitro* reconstituted pathway. The basic pathway is shown in Figure (5.9). Experimen-

tal conditions include additional components (not shown), such that concentrations of 3-phosphoglycerate (3PG) and pyruvate (PYR) can be considered as constant, while concentrations of 2,3-bisphosphoglycerate (BPG) and ADP can be changed independently. The flux through phosphoglycerate mutase (PGM), enolase (ENO) and pyruvate kinase (PK) is in a steady state as well as concentrations of 2-phosphoglycerate (2PG) and phosphoenolpyruvate (PEP). For an exact description the reader is referred to Giersch (1994) or Wu *et al.* (2004).

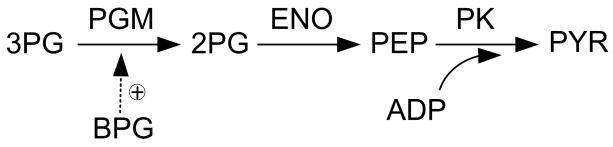

Figure 5.9.: The reconstituted pathway of Giersch (1995). BPG is a positive effector of PGM, indicated by the dashed arrow.

Wu *et al.* (2004) present the data set in Table (A.8), that was originally obtained by Giersch (1995). The data comprises enzyme and metabolite concentrations, as well as the steady state fluxes of the pathway in Figure (5.9). Elasticities are estimated by multiple linear regression of the data set to Eq.(5.9) and Eq.(5.11). It is assumed, that the three reactions are influenced by all metabolites (maximum connectivity). The metabolic states with highest R^2 are: metabolic state 2 for the lin-log approach and metabolic state 1 for the double modulation method. The metabolic state with metabolite levels near the center of the data set is metabolic state 11. Wu *et al.* (2004) demonstrate the quality of the estimated elasticities by means of parity plots, opposing measured steady state values (flux, 2PG and PEP concentrations) to values calculated from the lin-log model. For the lin-log formulation, the analytical solution of the steady state mass balances is described by Visser and Heijnen (2003). The analytical steady state solution of the power-law model is calculated according to Savageau (1969b). Figure (5.10) shows the parity plots of measured and calculated steady state values using both models. The elasticities with highest R^2 are used as model parameters.

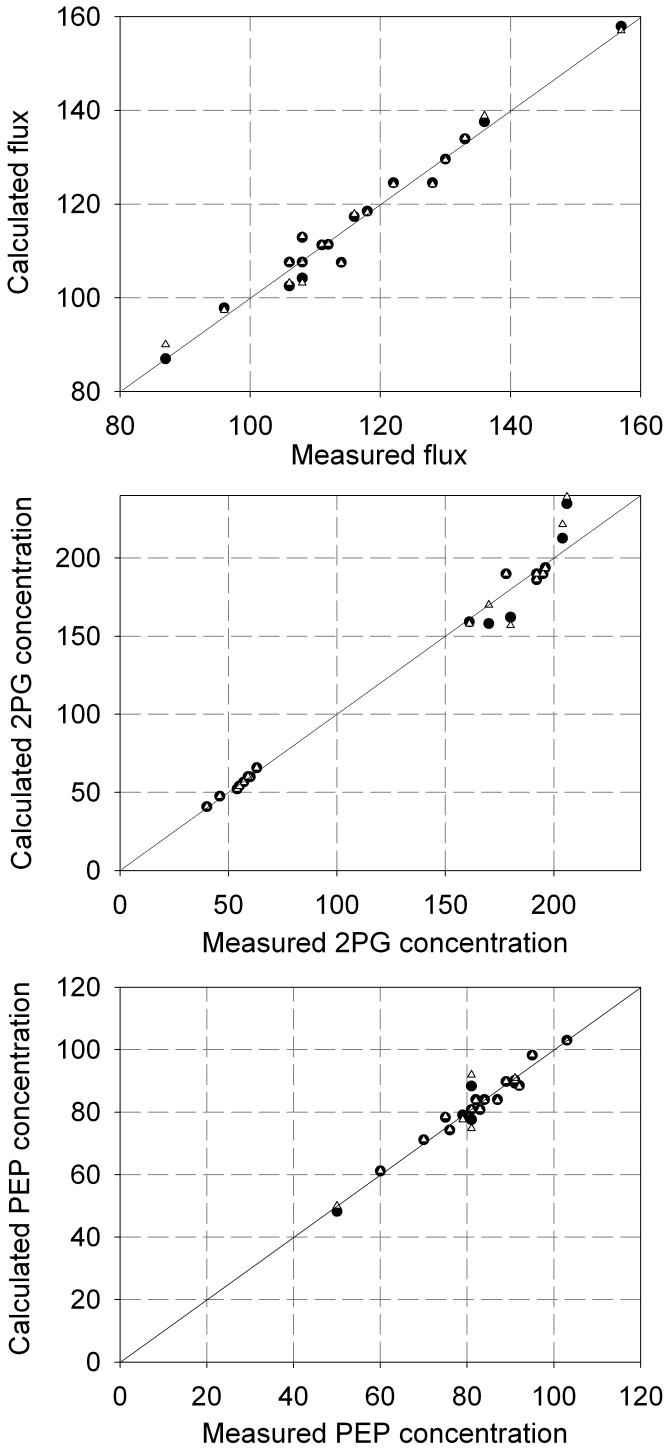

Figure 5.10.: Parity plots of measured and calculated steady state fluxes (in μmol L^{-1} h^{-1}), as well as 2PG and PEP steady state concentrations (in μmol L^{-1}) . The values are calculated by the analytical solution of mass balances using lin-log (filled circles) and power-law kinetics (diamonds). Elasticities at the reference state with highest R^2 are used as model parameters (lin-log: metabolic state 2; power-law: metabolic state 1).

Fluxes and metabolite concentrations calculated from both models are close to the measured values. Beside a slightly higher correlation in case of the lin-log model there are no noticeable differences. In order to further compare both approaches, elasticities are estimated for all metabolic states in Table (A.8). Figure (5.11) shows the distribution of the 19 elasticities by means of box plots. Elasticities for the metabolic state with highest R^2 and for the central metabolite level are additionally indicated in Figure (5.11).

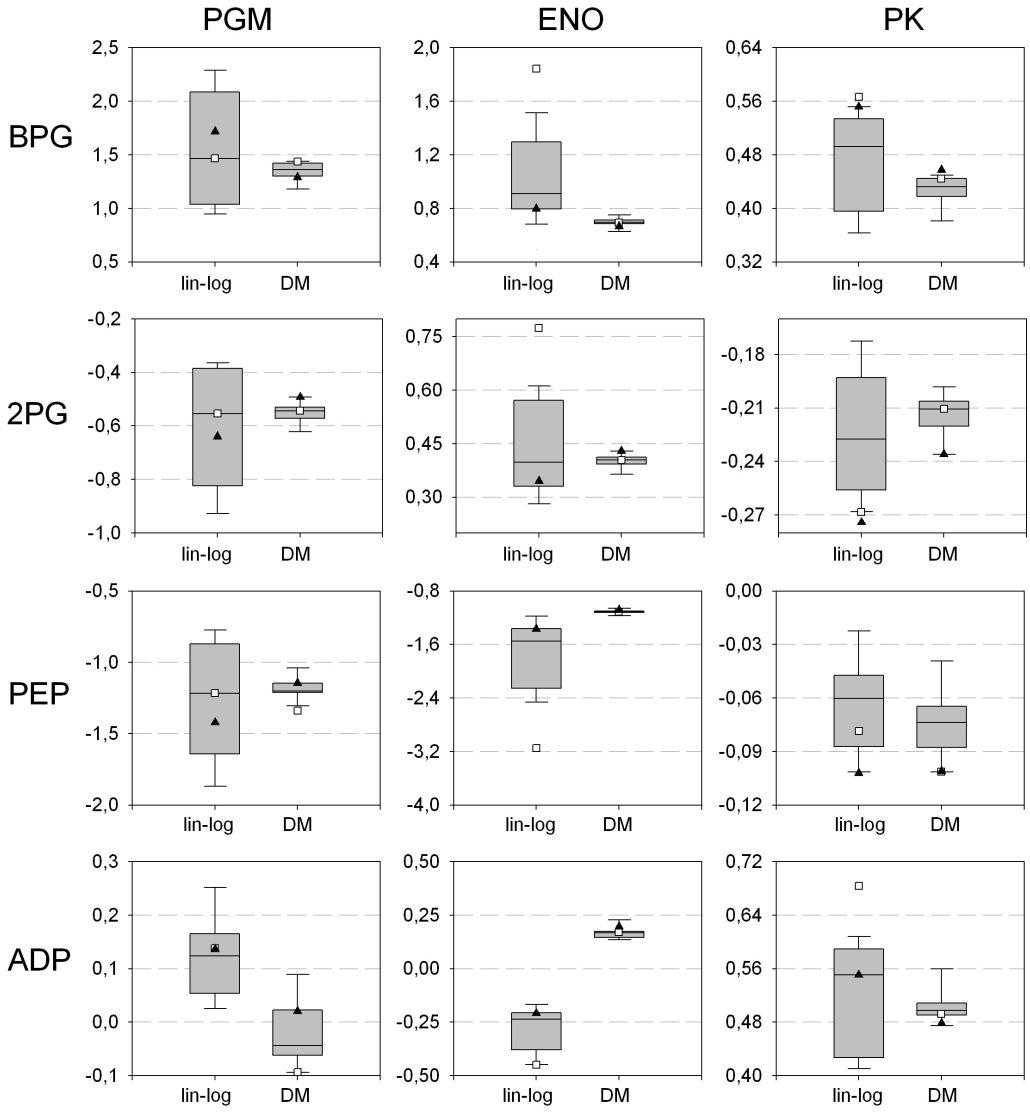

Figure 5.11.: Elasticities obtained from the data set in Table (A.8) using the lin-log approach (lin-log) and the double modulation method (DM). The distribution of the 19 estimates are shown by means of box plots (the boxes contain the middle of 50% of the data, the median is indicated, whiskers above and below the box indicate the 10th and 90th percentiles). Individual elasticities are shown for the reference state with highest R^2 (squares) and for the state with central metabolite levels (filled triangles). Figures in columns refer to elasticities with respect to the indicated reaction and figures in rows to the particular metabolite.

All elasticities that follow from the lin-log approach are distributed over a larger interval than those estimated with the double modulation method. Irrespective of the reference state the double modulation method estimates values near the median (including elasticities of metabolic state 1 and 11). In case of the lin-log approach it is worth to examine elasticities at the optimal reference state. Elasticities of PGM are inside the boxes in case of both reference criteria. Elasticities of ENO are out of the 10th and 90th percentiles if the R^2 criterion is applied, whereas elasticities at the central metabolite level are located within the boxes. In contrast, the elasticities of PK with respect to BPG, 2PG, and PEP are out of the 10th and 90th percentiles for the central metabolite level. However, compared to PGM and ENO, elasticities of PK are distributed over a smaller range and therefore the choice of reference should be less important. Especially in case of ENO the elasticities change over large intervals and estimates using the R^2 criterion are located at the rim. As demonstrated in Figure (5.7) such values might be biased. Elasticities at the central metabolite level are located near the median, improving the estimates.

5.2.4. Conclusions from theoretical considerations

After the *in silico* studies about steady state analysis the question remains, how experimental data of steady states can be obtained in an *in vivo* system. Since the double modulation method was introduced by Kacser and Burns (1979) many extensions and modifications were developed, most of them accounting for the networks structure and applying specific changes in one enzyme activity. However, the reconstituted pathway of Giersch (1995) already showed their experimental limitations: inducing small and specific changes is practically not feasible in most cases (especially not in an *in vivo* system). The original approach of Kacser and Burns (1979) considers the possibility of inducing metabolic states via external conditions such as substrate availability acting non-specific on the metabolic pathway. Especially for pathways, that are highly regulated on a metabolic level, e.g. the central carbon metabolism, it will be possible to induce different metabolic states via the fermentation media composition (e.g. addition of precursors and/or mixed carbon sources). The non-specific changes will result in large changes of metabolite levels and metabolic fluxes which can be analysed with the presented aproaches by linear regression. Even both methods account for multiple changes in enzyme levels it is difficult to quantify these changes, due to limitations of current methods like 2D gel-electrophoresis.

5.3. Steady state experiments with *E. coli* during a fed-batch cultivation

A prerequisite for steady state analysis of an industrial bioprocess is that the relevant phase of the process admits the assumption of a quasi steady state for the pathway of interest. This is the case for every phase with constant specific rates of fluxes that are connected to the pathway. The bioprocess is considered as the reference state and multiple metabolic perturbations are required for steady state analysis. The experimental approach of rapid media transition (RMT) was developed in order to expose cells from the bioprocess to divers environmental disturbances. The method tends to provide constant enzyme levels, due to the different time scales of enzyme synthesis and metabolic turnover. Several demands were made on the RMT experiments:

- a fast attainment of a metabolic steady state
- the steady state is significantly perturbed from the reference state
- the enzyme levels are constant

The approach was evaluated by means of *E. coli*'s central metabolism under conditions of a fed-batch cultivation, which is detailed in the following.

5.3.1. Fed-Batch cultivation of *E. coli*

A fed-batch cultivation of *E. coli* K12 was chosen as reference state for steady state perturbation experiments. An open-loop control of biomass formation assured high reproducibility of the process. In Figure (5.12 A) biomass concentrations measured during several cultivations is opposed to theoretical growth, following from a dynamic model. Additionally, OUR and CPR, as well as the DO signal during a fed-batch cultivation are depicted in Figure (5.12 B, C).

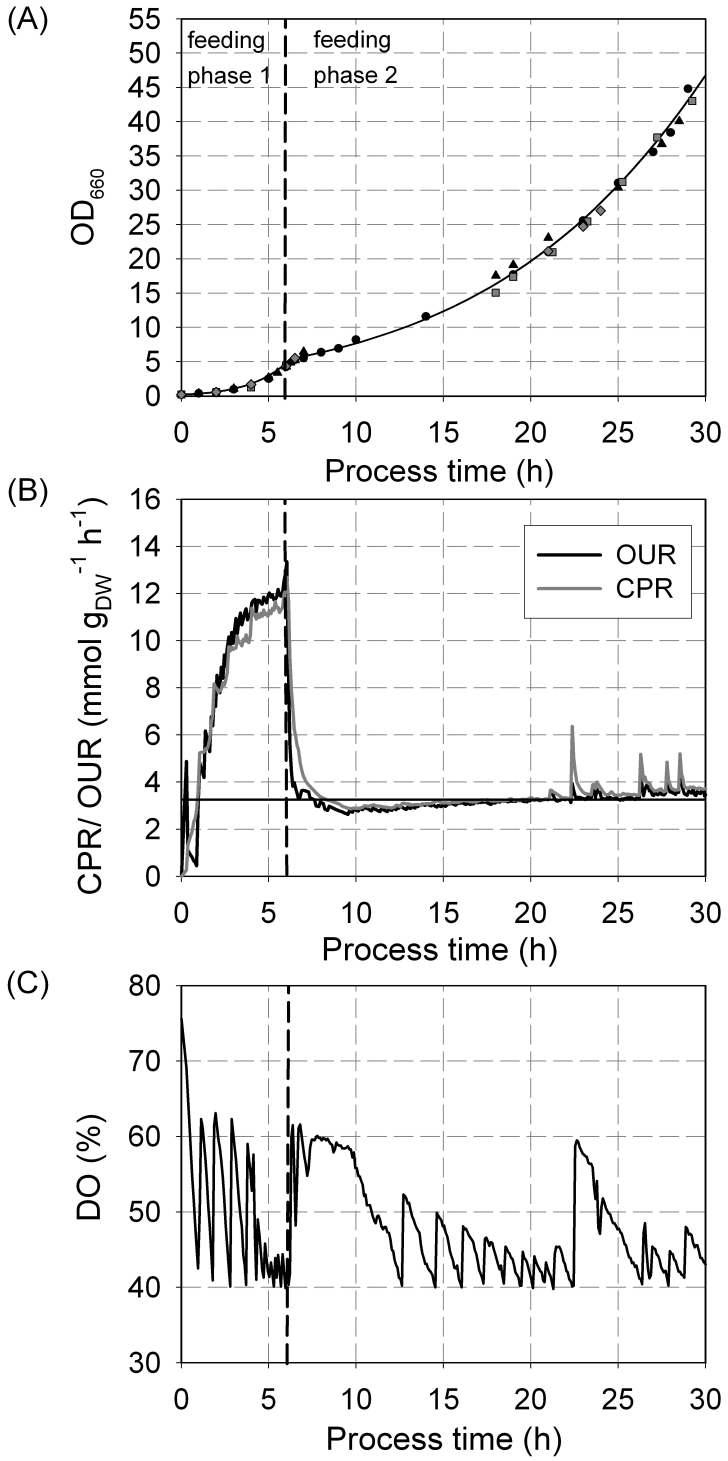

Figure 5.12.: Measured state variables during the *E. coli* fed-batch process. (A) Cellular growth predicted by the dynamic model (solid line) and measured optical densities (symbols refer to four different cultivations). (B) Oxygen uptake rate (OUR) and carbon dioxide production rate (CPR). (C) Dissolved oxyen (DO).

The theoretical biomass formation predicted by the dynamic model agrees well with measured biomass concentrations in four independent cultivations. Due to the open-loop control, specific substrate uptake and growth rate were fixed to constant values. Further, the process was robust against variations in parameters like the initial biomass concentration.

When the feeding rate was reduced after feeding phase 1, OUR and CPR immediately decreased and both reached 3 mmol g_{DW}^{-1} h^{-1}. Respiratory rates were almost constant during feeding phase 2 and increased only slightly. Peaks in OUR and CPR signals after 20 h result from a stepwise increase of the aeration rate. DO was controlled above 40 % by increasing stirrer speed and aeration.

The culture was glucose limited all the time and glucose as well as acetate were not detected in samples of the culture supernatant. With $dc_s/dt = 0$, $\mu_{set} = 0.1$ h^{-1} and $Y_{x,s} = 0.45$ g g^{-1}, specific glucose uptake rate during feeding phase 2 is estimated as 1.23 mmol g_{DW}^{-1} h^{-1}. OUR and CPR are approximately 3.2 mmol g_{DW}^{-1} h^{-1} and a relative error of 10% is assumed. Table (5.2) opposes these extracellular fluxes during the fed-batch process with best estimates resulting from elemental balances and FBA predictions.

Table 5.2.: Specific rates during the fed-batch process, given in mmol g_{DW}^{-1} h^{-1}. The specific growth rate is given in h^{-1}. Measured rates (r_m), best estimates ($\hat{r}_m$) and FBA predictions (r_{FBA}) are compared. The sum of weighted squares of residuals h is given in the last row.

Compound	r_m	$\hat{r}_m$	r_{FBA}
Glucose	1.23 ± 0.12	1.21	1.21[a]
O_2	3.2 ± 0.32	3.18	3.91
CO_2	3.2 ± 0.32	3.26	3.75
Biomass	0.10 ± 0.02	0.10	0.08
NH_3	-	0.99	0.86
h		0.135	

[a] FBA constraint

The measured rates are close to the best estimates, which conform to elemental balances of carbon, hydrogen, nitrogen and oxygen. Therefore, the extracellular rates in Table (5.2) contain no gross measurement errors and sufficiently describe reactions on the bioreactor level during feeding phase 2. Non-measured fluxes such as uptake of ammonia follow from Eq.(3.23). The predicted rates of FBA are given in the last column of Table (5.2). These rates depend only on information about glucose uptake, which was constrained to a maximal value of 1.21 mmol g_{DW}^{-1} h^{-1}. Even if the predicted growth rate is smaller and as a consequence CPR and OUR are higher than measured values, the differences are not greater than 20%. Uptake of ammonia is close to the value that was estimated by elemental balances.

Beside extracellular fluxes, FBA predicts values of all intercellular fluxes in the genome-scale model. In addition, stoichiometric MFA was used to estimate fluxes of central carbon metabolism. The results of both approaches are compared in Figure (5.13).

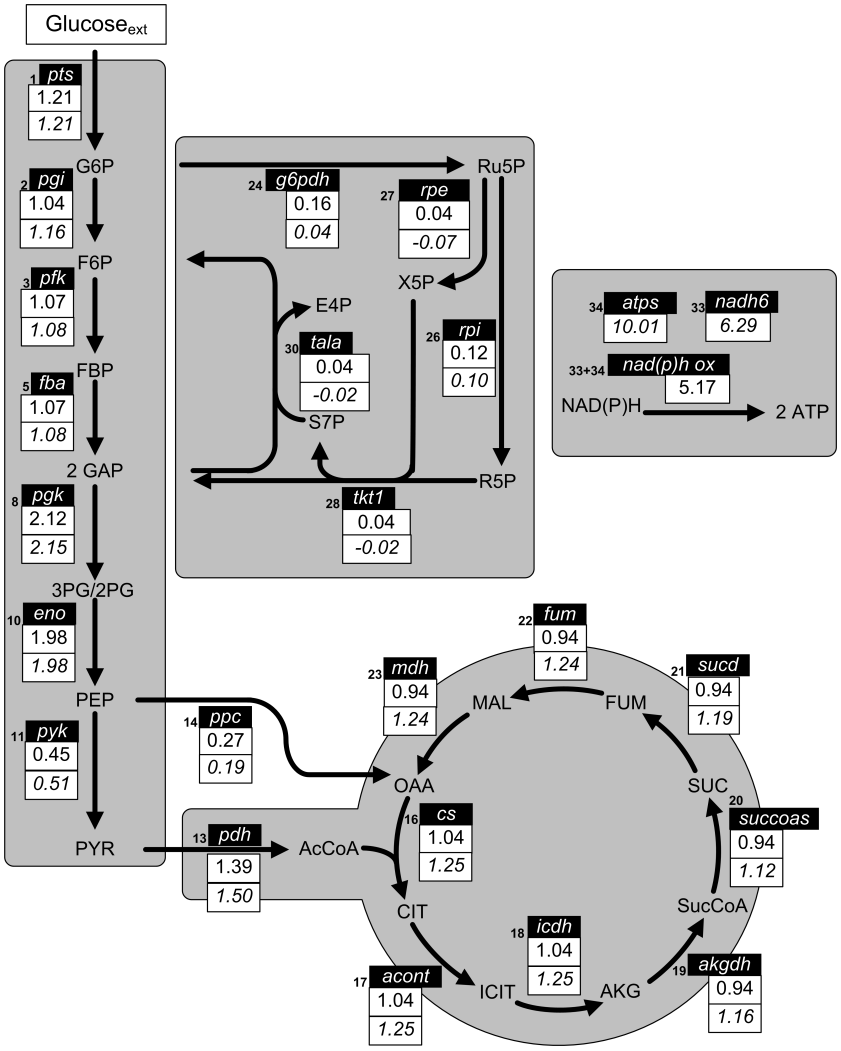

Figure 5.13.: Metabolic fluxes in central carbon metabolism during feeding phase 2 of the fed-batch process. Fluxes in mmol g_{DW}^{-1} h^{-1} were determined by stoichiometric metabolite balancing (upper boxes, normal letters) and by FBA (lower boxes, italic letters).

Both, FBA and MFA estimate similar values for glycolytic fluxes, TCA flux and also the anapleurotic ppc flux. Using MFA, the flux into PPP is approximately 13% of glucose uptake, opposed to only 3% using FBA. Different results about contribution of PPP to glucose metabolism are reported in literature.

Chassagnole *et al.* (2002) found that 70% of glucose is metabolized through PPP in an *E. coli* chemostat culture using MFA. Fischer and Sauer (2003a) estimated a ratio of 14-20% in *E. coli* batch cultures based on 1-^{13}C and U-^{13}C glucose experiments. A split ratio of 55% glycolysis and 44% PPP was estimated with dynamic and stationary U-^{13}C glucose experiments (Schaub *et al.* 2008). In addition to uncertainties about the oxidative part of PPP, FBA predicts negative fluxes in the non-oxidative part of the PPP. More reliable

information about PPP fluxes and NADPH metabolism is only feasible with ^{13}C labeling experiments, as shown by Sauer *et al.* (2004).

The flux into TCA is estimated as 86-100% of glucose uptake and FBA predicts a zero flux through the glyoxylate shunt (not shown in Figure (5.13)), which was not considered for stoichiometric MFA. Similarly, Schaub *et al.* (2008) estimated a TCA flux of 72-73% and did not consider glyoxylate shunt in their analysis. However, Fischer and Sauer (2003b) demonstrate the activity of a novel bi-functional PEP-glyoxylate cycle that operates in parallel to TCA cycle, which does involve enzymes of glyoxylate shunt. TCA fluxes in this study differ drastically from the distribution in Figure (5.13) and thereby point out the shortcoming of FBA and MFA: both approaches are strongly based on assumptions and not on data (Sauer 2006).

Even if oxidative phosphorylation is considered by a composite reaction in the MFA model, FBA predictions for ATP synthesis (atps) and NADH oxidoreductase (nadh6) agree well with MFA estimates for NAD(P)H oxidation (notice that only 1 mole ATP is produced by atps).

5.3.2. Rapid media transition in batch operation mode

The four RMT experiments in batch mode were performed with different carbon sources: glucose (gl), succinate (suc), acetate (ac) and pyruvate (pyr). Cells were harvested repeatedly from the fed-batch process during feeding phase 2 (gl: 20 h, pyr: 22 h; suc: 24 h; ac: 26 h) and transferred to a lab-scale stirred-tank reactor with fresh medium. Subsequently, the reaction of the cells to the different carbon sources was observed by measurements of extracellular fluxes and intracellular metabolite concentrations. OUR and CPR during the RMT experiments are shown in Figure (5.14).

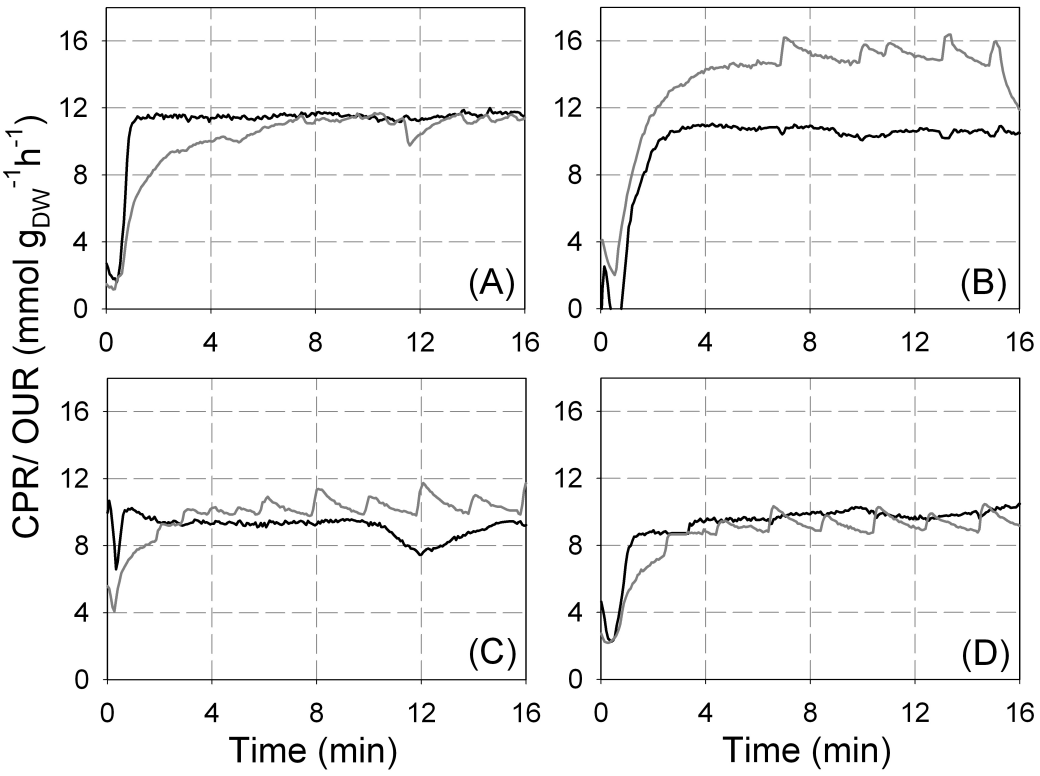

Figure 5.14.: Specific O_2 uptake rate (OUR; black lines) and the specific CO_2 production rate (CPR; grey lines) during RMT experiments with different substrates: (A) glucose, (B) pyruvate, (C) succinate and (D) acetate.

Within a few minutes OUR and CPR reached a constant value which was maintained during the analyses. Oscillations in case of CPR were caused by the pH depending equilibrium of carbonic acid in the medium. The characteristics in Figure (5.14) indicate pseudo stationary fluxes and steady state values for OUR and CPR are estimated from the mean during the last 8 minutes. The measurements of cell dry weight are depicted in Figure (5.15).

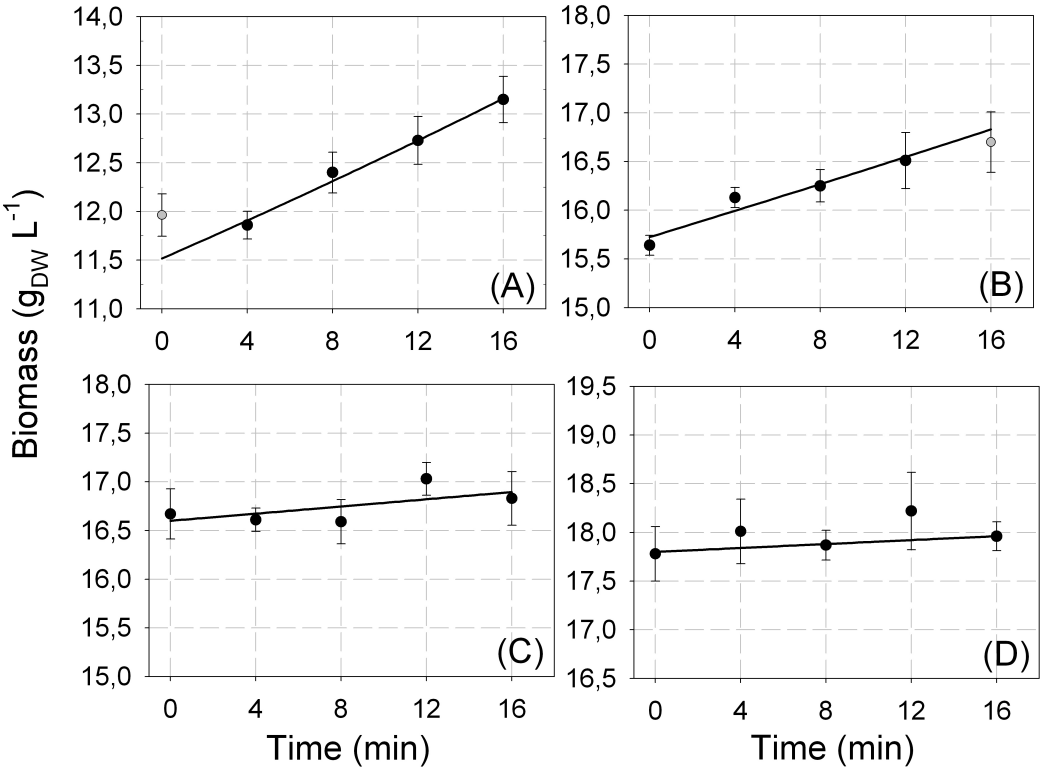

Figure 5.15.: Biomass concentration during RMT experiments with different substrates: (A) glucose, (B) pyruvate, (C) succinate and (D) acetate. Grey circles indicate measurements not used for logarithmic regression (black lines).

Biomass increased more than 1 g L^{-1} during the 16 minutes cultivation with glucose and pyruvate. During the first 4 minutes there was no growth on glucose and the first DW measurement is not used for regression analysis. With succinate and acetate there was almost no cellular growth and the small growth rates are hardly assessable. The results agree with the order of growth rate reported for *E. coli* in minimal medium (Chao *et al.* 1993). The corresponding concentrations of carbon sources are shown in Figure (5.16).

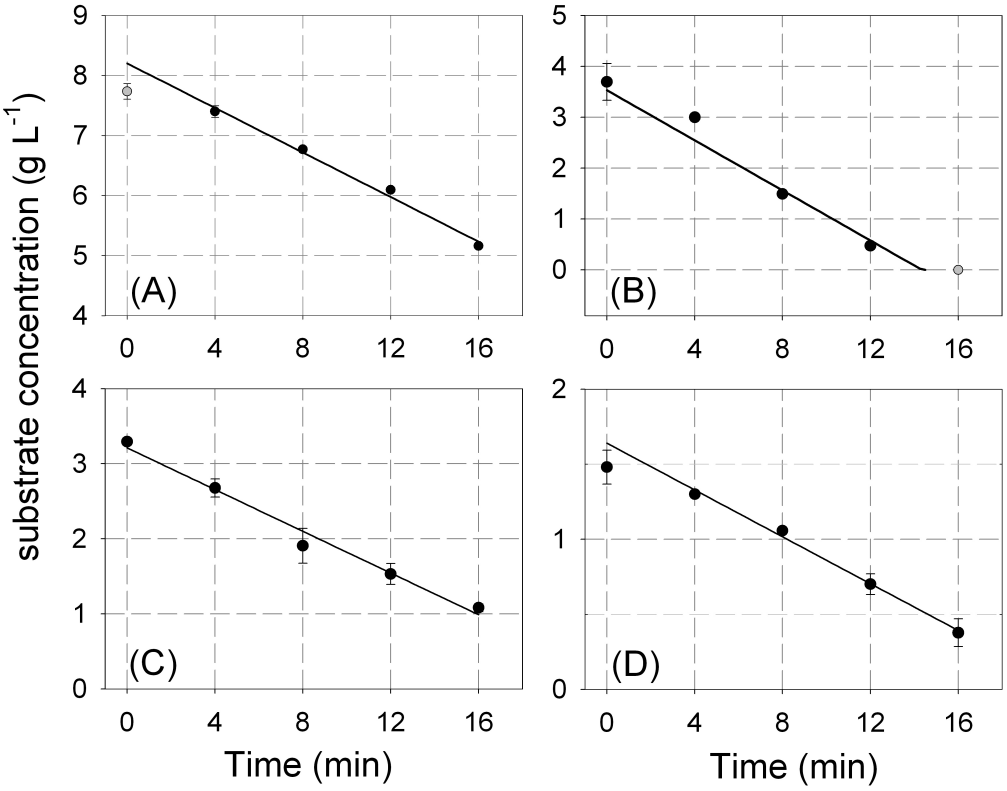

Figure 5.16.: Substrate concentrations during RMT experiments: (A) glucose, (B) pyruvate, (C) succinate and (D) acetate. Grey circles indicate measurements not used for regression analysis.

All carbon sources were immediately utilized by the cells and all substrate concentrations are continuously decreasing. The specific uptake rate of substrates was estimated by linear regression to Eq.(3.12) as indicated in Figure (5.16). The by-products acetate and formate were excreted during analyses with glucose and pyruvate. In the culture supernatant of the experiment with succinate the metabolites fumarate and α-ketoglutarate were detected. A constant increase of by-products was observed in all cases and specific production rates were estimated by linear regression. Table (5.3) summarizes the estimates of extracellular fluxes during the four perturbation experiments. The relative error of OUR and CPR was estimated as 10%. The errors of the remaining rates follow from the regression analysis. Best estimates, FBA predictions and the sum of weighted squares of residuals h are also given in Table (5.3).

As there are only small differences between original rates and the best estimates the measurements contain no gross errors. Additionally, the small values of the residuals h confirm the quality of the data. By-product formation was not predicted by FBA, as

Table 5.3.: Specific rates during the four RMT experiments on glucose, pyruvate, succinate and acetate, given in mmol g_{DW}^{-1} h^{-1}. The specific growth rate growth rate is given in h^{-1}. Measured rates (r_m), best estimates ($\hat{r}_m$) and FBA predictions (r_{FBA}) are compared. The sum of weighted squares of residuals h is given in the last row.

	Glucose			Pyruvate		
	r_m	$\hat{r}_m$	r_{FBA}	r_m	$\hat{r}_m$	r_{FBA}
Substrate	4.99 ± 0.69	5.45	5.45[(a)]	10.32 ± 1.80	9.89	9.89[(a)]
O_2	11.50 ± 1.15	11.38	10.67	10.53 ± 1.05	10.48	9.20
CO_2	11.20 ± 1.12	11.13	10.97	15.17 ± 1.52	15.35	14.40
Acetate	0.73 ± 0.10	0.74	0.74[(a)]	1.96 ± 0.16	1.97	1.97[(a)]
Formate	1.27 ± 0.27	1.25	1.25[(a)]	0.52 ± 0.05	0.53	0.53[(a)]
Biomass	0.50 ± 0.04	0.49	0.46	0.25 ± 0.05	0.26	0.26
h	0.538			0.077		

[(a)]FBA constraint

	Succinate			Acetate		
	r_m	$\hat{r}_m$	r_{FBA}	r_m	$\hat{r}_m$	r_{FBA}
Substrate	4.26 ± 0.34	4.09	4.09[(a)]	4.34 ± 0.23	4.50	4.50[(a)]
O_2	8.85 ± 0.88	9.05	7.11	9.87 ± 0.99	9.00	9.00
CO_2	10.63 ± 1.06	10.80	9.07	9.34 ± 0.93	9.00	9.00
Fumarate	0.17 ± 0.02	0.17	0.17[(a)]	-	-	-
AKG	0.20 ± 0.02	0.20	0.20[(a)]	-	-	-
Biomass	0.07 ± 0.05	0.10	0.14	0.03 ± 0.04	0.00	0.00
h	0.918			2.081		

[(a)]FBA constraint

it is not optimal with regard to maximized cellular growth. Therefore, exchange fluxes of by-products were constrained to minimum values as given in Table (5.3). With these constraints predictions of cellular growth as well as respiratory rates are close to measured values.

Initially, FBA predicted significant growth on acetate ($\mu = 0.2$ h^{-1}) and much lower CPR (6 mmol g_{DW}^{-1} h^{-1}) than observed in the experiment. The glyoxylate bypass is essential for growth on acetate since it prevents the loss of the carbon as carbon dioxide in the TCA cycle. Hence, activity of the glyoxylate bypass is predicted by FBA for the short-term cultivation with acetate. However, it is reported that the glyoxylate cycle is not active in glucose-limited chemostat cultures of *E. coli* (Yang *et al.* 2003, Hua *et al.* 2003). Deletion

of isocitrate lyase from the genome-scale model resulted in the values given in Table (5.3) and acetate carbon is completely metabolized to CO_2 without biomass formation. Hence, the rapid media transition experiment on acetate in combination with FBA gives evidence about a non-active glyoxylate bypass in the fed-batch process. In contrast, MFA allows no conclusions about the activity of the glyoxylate bypass.

Generally, the results demonstrate that *E. coli* utilizes the applied carbon sources immediately and extracellular fluxes are constant a few minutes after the cells are exposed to the new carbon source. Wu *et al.* (2006) made similar observations after a glucose pulse to an aerobic glucose-limited *S. cerevisae* chemostat culture, as a quasi steady state had been established after 150-300 seconds.

The immediate uptake of a substrate implies that the particular uptake systems and the required catabolic enzymes are available. Uptake of pyruvate and acetate will be an unspecific diffusion mechanism, whereas the dicarboxylic acid succinate requires an active transporter. It is reported that there is only the DctA dicarboxylic acid transporter in *E. coli* which is responsible for the uptake of succinate (Lo 1977). The DctA dicarboxylic acid transporter and other enzymes such as acetyl-CoA synthetase (acs) required for acetate utilization are subject to catabolite repression. Hence, the immediate utilization of succinate and acetate gives evidence that catabolite repression is absent in the fed-batch process. Similar results are reported in cases where the primary carbon source is in limited supply. Catabolite repression by glucose is absent at very low glucose concentrations in the culture media (Lendenmann and Egli 1995) and catabolic enzymes as well as acs are upregulated in a glucose limited fed-batch process (Raman *et al.* 2005).

The corrected rates in Table (5.3) conform to the elemental balances and were used for MFA and FBA. Figure (5.17) and (5.18) depict intracellular fluxes during the four perturbation experiments, given in mmol g_{DW}^{-1} h^{-1}.

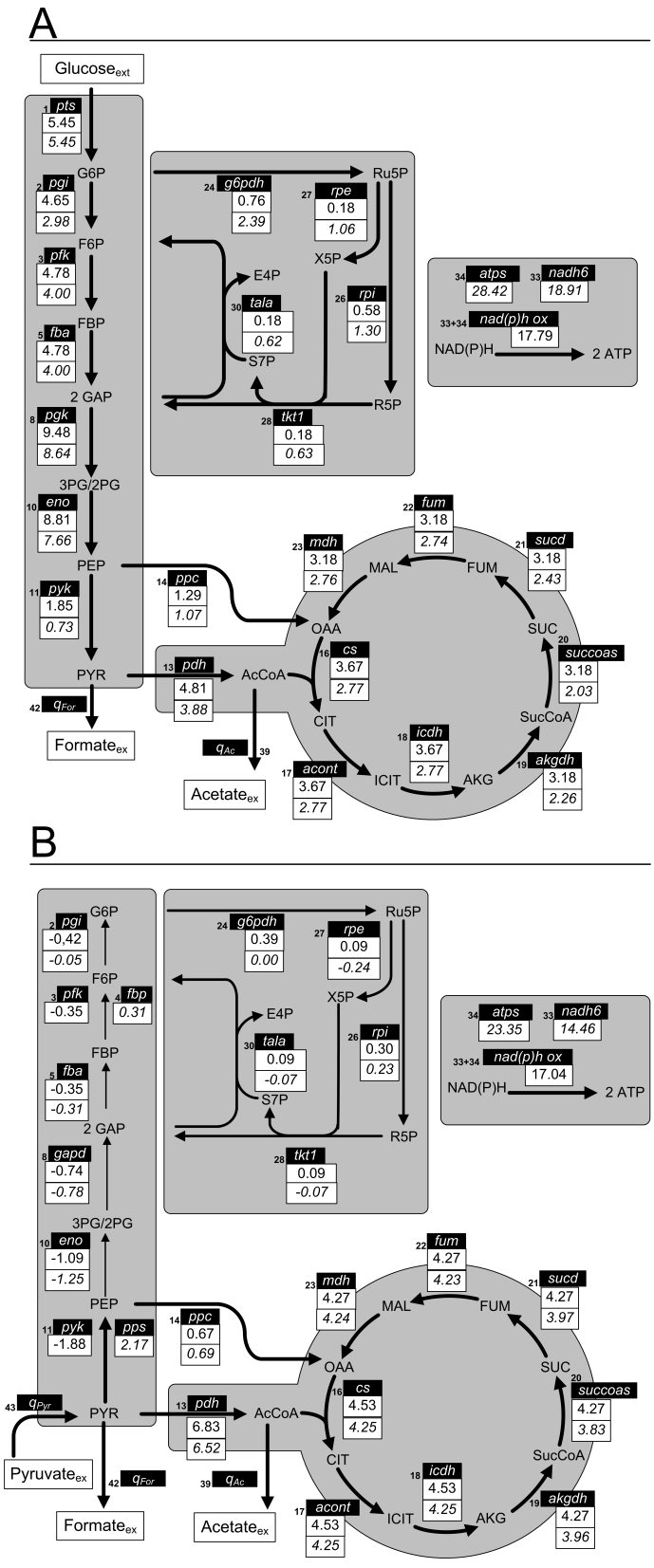

Figure 5.17.: Metabolic fluxes in central carbon metabolism during perturbation experiments with different substrates: (A) glucose, (B) pyruvate. Fluxes in mmol g_{DW}^{-1} h^{-1} were determined by stoichiometric metabolite balancing (upper boxes, normal letters) and by FBA (lower boxes, italic letters).

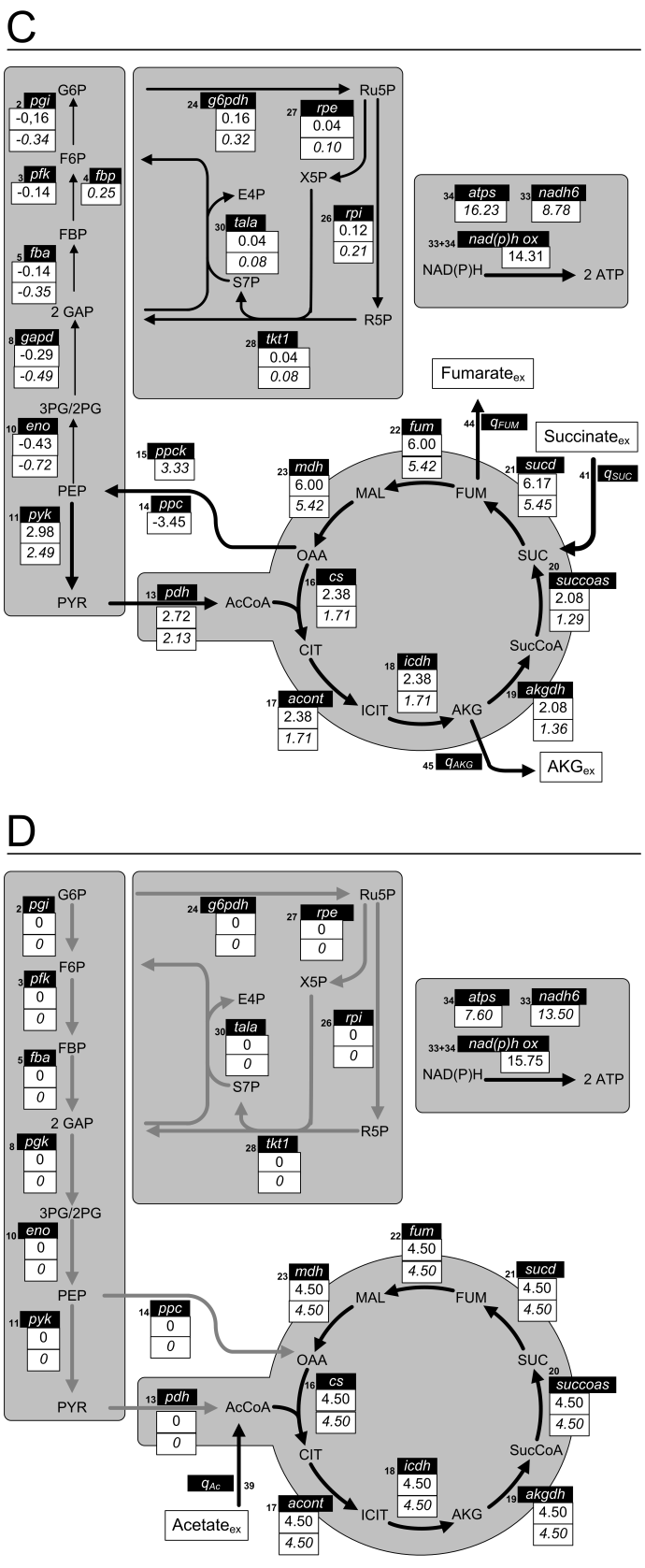

Figure 5.18.: Metabolic fluxes in central carbon metabolism during perturbation experiments with different substrates: (C) succinate and (D) acetate. Fluxes in mmol g_{DW}^{-1} h^{-1} were determined by stoichiometric metabolite balancing (upper boxes, normal letters) and by FBA (lower boxes, italic letters).

Compared to the fed-batch process, glucose uptake increased more than 450% in the RMT experiment with an excess of glucose. As a consequence most fluxes increase to a similar extend. However, ratios of glucose metabolized by PPP and channeled into TCA cycle differ from the fed-batch process. TCA flux in the fed-batch process is 75-100 molar-% of the glucose uptake, whereas TCA flux is only 50-60 % in the batch RMT experiment. FBA predicts, that almost 50 % of glucose is metabolized by PPP. Generally, the PPP ratio is the most striking difference of FBA and MFA. The reason for this is that PPP flux in the MFA model is mainly required for precursor supply, whereas the FBA model accounts for NADPH metabolism. Despite such discrepancies, the overall flux distribution of both approaches is consistent. Gluconeogenic flux with pyruvate and succinate involves the irreversible steps pps and ppck respectively. MFA does not separate between pyk and pps (accordingly ppc and ppck) and therefore predicts a negative flux through pyk and ppc. Nevertheless, the MFA estimates agree with values of pps and ppck predicted by FBA. These reactions are supposed to control gluconeogenic growth of *E. coli*, as overexpression of these enzyme increased growth rate on pyruvate and succinate (Chao *et al.* 1993). During cultivation with acetate, icdh produces an excess of NADPH and FBA predicts reoxidation of NADPH by a transhydrogenase, which is not considered in the MFA model.

In general, fluxes in the RMT experiments change in magnitude and are drastically redistributed compared to the fed-batch process. Due to the short-term cultivation it may be assumed that the drastic changes of fluxes are caused by kinetic effects at the metabolome level, rather than by changed enzyme levels. Samples for metabolome analysis were taken after 6, 10, and 14 minutes of each perturbation experiment using sampling protocol SP2. Additionally, a sample from the fed-batch process was withdrawn prior to each experiment. Metabolite concentrations are related to the intracellular volume, which was determined as 1.3 μL mg_{DW}^{-1} (Figure 5.2). Intracellular metabolite concentrations of four samples from the fed-batch process (black bars) are shown together with the three samples from each perturbation experiment in Figure (5.19) and (5.20).

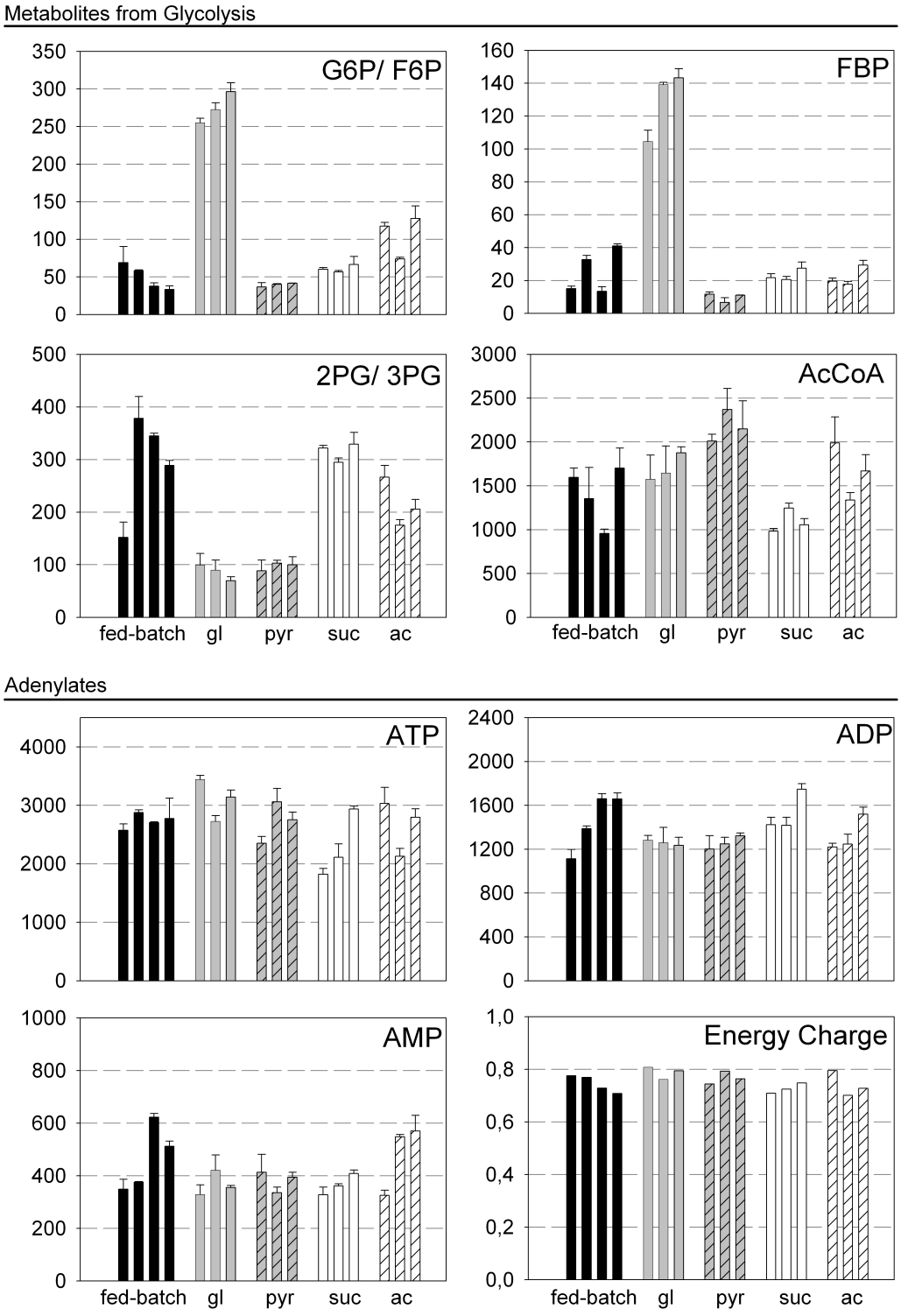

Figure 5.19.: Intracellular concentrations of metabolites from glycolysis and concentrations of adenylates given in μM. Four samples from the fed-batch process (black bars) are compared with the three samples (6, 10 and 14 minutes) from each rapid media transition experiment: glucose (grey bars), pyruvate (grey striped bars), succinate (white bars) and acetate (white striped bars). According to Eq.(5.1) the energy charge has no dimension.

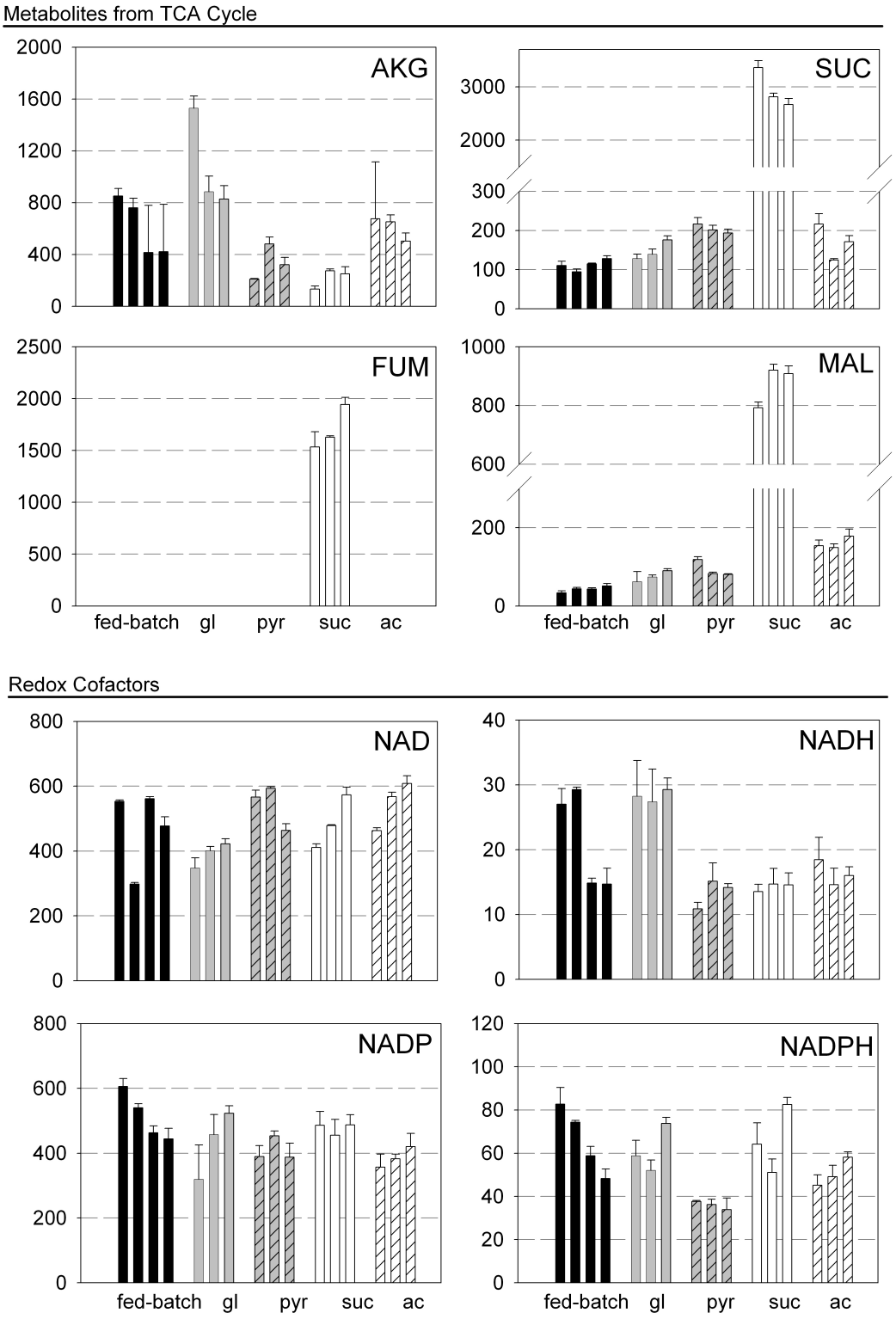

Figure 5.20.: Intracellular concentrations of metabolites from TCA cycle and redox cofactors given in μM. Four samples from the fed-batch process (black bars) are compared with the three samples (6, 10 and 14 minutes) from each rapid media transition experiment: glucose (grey bars), pyruvate (grey striped bars), succinate (white bars) and acetate (white striped bars).

The three measurements of each metabolic state in Figure (5.19) and (5.20) suggest a metabolic steady state. Generally, it is possible to confine all metabolite pools to small concentration ranges for one particular metabolic state. Considering the high-turn over of metabolites in central metabolism the differences of measured concentrations within one metabolic state are marginal. For example the several reactions producing and consuming AcCoA have to be in a quasi steady state, otherwise there would be more drastic differences as seen in Figure (5.19).

The concentrations of G6P/ F6P as well as FBP are significantly increased during cultivation with excess of glucose, correlating with the increased glycolytic flux. Conversely, the pool of 2PG and 3PG decreases during the RMT experiment with glucose. Concentrations of AcCoA are in the mM range and significantly higher compared to other metabolites from glycolysis. The lowest AcCoA concentrations were measured during the experiment with succinate. Concentrations of adenylates are almost not affected by the RMT experiments. In average, concentration of ATP is approximately 3 mM and just during cultivation with succinate a stepwise increase from 2 mM to 3 mM is observed. Similarly, ADP and AMP are constant during all experiments at a level around 1.2 mM and 0.4 mM respectively. As a consequence, the adenylates energy charge varies in a small range between 0.76 and 0.80.

Concentrations of redox cofactors NAD and NADH in Figure (5.20) are also constant within small bounds of 400-600 μM and 15-30 μM. The decrease of NAD during cultivation with an excess of glucose correlates with an increased NADH pool, probably caused by limitations of oxidative phosphorylation. However, a balanced NAD/NADH pool would require higher increases of NADH in response to the observed decrease of NAD. NADP and NADPH are also constrained to concentrations between 400-600 μM and 40-80 μM. An excess of NADPH, generated by icdh is not observed during cultivation on acetate.

The increase of TCA flux during cultivation with succinate is reflected in a more than 10-fold increase of intracellular malate, succinate and fumarate, whereas the AKG pool decreases with higher TCA flux. As fumarate, succinate and also AKG were present in the cultivation medium, they have to be distinguished from intracellular concentrations. Therefore, the cells were separated prior to extraction and additionally washed in quenching fluid. Even the washing step is essential in this case, it introduces additional sources of error.

Possible sources of error

The error bars in Figure (5.19) and (5.20) result from three independent extractions of one sample and reflect the statistical variability of extraction and LC-MS analysis. In most cases the relative error is below 10% and sampling protocol SP2 seems to be robust against statistical errors. It is not sure wether differences between the three samples of one metabolic state result from biological or analytical variations. However, small statistical errors do not reflect systematic errors caused by cellular leakage, thermal degradation and ion suppression in the ESI interface.

As mentioned above a critical point of metabolome analysis are metabolites, that are also present in the extracellular medium. Even after cells were separated from the culture supernatant, extracellular metabolites in the moist mass still divert measurements of intracellular concentrations. Therefore a washing step is required if significant amounts of metabolites are present in the extracellular medium. For measurements of intracellular metabolites shown in Figure (5.19) and (5.20) cells were separated from the cultivation supernatant and washed in cold quenching fluid (-20°C). The same metabolites were measured during an identical experiment without washing the cells before metabolite extraction. The results are compared in Figure (5.21) with metabolite concentrations already shown in Figure (5.19) and (5.20).

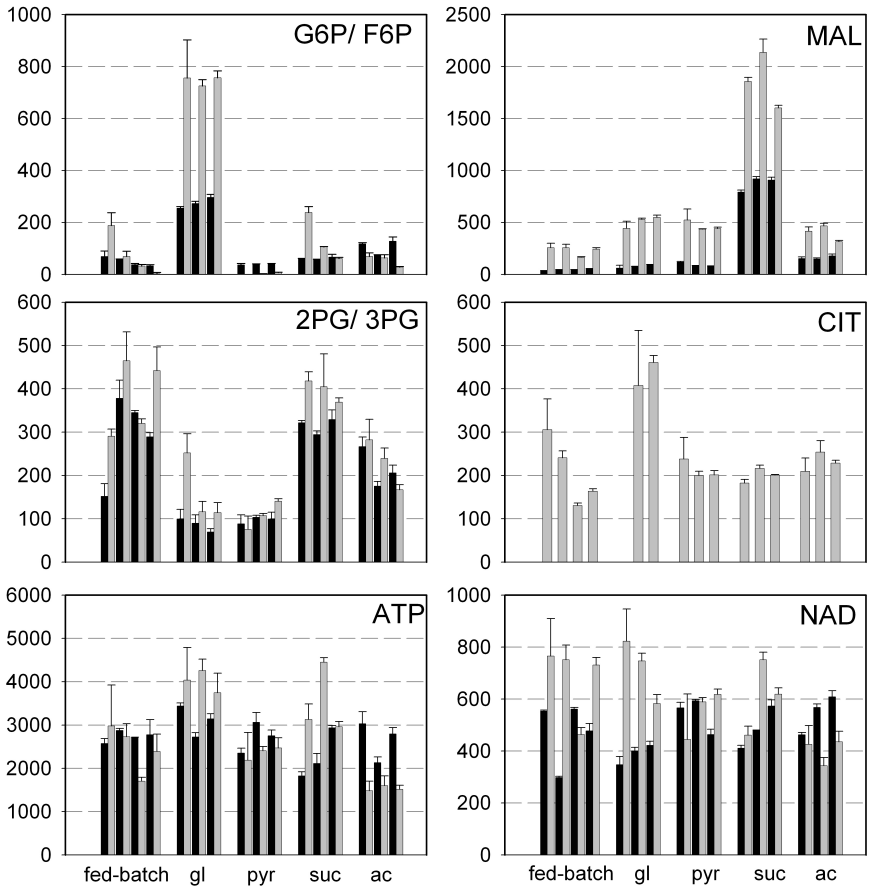

Figure 5.21.: Intracellular concentrations of metabolites measured during the fed-batch process and during RMT experiments with glucose (gl), pyruvate (pyr), succinate (suc) and acetate (ac). Black bars are the concentrations shown in Figures (5.19) and (5.20). Grey bars are concentrations in a reproduced experiment, without a washing step for metabolome analysis. Concentrations are given in μM.

The results in Figure (5.21) demonstrate, that even if absolute values are significantly different the relative metabolite profiles are consistent. Reproducibility was also given for substrate uptake and exhaust gas measurements (data not shown).

Without a washing step, higher metabolite concentrations were measured in all cases. The differences are mainly caused by two opposing effects: removal of extracellular metabolites and cellular leakage during the washing step. In case of samples from the RMT experiment with succinate as carbon source removal of extracellular succinate by the washing step is the main reason for smaller concentrations. In contrast, different concentrations of other metabolites result very likely from cellular leakage during the washing step. As shown before, cellular leakage is less pronounced for metabolites like ATP and NAD.

Consequently, concentrations of these metabolites are less affected by the washing step. In case of G6P/F6P, FBP and also malate there is a drastic difference between concentrations measured with both approaches, which is probably caused by cellular leakage. Leakage of citrate was even more severe, as this metabolite was only detected if no washing step was applied. Even if glycerol reduced leakage of some metabolites like ATP, other metabolites still leak during quenching and washing steps. Canelas *et al.* (2008) found that smaller metabolites tend to leak more than larger ones, since smaller metabolites are expected to have higher diffusivities. These findings are in accordance with the results in Figure (5.21), where concentrations of small organic acids like malate and citrate strongly depend on the applied protocol.

5.3.3. Rapid media transition in fed-batch mode

RMT experiments in batch mode have shown, that *E. coli* immediately utilizes certain substrates after the cells were separated from the glucose limited fed-batch process. Even if a metabolic steady state was achieved quickly and maintained during the analysis, the perturbations were quite large. For example the flux through the upper part of TCA cycle increased almost by 700% compared to the fed-batch process. In batch mode metabolism seemed perturbed to a maximum and consequently metabolic overflow and by-product formation was observed. In case of cultivation with succinate, the extracellular metabolites interfered with intracellular measurements.

Controlling substrate uptake is a promising possibility to adjust metabolic fluxes and additionally reduces metabolic overflow. Therefore, substrate was supplied with a constant rate to the lab-scale bioreactor. The feeding rate was adjusted, such that substrate uptake was always below the maximum uptake capacities, which were estimated from previous experiments in batch mode. A further advantage of the feeding strategy was the possibility of analyzing several steady states during one RMT experiment. After holding a feeding rate several minutes samples were withdrawn and the feeding rate was reduced to achieve accordingly lower fluxes. The fed-batch RMT approach was evaluated in four experiments with glucose (aerobic), glucose (anaerobic), pyruvate and succinate. Experiments with acetate feeding were not applicable, since acetate was not utilized until a certain concentration in the medium was achieved (approximately 1 g L^{-1}). OUR and CPR during the experiments with glucose (aerobic), pyruvate and succinate are shown in Figure (5.22). During anaerobic cultivation no CO_2 was measured in the off-gas. Predictions of FBA are indicated by straight lines in Figure (5.22).

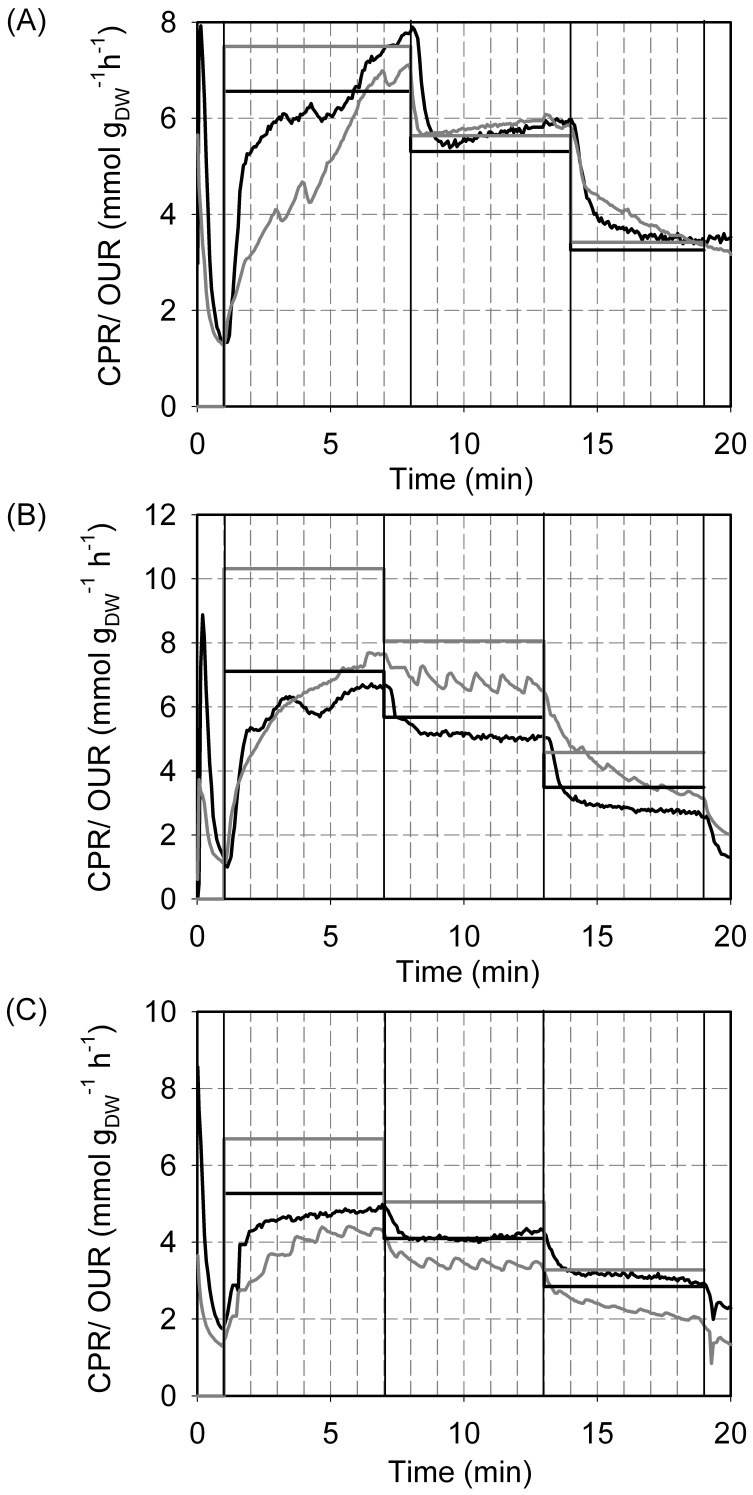

Figure 5.22.: Specific O_2 uptake rate (OUR; black lines) and the specific CO_2 production rate (CPR; grey lines) during RMT experiments in fed-batch mode with different substrates: (A) glucose, (B) pyruvate and (C) succinate. The FBA predictions for OUR and CPR are indicated by straight lines.

OUR immediately reached a constant value during each feeding interval, with exception of the first interval with glucose. The measured values of OUR are similar to values predicted by FBA. The characteristics of CPR are not as distinct as in case of OUR and differ more from FBA predictions. Reasons for this are the high aeration rate (10 vvm) and the accordingly low CO_2 signal in the exhaust gas (between 0.1 and 0.5 %). Additionally, the equilibrium of carbonic acid in the medium overlaid with the exhaust gas measurements. Nevertheless, mean values of OUR and CPR during the last minute of each interval were subjected to elemental balances, assuming a relative error of 20%.

None of the substrates was detected in the culture supernatant using HPLC (level of detection 0.1 g L^{-1}). Therefore, the culture supernatant was additionally analyzed with LC-MS (LOD 1 μM). No pyruvate was detected in the culture supernatant, particularly not in samples from the experiment with pyruvate as feeding carbon source. Extracellular succinate was detected in concentrations below 50 μM (0.01 g L^{-1}) in all samples and was not higher in case of the experiment with succinate feeding. As a consequence of the immediate substrate utilization ($c_s = 0$), it is possible to determine the specific substrate uptake rate by Eq.(3.5). Due to the small volumetric feeding and growth rates, reaction volume and biomass concentration are considered constant during the experiments. Biomass concentration was averaged over the four samples and the feeding rate ($\dot{V}_{in}$) was estimated by an analytical balance. Substrate concentration in the feed c_s^{in} was re-checked by HPLC analysis of a sample from the feeding solution.

Formation of by-products was only noticed in small amounts during the first feeding interval with glucose and pyruvate. No by-products were detected in samples from the experiment with succinate. During the anaerobic RMT experiment, glucose was completely converted into the by-products acetate, formate and ethanol. Specific rates were estimated from differences of concentrations between each feeding interval. They are given in Figure (5.23) on a C-mol basis.

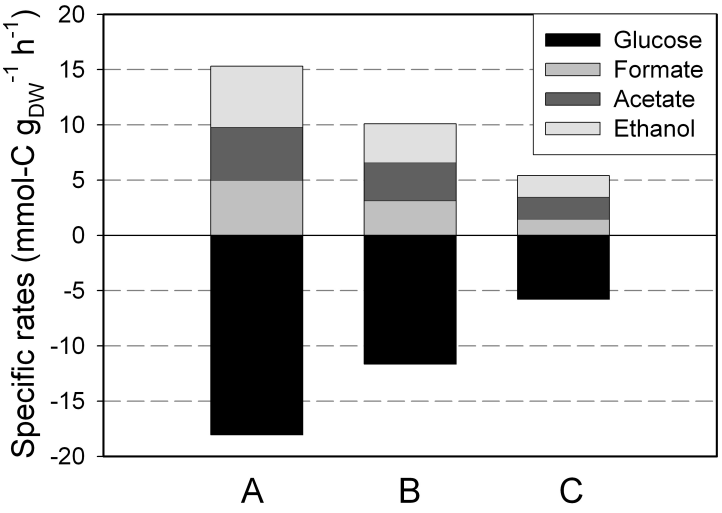

Figure 5.23.: Specific rates on C-mol basis during the three feeding intervals A,B and C in the anaerobic RMT experiment with glucose.

Even if the rates in Figure (5.23) are estimated from samples taken within step time of 6 minutes, carbon balances are closed by 90%. The precise estimation of by-product formation is a consequence of the high biomass concentration (26 g L^{-1}) and the accordingly high concentrations of by-products. Despite the high biomass concentration it was not possible to determine specific growth rates from DW measurements in 6 minute intervals.

Table (5.4) and Table (5.5) summarize measured extracellular rates (r_m) and their best estimates ($\hat{r}_m$) following from elemental balances. Cellular growth was considered as an unknown rate and was calculated from the the best estimates with Eq.(3.23). Additionally values of OUR, CPR and cellular growth predicted by FBA are given (r_{FBA}).

Table 5.4.: Specific rates during the RMT experiments in fed-batch mode with three feeding rates (A,B, and C) of glucose (aerobic) and pyruvate. Measured rates (r_m), best estimates ($\hat{r}_m$) and rates predicted by FBA (r_{FBA}) are given in mmol g_{DW}^{-1} h^{-1}. The specific growth rate is given in h^{-1}. The sum of weighted squares of residuals h is given in the last row.

Glucose (aerobic)

	A			**B**			**C**		
	r_m	$\hat{r}_m$	r_{FBA}	r_m	$\hat{r}_m$	r_{FBA}	r_m	$\hat{r}_m$	r_{FBA}
Glucose	3.26	3.24	3.24[(a)]	2.17	2.16	2.16[(a)]	1.05	1.08	1.08[(a)]
O_2	7.64	6.78	6.56	5.92	5.60	5.31	3.51	3.09	3.26
CO_2	6.87	7.27	7.50	5.89	6.07	5.64	3.23	3.29	3.42
Ethanol	0.75	0.75	0.75[(a)]	0.13	0.13	0.13[(a)]	0.19	0.19	0.19[(a)]
Formate	0.57	0.57	0.57[(a)]	0.25	0.25	0.25[(a)]	0.28	0.28	0.28[(a)]
Biomass	-	0.27	0.24	-	0.17	0.16	-	0.07	0.06
h		0.33			1.00			0.80	

Pyruvate

	A			**B**			**C**		
	r_m	$\hat{r}_m$	r_{FBA}	r_m	$\hat{r}_m$	r_{FBA}	r_m	$\hat{r}_m$	r_{FBA}
Pyruvate	6.47	6.48	6.48[(a)]	4.30	4.32	4.32[(a)]	2.09	2.03	2.03[(a)]
O_2	6.63	5.38	7.11	5.03	4.49	5.68	2.69	2.50	3.49
CO_2	7.50	8.52	10.32	6.64	7.08	8.06	3.26	3.64	4.58
Acetate	0.75	0.76	0.76[(a)]	0.00	0.00	0.00	0.00	0.00	0.00
Formate	0.58	0.58	0.58[(a)]	0.00	0.00	0.00	0.00	0.00	0.00
Biomass	-	0.24	0.17	-	0.16	0.12	-	0.09	0.04
h		2.43			0.117			0.085	

[(a)]FBA constraint

In all cases substrate uptake was almost exactly 60%, 40% and 20% of the uptake rate determined in the batch experiments. The specific rates estimated for the aerobic experiment with glucose match the best estimates as well as the FBA predictions. The small values of weighted squares of residuals h confirm the absence of gross errors. Even if the specific growth rate was not determined experimentally, the estimates from elemental balances and FBA agree well. During cultivation with pyruvate, lower values of OUR and higher values of CPR follow from elemental balances, whereas the FBA predictions are both higher compared to measured values. Except of the first feeding interval with a higher value of h the data of the pyruvate experiment is consistent.

Table 5.5.: Specific rates during the RMT experiments in fed-batch mode with three feeding rates (A,B, and C) of succinate and glucose (anaerobic). Measured rates (r_m), best estimates ($\hat{r}_m$) and rates predicted by FBA (r_{FBA}) are given in mmol g_{DW}^{-1} h^{-1}. The specific growth rate is given in h^{-1}. The sum of weighted squares of residuals h is given in the last row.

Succinate

	A			**B**			**C**		
	r_m	$\hat{r}_m$	r_{FBA}	r_m	$\hat{r}_m$	r_{FBA}	r_m	$\hat{r}_m$	r_{FBA}
Succinate	2.52	2.48	2.48[(a)]	1.72	1.72	1.72[(a)]	0.82	0.86	0.86[(a)]
O_2	4.82	3.80	5.27	4.24	2.65	4.10	3.00	1.66	2.85
CO_2	4.29	5.02	6.69	3.40	3.39	5.05	2.03	2.47	3.28
Biomass	-	0.13	0.08	-	0.09	0.04	-	0.03	0.00
h		10.72			3.10			32	

Glucose (anaerobic)

	A			**B**			**C**		
	r_m	$\hat{r}_m$	r_{FBA}	r_m	$\hat{r}_m$	r_{FBA}	r_m	$\hat{r}_m$	r_{FBA}
Glucose	3.01	3.01	3.01[(a)]	1.94	1.94	-	0.96	0.96	-
O_2	0.00	0.00	0.00	0.00	0.00	-	0.00	0.00	-
CO_2	0.00	0.00	0.00	0.00	0.00	-	0.00	0.00	-
Formate	5.00	5.10	5.94	3.14	3.21	-	1.48	1.55	-
Acetate	2.40	2.41	2.95	1.72	1.72	-	1.00	1.00	-
Ethanol	2.76	2.62	2.95	1.76	1.66	-	0.96	0.86	-
Biomass	-	0.06	0.01	-	0.04	-	-	0.01	-
h		0.033			0.006			0.072	

[(a)]FBA constraint

Measurements of OUR and CPR during cultivation with succinate are less conform to elemental balances. This is mainly caused by the small respiratory rates, that could not be determined with sufficient accuracy. In contrast, the specific rates during the anaerobic cultivation with glucose match elemental balances to the same extend as FBA predictions. In case of anaerobic feeding intervals B and C, the linear program used for FBA could not find a solution, probably because of very small growth rates.

Intracellular fluxes were estimated by MFA and FBA in the same way as for the RMT experiments in batch mode. The rates are given in mmol g_{DW}^{-1} h^{-1} for MFA (v_{MFA}) and FBA (v_{FBA}) in Tables (A.14)-(A.17). In general, the relative flux distribution of experiments with glucose, pyruvate and succinate was not different from the experiments in batch mode and only absolute values decreased according to substrate uptake by 60%,

40% and 20%.

During anaerobic cultivation with glucose, carbon is almost completely converted to pyruvate by a high glycolytic flux. Pyruvate is utilized by pathways of mixed acid fermentation, producing acetate, formate and ethanol. Under anaerobic conditions FBA predicts a zero flux through TCA cycle and PPP. Using MFA a small flux through PPP is estimated and a negative flux through TCA cycle (converting OAA to citrate). A branched, noncyclic operation of the TCA cycle under anaerobic conditions was observed by Fischer and Sauer (2003a). As extracellular succinate was detected in small amounts (not affecting the carbon balance), a flux from OAA to succinate is reasonable. The absence of CO_2 in the exhaust gas suggests a zero flux through PPP, as CO_2 is produced by G6P dehydrogenase and phosphogluconate dehydrogenase. Fischer and Sauer (2003) found that PPP is active under anaerobic conditions, but its contribution to glucose metabolism decreases to 5%. A similar anaerobic perturbation experiment is reported for a glucose limited *Saccharomyces cerevisiae* culture, which was shifted to anaerobic conditions with glucose excess (van den Brink *et al.* 2008). The authors report that under anaerobic conditions 4% and 2% of the glucose influx is channeled into PPP and TCA cycle. A further important conclusion of their study is that enzyme capacities only marginally contribute to regulation of glycolytic flux, whereas metabolite profiles strongly influence metabolic fluxes. Similar findings for *E. coli* under anaerobic conditions are reported by Smith and Neidhardt (1983).

Samples for metabolome analysis were taken at the end of each feeding interval of the RMT experiments. In order to circumvent problems with cellular leakage the whole culture broth was extracted according to sampling protocol SP3. Concentrations of extracellular metabolites should be low in fed-batch RMT experiments, as they were performed with fresh medium and no metabolic overflow was expected. Figure (5.24) depicts concentrations of metabolites, quantified by IDMS. One sample of the fed-batch process (black bar) is shown together with one sample of each feeding interval of the particular perturbation experiment.

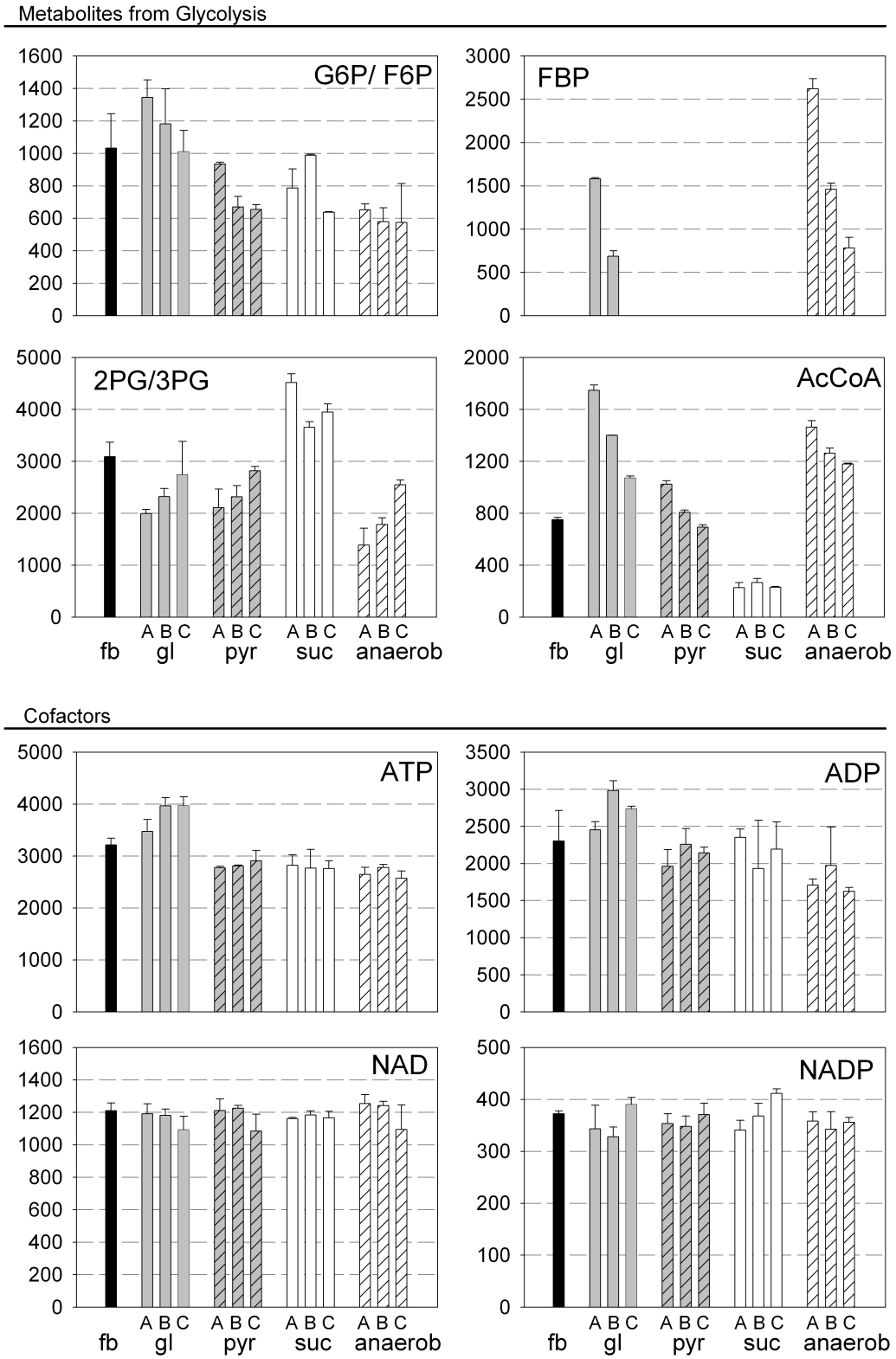

Figure 5.24.: Intracellular concentrations of metabolites from glycolysis and cofactors quantified by IDMS. One sample from the fed-batch process (black bars) is compared with the samples of each feeding interval (A, B and C) from the rapid media transition experiments in batch mode: glucose (grey bars), pyruvate (grey striped bars), succinate (white bars) and anaerobic glucose (white striped bars). Concentrations are given in μM.

At first view, concentrations of G6P/F6P, FBP and especially 2PG/3PG are significantly higher compared to concentrations measured in batch experiments. These metabolites were supposed to leak during sampling with protocol SP2 and thus extraction of the whole culture broth has strong influence on absolute values. Leakage of AcCoA was not noticed with any protocol and therefore concentrations are similar to the batch experiments.

Regarding relative values, some metabolite profiles are similar as observed in the batch experiment and others differ. For example, there is only a slight increase of the G6P/F6P pool, from 1 mM in the fed-batch process to 1.4 mM during glucose feeding interval A, whereas a more than 5-fold increase was observed in the batch experiment. In contrast to G6P/F6P, the concentration of FBP increases drastically with the glycolytic flux under aerobic and also anaerobic conditions. FBP was only detected in five samples, whereas U-^{13}C labeled FBP was detected in all samples. The internal standard assures, that a low (unlabeled) FBP signal is not caused by degradation during sample processing or ion suppression during analysis. A decrease of 2PG/3PG with increasing glycolytic flux was already observed in batch experiments. Another profile noticed in the batch experiments is the increased concentration of 2PG/3PG in combination with a decreased AcCoA pool during cultivation with succinate.

Metabolite concentrations of glucose interval C are of particular interest, as this metabolic state is expected to be almost similar to the fed-batch reference state. In all cases the concentrations of the reference state and feeding interval C are not contradictory. For example the G6P/F6P pool decreased to 1 mM during interval C, which is exactly the value determined for the reference state.

The stepwise feeding profile is most pronounced for FBP and AcCoA, but is still noticeable for the isobaric metabolites 2PG/3PG and G6P/F6P. On the contrary, concentrations of cofactors and adenylates were not considerably perturbed during the RMT experiments. ATP is in the same range of 3-4 mM, as determined in batch experiments with protocol SP2. In the experiment with glucose, ATP increased from 3 mM in the reference state to 4 mM, but did not decrease to the reference level during feeding interval C. Concentrations of ADP are slightly higher (1.6 - 3 mM) compared to batch experiments (1.2 - 1.6 mM). AMP was not quantified with sampling protocol SP3, because neither the U-^{13}C labeled AMP signal nor the unlabeled signal was detected in the samples.

Concentrations of NAD are twice as high as determined with protocol SP2 in batch experiments, whereas the same concentrations were estimated in case of NADP. The reduced cofactors NADPH and NADH were not detected with sampling protocol SP3.

The metabolites in Figure (5.25) were quantified with external calibration. They were not detected in samples with U-^{13}C-labeled standard, probably due to the high salt content in the labeled cell extract, which caused degradation during lyophilization and shifts of retention times. One sample from the fed-batch process (black bar) is shown together with one sample from each feeding interval of the particular perturbation experiment.

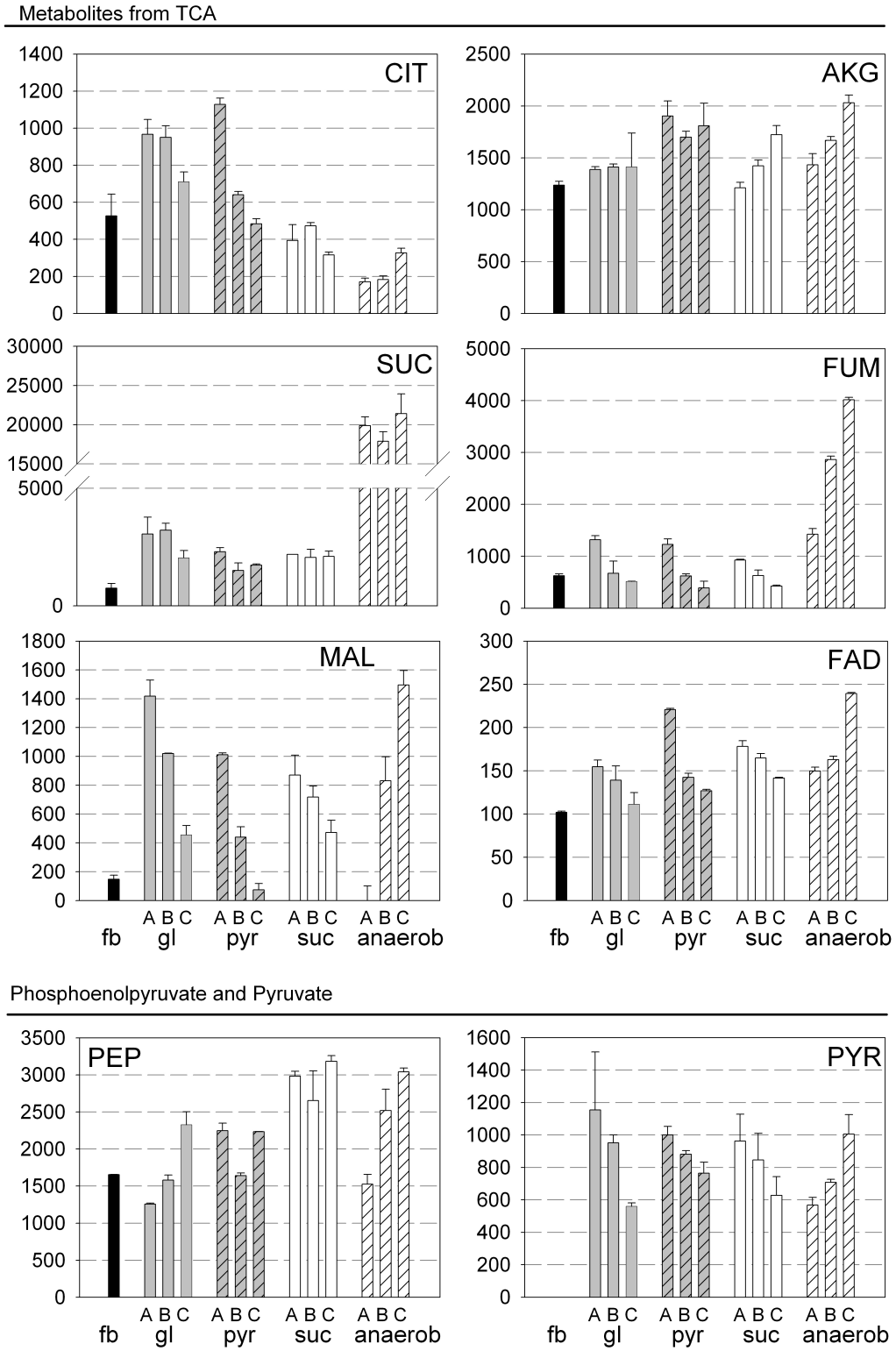

Figure 5.25.: Intracellular concentrations of metabolites from TCA cycle, phosphoenolpyruvate and pyruvate. One sample from the fed-batch process (black bars) is compared with the samples of each feeding interval (A, B and C) from the rapid media transition experiments: glucose (grey bars), pyruvate (grey striped bars), succinate (white bars) and anaerobic glucose (white striped bars). Concentrations are given in μM.

Generally, concentrations of organic acids in Figure (5.25) are higher when compared to batch experiments, due to absence of cellular leakage. Malate, citrate and fumarate decrease in the same stepwise manner as substrate uptake. Also FAD, the reducing cofactor of sucd, increases gradually. The profiles of AKG and succinate are less pronounced and rather constant. Particularly during the experiment with succinate feeding, intracellular succinate is not increased compared to experiments with glucose and pyruvate. In contrast, succinate is drastically increased during anaerobic cultivation with glucose. The intracellular concentration of 20 mM is already corrected for extracellular succinate as shown below. The distinct metabolite profiles of malate, fumarate and succinate during anaerobic cultivation confirm a flux from OAA to succinate, as suspected above. Further, the low citrate concentrations might indicate a zero flux through citrate synthase.

PEP and pyruvate were only detected in significant amounts with protocol SP3. It is assumed that these metabolites, especially the small molecule pyruvate, are susceptible to cellular leakage and therefore were not detected with protocol SP1 and SP2. Surprisingly, intracellular pyruvate is not increased during cultivation with pyruvate and gradually decreases with reduced pyruvate uptake. Pyruvate was not detected in the sample from the fed-batch process. As no U-^{13}C-labelled standard was applied it is not sure whether this is a result of sample processing or a low intracellular pyruvate level. PEP is obviously decreasing with an increased glycolytic flux. Schaub and Reuss (2008) observed the same decrease of PEP (and also 2PG/3PG) with increasing glycolytic fluxes in *E. coli*. They suspect a decrease in protein content to cause this decline of precursor metabolites. However, intracellular metabolites should be considered as regulatory effectors of a supply flux rather than sustainable precursor pools.

Possible sources of error

The RMT experiments in fed-batch mode were repeated and metabolites were quantified with external calibration. Differences of IDMS and external calibration are demonstrated in Figure (5.26). Grey bars are metabolites as shown in Figure (5.24) and black bars are concentrations estimated with external calibration.

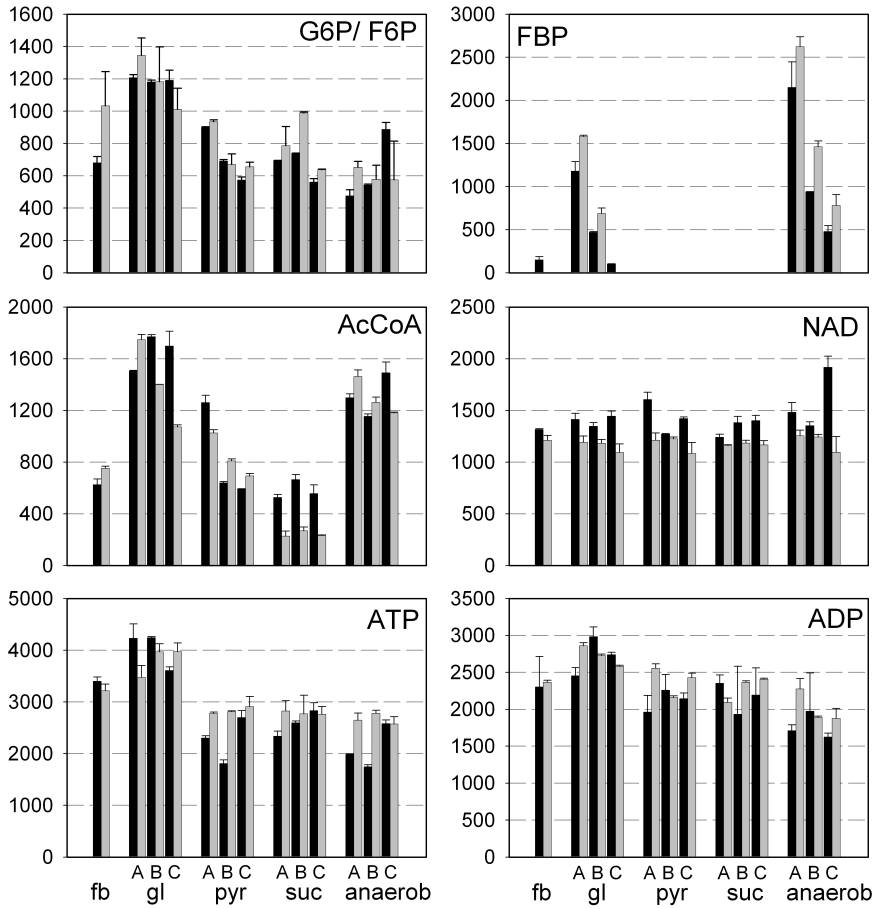

Figure 5.26.: Intracellular concentrations of metabolites measured during the fed-batch process and during RMT experiments with glucose (gl), pyruvate (pyr), succinate (suc) and anaerobic glucose (anaerobic). Grey bars are concentrations estimated with IDMS, as shown in Figure (5.24). Black bars are concentrations in a reproduced experiment, quantified with external calibration. Concentrations are given in μM.

Even if two different methods were applied in independent experiments, the metabolite levels in Figure (5.24) are almost identical. Upon close inspection, the advantages of IDMS are obvious. For example, the subtle gradual profiles of AcCoA and G6P/F6P are only resolved with IDMS. Further, variations of ATP and NAD become smaller due to application of an internal standard. The reproducibility observed for intracellular metabolites was also given for extracellular rates and metabolites (data not shown).

According to the differential method, the whole culture broth was extracted and metabolites were additionally quantified in culture supernatant. Only malate, succinate, citrate and 2PG/3PG were detected in the culture supernatant. PEP was detected only in the supernatant of samples from the fed-batch process. The amount of metabolites in the

medium is opposed to intracellular concentrations in Figure (5.27).

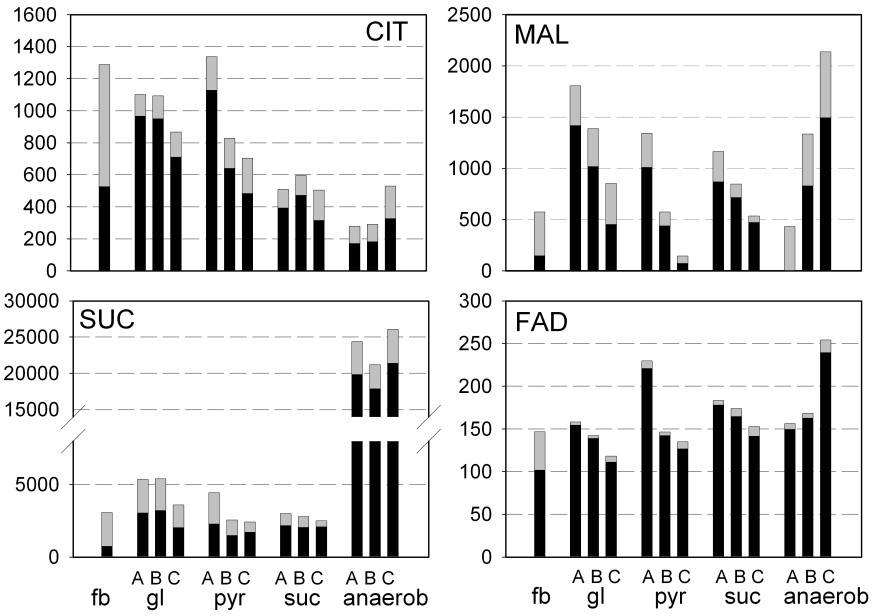

Figure 5.27.: Intracellular concentrations of metabolites measured during the fed-batch process and during RMT experiments with glucose (gl), pyruvate (pyr), succinate (suc) and anaerobic glucose (anaerobic). Black bars are intracellular concentrations, as shown in Figure (5.24). Grey bars reflect the amount measured in the culture supernatant. Concentrations are given in μM.

More than 50% of the total amount of malate, citrate and succinate extracted from the whole culture broth of the fed-batch process, originates from the extracellular medium. A smaller amount was found in the supernatant of the RMT experiments, as they were performed with fresh medium. Similarly, extracellular FAD is higher in the fed-batch process, than in the RMT experiments. The high concentration of succinate is attributed to intracellular succinate during anaerobic cultivation. In conclusion, extracellular metabolites did not detract measurements of most intracellular levels using the differential method. RMT experiments in fed-batch mode seem to be particularly suited if the whole culture broth is extracted for metabolome analysis. The amount of extracellular metabolites could be further reduced by a washing step after cells are separated from the production process.

5.4. Proteome analysis

Proteome analysis of samples from the fed-batch process and RMT experiments was performed by Protagen AG (Dortmund, Germany). Materials and methods are further described in appendix A.9. 2-DE gels of protein samples after 19 h fed-batch cultivation (c_x = 10 g_{DW} L^{-1}) were compared with gels of samples after 23 h (c_x = 14.5 g_{DW} L^{-1}). Figure (5.28) shows an overlay of false-color images of both gels, visualizing changes of the proteome. Unchanged spots appear black, whereas changes appear orange or blue.

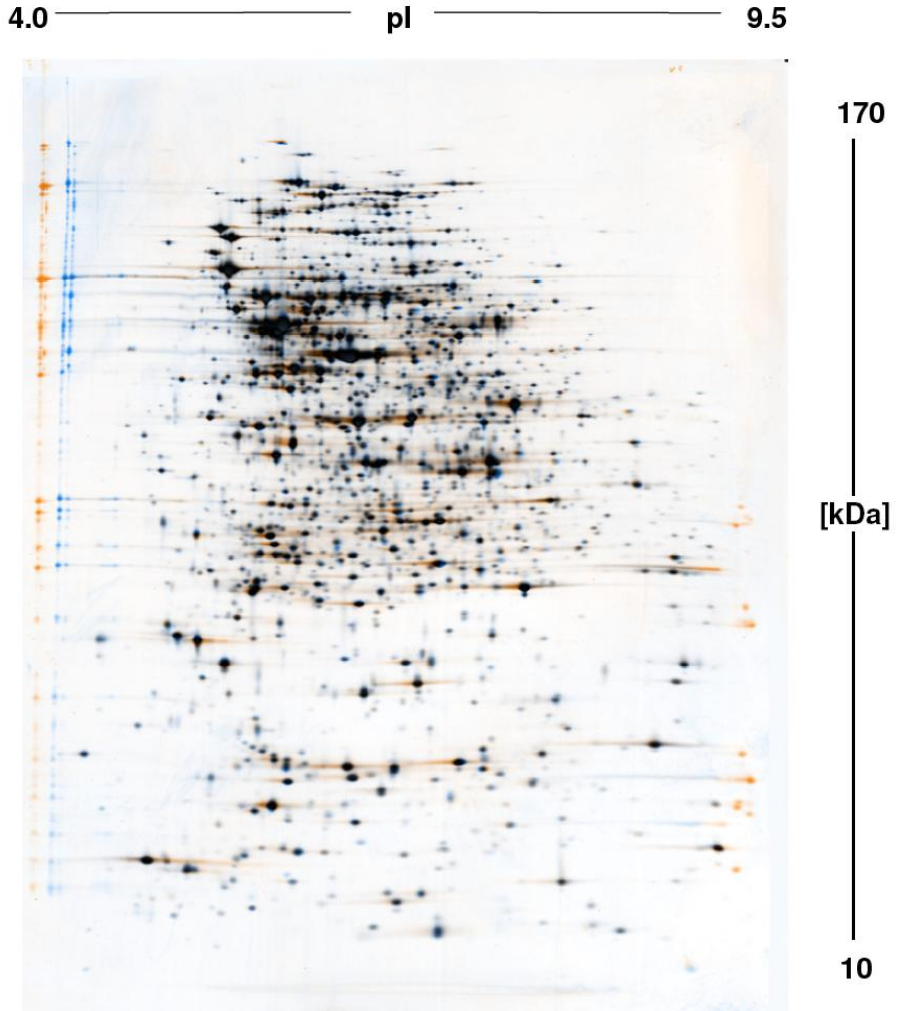

Figure 5.28.: Overlay of false-color images of gels from protein samples from the fed-batch process (19 h and 24 h). Unchanged spots appear black, whereas changes appear orange or blue.

The exclusively black spots in Figure (5.28) indicate an unchanged proteome. Further, quantitative evaluation confirmed that 99.5% of 1130 spots matched within a differential expression range of 0.3-3 (Figure (A.4)).

Figure (5.29) compares gels of the 19 h fed-batch sample and a sample from the batch RMT experiment with succinate (taken after 16 min).

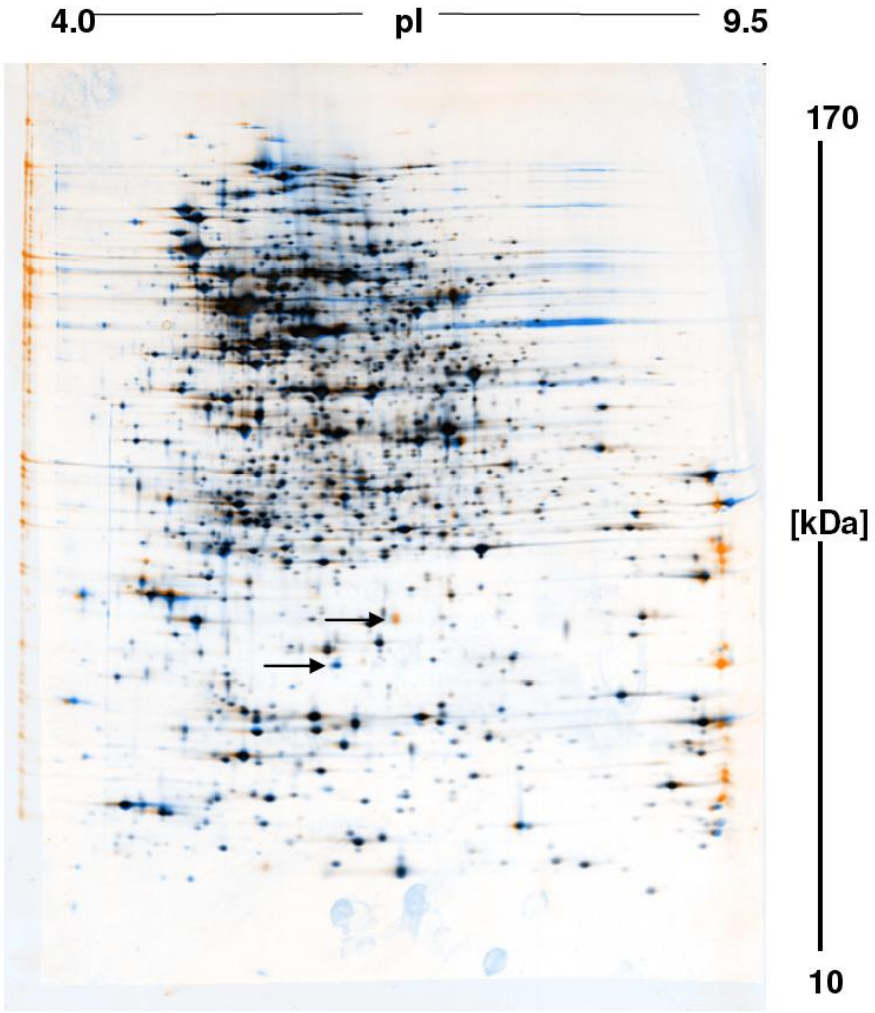

Figure 5.29.: Overlay of false-color images of gels from protein samples from the fed-batch process (19 h) and the batch RMT experiment with succinate (16 min). Unchanged spots appear black, whereas changes appear orange or blue.

Beside two differential spots (indicated by arrows) there are no significant changes between both gels. Similarly, samples from other batch RMT experiments confirmed an unchanged proteome. Figure (A.5) - (A.8) shown in the appendix compare a sample from the fed-batch process (24 h) with samples from fed-batch RMT experiments. Protein samples were taken directly after transfer to the lab-scale reactor and are compared with samples from the fed-batch process before the transfer (Figure (A.5)). Similar to the samples from the fed-batch process (Figure (5.28)), no changes in the proteome are noticeable in response to the transfer. Generally, proteome samples indicated in every case the absence

of proteins involved in stress protection.

Protein samples of cells after 18 min fed-batch RMT experiments with glucose, succinate and pyruvate show a constant proteome (Figure (A.6) - (A.8)). Only one differential spot is identified, the same as observed in samples from batch RMT experiments (indicated with a box in the particular Figures). Protagen could not identify the according enzyme.

5.5. Kinetic analysis

Proteome analysis suggests constant enzyme levels and consequently the only possibility to enhance or decrease a particular reaction rate is to vary metabolite concentrations that influence the reaction rate. The relation of metabolic fluxes and metabolite concentrations is evaluated graphically in this section and a quantitative evaluation is exemplified by means of the lin-log approach.

5.5.1. Reaction rate and substrate concentration

In the most simple case enzyme-catalyzed reactions depend exclusively on the concentration of their substrate and follow saturation type kinetics. Hence, an increased substrate concentration correlates with higher reaction rates. In this sense, a major issue with data from batch RMT experiments is demonstrated by means of *in vivo* kinetics of mdh. The increase of TCA flux during the batch RMT experiment with succinate was reflected in a more than 10-fold increase of intracellular malate. Figure (5.30) shows steady state concentrations of malate (averages of values in Figure 5.20) plotted against flux through mdh in the fed-batch reference state and the perturbed steady states. Error bars of metabolite concentrations reflect variations of the three samples. Error bars of reaction rates follow from differences between MFA and FBA predictions. The reference state in Figure (5.30) and subsequent Figures is highlighted by a circle.

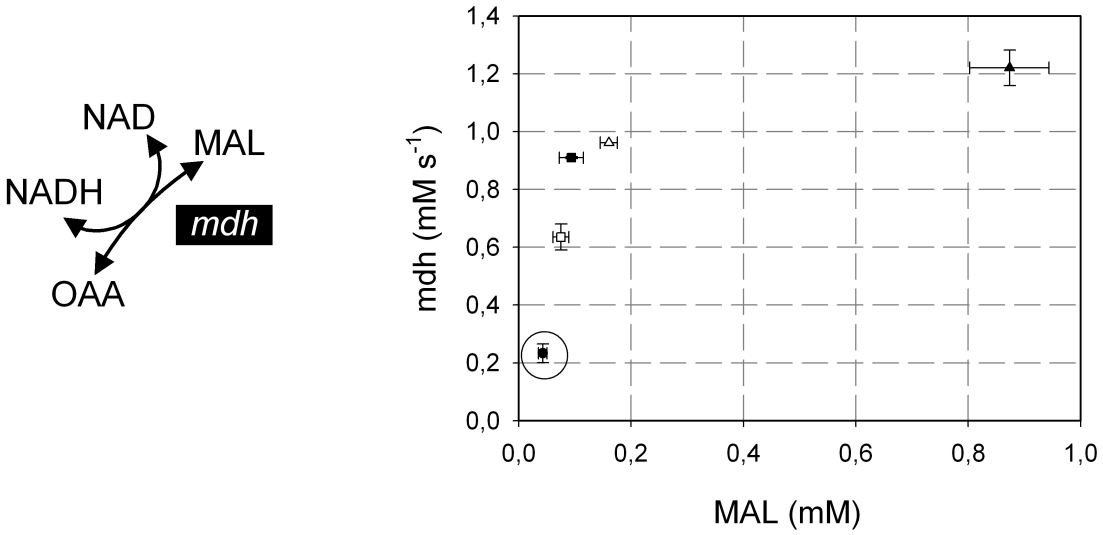

Figure 5.30.: Correlation of steady state fluxes through malate dehydrogenase (mdh) with intracellular malate during the fed-batch process (black dot) and the perturbation experiments with glucose (black square), pyruvate (white square), succinate (black triangle) and acetate (white triangle).

Figure (5.30) demonstrates that the 5 steady states lie at different regimes in the saturation kinetics of mdh. The enzyme is not saturated in the fed-batch reference state and an increase of mdh flux is achieved by increasing concentrations of malate. Similarly, the five-fold increase of G6P/F6P during batch RMT experiments with glucose was not observed in fed-batch RMT experiments with accordingly lower glycolytic fluxes. These results suggest, that in particular enzymes near the carbon source entry shift from a non-saturated regime in the reference state, towards a saturated state in the batch RMT experiment. Such data is not applicable for MCA, which is based on a linearization around the reference state. If a reaction is non-saturated in the reference state the perturbed steady state has to remain in the non-saturated regime. As shown in the following, perturbations of fed-batch RMT experiments are more subtle and closer to the reference state.

Relations of metabolic fluxes and metabolite pools of the fed-batch RMT experiments are visualized in the following. The flux into PPP via g6pdh is related to the G6P/F6P pool in Figure (5.31). Error bars of metabolite concentrations are the same as depicted in Figure (5.24) and (5.25). Error bars of reaction rates follow from differences between MFA and FBA predictions.

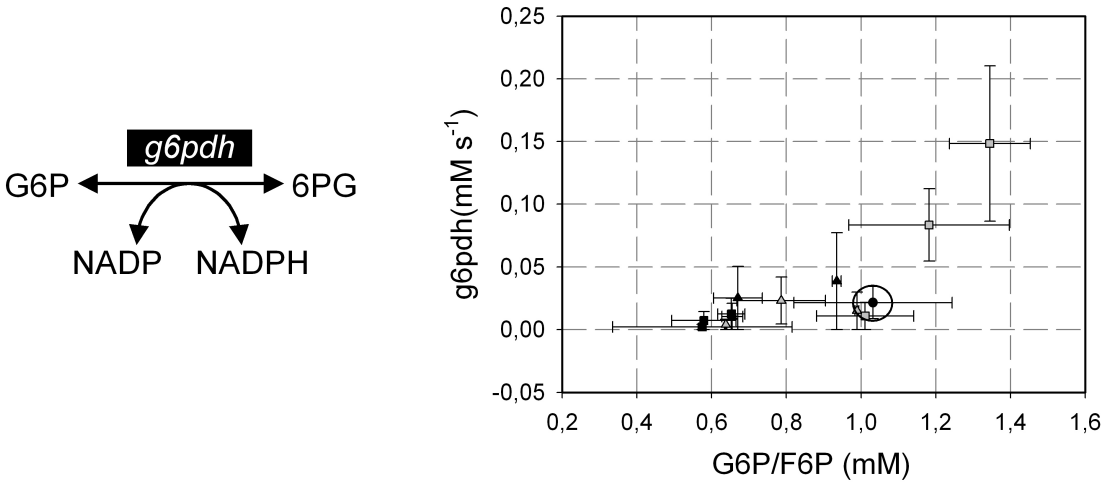

Figure 5.31.: Flux of glucose-6-phosphate dehydrogenase (g6pdh) is plotted against the G6P/F6P concentration: fed-batch process (black dot), glucose (grey squares), pyruvate (black triangles), succinate (grey triangles) and glucose anaerobic (black squares).

The relation of PPP flux and G6P/F6P suggests a linear dependency of g6pdh and its substrate G6P. The concentration of G6P/F6P decreases to 0.6 mM during anaerobic fed-batch experiments and is in a similar range during experiments with gluconeogenic flux. Therefore, it is hypothesized that G6P/F6P has no regulatory effect on glycolytic flux. Rather the flux into PPP, which is different under anaerobic and aerobic conditions, is effected by the G6P/F6P level.

Different findings are reported for *S. cerevisiae* by Vaseghi *et al.* (1999). The authors conclude from *in vivo* dynamics, that the PPP flux is independent from the G6P concentration and primarily regulated by MgATP and the NADP/NADPH ratio. In their study MgATP is directly related to ATP measurements. The results shown above do not support inhibition of g6pdh by ATP, as ATP is increased during RMT experiments with glucose (batch and fed-batch) and an accordingly higher PPP flux.

The glycolytic flux (exemplified by fba and pgm) is related to the FBP and 2PG/3PG concentrations in Figure (5.32).

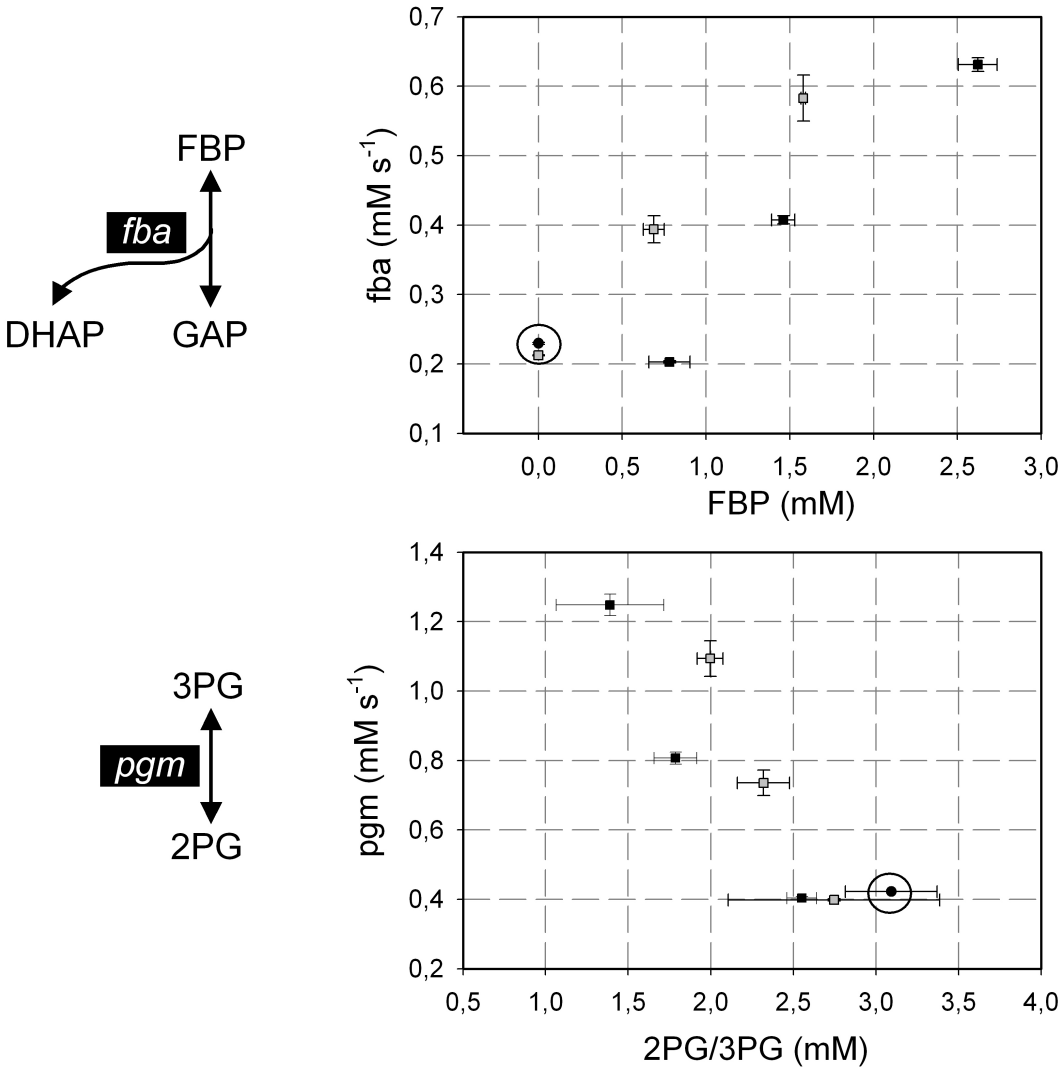

Figure 5.32.: Fluxes of fructose bisphosphate aldolase (fba) and phosphoglycerate mutase (pgm) are plotted against the FBP and 2PG/3PG concentrations: fed-batch process (black dot), glucose (grey squares) and glucose anaerobic (black squares).

The flux through fba lineraly depends on the concentration of its substrate FBP and 2PG/3PG linearly decreases with flux through pgm. The same correlations were observed in *E. coli* chemostat cultures (Schaub and Reuss 2008) and in case of the dynamic response of glucose-limited *S. cerevisiae* to a glucose pulse (Wu *et al.* 2005). In Figure (5.33) AcCoA is related to the flux channeled into TCA cycle via citrate synthase.

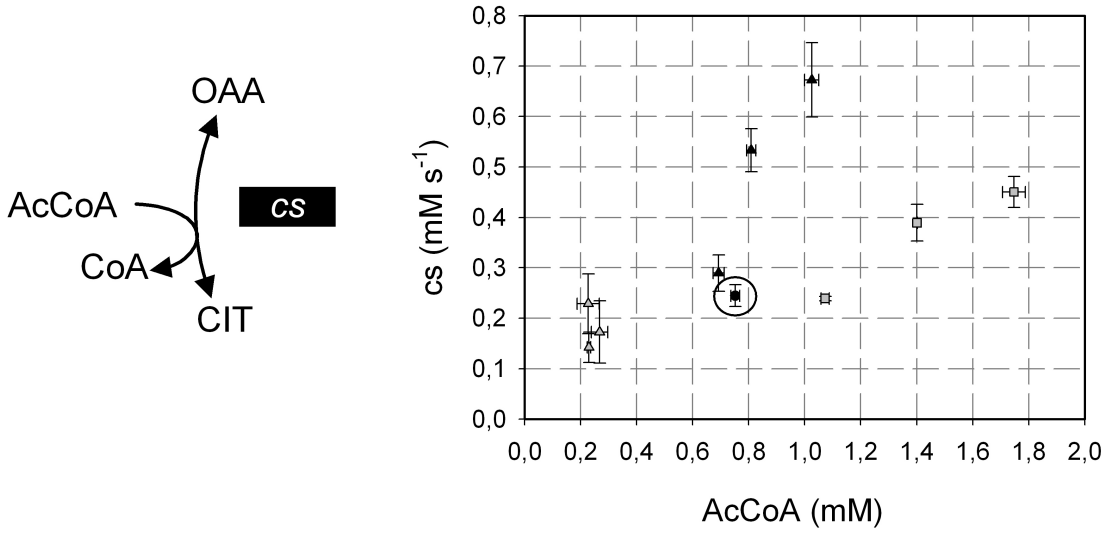

Figure 5.33.: Flux of citrate synthase (cs) is plotted against the AcCoA concentration: fed-batch process (black dot), glucose (grey squares), pyruvate (black triangles), succinate (grey triangles) and glucose anaerobic (black squares).

The flux through citrate synthase obviously depends not solely on the AcCoA concentration, rather the product citrate or other regulatory effectors such as AKG or NADH will additionally influence the reaction rate. The relation of other TCA fluxes with their substrates is shown in Figure (5.34).

The flux through icdh correlates linearly with the citrate/isocitrate level. In case of mdh and fum the correlation is less pronounced but still noticeable. The reaction rate of sucd is less affected by succinate, rather than by the cofactor FAD which increases linearly with sucd flux. In combination with the results from batch experiments it might be concluded that a significant increase of TCA flux is achieved by only a moderate increase of TCA metabolites.

Similarly, Wu *et al.* (2005) report that TCA metabolites are much less perturbed by a glucose pulse to a *S. cerevisiae* chemostat culture. The hypothesis, that TCA enzymes are not saturated is supported by proteome and transcriptome studies of Raman *et al.* (2005). They report, that under glucose-limited conditions enzymes of the TCA cycle are upregulated for satisfying the cellular energy needs. However, if every reaction in the metabolic network would solely depend on the particular substrate, there would be rather low flexibility to control fluxes. For this reason regulatory mechanisms such as feedback inhibition and allosteric activation are required.

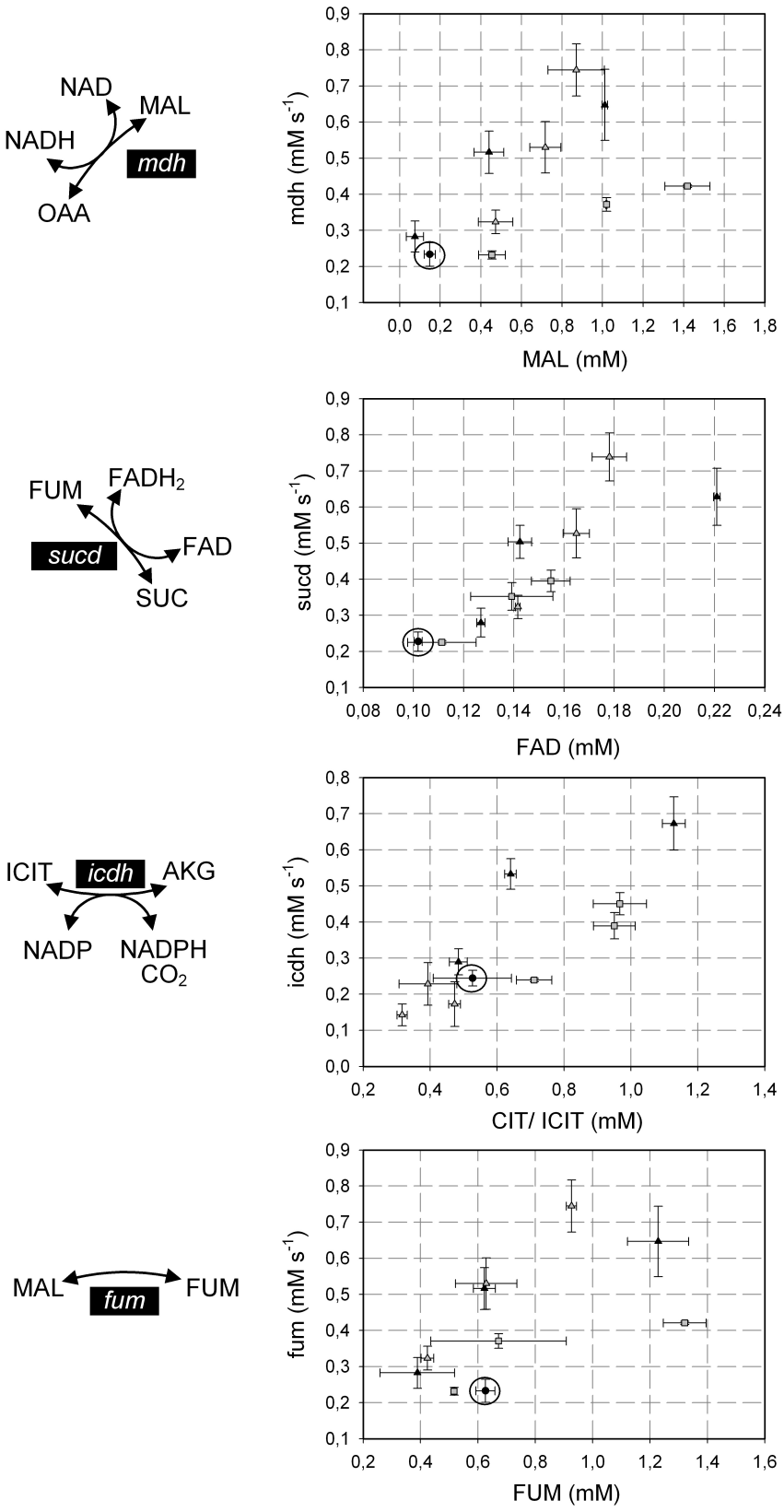

Figure 5.34.: Fluxes of isocitrate dehydrogenase (icdh), malate dehydrogenase (mdh), fumarate reductase (fum) and succinate dehydrogenase (sucd) are plotted against the concentration of their particular substrate (co-substrate in case of sucd). Fed-batch process (black dot), glucose (grey squares), pyruvate (black triangles) and succinate (grey triangles).

5.5.2. Active regulation

Two reactions, catalyzed by pfk and pyk are considered as key regulatory steps of glycolysis. Figure (5.35) shows the flux through pfk and pyk related to the concentration of their regulatory effectors PEP and FBP during experiments with glycolytic flux.

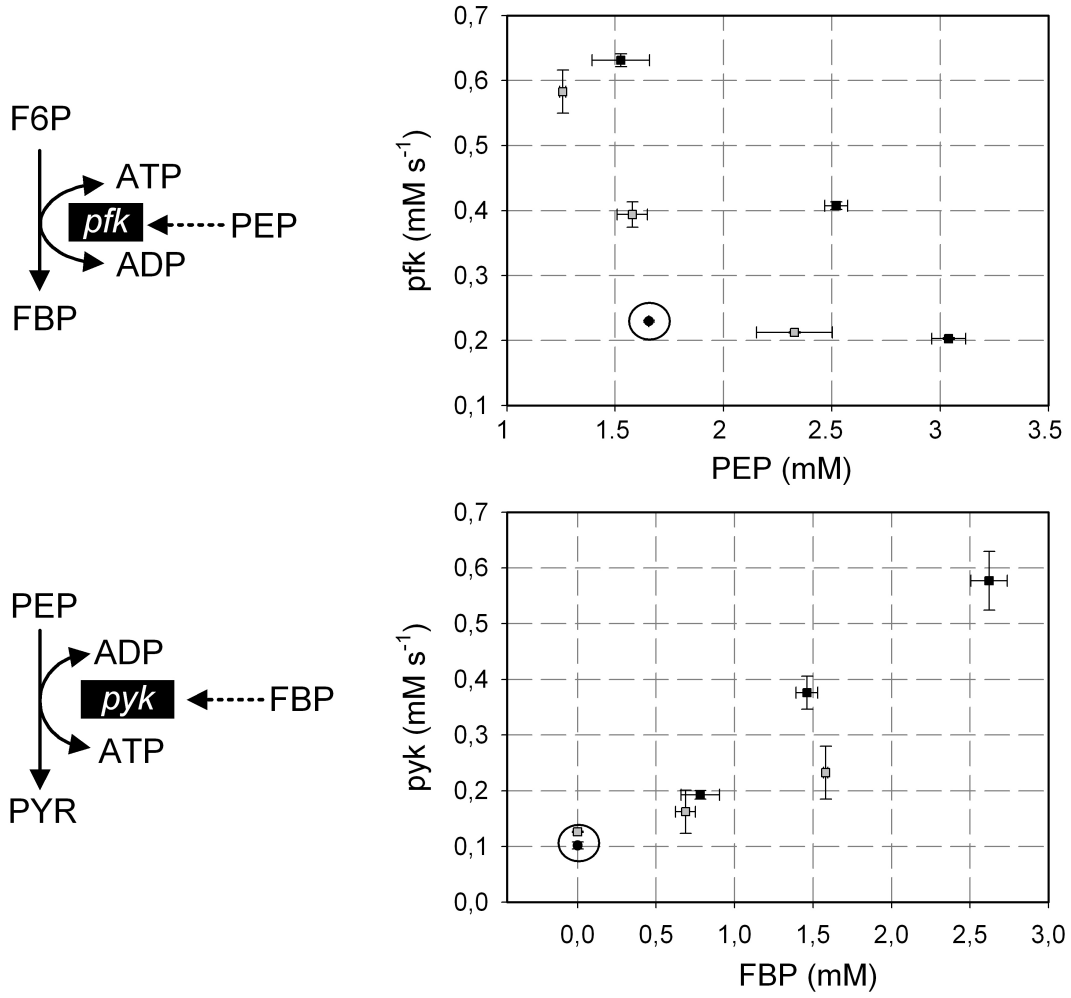

Figure 5.35.: Fluxes of phosphofructokinase (pfk) and pyruvate kinase (pyk) are plotted against the concentration of their regulatory effectors PEP and FBP in experiments with glycolytic flux. Fed-batch process (black dot), glucose (grey squares) and glucose anaerobic (black squares).

In accordance with *in vitro* studies (Kotlarz and Buc 1982), the *in vivo* kinetics show inhibition of pfk with increasing PEP concentration. Consequently, the lowest PEP concentration was measured during glucose interval A (aerobic and anaerobic). The decline of PEP with increasing glycolytic flux was also noticed *in vivo* for *S. cerevisiae* (Wu *et al.* 2005, van den Brink *et al.* 2008). Several authors observed allosteric activation of pyk

by FBP (Johannes and Hess 1973, Malcovati and Valentini 1982). The linear correlation of FBP and flux through pyk supports this regulatory effect under *in vivo* conditions.

5.5.3. The lin-log approach

Elasticity coefficients are a quantitative measure to express kinetic properties shown in Figures (5.31)-(5.35). Basically, the elasticity coefficients within MCA express the ratio of metabolite de-/increase and reaction rate de-/increase. As shown above elasticity coefficients are straightforward estimated from steady state data using the double modulation method or the lin-log approach. The lin-log approach is exemplified by means of icdh fluxes (v_{icdh}) and citrate/isocitrate levels (x_{CIT}), which were evaluated with Eq.(5.15).

$$\frac{v_{\mathrm{icdh}}}{v_{\mathrm{icdh},0}} = 1 + \varepsilon_{\mathrm{CIT}}^{\mathrm{icdh}} \cdot \ln\left(\frac{x_{\mathrm{CIT}}}{x_{\mathrm{CIT},0}}\right) \tag{5.15}$$

The only unknown in Eq.(5.15) is the elasticity of citrate/isocitrate towards icdh, which was estimated with the lin-log approach as $\varepsilon_{\mathrm{CIT}}^{\mathrm{icdh}} = 1.38$. In Figure (5.36) the lin-log model is opposed to the measurements.

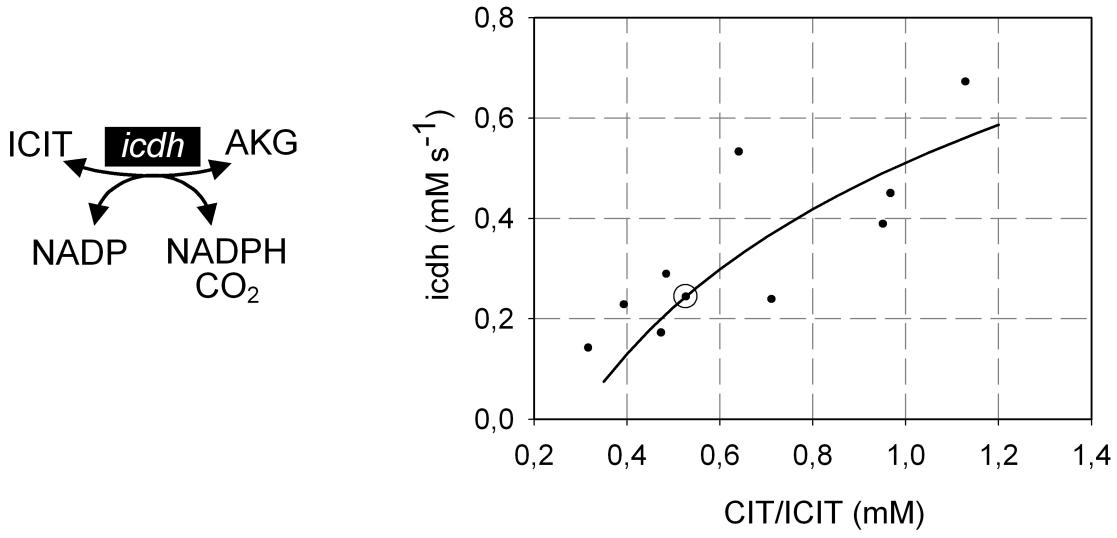

Figure 5.36.: Measured CIT/ICIT concentrations and icdh reaction rates are opposed to the lin-log model in Eq.(5.15).

The relationship of fluxes and metabolite concentrations is well reflected by the hyperbolic lin-log model. However, rather the value of the elasticity coefficient than the descriptive properties of the applied model is important in the sense of MCA. As shown in section

5.2.3 an accurate description of experimental data does not necessarily imply a correct estimate of the elasticity coefficient. A detailed in-silico study and identifiability analysis of elasticity coefficients is given by Nikerel *et al.* (2006 and 2009).

If more than one metabolite effects the reaction rate, more elasticities are included in the lin-log model. Figure (5.37) exemplifies the aforementioned inhibition of pfk by PEP ($\varepsilon^{pfk}_{PEP} = -0.89$), considering additional influences of the substrate FBP ($\varepsilon^{pfk}_{FBP} = 0.48$).

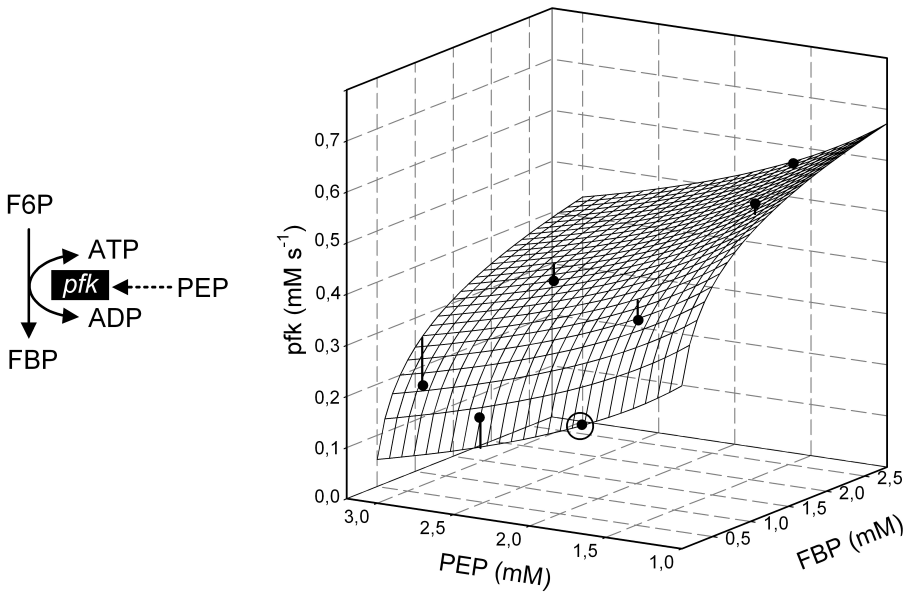

Figure 5.37.: Measured PEP and FBP concentrations are plotted against the flux through pfk (dots). The surface depicts a lin-log model with two parameters $\varepsilon^{pfk}_{FBP} = 0.48$ and $\varepsilon^{pfk}_{PEP} = -0.89$. Error of predictors are indicated by perpendicular lines between data points and surface.

Figure (5.37) visualizes the lin-log model and deviations of its predictions with experimental data. Activation of pfk by the product FBP was observed in pfk from rat skeletal muscle (Tornheim 1985) and a strong activating effect of fructose-2,6-bisphosphate on pfk is reported by Avigad (1981). Inhibition of pfk by ATP and activation by AMP are not considered in the lin-log model as the concentrations of adenylates were constant in all experiments. However, they are predominant effectors in other studies (Teusink *et al.* 2000, Chassagnole *et al.* 2002, van den Brink *et al.* 2008).

5.5.4. Redox and energy cofactors

Catabolic and anabolic reactions are coupled by redox and energy cofactors. The catabolic reactions provide phosphorylation and reducing power which satisfy anabolic demands for biosynthesis and maintenance. Hofmeyr and Cornish-Bowden (2000) investigated the regulation of such an economic system, consisting of one block of catabolic supply and a second block of anabolic demand. The authors could show that when flux is controlled by one block, the other block determines to which degree the concentration of the linking metabolite is homeostatically maintained.

The homeostatic maintenance of ATP might cause that regulatory effects of reactions towards ATP are not revealed by steady state experiments. For example, two contrary regulatory mechanisms are conceivable. One possibility is, that an increase of ATP might be compensated by a decrease of ATP producing reactions, due to feedback inhibition. Conversely, feedback inhibition is not required if the demand block has high elasticity towards ATP. In this case, an increase of ATP is compensated by an increase of ATP consuming reactions.

Hofmeyr and Cornish-Bowden (2000) could show, that feedback inhibition of biosynthetic pathways is required to maintain homeostatic concentrations away from thermodynamic equilibrium. There is no thermodynamic equilibrium in case of anabolic demand and catabolic supply. Therefore, feedback inhibition of ATP on central metabolic pathways is not necessarily required to maintain a constant ATP level.

Actually, glucose uptake by bacterial pts is not effected by energy cofactors, such as hexokinase in yeast which is inhibited by ATP. Furthermore, there are contradictory findings wether pfk is inhibited by ATP. Zheng and Kemp (1992) found that ATP inhibition of pfk is minimal at pH 7. The increased concentration of ATP during the aerobic glucose experiment (observed similarly in the fed-batch experiment) indicates absence of ATP inhibition. Detailed information about regulatory effects of ATP and other cofactors is not revealed by RMT experiments. Rather, the results suggest that energy and redox cofactors are tightly controlled at constants levels. Further discussion about the implications of metabolic homeostasis regarding the ability to control flux by variations of metabolite levels is given by Kacser and Acerenza (1993) or by Thomas and Fell (1996).

5.6. Thermodynamic analysis

The second law of thermodynamics constrains metabolite concentrations and defines feasible ranges of Gibbs energy of reaction, considering directions of reactions and operation of the network. Metabolome data and information about directions of metabolic fluxes of the fed-batch process and the RMT experiments were subjected to NET analysis using the anNET software (Zamboni *et al.* 2008). Figure (5.38) shows feasible ranges of Gibbs energies of reactions in the fed-batch process.

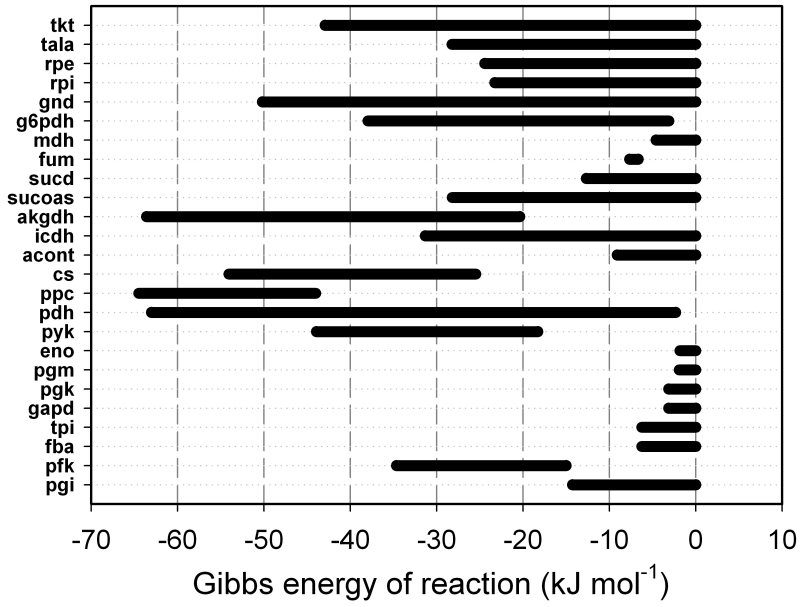

Figure 5.38.: Feasible ranges of Gibbs energies of reactions in the fed-batch process estimated by NET analysis.

The results show, that except of pfk and pyk most reactions of glycolysis are limited to a range of Gibbs energy close to zero and operate near thermodynamic equilibrium. Reactions that operate far from equilibrium have a displacement from zero, that is at least 10 kJ mol^{-1} (Zamboni *et al.* 2008). In particular decarboxylations catalyzed by akgdh, pdh, icdh and ppc are far from equilibrium. Also the reaction channeling glucose into PPP and TCA (g6pdh and cs) have large Gibbs energies of reaction. Kümmel *et al.* (2006) report similar results for an *E. coli* data set, with the exception that fba is far from equilibrium. The reason for this disagreement is the high FBP concentration (1.11 mM) of the employed data set of Schaub *et al.* (2006). Here, the FBP pool was below 0.1 mM, constraining $\Delta_r G_{\mathrm{fba}}$ close to zero.

In case of PPP only g6pdh could be identified as far from equilibrium. As metabolites of PPP were not quantified the Gibbs energies of reactions catalyzed by rpi, rpe, tkt and tala are rather uncertain. However, near equilibrium conditions were assumed by Chassagnole *et al.* (2002) for these reactions. Additionally, Kümmel *et al.* (2006) found that rpi and rpe are close to equilibrium in *E. coli*.

Initially, the consistency of several data sets were not approved by NET analysis. Data sets from the RMT experiments with glucose (aerobic and anaerobic) were not feasible with the measured metabolite concentrations and the assumed directions of metabolic fluxes. The anNET software identified the reaction of enolase as not feasible with the provided data of 2PG/3PG and PEP. This caused a revision of PEP and 2PG/3PG measurements. The pool size of 2PG/3PG was estimated using IDMS and therefore considered as reliable. All data sets were feasible when removing constraints of measured PEP concentrations. The reason for unfeasible PEP concentrations is clarified in Figure (5.39), which opposes constraints on PEP concentrations and measured values.

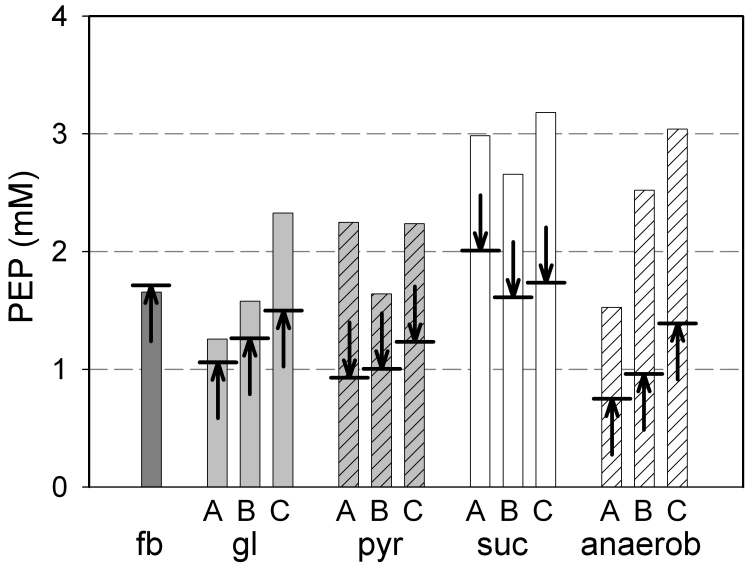

Figure 5.39.: Arrows indicate maximal PEP concentrations (in case of a glycolytic flux) and minimal PEP concentrations (in case of a gluconeogenic flux) estimated by NET analysis. They are opposed to measured PEP concentrations (values in mM).

NET analysis revealed, that the glycolytic flux from 2PG towards PEP catalyzed by enolase constrains PEP to a maximum value. In case of the RMT experiments with glucose this maximum is below the measured pool size and caused the discrepancies. In case of experiments with gluconeogenic substrates succinate and pyruvate the reverse flux

through enolase constrains PEP to minimal concentrations, which agree with measured values. Figure (5.39) illustrates, that even if absolute values are contradictory, the relative profiles of constraints and measured PEP levels suggest correlation of thermodynamic constraints and steady state metabolite profiles.

NET analysis further predicted feasible concentration ranges of non-measured metabolites and isobaric metabolites G6P/F6P, 2PG/3PG and citrate/isocitrate, which are shown in Figure (5.40).

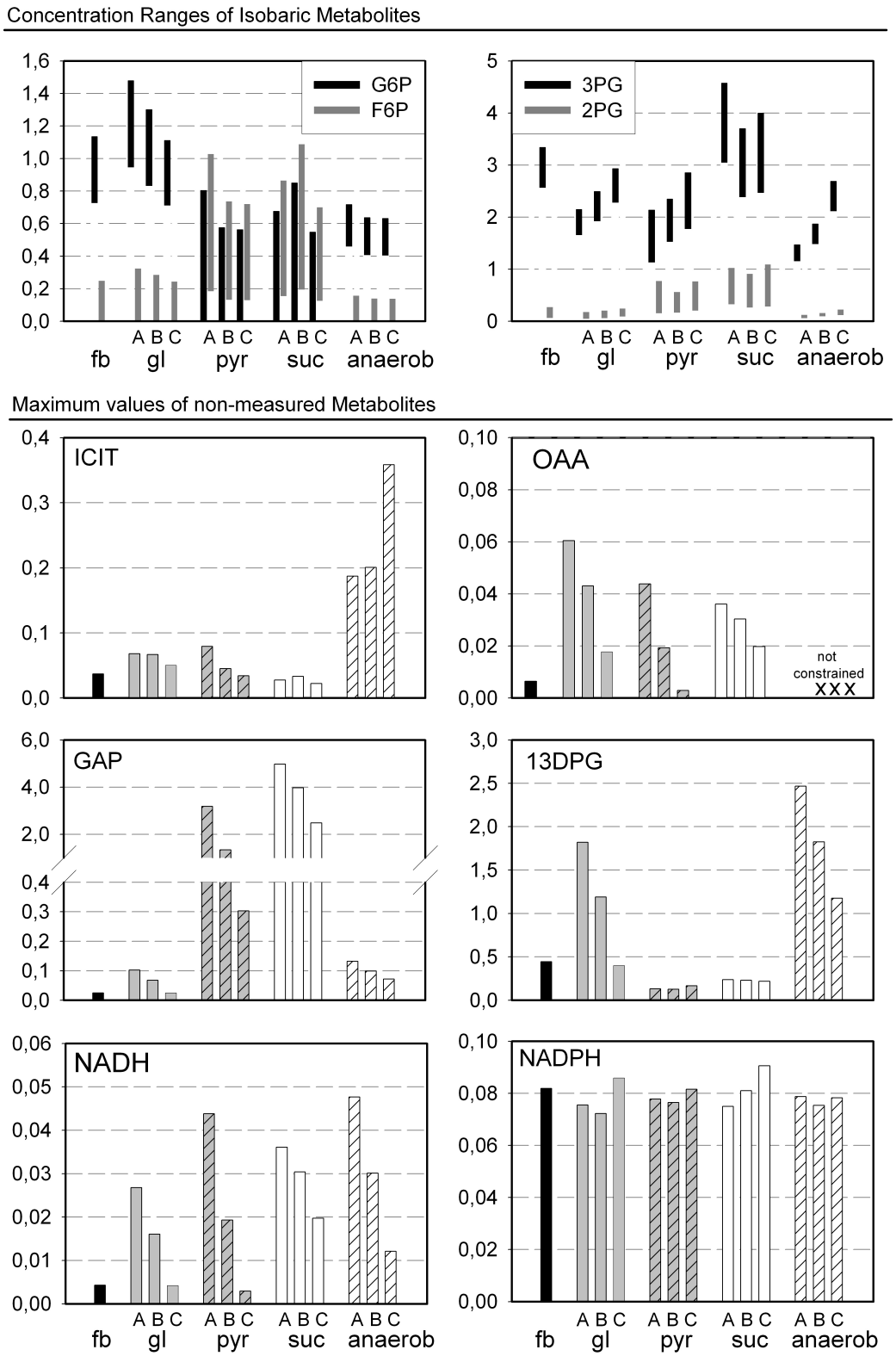

Figure 5.40.: Concentration ranges of non-measured metabolites and isobaric metabolites G6P/F6P, 2PG/3PG and CIT/ICIT predicted by NET analysis (values in mM).

The pooled concentration of isobaric molecules G6P/F6P were resolved by NET analysis. A glycolytic flux requires negative Gibbs energy for the reaction catalyzed by pgi. This thermodynamic constraint restricts F6P concentrations to approximately 1/4 of G6P concentrations. This result agrees with data from enzymatic assays, which distinguished G6P and F6P and yielded low F6P concentrations (data not shown). The thermodynamic constraint relaxes if pgi flux occurs in the reverse direction. In this case a minimum F6P concentration is required. Similar thermodynamic constraints confine 2PG and 3PG to small concentration ranges. Isocitrate constitutes only a fractional amount of the citrate/isocitrate pool and is limited to concentrations below 0.1 μM. During anaerobic cultivation TCA flux was not restricted to a particular direction, hence there is no constraint on the isocitrate pool size. This relief from thermodynamic constraints might be an explanation for increased concentrations of other organic acids during anaerobic cultivation. Maximum OAA concentrations are also very low and obviously related to measured malate concentrations. Depending on the direction of glycolytic flux, GAP and 13DPG are also restricted to small concentration ranges. As expected, the reduced redox cofactors NADPH and NADH are limited to concentrations in the low μM range. The maximum concentration of these metabolites are close to values measured in the batch RMT experiments (40-80 μM NADPH and 10-30 μM NADH).

Obviously, the stepwise profile of measured metabolites propagates into thermodynamic constraints of non-measured metabolites. This observation rises the question whether a metabolite profile originates from thermodynamic constraints or if it is kinetically regulated. Hofmeyr (1995) shows that metabolic control parameters are composed of a thermodynamic term and a kinetic term. Further relationships of thermodynamics and metabolic control analysis are discussed by Heuett *et al.* (2008). Nielsen (1997) shows, that in particular, substrates and products of reactions operating near equilibrium have high elasticity coefficients. Reactions far from equilibrium are less often regulated by their substrate, rather they are actively regulated by activation/inactivation and also enzyme synthesis. With this assumption, Kümmel *et al.* (2008) were able to spot regulatory sites by NET analysis of metabolome data of *E. coli*.

5.7. Metabolic Control Analysis

Studies of kinetics and thermodynamics as shown above are conceptually different from the control structure of a metabolic system. Observations during RMT experiments demonstrated robustness and simultaneous flexibility of *E. coli*'s central metabolism to disturbances in the environment. Hofmeyr and Cornish-Bowden (1991) proposed that such a well-regulated system would have control sites that could act on the flux without great perturbation in metabolite concentrations. In this sense, potential control sites and global properties of *E. coli*'s central metabolism were evaluated by means of MCA.

5.7.1. Metabolic network and stoichiometry

It is important to be conscious that MCA is a linearization around a reference state, the fed-batch process in this case. As all variables are normalized to the reference state it is not possible to consider reactions with a zero flux in the reference state. The stoichiometric model employed for MCA consisted of the reactions 1-30 in Table (A.9). Reactions with zero flux in the fed-batch process are: the irreversible steps of gluconeogenesis (fbp and pps), the anapleurotic reaction ppck and all reactions of mixed acid fermentation. Oxidative phosphorylation was considered by composite reactions of electron transfer from NADH to cytochrome oxidase and ATP synthesis (nadhox). Similarly a reaction fadh2ox is considered for regeneration of $FADH_2$. ATP produced by oxidative and substrate-level phosphorylation is consumed by several processes. They are represented by a reaction ATPase, which was applied by several authors (Thomas and Fell 1998, Teusink *et al.* 2000, Wang *et al.* 2004). Biomass formation consisted of the same biosynthetic fluxes applied in the MFA model (Table (A.12)). Reactions of the MCA model are summarized in Table (A.10).

Beside the metabolic network the bioreactor processes have to be included in the analysis. Several authors developed methods to incorporate bioreactor processes into MCA (Wang and Hatzimanikatis 2006a,b) and converse approaches separating control of physical and biological components (Small 1994, Snoep *et al.* 1994). Without further discussion of these approaches the problem will be addressed by a proper definition of system boundaries as shown in Figure (5.41).

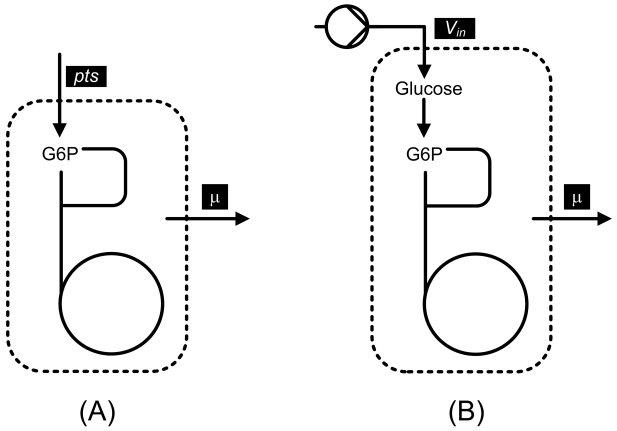

Figure 5.41.: System boundaries of (A) the intracellular model, (B) the fed-batch model.

Commonly, system boundaries separate compounds that are internal to a system from external variables. System boundaries in Figure (5.41 A) separate metabolic processes from bioreactor processes and a constant influx through pts serves as input. Bioreactor processes are incorporated by inclusion of extracellular glucose and a constant glucose influx V_{in}. It is important to notice that only if glucose has no regulatory effect on intracellular fluxes, it is possible to consider extra- and intracellular compounds as internal variables of the system (spatial separation by the cell envelope has no further influence on normalized fluxes and concentrations). Cellular growth serves as output of both systems. Biomass is not considered as an external variable, as it is supposed to have no effect on internal variables and fluxes. In the following, models according to Figure (5.41 A) and (5.41 B) will be termed the intracellular model and the fed-batch model.

The metabolic network without bioreactor processes, consisted of 30 reactions and 34 metabolites. In order to deduce the reduced stoichiometric matrix $\mathbf{N}_R$, the $m = 34$ metabolites considered in the metabolic network are separated into m_d dependend and m_i independent metabolites. The complete (34×30) stoichiometric matrix $\mathbf{N}$ had rank 29 and therefore $m_d = 5$ metabolites are dependent. The dependent metabolites are recovered by inspection of conserved moieties, that are ATP/ADP, NAD/NADH, NADP/NADPH, FAD/$FADH_2$ and SucCoA/AcCoA/CoA. Consequently, ADP, NADH, NADPH, $FADH_2$ and CoA were defined as dependent metabolites. The reduced stoichiometric matrix was derived from the remaining 29 independent metabolites and is related to the complete network by the link matrix as described by Eq.(3.34).

In case of the bioreactor model, $\mathbf{N}$ is augmented by one flux (glucose feed) and one metabolite (external glucose). The structural properties are not altered and there are still 5 dependent metabolites in the network.

5.7.2. Elasticity coefficients

According to Eq.(3.62) control coefficients are derived from elasticity coefficients, which describe kinetic properties of the entire network. To this end, matrix **E** is required, which comprises elasticity coefficients of 30 reactions (rows of **E**) towards 34 metabolites (columns of **E**). Elasticity coefficients of reactions far from thermodynamic equilibrium were estimated with the lin-log approach in Eq.(5.11). In case of reactions near equilibrium, elasticity coefficients were derived with the approach proposed by Nielsen (1997) (see Eq.(3.56)).

A Monte Carlo simulation was applied to account for uncertainties in metabolite concentrations, fluxes and distances from thermodynamic equilibrium. Wang *et al.* (2004) introduced the framework of MCA under uncertainty, a monte carlo sampling procedure to generate either random elasticities or partially incorporate knowledge about kinetic mechanisms. Similarly, metabolite concentrations, fluxes and Gibbs energies of reactions were randomly sampled from intervals, following from experimental data and NET analysis. Reactions close to equilibrium are listed in Table (5.6) together with the range of Gibbs free energy estimated by NET analysis. As $\Delta_r G$ approximates zero, elasticity coefficients according to Eq.(3.56) have abnormally high values and the maximum limit of Gibbs free energy is -1. A near-equilibrium assumption was made for sucoas, rpe, rpi,tkt and tala, by setting the minimum of $\Delta_r G$ to a default value of -10 kJ mol^{-1}.

Table 5.6.: Ranges of Gibbs energy of reactions in the MCA model, which are considered close to equilibrium (given in kJ mol^{-1}). Default values are -10 and -1 kJ mol^{-1}, in case no information from NET analysis is available.

Reaction	$\Delta_r G_{\min}$	$\Delta_r G_{\max}$
pgi	-14,28	-1,00
fba	-6,26	-1,00
tpi	-6,26	-1,00
gapd	-3,31	-1,00
pgk	-3,31	-1,00
pgm	-1,93	-1,00
eno	-1,82	-1,00
acont	-9,12	-1,00
sucoas	-10,00	-1,00
fum	-7,67	-6,67
mdh	-4,61	-1,00
rpe	-10,00	-1,00
rpi	-10,00	-1,00
tkt1	-10,00	-1,00
tala	-10,00	-1,00

The relationship between elasticity coefficients and $\Delta_r G$ according to Eq.(3.56) is illustrated in Figure (5.42).

The majority of elasticity coefficients is within a range of 0.25 and 1, due to the non-linear dependency on Gibbs energy of reaction. Eq.(3.56) implies that elasticities of substrates and products are correlated and only differ in algebraic sign. There are other approaches that involve near equilibrium assumptions within MCA. Wang *et al.* (2004) separated reactions in a model of glycolysis in *S. cerevisae* into forward and backward reactions and point out, that for reversible reactions elasticities with respect to substrate and products are correlated. Groen *et al.* (1986) derived similar equations to calculate elasticity coefficients from mass-action ratios and equilibrium coefficients. Other approaches that account for near-equilibrium assumption involve time hierarchy analysis to calculate control coefficients from elasticities of slow reactions (Kholodenko *et al.* 1998) or to solve problems with identification of elasticities in dynamic lin-log models (Nikerel *et al.* 2009).

Elasticity coefficients of 15 reactions far from equilibrium were assigned with the lin-log approach, which was integrated into the Monte Carlo procedure. Upper and lower boundaries for concentrations of all metabolites in the network were defined for the reference

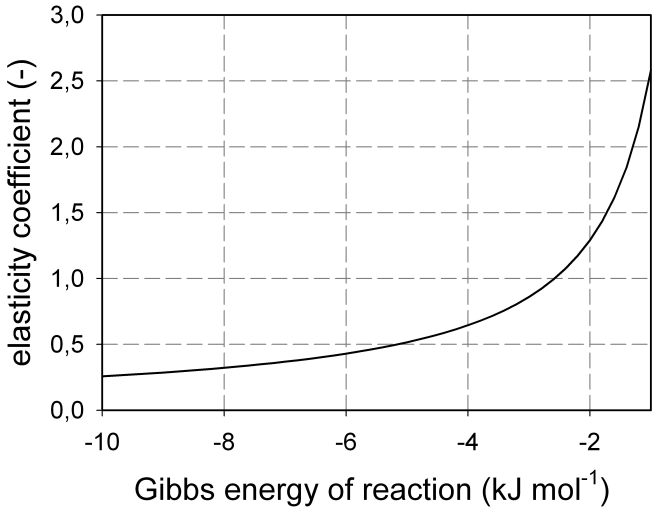

Figure 5.42.: Relationship between $\Delta_r G$ and the elasticity coefficient of a substrate towards a reaction near thermodynamic equilibrium.

state and the 12 metabolic states from fed-batch RMT experiments. The limits where either 10% of measured concentrations or the feasible ranges estimated by NET analysis in case of non-measured metabolites. Concentrations of metabolites with regulatory effect on a particular reaction rate were randomly sampled from these intervals. Similarly, metabolic fluxes were sampled from intervalls defined by results of MFA and FBA. 5000 data sets of metabolic fluxes and metabolite concentrations were evaluated with the lin-log approach. The results are discussed in the following, together with information about potential regulatory effectors, found in literature.

Glucose uptake by pts

Several authors report that the PEP/PYR ratio is a regulatory factor of glucose uptake by pts (Liao *et al.* 1996, Kremling *et al.* 2008). Clark and Holms (1976) report inhibition of pts by hexose phosphate such as G6P. Also Kaback (1969) identified two inhibitory sites of pts in *E. coli* membrane isolations, one specific for G6P the other for G1P. Consequently PEP, pyruvate and G6P were considered as regulatory effectors of pts in the MCA network. Figure (5.43) shows elasticities of pts obtained from 5000 data sets as described above.

Generally, the box plots illustrate the distribution of estimated elasticities. Boxes contain 50% of the data and the line inside indicates the median. Error bars correspond to the 25th and 75th percentiles and dots to the 5th and 95th percentiles. Similar to a

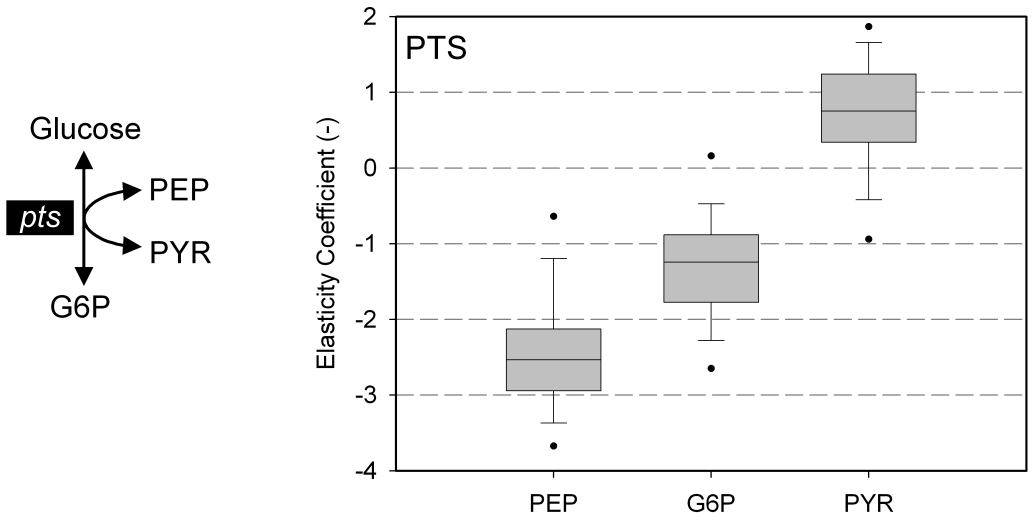

Figure 5.43.: Distribution of 5000 elasticity coefficients of pts towards PEP, G6P and PYR. Boxes contain 50% of the data and the line inside indicates the median. Error bars correspond to the 25th and 75th percentiles and dots to the 5th and 95th percentiles.

method proposed by Joshi *et al.* (2006), the distribution reflects confidence intervals of the estimates. The narrower the distribution, the better the estimates. Elasticity coefficients of pts towards PEP are exclusively negative and 50% of the values are between -2 and -3. A weaker inhibition of G6P is reflected in significantly higher elasticities. Elasticities of pyruvate are positive in most cases. Inhibition of G6P is in accordance with the findings of Clark and Holmes (1976) and was also applied within a dynamic model of central metabolism of *E. coli* (Chassagnole *et al.* 2002). However, the results of PEP and pyruvate are contradictory to the rate expression proposed by Liao *et al.* (1996). Their results imply a positive elasticity of PEP towards pts and a negative value of pyruvate, as a high PEP/PYR ratio increases v_{max} and reduces affinity of glucose in their kinetic expression for pts. More recent findings of Kremling *et al.* (2008) support the elasticities of PEP and pyruvate in Figure (5.43). The authors show, that high glycolytic fluxes are realized by lowering the PEP concentration. Their detailed model of the pts output (phosphorylation of pts enzmyes) suggests, that pyruvate increases with increasing glucose uptake while PEP decreases. This model results in negative elasticity coefficients of PEP and positive values for pyruvate.

As shown in Figure (5.41) the linking metabolite of bioreactor processes and metabolic processes is external glucose. In case of the fed-batch model, the elasticity of pts towards extracellular glucose was randomly sampled between 0.5 and 1.

Glycolysis

The activity of pfk is sensitive to various metabolites. The effects of several activating compounds (ADP, AMP and FBP) and inhibitors (PEP, ATP) were described (Kotlarz and Buc 1982, Zheng and Kemp 1992). Zheng and Kemp (1992) observed only weak inhibition of pfk by ATP at pH 7 and cooperativity with the substrate F6P. The substrate F6P, the product FBP and the inhibitor PEP were considered to have an effect on pfk reaction rate as shown in Figure (5.44).

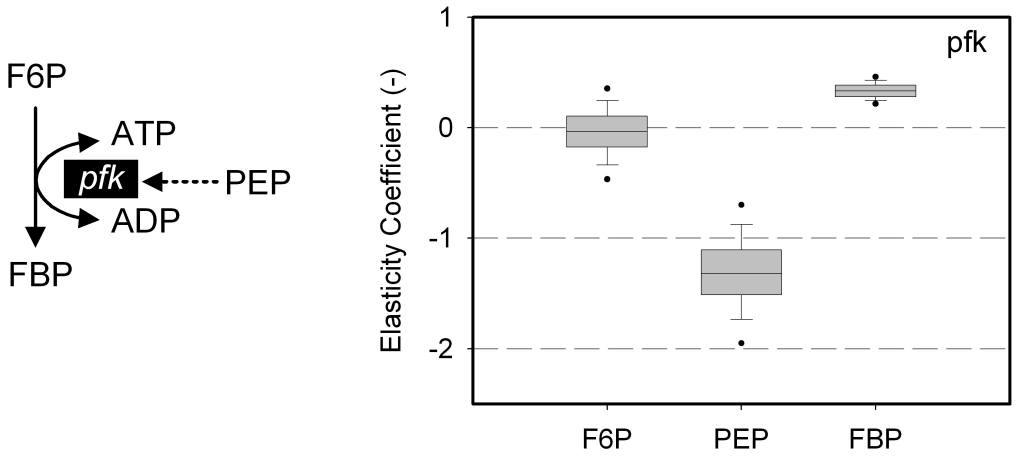

Figure 5.44.: Distribution of 5000 elasticity coefficients of pfk towards F6P, PEP and FBP.

The distribution of elasticity of pfk towards F6P reflects, that F6P has only marginal influence on the reaction rate. In contrast, the results suggest strong inhibition of pfk by PEP and activation by FBP. Positive elasticities of pfk towards the product FBP, agree with observations of Tornheim (1985) and Avigad (1981).

Two reactions, pyk and ppc divert PEP from the lower part of glycolysis. They both have the same activator FBP. Wohl and Markus (1972) report that activation of ppc by FBP is even stronger in presence of AcCoA. Regulatory effects of ATP and AMP on pyk and ppc were not considered. Elasticities for both reactions are shown in in Figure (5.45).

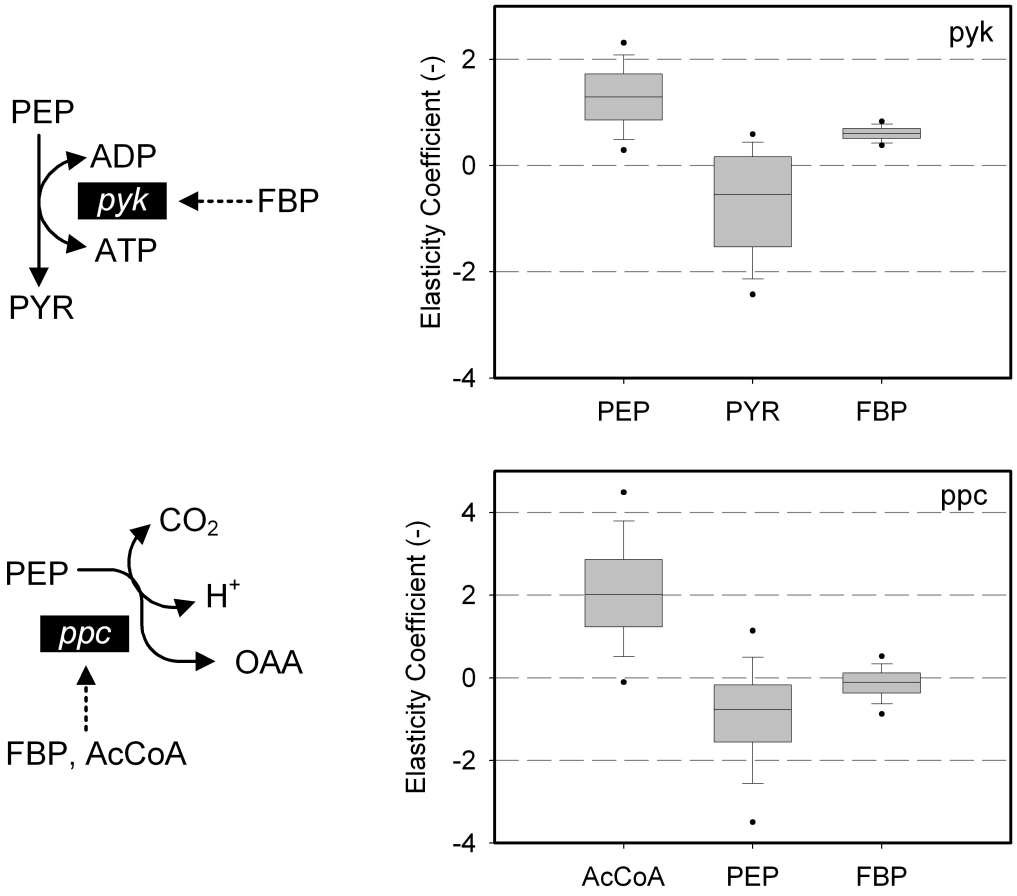

Figure 5.45.: Distribution of 5000 elasticity coefficients of pyk and ppc towards substrates, products and regulatory effectors.

Activating compounds have exclusively positive elasticity coefficients, such as FBP on pyk or AcCoA on ppc. Activation of ppc by FBP as proposed by Wohl and Markus (1972) is not observed here, rather the result suggests a negative effect of PEP.

No regulatory effectors of pdh are reported so far. As Chassagnole *et al.* (2002) assumed Hill kinetics for pdh, pyruvate is considered as the only effector. Distributions of elasticities are shown in Figure (5.46).

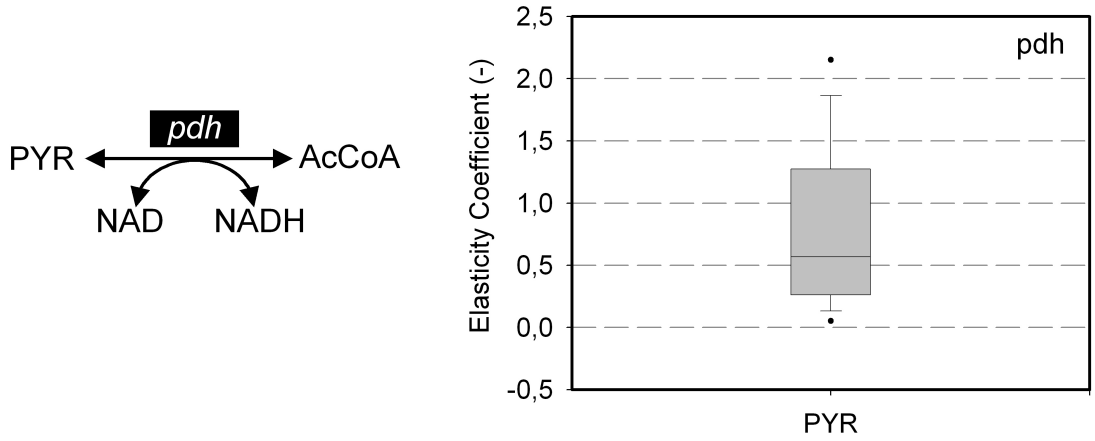

Figure 5.46.: Distribution of 5000 elasticity coefficients of pdh towards pyruvate.

Chassagnole *et al.* (2002) estimated a Hill coefficient of 3.68 for pdh. As elasticity coefficients are limited between 0 and the Hill coefficient the estimates for pdh are reasonable.

TCA cycle

Citrate synthase catalyses the introduction of AcCoA into the TCA cycle and may be an important site of control. Robinson *et al.* (1983) report sigmoidal dependence of cs on AcCoA and OAA concentrations and inhibition by NADH and AKG. Elasticity coefficients of cs towards the substrates AcCoA and OAA are shown in Figure (5.47). No regulatory effects of NADH and AKG were identified from the available data set. Further, the distribution of elasticities of icdh towards the substrate isocitrate is depicted.

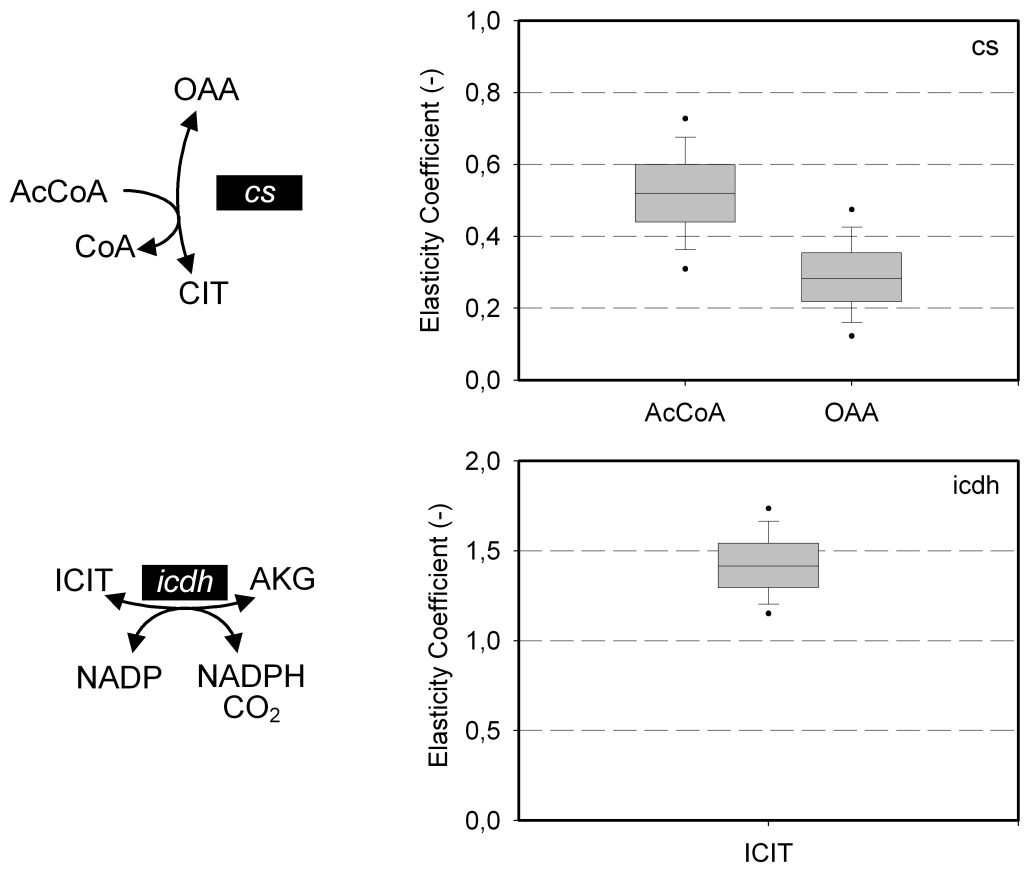

Figure 5.47.: Distribution of 5000 elasticity coefficients of cs and icdh towards their substrates.

As expected, both reactions have positive elasticities towards their substrates. Even if OAA was not experimentally determined, the constraints resulting from NET analysis allow good estimates of elasticities towards this metabolite. The second substrate of icdh is NADP, which was constant in all samples and was not considered to have regulatory effects on icdh. A potential inhibition of cs by NADH was introduced by sampling random elasticities between -1 and -0.1. This subsequent assignment is formally not correct, as elasticities of cs towards OAA and AcCoA were estimated without consideration of NADH.

The enzyme complex akgdh is supposed to be a key regulatory step of TCA and regulation has been considered in the biochemical literature very rarely. Inhibition by SucCoA, ATP, NADH and activation by AMP is reported (Strumilo 2005). A recent study suggests that OAA inhibits akdh and allows coordinated activity within TCA cycle (Frank *et al.* 2007). The data did not reveal any information about akgdh kinetics and elasticities of akgdh towards the substrate AKG were randomly sampled between 0.5 and 1.5. Inhibition by OAA was considered with a random elasticity between -1 and -0.1.

Succinate dehydrogenase is expressed during aerobic respiration rather than the related enzyme fumarate reductase (Yankovskaya *et al.* 2003). Sucd is a membrane bound enzyme complex with covalently bound FAD. Figure (5.48) shows elasticities of sdh towards succinate and FAD.

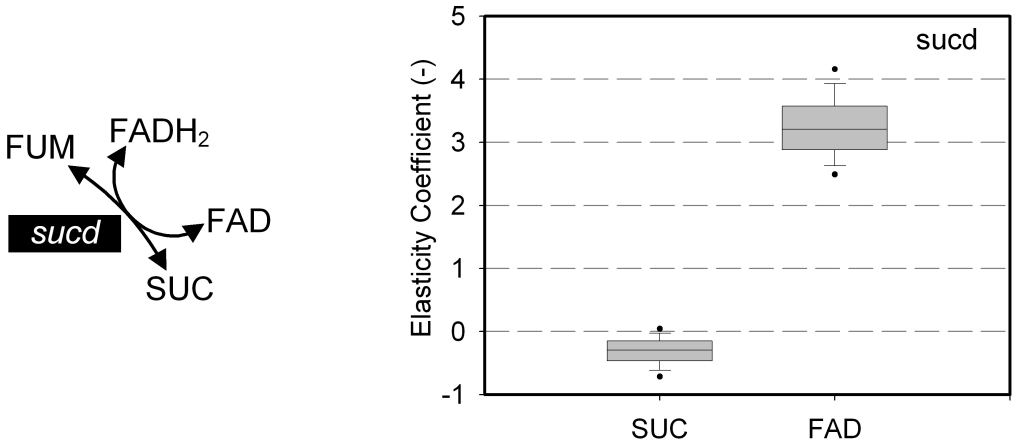

Figure 5.48.: Distribution of 5000 elasticity coefficients of sucd towards succinate and FAD.

Beside a small negative effect of succinate the activation of sucd by FAD is distinctive. Sucheta *et al.* (1992) show, that sucd behaves as a diode that essentially allows electron flow in one direction only. This behavior is addressed to the oxidation state of a redox group on the enzyme, what might be an explanation of the high elasticity towards FAD as observed here.

Pentose Phosphate Pathway

The elasticity of G6P towards g6pdh was estimated from experimental data. The results are shown in Figure (5.49). Beside G6P other regulatory effectors will certainly control PPP flux. Chassagnole *et al.* (2002) consider regulation of the oxidative part of PPP by NADPH inhibition of g6pdh and gnd. Moritz *et al.* (2000) found also NADPH inhibition of g6pdh and gnd in *Corynebacterium glutamicum*. Even if gnd is inhibited by additional metabolites (ATP, FBP, GAP, E4P, Ru5P) the authors conclude that both enzymes and thus PPP flux is mainly regulated by the ratio of NADPH and NADP concentrations. Inhibition of NADPH was considered by randomly sampling elasticities between -1 and -0.1 for g6pdh and gnd towards NADPH.

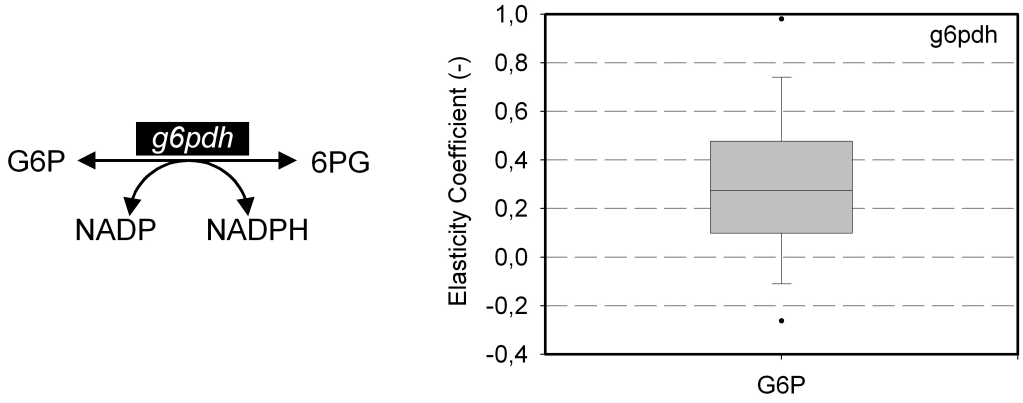

Figure 5.49.: Distribution of 5000 elasticity coefficients of g6pdh towards G6P/F6P.

Energy metabolism (nadhox, fadh2ox and ATPase)

Oxidative phosphorylation was considered by composite ATP producing and NADH/ $FADH_2$ consuming reactions nadhox and fadh2ox. Detailed information about kinetics of electron transfer from NADH to cytochrom oxidase and ATPase reaction is not available. Here it is assumed that these processes are irreversible and follow linear kinetics. The elasticites of such first order kinetics towards the substrate are always equal to 1. First order kinetics for the ATPase reaction were applied by Teusink *et al.* (2000) and by Wang *et al.* (2004). Thomas and Fell (1998) investigated the effect of different elasticities coefficients for ATPase towards ATP and included inhibition by ADP. Here, no inhibition of ATPase by ADP is assumed and only ATP effects the rate of ATP hydrolysis with $\varepsilon_{ATP}^{ATPase} = 1$.

Biomass formation

The elasticities of specific growth rate follow straightforward from biosynthetic fluxes in the reference state, the fraction of carbon moles from all precursors φ_i (Table (A.12)) and the elasticities of biosynthetic fluxes. The method is detailed by Wang and Hatzimanikatis (2004a,b). According to one of their assumptions it is hypothesized that biosynthetic fluxes depend only on the concentration of the particular precursor.

All assumptions about elasticity coefficients are summarized in Table (A.10). Each reaction in the model is either classified as close to equilibrium or the metabolites with regulatory effects on the reaction are listed.

5.7.3. Flux control coefficients

Within one iteration of the Monte Carlo sampling loop elasticities of actively regulated reactions and reactions near-equilibrium were sampled as described above and collected in matrix **E**. Further, the reference state was randomly chosen from the data set of the fed-batch process, in order to define matrices $\mathbf{J}_0$ and $\mathbf{x}_0$. Control coefficients were estimated according to Eq.(3.61) and (3.62). The (Log)linear approach of Hatzimanikatis and Bailey (1996) was additionally applied and yielded identical results.

Control structure of the intracellular model

Figure (5.50) shows mean values of 5000 flux control coefficients estimated with the Monte Carlo approach for the intracellular model.

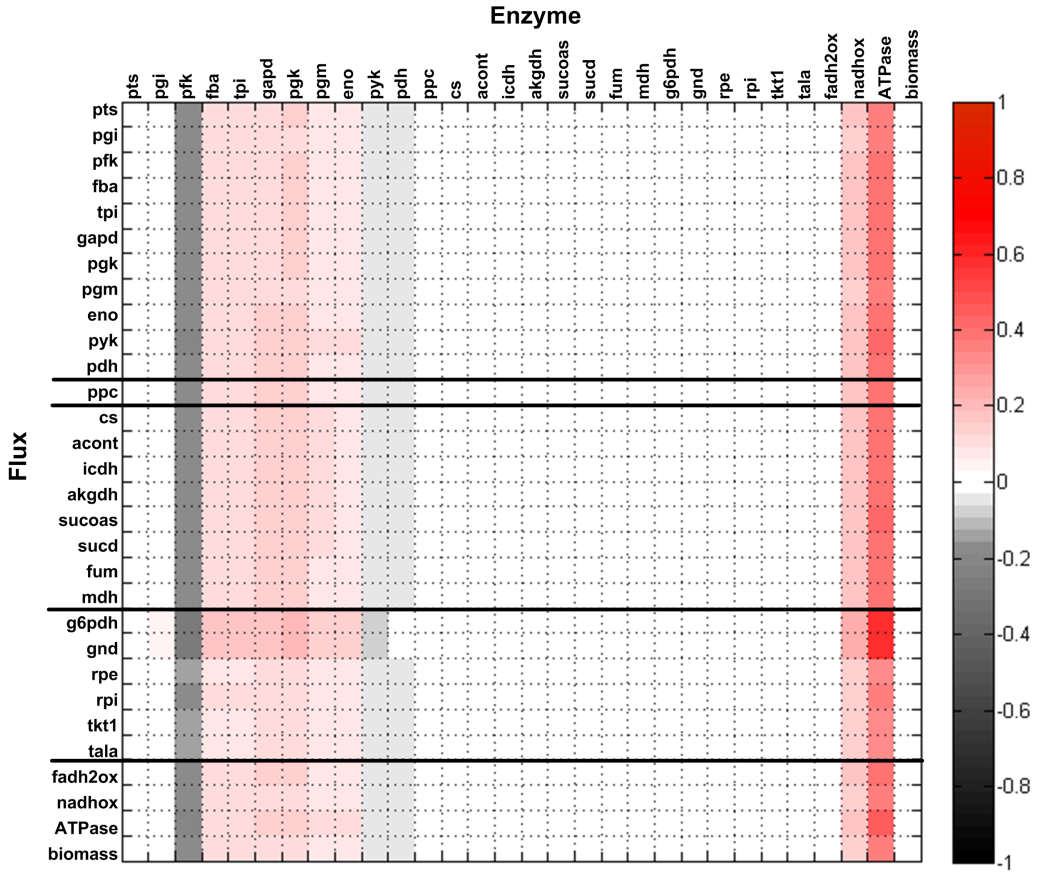

Figure 5.50.: Flux control coefficients of intracellular reactions of the stoichiometric model in Table (A.10). Extracellular glucose and glucose feeding is not considered. Each column corresponds to the perturbed enzyme. The rows correspond to the responding steady state flux.

A striking feature of control coefficients in Figure (5.50) is the fact that most of them are zero or at least smaller than one. Control coefficients express the percentage change of the steady state flux in response to a unit percentage change of enzyme activity. Hence, values between zero and one are reasonable, as it was shown that small control coefficients are a prerequisite of a stable metabolic network (Mazat *et al.* 1996). Briefly, the authors argument is, that high control coefficients would have deleterious effects on metabolism in case of small variations in enzyme levels.

A further distinct characteristic in Figure (5.50) are the high control coefficients of ATPase on all reactions in the network. Koebmann *et al.* (2002) enhanced hydrolization of ATP by expression of a soluble ATPase in *E. coli*. This ATPase is uncoupled from other reactions, in the same way as the ATP consuming reaction in the MCA model. The studies of Koebmann *et al.* (2002) gave almost similar results as shown in Figure (5.50): the demand for ATP controls the flux. The significance of this finding is, that the majority

of flux control resides not inside but outside the pathway. For example, Groen *et al.* (1986) found that control of gluconeogenesis in rat liver cells resides partially in steps outside the pathway, such as a adenine-nucleotide translocating reaction.

The small control coefficients agree with the several unsuccessful attempts to increase glycolytic flux by overexpression of enzymes, that were considered as rate-limiting steps. For example, experimental studies have shown, that pts and hence glucose uptake has no control on fluxes of central metabolism. Ruyter *et al.* (1991) studied effects of variation of the membrane-bound pts enzyme II^{Glc}, which catalyzes glucose transport and phosphorylation. They estimated a low control coefficient of this enzyme on growth rate and glucose metabolism, as it is the case in Figure (5.50).

Furthermore, the control coefficients suggest that enzymes of TCA have no flux control. Such behavior was experimentally observed by Walsh and Koshland (1985). In their study carbon flow of *E. coli* growing on glucose was not affected by a 90% decrease in the level of citrate synthase.

Beside control by ATPase, flux control is distributed among reactions of glycolysis. The actively regulated reactions pfk, pyk and pdh have negative control coefficients, whereas reactions at equilibrium have positive values. In order to examine whether these values are significant and not just uncertainties propagated through the Monte Carlo procedure, the distribution of flux control coefficients was analyzed in more detail. Figure (5.51) shows the distribution of 5000 control coefficients of pfk on every reactions in the network by means of box plots.

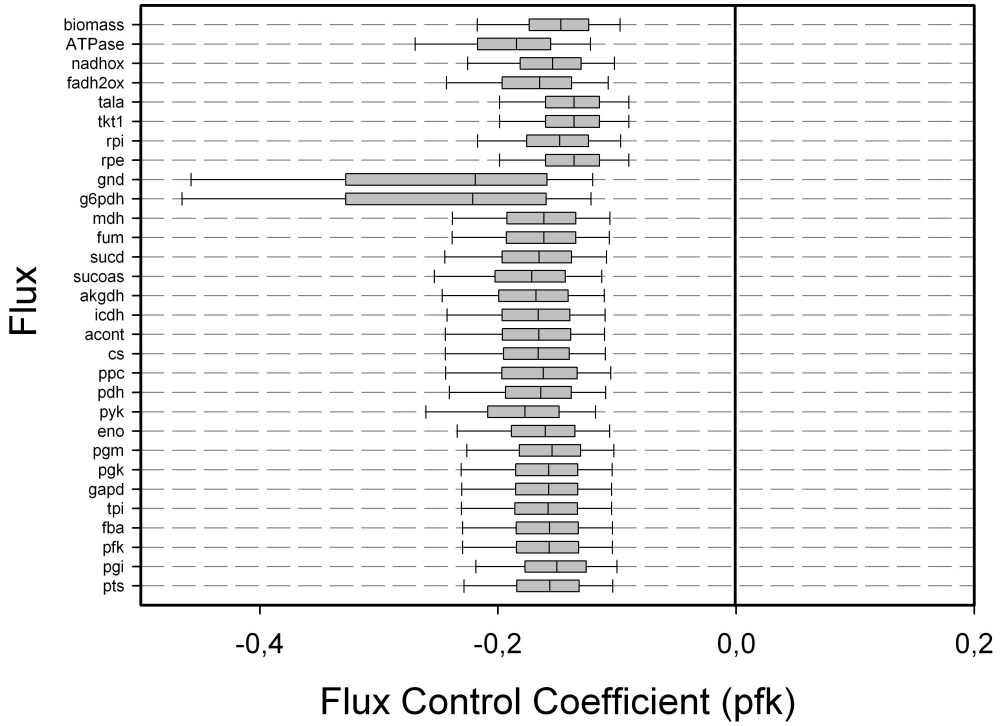

Figure 5.51.: Distribution of flux control coefficients of pfk. Boxes contain 50% of the data and the line inside indicates the median. Error bars indicate 25th and 75th percentiles.

The boxplots indicate, that the control coefficients of pfk are significantly below zero and for most reactions constrained to a small range between -0.3 and -0.1. Similarly, control coefficients of reactions near equilibrium have exclusively positive control coefficients. The control coefficients of pyk are also significantly below zero, whereas in case of pdh the values are distributed between -0.1 and 0.1 and hence not significant.

An explanation of this control structure is certainly the feedback-loop of pyk activation by FBP and allosteric inhibition of pfk by PEP, in combination with reactions near thermodynamic equilibrium located in-between. It is reported that enzymes near the beginning of a pathway subject to feedback inhibition would tend to have low flux control coefficients, whilst the flux control coefficients of the enzymes after the feedback metabolite would tend to be high (Kacser and Burns 1973, Thomas and Fell 1996). Since pfk and pyk are commonly considered the controlling steps in glycolysis several metabolic engineering approaches included alteration of these enzymes. However, overexpression of pfk and pyk did not yield significant changes of glycolytic flux (Schaaff *et al.* 1989). Sauer *et al.* (1999) have shown, that a pyk-deficient *E. coli* exhibits exactly the same glucose consumption and growth rate as the parental strain. Despite the overall physiological similarities, they found significant changes at the branch point between glycolysis and TCA, which are not

predicted by the control coeffcients in Figure (5.50). Such large perturbations caused by complete inactivation of an enzyme are of course not covered by the MCA model.

Emmerling *et al.* (1999) studied the effect of overexpressing heterologous and native pfk and pyk in *E. coli*. During exponential growth the alteration of these enzymes had neither an effect on growth rate nor on glucose consumption. Actually, overexpression of heterologous pfk and pyk had a negative effect of glucose uptake in the stationary phase, as suggested by the negative control coefficients in Figure (5.50).

Control structure of the fed-batch model

The control structure in Figure (5.50) represents the internal control structure, as extracellular components and bioreactor processes are not considered. In the same way as above, 5000 flux control coefficients of the fed-batch model were estimated with the Monte Carlo procedure. In analogy to Figure (5.50) flux control coefficients are shown in Figure (5.52).

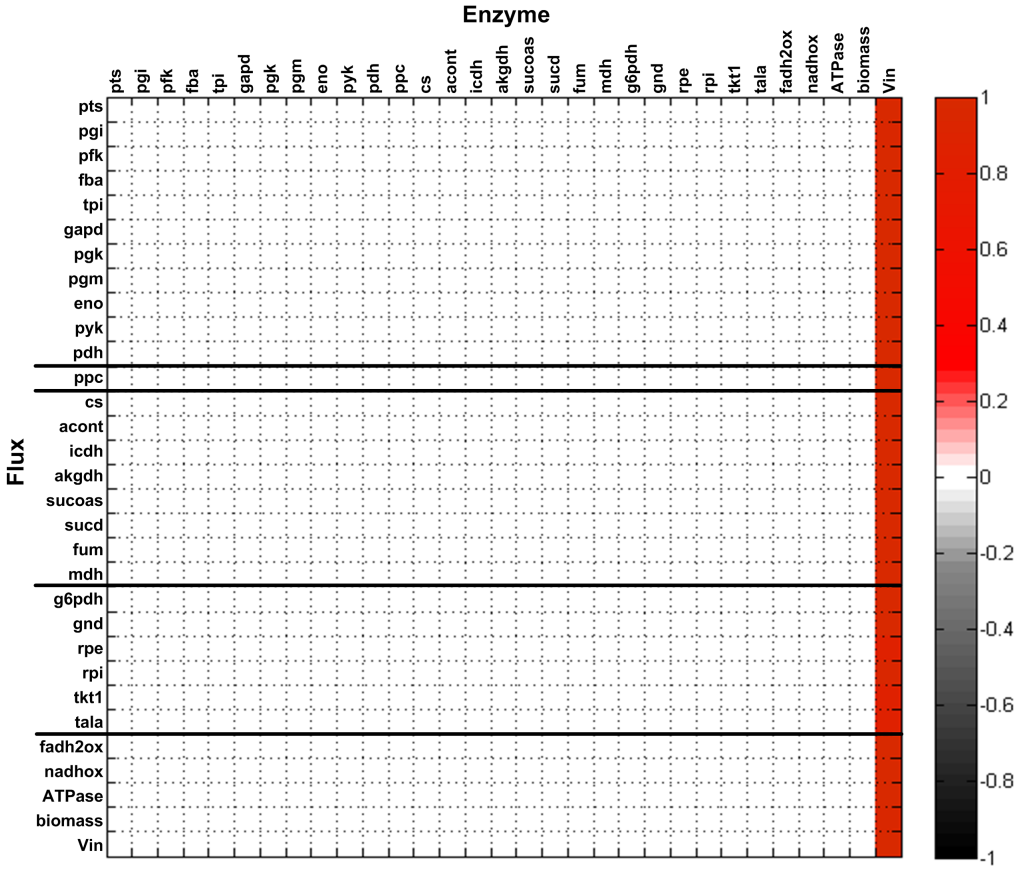

Figure 5.52.: Flux control coefficients of intracellular reactions of the stoichiometric model in Table (A.10) including extracellular glucose and glucose feeding. Each column corresponds to the perturbed enzyme. The rows correspond to the responding steady state flux.

Without exception, control coefficients of intracellular reactions are indistinguishable from zero and control coefficients of glucose feeding rate V_{in} are close to 1. Distributions of control coefficients of glucose feeding rate on every reaction in the network are shown in Figure (5.53).

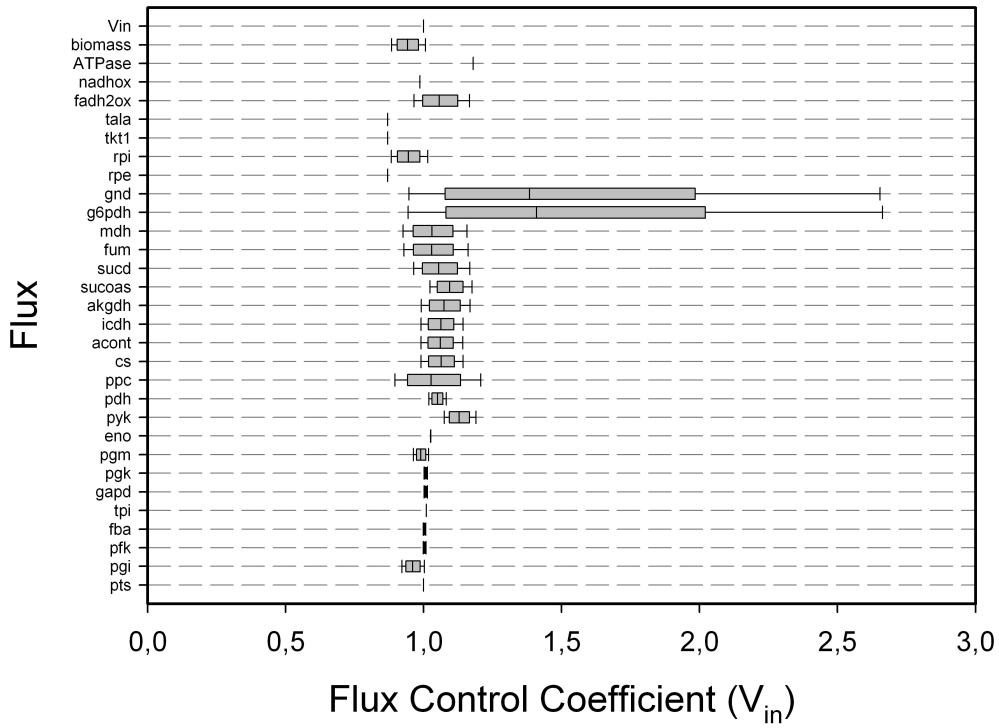

Figure 5.53.: Distribution of flux control coefficients of the feeding rate V_{in}. Boxes contain 50% of the data and the line inside indicates the median. Error bars indicate 25th and 75th percentiles.

Even if some reactions like g6pdh and gnd vary in a quite large interval, most control coefficients are confined to a range close to one. Such behavior is expected intuitively if properties of the fed-batch process are considered. A unit percentage change of any enzyme activity will not change the flux through any reaction, because the glucose influx is constant. In contrast, a unit percentage change of glucose influx results in proportional increase of every other flux, as glucose metabolism is far below the maximal capacities. Although these results appear obvious, they are not based upon mass balances as in case of stoichiometric MFA. Even if MCA is based upon linearization in the steady state, there are no constrains such as $\mathbf{Nv} = \mathbf{0}$, rather an increase of glucose influx increases glucose concentration, which then causes a cascade of regulatory mechanisms.

Wang *et al.* (2004) include stability analysis into the stochastic MCA approach, as they discard a set of elasticity coefficients if the steady state is not stable. Stability analysis is based on the eigenvalues of the Jacobian matrix, which have negative real parts in case of an asymptotically stable steady state. The MCA models applied above did not provide evidence for stability. Stability was evaluated for the (Log)linear approach by the equation provided by Wang *et al.* (2004). Even if a few samples of fluxes, metabolites

and elasticities resulted in negative real parts of eigenvalues, most solutions had some positive values and were therefore not stable. This behavior was confirmed by numerical integration of the lin-log model, as not all concentrations returned to the steady state after initial perturbations. There are several reasons for instabilities, such as missing reactions in the stoichiometric network (structural properties) or additional allosteric regulatory mechanisms, required to enforce stability of certain metabolites. Finally, the concentration ranges of the various metabolites differ in orders of magnitude (from μM to the mM range) and might cause instabilities.

6. Conclusions and Future Perspectives

Conclusions

Rapid Media Transition (RMT) was developed and evaluated as an experimental approach for steady state analysis of metabolic pathways. In contrast to commonly applied continuous cultures, the approach allows steady state analysis of cells in parallel to non-stationary fed-batch fermentation processes. Metabolic capabilities and control mechanisms of central metabolism of *Escherichia coli* under conditions of a fed-batch process were identified with the proposed approach.

Different carbon sources were immediately utilized after *E. coli* cells were separated from a 30 L scale fed-batch process and transferred into a lab-scale stirred-tank bioreactor. Several experimental results indicated a metabolic steady state during the 15-18 minutes RMT experiments. Respiratory rates were constant within a few minutes after the perturbation and the concentrations of substrates were continuously decreasing. The constant metabolite pools measured during perturbation experiments gave further evidence of steady state conditions inside the cells. Large changes of fluxes occurred during the perturbation experiments, which were attributed to altered metabolite concentrations. Despite large changes of the metabolic state, concentrations of redox and energy cofactors were not disturbed by RMT experiments. These findings are exemplified in Figure (6.1). Results from a RMT experiment with succinate are compared to measurements during the fed-batch process.

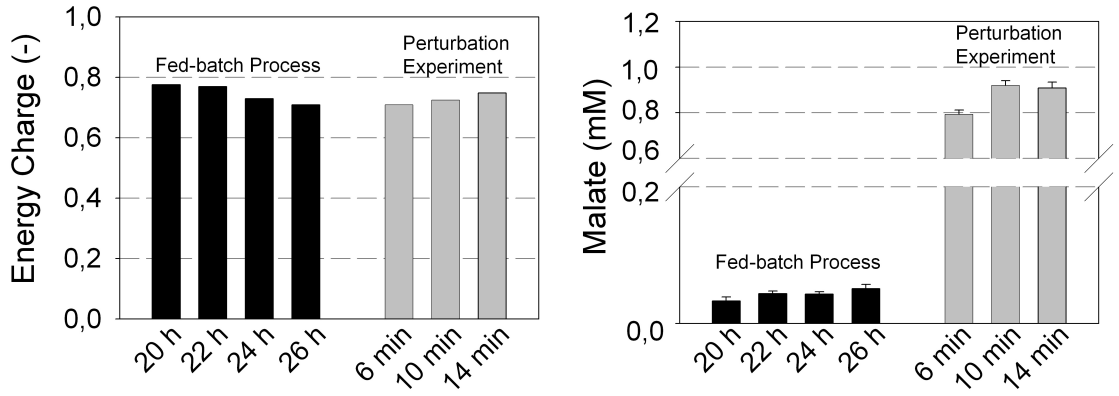

Figure 6.1.: Energy charge and intracellular malate concentrations during the fed-batch cultivation process (black bars) and a perturbation experiment with succinate (grey bars).

The results in Figure (6.1) are representative for other metabolite profiles. In response to environmental disturbances, some metabolites increased by an order of magnitude, while others are almost not affected. The increase of intracellular malate during the perturbation experiment correlates with increased TCA flux. Energy cofactors such as ATP were unperturbed, reflected by a constant energy charge.

RMT experiments were performed in fed-batch operation mode, such that perturbations are controlled and almost no substrate (and by-products) was detected in the cultivation medium. This strategy provides several advantages, such as accurate estimation of specific uptake rates by the amount of supplied substrate. Further, the approach is particularly suited for measurements of intracellular metabolites with the differential method (Taymaz-Nikerel *et al.* 2009). Concentrations of extracellular metabolites are low, as metabolome analysis is performed with fresh medium and without formation of by-products during analysis.

The presented approach clarifies that beside analytical and computational techniques, cultivation strategies and well-engineered process control is required for systems biotechnology approaches. The wide-spread chemostat experiments might serve as a convenient approach to achieve constant growth and exchange fluxes, but the physiology of cells is divers and probably differs from most industrial bioprocesses. In contrast, RMT experiments enable metabolic analysis of cells, equipped with the same enzymes, transporters and cofactors as provided in an interesting phase of a fed-batch production process.

Experimental data of RMT experiments was subjected to kinetic analysis, thermodynamic analysis and metabolic control analysis. All approaches gave further insights into properties of central metabolic pathways. For example, an increasing FBP pool in combination with decreasing PEP and 2PG/3PG levels is one of several characteristics associated with increasing glycolytic fluxes. Similar profiles are reported for *E. coli* (Schaub and Reuss 2008) and for the dynamic response of yeast to a glucose pulse (Wu *et al.* 2005). Kinetic analysis in combination with thermodynamic analysis raised the question, whether such behavior is a consequence of kinetic or thermodynamic effects. Several theoretical studies addressed the influence of kinetic and thermodynamic interactions in metabolic networks (Thomas and Fell 1996, Hofmeyr and Cornish-Bowden 2000). Here, NET analysis was successfully applied to distinguish reactions operating near and far from thermodynamic equilibrium. It was shown that thermodynamic constraints on maximal intracellular metabolite concentrations correlate with measured values.

Active response to the environment at the level of gene expressions is a widespread phenotype of *E. coli* and is supposed to be a common strategy that the cell can use when it

faces environmental changes (Ishii *et al.* 2007). Another response at the level of metabolic regulation was shown in this work. With RMT experiments it was possible to distinguish regulatory mechanisms at the different levels of cellular function. Short-term disturbances did hardly affect enzyme levels as confirmed by proteom analysis, whereas large flux changes were realized by relatively small changes of metabolite levels. The results confirmed stability and robustness of central metabolism, but further they revealed its remarkable flexibility. *E. coli* reacts almost instantly to changes in the environment and effectively redirects metabolic fluxes. Metabolic Control Analysis of central metabolism revealed the control structure of such a tightly controlled system. Kinetic and thermodynamic information was included in a stochastic MCA approach. The results revealed that control coefficients of reactions in central metabolism are small. Such a robust control structure agrees with the stable physiological characteristics observed during the experiments. The only reaction with significant flux control was identified as reaction hydrolyzing ATP. In fact, it was shown by Koebmann *et al.* (2002), that glycolytic flux in *E. coli* is controlled by the demand for ATP.

Perspectives

Beside fermentation strategies and data analysis, the obvious and intensively discussed uncertainties associated with microbial metabolome analysis require attention in future studies. It was shown that cellular leakage during cold methanol quenching of *E. coli* results in high systematic errors. Even though cold glycerol reduced cellular leakage, small metabolites such as pyruvate were still susceptible to leakage. An effective and leakage-free inactivation of metabolism, as well as quantitative extraction of metabolites have to be assured, to get the *in vivo* metabolic snapshot into sharper focus. This is particularly important in the light of metabolic homoeostasis, as only small perturbations of metabolite concentrations are expected in response to genetic and environmental disturbances. Further, ^{13}C based flux analysis is required in order to obtain information about reactions and pathways, which are hardly assessable by measurements of extracellular rates only.

RMT experiments with single-gene knockout mutants will probably gain further insight about properties of metabolic pathways in the face of combined genetic and environmental perturbations. Comparative studies with genetically modified strains could be performed in parallel steady state experiments in milliter-scale stirred-tank bioreactors.

Straight-forward data analysis requires a graphical user interface which enables proper and flexible data management for metabolic control analysis. The network structure should

be presented graphically in combination with regulatory effectors and information about thermodynamic equilibrium of a particular reaction. Integration of NET analysis into the framework of MCA under uncertainty is a promising possibility to combine information about thermodynamic and kinetic regulation in metabolic networks.

Finally, future studies will apply RMT experiments to problems such as decreasing productivity during industrial production processes. Metabolic properties of a biosynthetic pathway will be analyzed with the presented tools in order to identify limiting enzymes in the producer strain or limiting resources in the cultivation medium.

7. References

Abdel-Hamid A, Attwood M, Guest J (2001): Pyruvate oxidase contributes to the aerobic growth efficiency of *Escherichia coli*. *Microbiology* 147, 1483-1498.

Acerenza L, Cornish-Bowden A (1997): Generalization of the double-modulation method for in situ determination of elasticities. *Biochem J* 327, 217-223.

Al Zaid Siddiquee K, Arauzo-Bravo MJ, Shimizu K (2004): Metabolic flux analysis of pykF gene knockout *Escherichia coli* based on ^{13}C-labeling experiments together with measurements of enzyme activities and intracellular metabolite concentrations. *Appl Microbiol Biotechnol* 63, 407-417.

Alberts B, Bray D, Lewis J, Raff M, Roberts K, Watson JD (1995): Molekularbiologie der Zelle. VCH Verlag.

Alvarez-Vasquez F, Sims KJ, Cowart LA, Okamoto Y, Voit EO, Hannun YA (2005): Simulation and validation of modelled sphingolipid metabolism in *Saccharomyces cerevisiae*. *Nature* 433, 425-430.

Andersen KB, von Meyenburg K (1980): Are growth rates of *Escherichia coli* in batch cultures limited by respiration? *J Bacteriol* 144, 114-123.

Avigad G (1981): Stimulation of yeast phosphofructokinase activity by fructose-2,6-bisphosphate. *Biochem Biophys Res Commun* 102, 985-991.

Bailey J (1991): Toward a science of metabolic engineering. *Science* 252, 1668-1675.

Becker SA, Feist AM, Mo ML, Hannum G, Palsson BØ, Herrgard MJ (2007): Quantitative prediction of cellular metabolism with constraint-based models: the COBRA Toolbox. *Nat Protoc* 2, 727-738.

Bernhardt J, Büttner K, Scharf C, Hecker M (1999): Dual channel imaging of two dimensional electropherograms in *Bacillus subtilis*. *Electrophoresis* 20, 2225-2240.

Bernhardt J, Weibezahn J, Scharf C, Hecker M (2003): *Bacillus subtilis* during feast and famine: visualization of the overall regulation of protein synthesis during glucose starvation by Proteome analysis. *Genome Res* 13, 224-237.

Bolten CJ, Kiefer P, Letisse F, Portais JC, Wittmann C (2007): Sampling for metabolome analysis of microorganisms. *Anal Chem* 79, 3843-3849.

Buchholz A, Takors R, Wandrey C (2001): Quantification of intracellular metabolites in *Escherichia coli* K12 using liquid chromatographic-electrospray ionization tandem mass spectrometric techniques. *Anal Biochem* 295, 129-137.

Buziol S, Bashir I, Baumeister A, Claassen W, Noisommit-Rizzi N, Mailinger W, Reuss M (2002): New bioreactor-coupled rapid stopped-flow sampling technique for measurements of metabolite dynamics on a subsecond time scale. *Biotechnol Bioeng* 80, 632-636.

Calhoun MW, Oden KL, Gennis RB, de Mattos MJ, Neijssel OM (1993): Energetic Efficiency of *Escherichia coli*: Effects of Mutations in Components of the Aerobic Respiratory Chain. *J Bacteriol* 175, 3020-3025.

Canelas AB, Ras C, ten Pierick A, van Dam JC, Heijnen JJ, van Gulik WM (2008): Leakage-free rapid quenching technique for yeast metabolomics. *Metabolomics* 4, 226-239.

Chao YP, Patnaik R, Roof WD, Young RF, Liao JC (1993): Control of gluconeogenic growth by pps and pck in *Escherichia coli*. *J Bacteriol* 175, 6939-6944.

Chassagnole C, Noisommit-Rizzi N, Schmid JW, Mauch K, Reuss M (2002): Dynamic modeling of the central carbon metabolism of *Escherichia coli*. *Biotechnol Bioeng* 79, 53-71.

Clark B, Holms WH (1976): Control of the sequential utilization of glucose and fructose by *Escherichia coli*. *J Gen Microbiol* 96, 191-201.

Drysch A, Massaoudi ME, Mack C, Takors R, de Graaf A, Sahm H (2003): Production process monitoring by serial mapping of microbial carbon flux distributions using a novel sensor reactor approach: II 13C-labeling-based metabolic flux analysis and L-lysine production. *Metab Eng* 5, 96-107.

Edwards JS, Ibarra RU, Palsson BØ (2001): In silico predictions of *Escherichia coli* metabolic capabilities are consistent with experimental data. *Nature Biotechnol* 19, 125-130.

Edwards JS, Palsson BØ (2000): The *Escherichia coli* MG1655 in silico metabolic genotype: its definition, characteristics, and capabilities. *Proc Natl Acad Sci USA* 10, 5528-5533.

Edwards JS, Palsson BØ (1998): How will bioinformatics influence metabolic engineering? *Biotechnol Bioeng* 58, 162-169.

Ehlde M, Zacchi G (1997): A general formalism for metabolic control analysis. *Chem Eng Sci* 52, 2599-2606.

Emmerling M, Bailey JE, Sauer U (1999): Glucose catabolism of *Escherichia coli* strains with increased activity and altered regulation of key glycolytic enzymes. *Metab Eng* 1, 117-127.

Faijes M, Mars AE, Smid EJ (2007): Comparison of quenching and extraction methodologies for metabolome analysis of *Lactobacillus plantarum*. *Microb Cell Fact* 6, 27.

Farewell A, Neidhardt FC (1998): Effect of Temperature on In Vivo Protein Synthetic Capacity in *Escherichia coli* . *J Bacteriol* 180,4704-4710.

Fell DA (1992): Metabolic control analysis: a survey of its theoretical and experimental development. *Biochem J* 186, 313-330.

Ferenci T (2008): Bacterial physiology, regulation and mutational adaptation in a chemostat environment. *Adv Microb Physiol* 53, 169-229.

Fischer E, Sauer U (2003a): Metabolic flux profiling of *Escherichia coli* mutants in central carbon metabolism using GC-MS. *Eur J Biochem* 270, 880-891.

Fischer E, Sauer U (2003b): A novel metabolic cycle catalyzes glucose oxidation and anaplerosis in hungry *Escherichia coli*. *J Biol Chem* 278, 46446-46451.

Frank RA, Price AJ, Northrop FD, Perham RN, Luisi BF (2007): Crystal structure of the E1 component of the *Escherichia coli* 2-oxoglutarate dehydrogenase multienzyme complex. *J Mol Biol* 368, 639-651.

Giersch C (1988a): Control analysis of metabolic networks. 1. Homogeneous functions and the summation theorems for control coefficients. *Eur J Biochem* 174, 509-513.

Giersch C (1988b): Control analysis of metabolic networks. 2. Total differentials and general formulation of the connectivity relations. *Eur J Biochem* 174, 515-519.

Giersch C (1994): Determining elasticities from multiple measurements of steady-state flux rates and metabolite concentrations: Theory. *J Theor Biol* 169, 89-99.

Giersch C (1995): Determining elasticities from multiple measurements of steady-state flux rates and metabolite concentrations. Application of the multiple modulation method to a reconstituted pathway. *Eur J Biochem* 227, 194-201.

Gottesman S, Neidhardt FC (1983) Global control systems. In: Beckwith J, Davies J, Gallant JA (eds) Gene function in prokaryotes. Cold Spring Harbor Laboratory, Cold Spring Harbor, NY.

Groen AK, van Roermund CW, Vervoorn RC, Tager JM (1986): Control of gluconeogenesis in rat liver cells. Flux control coefficients of the enzymes in the gluconeogenic pathway in the absence and presence of glucagon. *Biochem J* 237, 379-389.

Giersch C, Cornish-Bowden A (1996): Extending double modulation: combinatorial rules for identifying the modulations necessary for determining elasticities in metabolic pathways. *J Theor Biol* 182, 361-369.

Han MJ, Lee SY (2006): The *Escherichia coli* Proteome: Past, Present, and Future Prospects. *Microbiol Mol Biol Rev* 70, 362 -439

Hatzimanikatis V, Bailey JE (1996): MCA has more to say. *J Theor Biol* 182, 233-242.

Heijnen JJ (2005): Approximative kinetic formats used in metabolic network modeling. *Biotechnol Bioeng* 91, 534-545.

Heinrich R, Rapoport TA (1974): A linear steady-state treatment of enzymatic chains. General properties, control and effector strength. *Eur J Biochem* 42, 89-95.

Heinrich R, Rapoport SM, Rapoport TA (1977): Metabolic regulation and mathematical models. *Prog Biophys Mol Biol* 32, 1-82.

Heinrich R, Schuster S, (1996) The Regulation of Cellular Systems. Kluwer Academic Publishers, Dordrecht.

Henry CS, Broadbelt LJ, Hatzimanikatis V (2007): Thermodynamics-based metabolic flux analysis. *Biophys J* 92, 1792-805.

Heuett WJ, Beard DA, Qian H (2008): Linear analysis near a steady-state of biochemical networks: control analysis, correlation metrics and circuit theory. *BMC Systems Biology* 2, 44.

Hiller J, Franco-Lara E, Papaioannou V, Weuster-Botz D (2007a): Fast sampling and quenching procedures for microbial metabolic profiling. *Biotechnol Lett* 29, 1161-1167.

Hiller J, Franco-Lara E, Weuster-Botz D (2007b): Metabolic profiling of *Escherichia coli* cultivations: evaluation of extraction and metabolite analysis procedures. *Biotechnol Lett* 29, 1169-1178.

Hofmeyr JHS, Cornish-Bowden A (1991): Quantitative assessment of regulation in metabolic systems. *Eur J Biochem* 200, 223-236.

Hofmeyr JHS, Cornish-Bowden A, Rohwer JM (1993): Taking enzyme kinetics out of control; putting control into regulation. *Eur J Biochem* 212, 833-837.

Hofmeyr JHS (1995) Metabolic regulation: a control analytic perspective. *J Bioenerg Biomembr* 27, 479-90.

Hofmeyr JHS, Cornish-Bowden A (1996): Co-response analysis: a new experimental strategy for metabolic control analysis. *J Theor Biol* 182, 371-380.

Hofmeyr JHS, Cornish-Bowden A (2000): Regulating the cellular economy of supply and demand. *FEBS Lett* 476, 47-51.

Holms H (2001): Flux Analysis: A Basic Tool of Microbial Physiology. *Adv Microb Physiol* 45, 271-340.

Hoque MA, Ushiyama H, Tomita M, Shimizu K (2005): Dynamic responses of the intracellular metabolite concentrations of the wild type and pykA mutant *Escherichia coli* against pulse addition of glucose or NH_3 under those limiting continuous cultures. *Biochem Eng J* 26, 38-49.

Hua Q, Yang C, Baba T, Mori H, Shimizu K (2003): Responses of the central metabolism in *Escherichia coli* to phosphoglucose isomerase and glucose-6-phosphate dehydrogenase knockouts. *J Bacteriol* 185, 7053-7067.

Hua Q, Yang C, Oshima T, Mori H, Shimizu K (2004): Analysis of Gene Expression in *Escherichia coli* in Response to Changes of Growth-Limiting Nutrient in Chemostat Cultures. *Appl Env Micro* 70, 2354-2366.

Ingraham JL, Maaløe O, Neidhardt FC (1983): Growth of the Bacterial Cell. Sunderland, MA, Sinauer Associates Inc.

Ishii N, Nakahigashi K, Baba T, Robert M, Soga T, Kanai A, Hirasawa T, Naba M, Hirai K, Hoque A, Ho PY, Kakazu Y, Sugawara K, Igarashi S, Harada S, Masuda T, Sugiyama N, Togashi T, Hasegawa M, Takai Y, Yugi K, Arakawa K, Iwata N, Toya Y, Nakayama Y, Nishioka T, Shimizu K, Mori H, Tomita M (2007): Multiple high-throughput analyses monitor the response of *E. coli* to perturbations. *Science* 316, 593-597.

Jensen NB, Jokumsen KV, Villadsen J (1999): Determination of the phosphorylated sugars of the Embden-Meyerhoff-Parnas pathway in *Lactococcus lactis* using a fast sampling technique and solid phase extraction. *Biotechnol Bioeng* 63, 356-362.

Jenzsch M, Gnoth S, Beck M, Kleinschmidt M, Simutis R, Lübbert A (2006): Open-loop control of the biomass concentration within the growth phase of recombinant protein production processes. *J Biotechnol* 127, 84-94.

Johannes KJ, Hess B (1973): Allosteric kinetics of pyruvate kinase of *Saccharomyces carlsbergensis*. *J Mol Biol* 76, 181-205.

Joshi M, Seidel-Morgenstern A, Kremling A (2006): Exploiting the bootstrap method for quantifying parameter confidence intervals in dynamical systems. *Metab Eng* 8, 447-455.

Kaback HR (1969): Regulation of sugar transport in isolated bacterial membrane preparations from *Escherichia coli*. *Proc Natl Acad Sci USA* 63, 724-31.

Kacser H, Acerenza L (1993): A universal method of achieving increases in metabolite production. *Eur J Biochem* 216, 361-367

Kacser H, Burns JA (1979): Molecular democracy: Who shares the controls? *Biochem Soc Trans* 7, 1149-1160.

Kacser H, Burns JA, (1973): The control of flux. *Symp Soc Exp Biol* 27, 65-104.

Karp PD, Riley M, Saier M, Paulsen IT, Collado-Vides J, Paley SM, Pellegrini-Toole A, Bonavides C, Gama-Castro S (2002): The EcoCyc Database. *Nucleic Acids Research* 30, 56-58.

Klamt S, Schuster S, Gilles ED (2002): Calculability Analysis in Underdetermined Metabolic Networks illustrated by a model of the central metabolism in purple nonsulfur bacteria. *Biotechnol Bioeng* 77, 734-751.

Kholodenko BN, Schuster S, Garcia J, Westerhoff HV, Cascante M (1998): Control analysis of metabolic systems involving quasi-equilibrium reactions. *Biochim Biophys Acta* 1379, 337-352.

Koebmann BJ, Westerhoff HV, Snoep JL, Nilsson D, Jensen PR (2002): The glycolytic flux in *Escherichia coli* is controlled by the demand for ATP. *J Bacteriol* 184, 3909-3916.

Kotlarz D, Buc H (1982): Phosphofructokinases from *Escherichia coli*. *Methods Enzymol* 90, 60-70.

Kremling A, Bettenbrock K, Gilles ED (2008): A feed-forward loop guarantees robust behavior in *Escherichia coli* carbohydrate uptake. *Bioinformatics* 24, 704-710.

Kümmel A, Panke S, Heinemann M (2006): Putative regulatory sites unraveled by network-embedded thermodynamic analysis of metabolome data. *Mol Syst Biol* 2, 2006.0034.

Lendenmann U, Egli T (1995): Is *Escherichia* coli growing in glucose-limited chemostat culture able to utilize other sugars without lag? *Microbiology* 141, 71-78.

Liao JC, Hou SY, Chao YP (1996): Pathway analysis, engineering, and physiological considerations for redirecting central metabolism. *Biotechnol Bioeng* 52, 129-40.

Lo TC (1977): The molecular mechanism of dicarboxylic acid transport in *Escherichia coli* K 12. *J Supramol Struct* 7, 463-480.

Link H, Weuster-Botz D (2006) Genetic algorithm for multi-objective experimental optimization. *Bioprocess Biosyst Eng* 29, 385-390.

Luo B, Groenke K, Takors R, Wandrey C, Oldiges M (2007): Simultaneous determination of multiple intracellular metabolites in glycolysis, pentose phosphate pathway and tricarboxylic acid cycle by liquid chromatography-mass spectrometry. *J Chrom A* 1147, 153-164.

Magnus JB, Hollwedel D, Oldiges M, Takors R (2006): Monitoring and modeling of the reaction dynamics in the valine/leucine synthesis pathway in *Corynebacterium glutamicum*. *Biotechnol Prog* 22, 1071-1083.

Maharjan RP, Ferenci T (2003): Global metabolite analysis: the influence of extraction methodology on metabolome profiles of *Escherichia coli*. *Anal Biochem* 313, 145-154.

Malcovati M, Valentini G (1982): AMP- and fructose 1,6-bisphosphate-activated pyruvate kinases from *Escherichia coli*. *Methods Enzymol* 90, 170-179.

Mashego MR, Rumbold K, De Mey M, Vandamme E, Soetaert W, Heijnen JJ (2007): Microbial metabolomics: past, present and future methodologies. *Biotechnol Lett* 29, 1-16.

Massaoudi ME, Spelthahn J, Drysch A, de Graaf A, Takors R (2003) Production process monitoring by serial mapping of microbial carbon flux distributions using a novel sensor reactor approach: I sensor resactor system. *Metab Eng* 5, 86-95.

Mavrovouniotis ML (1991): Estimation of standard Gibbs energy changes of biotransformations. *J Biol Chem* 266, 14440-14445.

Mazat JP, Reder C, Letellier T (1996): Why are most flux control coefficients so small? *J Theor Biol* 182, 253-258.

Monod J (1949): The growth of bacterial cultures. *Ann Rev Microbiol* 3, 371-378.

Moritz B, Striegel K, De Graaf AA, Sahm H (2000): Kinetic properties of the glucose-6-phosphate and 6-phosphogluconate dehydrogenases from *Corynebacterium glutamicum*

and their application for predicting pentose phosphate pathway flux in vivo. *Eur J Biochem* 267, 3442-3452.

Nasution U, van Gulik WM, Kleijn RJ, van Winden WA, Proell A, Heijnen JJ (2006): Measurement of intracellular metabolites of primary metabolism and adenine nucleotides in chemostat cultivated Penicillium chrysogenum. *Biotechnol Bioeng* 94, 159-166.

Nasution U, van Gulik WM, Ras C, Proell A, Heijnen JJ (2008): A metabolome study of the steady-state relation between central metabolism, amino acid biosynthesis and penicillin production in *Penicillium chrysogenum*. *Metab Eng* 10, 10-23.

Nicolas C, Kiefer P, Letisse F, Kramer J, Massou S, Soucaille P, Wittmann C, Lindley ND, Portais JC (2007): Response of the central metabolism of *Escherichia coli* to modified expression of the gene encoding the glucose-6-phosphate dehydrogenase. *FEBS Lett* 581, 3771-3776.

Nielsen J (1994): Physiological engineering-towards a new science. p. 30-38. Proceedings of the 1994 IChemE Research Event, London.

Nielsen J (1997): Metabolic control analysis of biochemical pathways based on a thermokinetic description of reaction rates. *Biochem J* 321, 133-138.

Nikerel IE, van Winden WA, van Gulik WM, Heijnen JJ (2006): A method for estimation of elasticities in metabolic networks using steady state and dynamic metabolomics data and linlog kinetics. *BMC Bioinformatics* 7, 540.

Nikerel IE, van Winden WA, Verheijen PJ, Heijnen JJ (2009): Model reduction and a priori kinetic parameter identifiability analysis using metabolome time series for metabolic reaction networks with linlog kinetics. *Metab Eng* 11, 20-30.

Oldiges M, Lütz S, Pflug S, Schroer K, Stein N, Wiendahl C (2007): Metabolomics: current state and evolving methodologies and tools. *Appl Microbiol Biotechnol* 76, 495-511.

Onsager L (1931): Reciprocal Relations in Irreversible Processes. I. *Phys Rev* 37, 405-426.

Palsson BØ (2000): The challenges of in silico biology. *Nature Biotechnol* 18, 1147-1150.

Park JH, Lee SY, Kim TY, Kim HU (2008): Application of systems biology for bioprocess development. *Trends Biotechnol* 26, 404-412.

Raman B, Nandakumar MP, Muthuvijayan V, Marten MR (2005): Proteome analysis to assess physiological changes in *Escherichia coli* grown under glucose limited fed-batch conditions. *Biotechnol Bioeng* 92, 384-392.

Reder C (1988): Metabolic control theory: a structural approach. *J Theor Biol* 135, 175-201.

Reed JL, Vo TD, Schilling CH, Palsson BØ (2003): An expanded genome-scale model of *Escherichia coli* K-12 (*i*JR904 GSM/GPR). *Genome Biol* 4, R54.

Reed JL, Palsson BØ (2003): Thirteen years of building constrained-based in silico models of *Escherichia coli*. *J Bacteriol* 185, 2692-2699.

Robinson MS, Easom RA, Danson MJ, Weitzman PD (1983): Citrate synthase of *Escherichia coli*. Characterisation of the enzyme from a plasmid-cloned gene and amplification of the intracellular levels. *FEBS Lett* 154, 51-54.

Rottenberg H (1973): The thermodynamic description of enzyme-catalyzed reactions. The linear relation between the reaction rate and the affinity. *Biophys J* 13, 503-511.

Ruyter GJ, Postma PW, van Dam K (1991): Control of glucose metabolism by enzyme IIGlc of the phosphoenolpyruvate-dependent phosphotransferase system in *Escherichia coli*. *J Bacteriol* 173, 6184-6191.

Sauer U (2006): Metabolic networks in motion: ^{13}C-based flux analysis. *Mol Syst Biol* 2, 62.

Sauer U, Canonaco F, Heri S, Perrenoud A, Fischer E (2004): The soluble and membrane-bound transhydrogenases UdhA and PntAB have divergent functions in NADPH metabolism of *Escherichia coli*. *J Biol Chem* 279, 6613-6619.

Sauer U, Lasko DR, Fiaux J, Hochuli M, Glaser R, Szyperski T, Wüthrich K, Bailey JE (1999): Metabolic flux ratio analysis of genetic and environmental modulations of *Escherichia coli* central carbon metabolism. *J Bacteriol* 181, 6679-6688.

Savageau M (1969a): Biochemical system analysis, I. Some mathematical properties of the rate law for the component enzymatic reactions. *J Theor Biol* 25, 365-369.

Savageau M (1969b): Biochemical system analysis, II. The steady-state solutions for an n-pool system using a power law approximation. *J Theor Biol* 25, 370-379.

Schaaff L, Heinisch J, Zimmermann FK (1989): Overproduction of glycolytic enzymes in yeast. *Yeast* 5, 285-290.

Schädel F, Franco-Lara E (2009): Rapid sampling devices for metabolic engineering applications. *Appl Microbiol Biotechnol* 83, 199-208.

Schaefer U, Boos W, Takors R, Weuster-Botz D (1999): Automated sampling device for monitoring intracellular metabolite dynamics. *Anal Biochem* 270, 88-96.

Schaub J, Mauch K, Reuss M (2008): Metabolic flux analysis in *Escherichia coli* by integrating isotopic dynamic and isotopic stationary ^{13}C labeling data. *Biotechnol Bioeng* 99, 1170-1185.

Schaub J, Reuss M (2008): In vivo dynamics of glycolysis in *Escherichia coli* shows need for growth-rate dependent metabolome analysis. *Biotechnol Prog* 24, 1402-1407.

Schaub J, Schiesling C, Reuss M, Dauner M (2006): Integrated sampling procedure for metabolome analysis. *Biotechnol Prog* 22, 1434-1442.

Schilling CH, Edwards JS, Letscher D, Palsson BØ (2000): Combining pathway analysis with flux balance analysis for the comprehensive study of metabolic systems. *Biotechnol Bioeng* 4, 286-306.

Schuetz R, Kuepfer L, Sauer U (2007): Systematic evaluation of objective functions for predicting intracellular fluxes in *Escherichia coli*. *Mol Syst Biol* 3, 119.

Shimizu H, Tanaka H, Nakato A, Nagahisa K, Shioya S (2002): Metabolic control analysis in glutamate synthetic pathway. p. 39-52. In Marten MR, Park TH, Nagamune T. Biological Systems analysis. ACS Symposium series. Oxford University Press. Washinghton.

Simpson TW, Shimizu H, Stephanopoulos G (1998): Experiemntal determination of group flux control coefficients in metabolic networks. *Biotechnol Bioeng* 58, 149-157.

Small JR (1994): Desing and analysis of chemostat experiments using Metabolic Control Analysis: a top-down approach. *Microbiol* 140, 2439-2449.

Small JR, Fell DA (1989): The matrix method of metabolic control analysis: its validity for complex pathway structures. *J Theor Biol* 136, 181-197.

Smith MW, Neidhardt FC (1983): Proteins induced by aerobiosis in *Escherichia coli*. *J Bacteriol* 154, 344-350.

Snoep JL, Jensen PR, Groeneveld P, Molenaar D, Kholodenko BN, Westerhoff HV (1994): How to determine control of growth rate in a chemostat. Using metabolic control analysis to resolve the paradox. *Biochem Mol Biol Int* 33, 1023-1032.

Snoep JL, Yomano LP, Westerhoff HV, Ingram LO (1995): Protein burden in *Zymomonas mobilis*: Negative flux and growth control due to overproduction of glycolytic enzymes. *Microbiol* 141, 2329-2337.

Stephanopoulos GN (2002): Metabolic engineering: Perspectives of a chemical engineer. *AIChE J* 48, 920-926.

Stephanopoulos GN, Aristidou AA, Nielsen J (1998): Metabolic Engineering: Principles and Methodologies. Academic Press, London.

Strumilo S (2005): Short-term regulation of the alpha-ketoglutarate dehydrogenase complex by energy-linked and some other effectors. *Biochemistry* 70, 726-729.

Sucheta A, Ackrell BA, Cochran B, Armstrong FA (1992): Diode-like behaviour of a mitochondrial electron-transport enzyme. *Nature* 356, 361-362.

Takors R, Bathe B, Rieping M, Hans S, Kelle R, Huthmacher K (2007): Systems biology for industrial strains and fermentation processes–example: amino acids. *J Biotechnol* 129, 181-190.

Taymaz-Nikerel H, de Mey M, Ras C, ten Pierick A, Seifar RM, van Dam JC, Heijnen JJ, van Gulik WM (2009): Development and application of a differential method for reliable metabolome analysis in *Escherichia coli*. *Anal Biochem* 386, 9-19.

Teusink B, Passarge J, Reijenga CA, Esgalhado E, van der Weijden CC, Schepper M, Walsh MC, Bakker BM, van Dam K, Westerhoff HV, Snoep JL (2000): Can yeast glycolysis be understood in terms of in vitro kinetics of the constituent enzymes? Testing biochemistry. *Eur J Biochem* 267, 5313-5329.

Theobald U, Mailinger W, Baltes M, Reuss M, Rizzi M (1997): In vivo analysis of metabolic dynamics in *Saccharomyces cerevisiae*: I. Experimental observations. *Biotechnol Bioeng* 55, 305-316.

Thomas S, Fell DA (1996): Design of metabolic control for large flux changes. *J Theor Biol* 182, 285-298.

Thomas S, Fell DA (1998): A control analysis exploration of the role of ATP utilisation in glycolytic-flux control and glycolytic-metabolite-concentration regulation. *Eur J Biochem* 258, 956-67.

Tornheim K (1985): Activation of muscle phosphofructokinase by fructose 2,6-bisphosphate and fructose 1,6-bisphosphate is differently affected by other regulatory metabolites. *J Biol Chem* 260, 7985-7989.

Vaidyanathan S (2005): Profiling microbial metabolomes: what do we stand to gain? *Metabolomics* 1,17-28.

Vallino JJ, Stephanopoulos G (1993): Metabolic flux distributions in *Corynebacterium glutamicum* during growth and lysine overproduction. *Biotechnol Bioeng* 41, 633-646.

van den Brink J, Canelas AB, van Gulik WM, Pronk JT, Heijnen JJ, de Winde JH, Daran-Lapujade P (2008): Dynamics of glycolytic regulation during adaptation of *Saccharomyces cerevisiae* to fermentative metabolism. *Appl Environ Microbiol* 74, 5710-5723.

Van der Meer R, Westerhoff HV, van Dam K (1980): Linear relation between rate and thermodynamic force in enzyme-catalyzed reactions. *Biochim Biophys Acta* 591, 488-493.

VanBogelen RA (2003): Probing the Molecular Physiology of the Microbial Organism *Escherichia coli* Using Proteomics. In Advances in Biochemical Engineering/ Biotechnology: Proteomics of Microorganisms. Fundamental Aspects and Application. Springer Verlag

Varma A, Palsson BØ(1994): Stoichiometric flux balance models quantitatively predict growth and metabolic by-product secretion in wild-type *Escherichia coli* W3110. *Appl Env Microbiol* 60, 3724-3731.

Vaseghi S, Baumeister A, Rizzi M, Reuss M (1999): In vivo dynamics of the pentose phosphate pathway in *Saccharomyces cerevisiae. Metab Eng* 1, 128-140.

Villas-Boas SG, Bruheim P (2007): Cold glycerol-saline: the promising quenching solution for accurate intracellular metabolite analysis of microbial cells. *Anal Biochem* 370, 87-97.

Visser D, Heijnen JJ (2002): The mathematics of metabolic control analysis revisited. *Metab Eng* 4, 114-123.

Visser D, van Zuylen GA, van Dam JC, Oudshoorn A, Eman MR, Ras C, van Gulik WM, Frank J, van Dedem GW, Heijnen JJ (2002): Rapid sampling for analysis of in vivo kinetics using the BioScope: a system for continuous-pulse experiments. *Biotechnol Bioeng* 79, 674-681.

Visser D, Heijnen JJ (2003): Dynamic simulation and metabolic re-design of a branched pathway using linlog kinetics. *Metab Eng* 5, 164-176.

Visser D, van Zuylen GA, van Dam JC, Eman MR, Proll A, Ras C, Wu L, van Gulik WM, Heijnen JJ (2004a): Analysis of in vivo kinetics of glycolysis in aerobic *Saccharomyces cerevisiae* by application of glucose and ethanol pulses. *Biotechnol Bioeng* 88, 157-167.

Visser D, Schmid JW, Mauch K, Reuss M, Heijnen, JJ (2004b): Optimal re-design of primary metabolism in *Escherichia coli* using linlog kinetics. *Metab Eng* 6, 378-390.

Walsh K, Koshland DE (1985): Characterization of rate-controlling steps in vivo by use of an adjustable expression vector. *Proc Natl Acad Sci USA* 82, 3577-3581.

Wang L, Birol I, Hatzimanikatis V (2004): Metabolic control analysis under uncertainty: framework development and case studies. *Biophys J* 87, 3750-63.

Wang L, Hatzimanikatis V (2006a): Metabolic engineering under uncertainty. I: framework development. *Metab Eng* 8, 133-141.

Wang L, Hatzimanikatis V (2006b): Metabolic engineering under uncertainty. II: analysis of yeast metabolism. *Metab Eng* 8, 142-159.

Wang Y, Wu SL, Hancock WS, Trala R, Kessler M, Taylor AH, Patel PS, Aon JC (2005) Proteomic profiling of *Escherichia coli* proteins under high cell density fed-batch cultivation with overexpression of phosphogluconolactonase. *Biotechnol Prog* 21, 1401-1411.

Weuster-Botz D (1997): Sampling tube device for monitoring intracellular metabolite dynamics. *Anal Biochem* 246, 225-233.

Wiback SJ, Mahadevan R, Palsson BØ (2004): Using metabolic flux data to further constrain the metabolic solution space and predict internal flux patterns: the *Escherichia coli* spectrum. *Biotechnol Bioeng* 86, 317-331.

Wiechert W, de Graaf AA (1996): In vivo stationary flux analysis by ^{13}C labeling experiments. *Adv Biochem Eng Biotechnol* 54, 109-54.

Wiechert W, de Graaf AA (1997): Bidirectional reaction steps in metabolic networks: II. Modeling and simulation of carbon isotope labeling experiments. *Biotechnol Bioeng* 55, 101-117.

Winder CL, Dunn WB, Schuler S, Broadhurst D, Jarvis R, Stephens GM, Goodacre R (2008): Global metabolic profiling of *Escherichia coli* cultures: an evaluation of methods for quenching and extraction of intracellular metabolites. *Anal Chem* 80, 2939-48.

Wittmann C, Kramer JO, Kiefer P, Binz T, Heinzle E (2004): Impact of the cold shock phenomenon on quantification of intracellular metabolites in bacteria. *Anal Biochem* 327, 135-139.

Wohl RC, Markus G (1972): Phosphoenolpyruvate carboxylase of *Escherichia coli*. Purification and some properties. *J Biol Chem* 247, 5785-5792.

Wu L, Mashego MR, van Dam JC, Proell AM, Vinke JL, Ras C, van Winden WA, van Gulik WM, Heijnen JJ (2005): Quantitative analysis of the microbial metabolome by isotope dilution mass spectrometry using uniformly ^{13}C-labeled cell extracts as internal standards. *Anal Biochem* 336, 164-171.

Wu L, van Dam J, Schipper D, Kresnowati MT, Proell AM, Ras C, van Winden WA, van Gulik WM, Heijnen JJ (2006): Short-term metabolome dynamics and carbon, electron, and ATP balances in chemostat-grown *Saccharomyces cerevisiae* CEN.PK 113-7D following a glucose pulse. *Appl Environ Microbiol* 72, 3566-3577.

Wu L, Wang W, van Winden WA, van Gulik WM, Heijnen JJ (2004): A new framework for the estimation of control parameters in metabolic pathways using lin-log kinetics. *Eur J Biochem* 271, 3348-3359.

Yang C, Hua Q, Baba T, Mori H, Shimizu K (2003): Analysis of *Escherichia coli* anaplerotic metabolism and its regulation mechanisms from the metabolic responses to altered dilution rates and phosphoenolpyruvate carboxykinase knockout. *Biotechnol Bioeng* 84, 129?144.

Yankovskaya V, Horsefield R, Törnroth S, Luna-Chavez C, Miyoshi H, Leger C, Byrne B, Cecchini G, Iwata S (2003): Architecture of succinate dehydrogenase and reactive oxygen species generation. *Science* 299, 700-704.

Yoon SH, Han MJ , Lee SY , Jeong KJ, Yoo JS (2003): Combined transcriptome and proteome analysis of *Escherichia coli* during high cell density culture. *Biotechnol Bioeng* 81, 753-767.

Zamboni N, Kümmel A, Heinemann M (2008): anNET: a tool for network-embedded thermodynamic analysis of quantitative metabolome data. *BMC Bioinformatics* 9, 199.

Zheng RL, Kemp RG (1992): The mechanism of ATP inhibition of wild type and mutant phosphofructo-1-kinase from *Escherichia coli*. *J Biol Chem* 267, 23640-23645.

8. Abbreviations

TCA	tricarboxylic acid cycle
PPP	pentose phosphate pathway
IDMS	isotope dilution mass spectrometry
MCA	metabolic control analysis
FBA	flux balance analysis
NET	network embedded thermodynamic analysis
LC-MS	liquid chromatography-mass spectrometry
GC-MS	gas chromatography-mass spectrometry
2-DE	two-dimensional gel electrophoresis
OUR	oxygen uptake rate
CPR	carbon dioxide production rate
OTR	oxygen transfer rate
RMT	rapid media transition
DW	dry weight
OD	optical density
MW	methanol/water
MG	methanol/glycerol

Metabolites

PEP	phosphoenolpyruvate
G6P	glucose-6-phosphate
F6P	fructose-6-phosphate
FBP	fructose-1,6-bisphosphate
DHAP	dihydroxy-acetone phosphate
GAP	glyceraldehyde-3-phosphate
13DPG	1,3-diphosphoglycerate
3PG	3-phosphoglycerate
2PG	2-phosphoglycerate
PYR	pyruvate
6PG	6-phosphogluconate
Ru5P	ribulose-5-phosphate
R5P	ribose-5-phosphate
X5P	xylose-5phosphate
S7P	sedoheptulose-7-phosphate

E4P	erythrose-4-phosphate
AcCoA	acetyl-coenzyme A
CoA	coenzyme A
OAA	oxaloacetate
CIT	citrate
ICIT	isocitrate
AKG	α-ketoglutarate
SucCoA	succinyl-coenzyme A
SUC	succinic acid
FUM	fumarate
MAL	malate
ATP	adenosine-5-triphosphate
ADP	adenosine-5-diphosphate
AMP	adenosine-5-monophosphate
NAD	nicotinamide adenine dinucleotide
NADH	nicotinamide adenine dinucleotide reduced
NADP	nicotinamide adenine dinucleotide phosphate
NADPH	nicotinamide adenine dinucleotide phosphate reduced

Reactions

pts	phosphotransferase system
pgi	phosphoglucose isomerase
pfk	phosphofructokinase
fba	fructose-1,6-bisphosphate aldolase
tpi	triosephosphate isomerase
gapd	glyceraldehyde-3-phosphate dehydrogenase
pgk	phosphoglycerate kinase
pgm	phosphoglycerate mutase
eno	Enolase
pyk	pyruvat kinase
pps	PEP synthase
fbp	fructose-biphosphatase
g6pdh	glucose-6-phosphate dehydrogenase
gnd	6-phosphogluconate dehydogenase
rpi	ribose-5-phosphate isomerase
rpe	ribose-5-phosphate epimerase

tkt	transketolase
tala	transaldolase
pdh	pyruvate dehydrogenase
cs	citrate synthase
acont	aconitase
akgdh	α-ketoglutarate dehydrogenase
icdh	isocitratedehydrogenase
fum	fumarase
mdh	malate dehydrogenase
sucoas	SucCoA synthetase
nadh6	NADH:ubuiqinone oxidoreductase
cytbd	cytochrome bo terminal oxidase
atps	ATP synthesis
thd	transhydrogenase
pfl	pyruvate formate-lyase
pox	pyruvate oxidase
pta	phosphate acetyltransferase
ack	acetate kinase
adh	alcohol dehydrogenase

A. Appendix

A.1. Chemicals and equipment

Table A.1.: List of applied chemicals.

Acetic Acid (LC-MS)	49199	Sigma-Aldrich
Cobalt chloride hexahydrate	109986	Merck
Clerol FBA 265		Cognis
Dipotassium phosphate	P749.2	Roth
Ferrum sulfate hexahydrate	103965	Merck
Ethanol	100983	Merck
Glucose-Monohydrat	108342	Merck
Glycerol	104091	Merck
Yeast extract	111926	Merck
Helium 6.0		Linde
Potassium dihydrogenphosphat	3907	Roth
Potassium hydroxid	814353	Merck
Copper chloride dihydrate	102790	Merck
Magnesium chloride	814733	Merck
Magnesium sulfate	105886	Merck
Manganese sulfate Monohydrate	105941	Merck
Methanol	106008	Merck
Methanol (HPLC grade)	7342.1	Roth
Sodium dihydrogenphosphate monohydrate	106370	Merck
Sodium acetate	116100	Merck
Sodium chloride	P029	Roth
Sodium hydroxide	106482	Merck
Sodium molybdate dihydrate	105621	Merck
Peptone	102239	Merck
Tributylamine	90781	Sigma-Aldrich
Triethanolamine	T1377	Sigma
U-^{13}C labeled glucose		Eurisotop
Zinc sulfate heptahydrate	108883	Merck

Table A.2.: List of metabolite standards.

3PG	P8877	Sigma-Aldrich
AcCoA	A2056	Sigma-Aldrich
ADP	A2754	Sigma-Aldrich
AMP	A1752	Sigma-Aldrich
ATP	A6559	Sigma-Aldrich
F6P	F3627	Sigma-Aldrich
FAD	F6625	Sigma-Aldrich
FBP	F6803	Sigma-Aldrich
G6P	G7879	Sigma-Aldrich
PEP	P7252	Sigma-Aldrich
Pyr	P2256	Sigma-Aldrich
SUC	S 3674	Sigma-Aldrich
FUM	F 1506	Sigma-Aldrich
MAL	M 2422	Sigma-Aldrich
AKG	75890	Sigma-Aldrich
NAD	10127965001	Roche-Diagnostics
NADH	10107735001	Roche-Diagnostics
NADP	10128031001	Roche-Diagnostics
NADPH	10107824001	Roche-Diagnostics

Table A.3.: Equipment for general purposes.

Analytical balance AG 285	Mettler Toledo, Gießen
Analytical balance E1M213	Ohaus, Gießen
Analytical balance E121245	Ohaus, Gießen
Photometer Spectronic Genesys 20	Thermo Electron, Dreieich
Dry freezer Alpha 1-2 LD Martin	Christ GmbH, Osterrode / Harz
Centrifuge Biofuge Stratos	Kendro-Heraeus, Langenselbold
pH-probe BlueLine 14 pH	Schott, Mainz
pH-probe CG 843	Schott, Mainz
Shaking incubator Multitron	Infors, Einsbach
Centrifuge Rotixa 50 RS	Hettich, Tuttlingen
Thermomixer Comfort	Eppendorf, Hamburg
Centrifuge Mikro 20	Hettich, Tuttlingen
Cell size counter Multisizer II	Beckman Coulter

Table A.4.: Fermentation systems.

Bench-top fermenter Labfors	**Infors, Einsbach**
vessel	double jacketed glass
total volume - working volume	2 L - 1.2 L
stirrer	2 flat-bladed Rushton impellors
drive	top, mechanical seal drive coupling
aeration	mass flow valve, sparger
process control software	Iris-NT Pro Version 4.11
pH-probe HA405-DPA-SC-S8	Mettler-Toledo, Giessen
DO-probe InPro 6000	Mettler-Toledo, Giessen
exhaust gas analyzer Easy Line	ABB-Frankfurt

Techfors fermenter system	**Infors, Einsbach**
vessel	double jacketed stainless steel
total volume - Working volume	42 L - 30 L
stirrer	3 flat-bladed Rushton impellors
drive	bottom, mechanical seal drive coupling
aeration	mass flow valve, sparger
process control software	Iris-NT Pro Version 4.11
pH-probe HA405-DPA-SC-S8	Mettler-Toledo, Giessen
DO-probe InPro 6000	Mettler-Toledo, Giessen
anti-foam probe Russel	Infors, Einsbach
pressure probe sensor PR-25HT/8931A	Keller, Winterthur, Schweiz
exhaust gas analyzer Easy Line	ABB, Frankfurt
peristaltic feeding pump Ecoline VC	Ismatech, Wertheim-Mondfeld

Table A.5.: LC-MS system.

software Xcalibur 1.2	Thermo Finnigan, Dreieich
autosampler AS 1000	Thermo Spectronic, Dreieich
quartenary HPLC-Pump P1100	Thermo Spectronic, Dreieich
degaser D 1100	Thermo Spectronic, Dreieich
diode array UV 1000	Thermo Spectronic, Dreieich
ESI masspectrometer LCQ-Advantage	Thermo Spectronic, Dreieich
Synergi Hydro-RP (C18) 150mm×2.1mm I.D., 4 μm 80 Å	Phenomenex, Aschaffenburg
nitrogen generator ESP 2	DWT, Essen

A.2. ESI parameter

Table A.6.: ESI parameter.

ESI Parameter	**Segment 1**	**Segment 2**	**Segment 3**
time	0-32 min	32-62 min	62-80 min
Capillary Temp (°C)	330	290	350
AGC	on	on	on
Sheath Gas Flow (-)	53	53	60
Aux Gas Flow (-)	31	31	20
Source Voltage (kV)	3	2,6	2,5
Capillary Voltage (V)	-15	-5	-21
Tube Lens Offset (V)	-4	-14,2	0
Multipole RF Amplifier (Vp-p)	400	400	400
Multipole 1 Offset (V)	7	7	3
Multipole 2 Offset (V)	9,5	9,5	6,5
InterMultipole Lens Voltage (V)	17,4	17,4	14

A.3. Elementary matrix

Table A.7.: Elementary matrix.

	o2	co2	gluc	pyr	suc	ac	for	etoh	c_x	nh3	h2o
C	0	1	1	1	1	1	1	1	1	0	0
H	0	0	2	1.3	1.5	2	2	3	1.93	3	2
O	2	2	1	1	1	1	2	0.5	0.55	0	1
N	0	0	0	0	0	0	0	0	0.26	1	0

A.4. External calibration

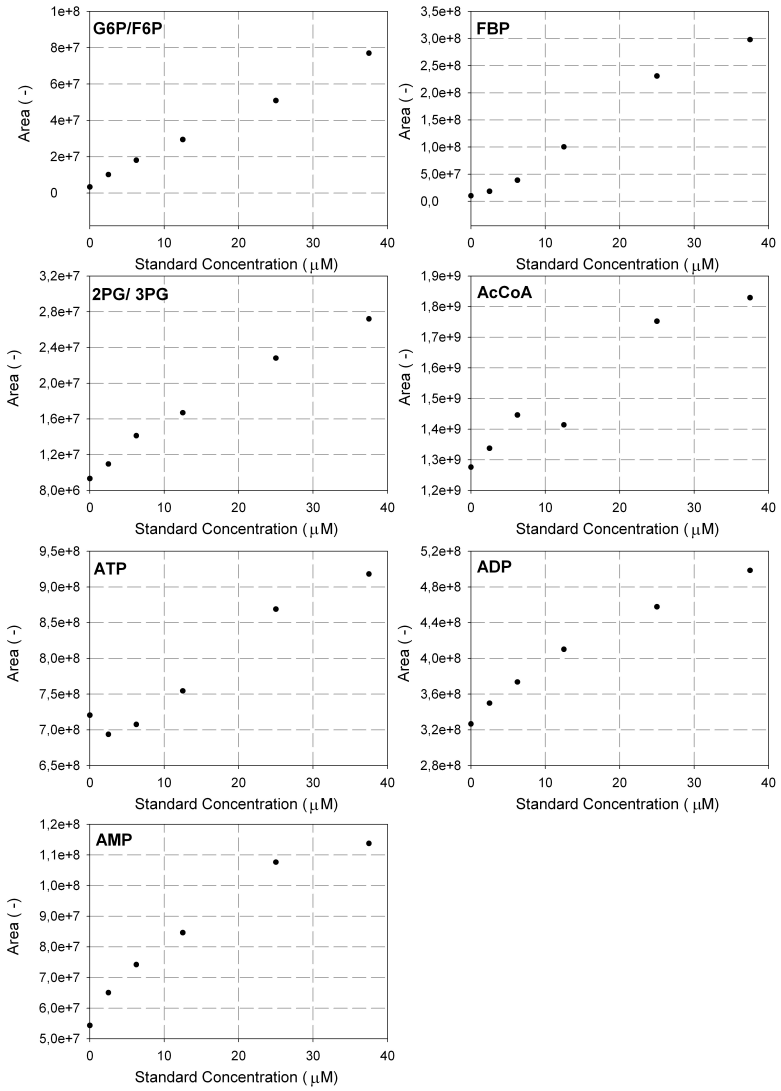

Figure A.1.: LC-MS calibration with standard solution of metabolites, mixed with culture broth and processed according to sampling protocol SP2.

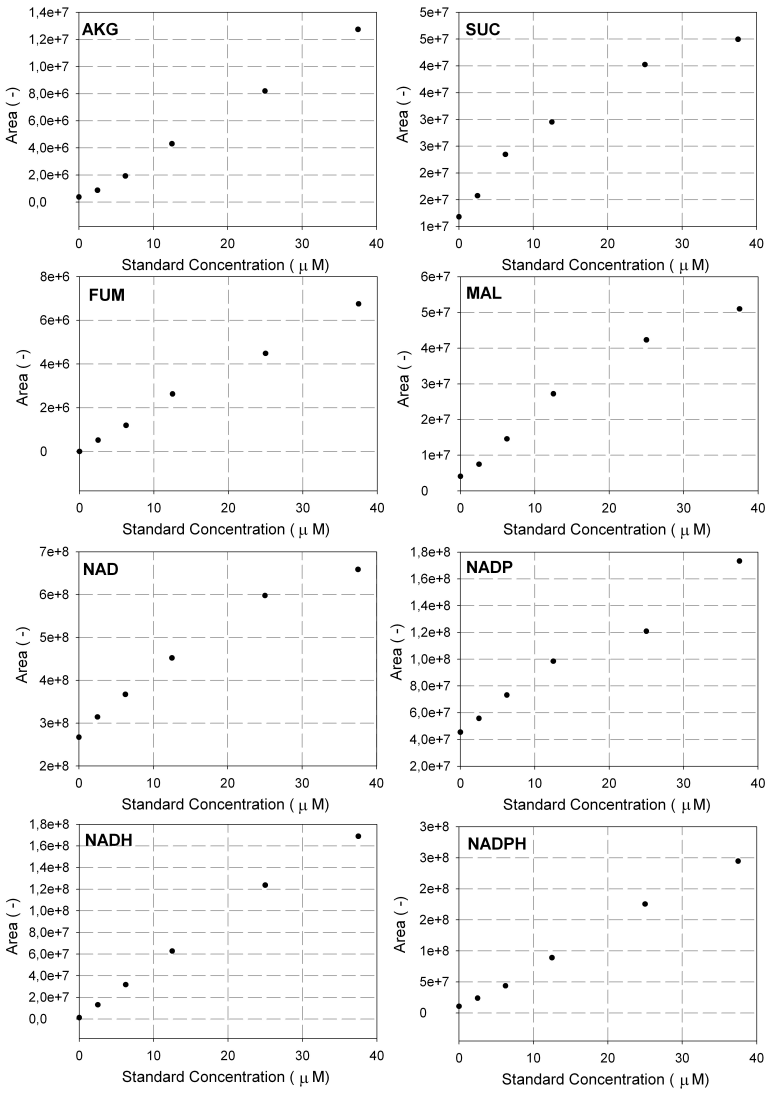

Figure A.2.: LC-MS calibration with standard solution of metabolites, mixed with culture broth and processed according to sampling protocol SP2.

A.5. IDMS calibration

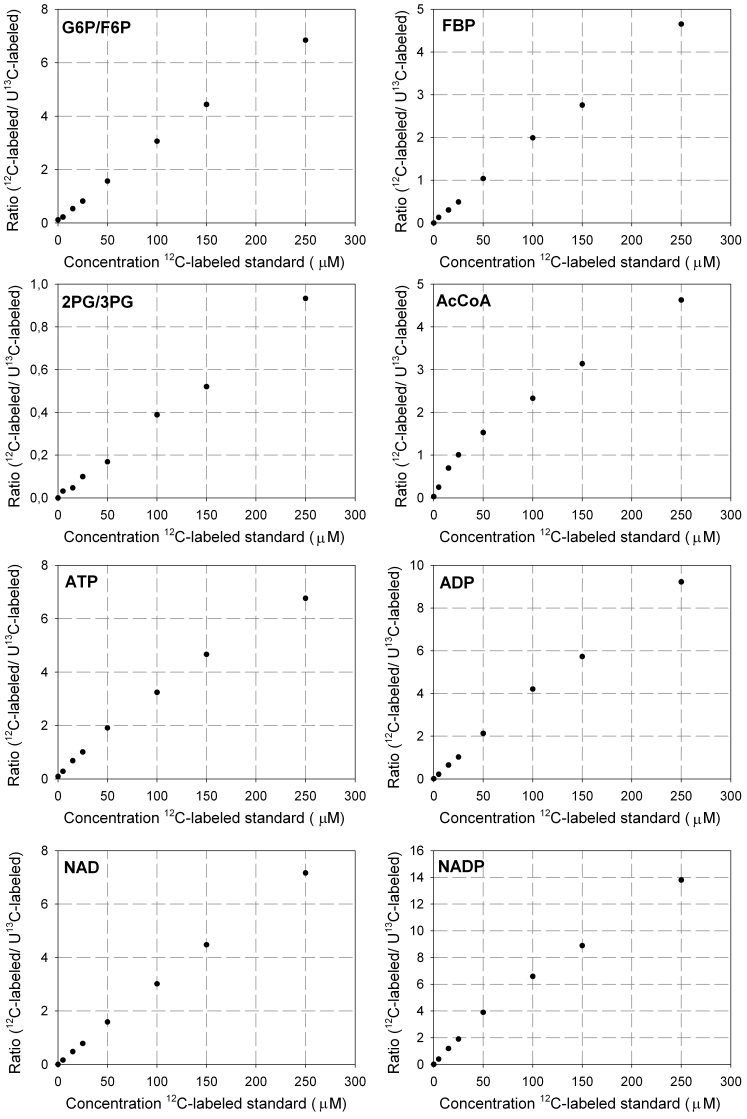

Figure A.3.: Calibration of U-^{13}C labeled cell extracts. Ratio of peak areas of ^{12}C and U-^{13}C metabolites is plotted against the concentration of ^{12}C metabolite in the 1:1 mixture of labeled cell extract and standard solution.

A.6. Data set of Giersch (1995)

Table A.8.: Experimental data of the reconstituted pathway in Fig. (5.9) as presented by Wu *et al.* (2004), originally obtained from Giersch (1995).

Experiment	PGM (U L^{-1})	ENO (U L^{-1})	PK (U L^{-1})	2PG (μM)	PEP (μM)	BPG (μM)	ADP (μM)	Flux (μM h^{-1})
1	31	5.6	46	170	50	13.2	107	157
2	25	12	30	60	103	13.2	61	87
3	25	12	30	57	91	13.2	83	114
4	25	12	30	55	83	13.2	107	128
5	25	12	30	54	76	13.2	130	136
6	25	12	30	40	60	8.5	107	111
7	25	12	30	46	70	10.8	107	118
8	25	12	30	55	81	13.2	107	122
9	25	12	30	59	89	15.6	107	130
10	25	12	30	63	95	18	107	133
11	36.8	6.5	34	161	81	13.2	107	108
12	45	6.5	34	178	82	13.2	107	108
13	53.2	6.5	34	204	81	13.2	107	108
14	45	5.3	34	206	75	13.2	107	106
15	45	6.5	34	195	87	13.2	107	108
16	45	7.7	34	180	92	13.2	107	112
17	45	6.5	30.9	192	91	13.2	107	96
18	45	6.5	34	192	84	13.2	107	106
19	45	6.5	37.1	196	79	13.2	107	116

A.7. Stoichiometric models

A.7.1. FBA and MFA models

Table A.9.: Reactions of the MFA model and *E. coli* *i*JR904.

	ID	***E. coli* iJR904**	**MFA Modell**
		Glycolysis	
1	pts	glc-D[e] + pep[c] -> g6p[c] + pyr[c]	glc-D[e] + pep[c] <=> g6p[c] + pyr[c]
2	pgi	g6p[c] <=> f6p[c]	g6p[c] <=> f6p[c]
3	pfk	atp[c] + f6p[c] -> adp[c] + fdp[c] + h[c]	{ atp[c] + f6p[c] <=> fdp[c]
4	fbp	fdp[c] + h2o[c] -> f6p[c] + pi[c]	
5	fba	fdp[c] <=> dhap[c] + g3p[c]	{ fdp[c] <=> 2 g3p[c]
6	tpi	dhap[c] <=> g3p[c]	
7	gapd	g3p[c] + nad[c] + pi[c] <=> 13dpg[c] + h[c] + nadh[c]	
8	pgk	13dpg[c] + adp[c] <=> 3pg[c] + atp[c]	{ g3p[c] <=> pg[c] + atp[c] + nad(p)h[c]
9	pgm	3pg[c] <=> 2pg[c]	
10	eno	2pg[c] <=> h2o[c] + pep[c]	pg[c] <=> pep[c]
11	pyk	adp[c] + h[c] + pep[c] -> atp[c] + pyr[c]	{ pep[c] <=> atp[c] + pyr[c]
12	pps	atp[c] + h2o[c] + pyr[c] -> amp[c] + 2 h[c] + pep[c] + pi[c]	
13	pdh	coa[c] + nad[c] + pyr[c] -> accoa[c] + co2[c] + nadh[c]	pyr[c] <=> accoa[c] + co2[c] + nad(p)h[c]
		Anapleurotic Reactions	
14	ppc	co2[c] + h2o[c] + pep[c] -> h[c] + oaa[c] + pi[c]	{ co2[c] + pep[c] <=> oaa[c]
15	ppck	oaa[c] + atp[c] -> co2[c] + adp[c] + pep[c]	
		TCA Cycle	
16	cs	accoa[c] + h2o[c] + oaa[c] -> cit[c] + coa[c] + h[c]	accoa[c] + oaa[c] <=> cit[c]
17	acont	cit[c] <=> icit[c]	cit[c] <=> icit[c]
18	icdh	icit[c] + nadp[c] <=> akg[c] + co2[c] + nadph[c]	icit[c] <=> akg[c] + co2[c] + nad(p)h[c]
19	akgdh	akg[c] + coa[c] + nad[c] -> co2[c] + nadh[c] + succoa[c]	akg[c] <=> co2[c] + nad(p)h[c] + succoa[c]
20	sucoas	adp[c] + pi[c] + succoa[c] <=> atp[c] + coa[c] + succ[c]	succoa[c] <=> atp[c] + succ[c]
21	sucd	fad[c] + succ[c] -> fadh2[c] + fum[c]	succ[c] <=> 0.5 nad(p)h[c] + fum[c]
22	fum	fum[c] + h2o[c] <=> mal-L[c]	fum[c] <=> mal-L[c]
23	mdh	mal-L[c] + nad[c] <=> h[c] + nadh[c] + oaa[c]	mal-L[c] <=> nad(p)h[c] + oaa[c]
		Pentose Phosphate Pathway	
24	g6pdh	g6p[c] + nadp[c] <=> 6pgl[c] + h[c] + nadph[c]	{ g6p[c] <=> co2[c] + 2 nad(p)h[c] + ru5p-D[c]
25	gnd	6pgc[c] + nadp[c] -> co2[c] + nadph[c] + ru5p-D[c]	
26	rpi	ru5p-D[c] <=> r5p[c]	ru5p-D[c] <=> r5p[c]
27	rpe	ru5p-D[c] <=> xu5p-D[c]	ru5p-D[c] <=> xu5p-D[c]
28	tkt1	r5p[c] + xu5p-D[c] <=> g3p[c] + s7p[c]	r5p[c] + xu5p-D[c] <=> g3p[c] + s7p[c]
29	tkt2	e4p[c] + xu5p-D[c] <=> f6p[c] + g3p[c]	reaction not considered
30	tala	g3p[c] + s7p[c] <=> e4p[c] + f6p[c]	g3p[c] + s7p[c] <=> e4p[c] + f6p[c]
		Oxidative Phosphorylation	
31	thd	2 h[e] + nadh[c] + nadp[c] -> 2 h[c] + nad[c] + nadph[c]	reaction not considered
32	cytbd	2 h[c] + 0.5 o2[c] + q8h2[c] -> h2o[c] + 2 h[e] + nad[c] + q8[c]	rection not considered
33	nadh6	5 h[c] + nadh[c] + q8[c] -> 4 h[e] + nad[c] + q8h2[c]	{ nad(p)h[c] <=> 2 atp[c]
34	atps	adp[c] + 4 h[e] + pi[c] <=> atp[c] + h2o[c] + 3 h[c]	
		Pyruvate Metabolism	
35	pfl	coa[c] + pyr[c] -> accoa[c] + for[c]	pyr[c] -> accoa[c] + for[c]
36	adh	accoa[c] + 2 h[c] + 2 nadh[c] <=> coa[c] + etoh[c] + 2 nad[c]	accoa[c] + 2 nad(p)h[c] <=> etoh[c]
37	pta	accoa[c] + pi[c] <=> actp[c] + coa[c]	{ accoa[c] <=> ac[c] + atp[c]
38	ack	ac[c] + atp[c] <=> actp[c] + adp[c]	
		ATP drain	
39	ATPase	reaction not considered	atp[c] ->
		Exchange Fluxes	
39	q_{ac}	ac[c] <=> ac[e]	ac[c] <=> ac[e]
40	q_{CO_2}	co2[c] <=> co2[e]	co2[c] <=> co2[e]
41	q_{suc}	succ[c] <=> succ[e]	succ[c] <=> succ[e]
42	q_{for}	for[c] <=> for[e]	for[c] <=> for[e]
43	q_{pyr}	pyr[c] <=> pyr[e]	pyr[c] <=> pyr[e]
44	q_{fum}	fum[c]<=> fum[e]	fum[c]<=> fum[e]
45	q_{akg}	akg[c] <=> akg[e]	akg[c] <=> akg[e]
46	q_{etoh}	etoh[c] <=> etoh[e]	etoh[c] <=> etoh[e]

A.7.2. MCA model

Table A.10.: Reactions considered for Metabolic Control Analysis.

	ID	Reaction	Effectors
		Glycolysis	
1	pts	glc-D[e] + pep[c] -> g6p[c] + pyr[c]	pyr[c], pep[c], g6p[c], (glc-D[e])
2	pgi	g6p[c] <=> f6p[c]	equilibrium
3	pfk	atp[c] + f6p[c] -> adp[c] + fdp[c] + h[c]	fdp[c], pep[c], f6p[c]
4	fba	fdp[c] <=> dhap[c] + g3p[c]	equilibrium
5	tpi	dhap[c] <=> g3p[c]	equilibrium
6	gapd	g3p[c] + nad[c] + pi[c] <=> 13dpg[c] + h[c] + nadh[c]	equilibrium
7	pgk	13dpg[c] + adp[c] <=> 3pg[c] + atp[c]	equilibrium
8	pgm	3pg[c] <=> 2pg[c]	equilibrium
9	eno	2pg[c] <=> h2o[c] + pep[c]	equilibrium
10	pyk	adp[c] + h[c] + pep[c] -> atp[c] + pyr[c]	pyr[c], pep[c], fdp[c]
11	pdh	coa[c] + nad[c] + pyr[c] -> accoa[c] + co2[c] + nadh[c]	pyr[c]
		Anapleurotic Reactions	
12	ppc	co2[c] + h2o[c] + pep[c] -> h[c] + oaa[c] + pi[c]	fdp[c], pep[c], accoa[c]
		TCA Cycle	
13	cs	accoa[c] + h2o[c] + oaa[c] -> cit[c] + coa[c] + h[c]	accoa[c], oaa[c], nadh[c]
14	acont	cit[c] <=> icit[c]	equilibrium
15	idh	icit[c] + nadp[c] <=> akg[c] + co2[c] + nadph[c]	icit[c]
16	akgdh	akg[c] + coa[c] + nad[c] -> co2[c] + nadh[c] + succoa[c]	akg[c], oaa[c]
17	sucoas	adp[c] + pi[c] + succoa[c] <=> atp[c] + coa[c] + succ[c]	equilibrium
18	sucd	fad[c] + succ[c] -> fadh2[c] + fum[c]	fad[c], succ[c]
19	fum	fum[c] + h2o[c] <=> mal-L[c]	equilibrium
20	mdh	mal-L[c] + nad[c] <=> h[c] + nadh[c] + oaa[c]	equilibrium
		Pentose Phosphate Pathway	
21	g6pdh	g6p[c] + nadp[c] <=> 6pgl[c] + h[c] + nadph[c]	g6p[c], nadph[c]
22	gnd	6pgc[c] + nadp[c] -> co2[c] + nadph[c] + ru5p-D[c]	6pgc[c], nadph[c]
23	rpi	ru5p-D[c] <=> r5p[c]	equilibrium
24	rpe	ru5p-D[c] <=> xu5p-D[c]	equilibrium
25	tkt1	r5p[c] + xu5p-D[c] <=> g3p[c] + s7p[c]	equilibrium
26	tala	g3p[c] + s7p[c] <=> e4p[c] + f6p[c]	equilibrium
		Energy Metabolism	
27	fadh2ox	adp[c] + fadh2[c] -> atp[c] + fad[c]	fadh2[c]
28	nadhox	2 adp[c] + nadh[c] -> 2 atp[c] + nad[c]	nadh[c]
29	ATPase	atp[c] <=> adp[c]	atp[c]
30	μ	see Table A.12	

A.8. Biomass composition

Table A.11.: Biosynthetic demand of *E. coli* *i*JR904 given in mmol g_{DW}^{-1}.

Amount	**ID**	**Name**
0.488	ala-L[c]	L-Alanine
0.281	arg-L[c]	L-Arginine
0.229	asn-L[c]	L-Asparagine
0.229	asp-L[c]	L-Asparatat
0.087	cys-L[c]	L-Cysteine
0.25	gln-L[c]	L-Glutamine
0.25	glu-L[c]	L-Glutamate
0.582	gly[c]	Glycine
0.09	his-L[c]	L-Histidine
0.276	ile-L[c]	L-Isoleucine
0.428	leu-L[c]	L-Leucine
0.326	lys-L[c]	L-Lysine
0.146	met-L[c]	L-Methionine
0.176	phe-L[c]	L-Phenylalanine
0.21	pro-L[c]	L-Proline
0.205	ser-L[c]	L-Serine
0.241	thr-L[c]	L-Threonine
0.054	trp-L[c]	L-Tryptophan
0.131	tyr-L[c]	L-Tyrosine
0.402	val-L[c]	L-Valine
0.05	5mthf[c]	5-Methyltetrahydrofolate
0.000129	clpn-EC[c]	Cardiolipin-Ecoli
0.154	glycogen[c]	glycogen
0.0084	lps-EC[c]	lipopolysaccharide-Ecoli
0.001935	pe-EC[c]	Phosphatidylethanolamine-ecoli
0.0276	peptido-EC[c]	Peptidoglycan-subunit-of-Escherichia-coli
0.000464	pg-EC[c]	Phosphatidylglycerol-Ecoli
5.2e-005	ps-EC[c]	phosphatidylserine-Ecoli

Amount	ID	Name
0.035	ptrc[c]	Putrescine
0.007	spmd[c]	Spermidine
0.003	udpg[c]	UDPglucose
0.136	utp[c]	UTP
45.7318	atp[c]	ATP
0.126	ctp[c]	CTP
0.203	gtp[c]	GTP
0.0247	datp[c]	dATP
0.0254	dctp[c]	dCTP
0.0254	dgtp[c]	dGTP
0.0247	dttp[c]	dTTP
0.001	amp[c]	AMP
0.00215	nad[c]	NAD
0.00005	nadh[c]	NADH
0.00013	nadp[c]	NADP
0.0004	nadph[c]	NADPH
0.00001	fad[c]	FAD
0.000003	succoa[c]	succoa[c]
0.00005	accoa[c]	accoa[c]
0.000006	coa[c]	coa[c]
45.5608	h2o[c]	h2o[c]

Table A.12.: Biomass synthetic precursors according to Wiback *et al.* (2004) and fraction of carbon moles φ_i of precursor i.

Metabolite	mmol g_{DW}^{-1}	φ_i
G6P	0.2	0.14
F6P	0.1	0.14
R5P	0.9	0.12
E4P	0.4	0.09
GAP	0.1	0.07
3PG	1.5	0.07
PEP	0.5	0.07
PYR	2.8	0.07
AcCoA	3.7	0.05
OAA	1.8	0.09
AKG	1.1	0.12
Succ	trace	-

A.9. Proteome analysis (2-DE gels)

Methods

Sampling

Approximately 10 mL culture broth was withdrawn and rapidly chilled on pre-cooled test tubes. Cells were separated (4500 g, 10 min, 4°C) and the cell pellet was washed in 10 mL PBS buffer. Cells were again separated (4500 g, 10 min, 4°C), resuspended in 1 mL PBS buffer and transfered into pre-weighted 2 mL test tubes. Again, cells were separated (10,000 g, 10 min, 4°C). The weight of the cell pellet was determined before it was frozen in liquid nitrogen and stored at -80°C.

Cell Lysis

The cell lysis of the samples was performed by ultrasonication in presence of protease inhibitors and CHAPS in phosphate buffer. For the isoelectric focusing (IEF, first dimension separation) of the proteins urea and thiourea were added to the sample to a final concentration of 7 M and 2 M, respectively. To denature the proteins 65 mM DTT was added. The homogenate was centrifuged (30 min, 226,000 g, 25°C). The resulting supernatant was used for proteome comparison, while the pellet consisting of cell debris and buffer insoluble proteins was not used for further analysis and stored at -70°C.

Protein Samples

The sample was diluted in sample buffer containing 4% CHAPS, protease inhibitor, 65mM DTT, 7M urea and 2M thiourea.

Protein Quantification

The protein amount of the sample prior to 2D gel electrophoresis was determined. Each sample was measured as duplicate. The sample was then supplemented with carrier ampholytes to give a final concentration of 2%.

Isoelectric Focusing

IEF was performed using 40 cm rod gels containing 9 M urea, 3.5% acrylamide, 0.3% piperazine diacrylamide and a total of 4 % carrier ampholytes pH 2-11. The samples were applied onto the IEF gels at the anodic side of the tube gels. The proteins were focused under nonequilibrium pH gradient electrophoresis conditions (NEPHGE).

20 cm SDS-PAGE for 2D Gel Electrophoresis

The IEF gels were applied onto SDS gels of 0.75x250x300 mm^3 containing 15% acrylamide and 0.2% bis-acrylamide using the IEF gels as stacking gels. The proteins were separated

according to their apparent molecular weight in a continuous buffer system (25 mM Tris, 192 mM glycine, and 0.1% SDS). The separated proteins were stained with silver to achieve highest sensitivity.

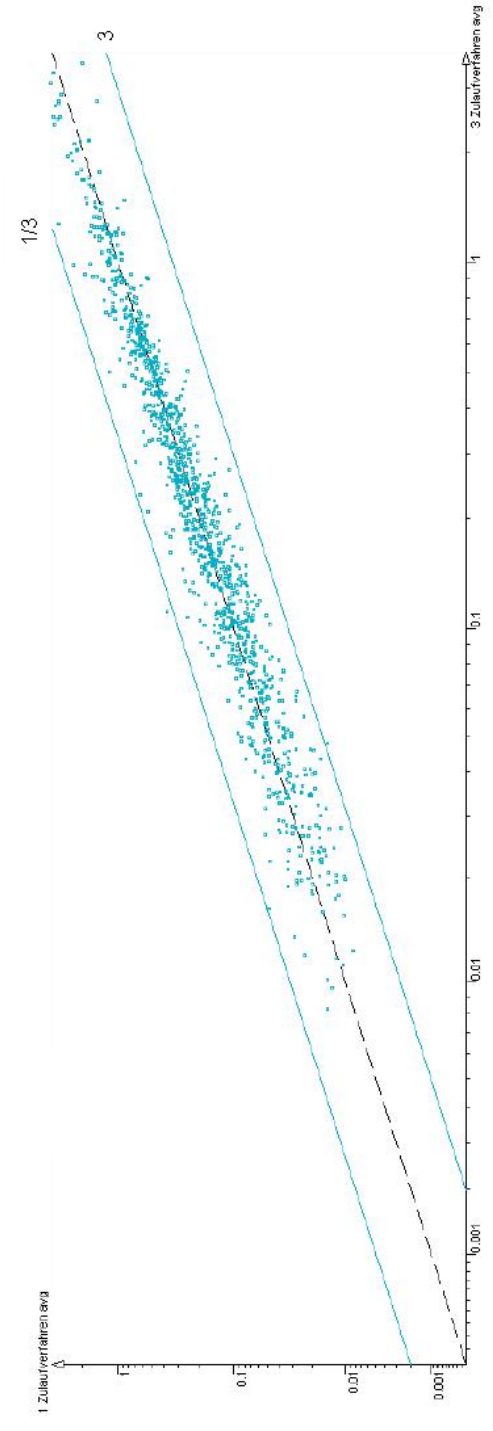

Figure A.4.: Parity plot of intensity of 1130 spots on 2-DE gels of samples from the fed-batch process (19 h and 24 h).

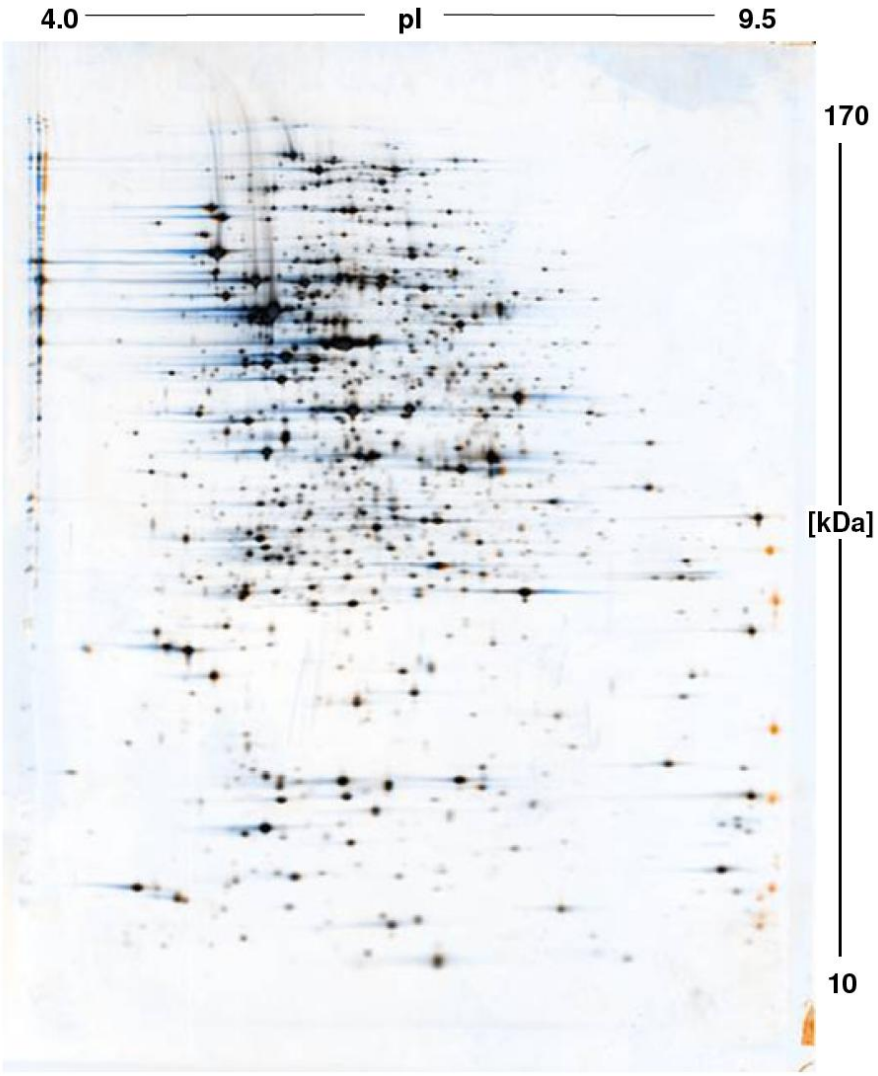

Figure A.5.: Overlay of false-color images of gels from protein samples from the fed-batch process (24h) and directly after transfer to the lab-scale fermenter. Unchanged spots appear black, whereas changes appear orange or blue.

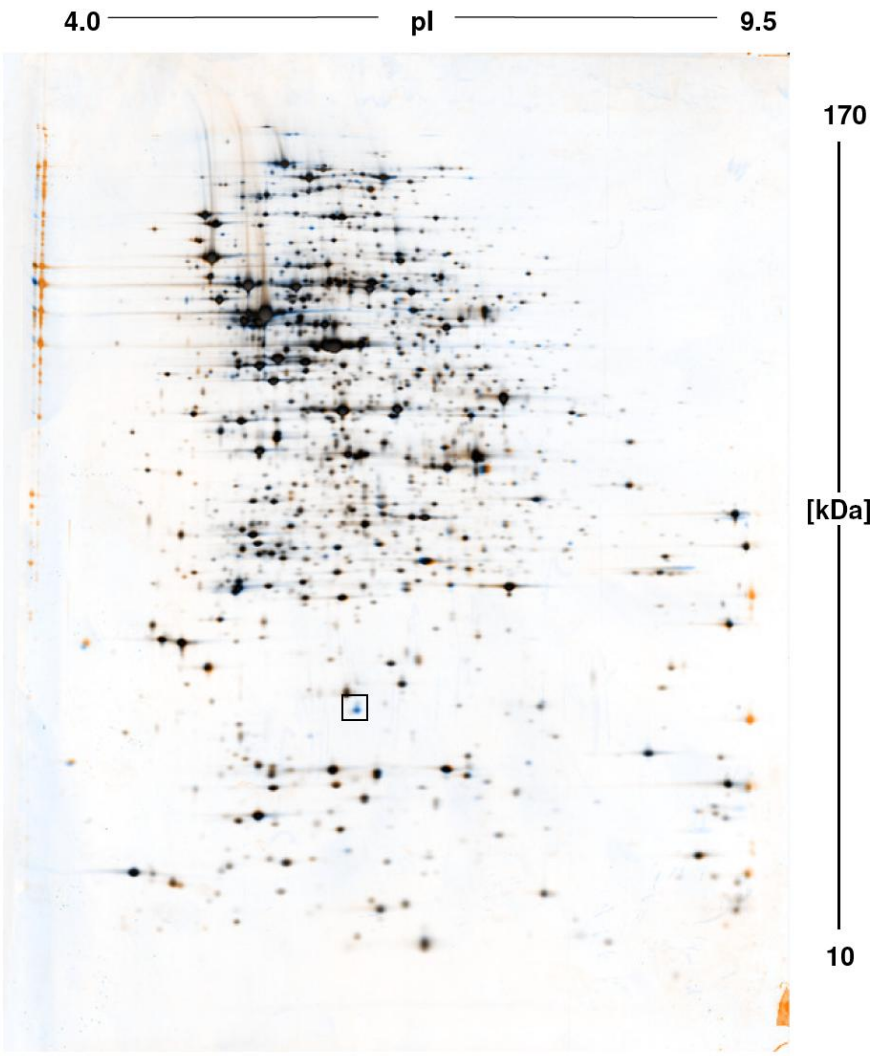

Figure A.6.: Overlay of false-color images of gels from protein samples from the fed-batch process (24h) and the fed-batch RMT experiment with glucose after 18 min. Unchanged spots appear black, whereas changes appear orange or blue.

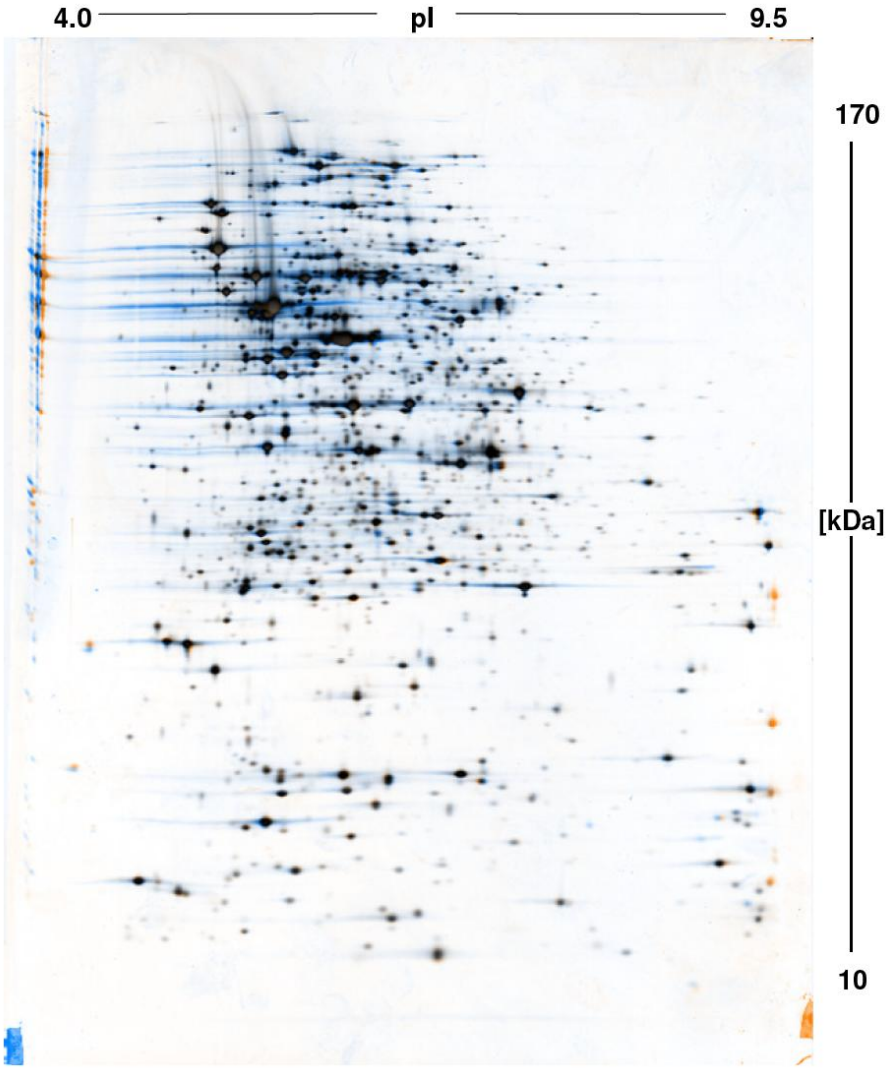

Figure A.7.: Overlay of false-color images of gels from protein samples from the fed-batch process (24h) and the fed-batch RMT experiment with succinate after 18 min. Unchanged spots appear black, whereas changes appear orange or blue.

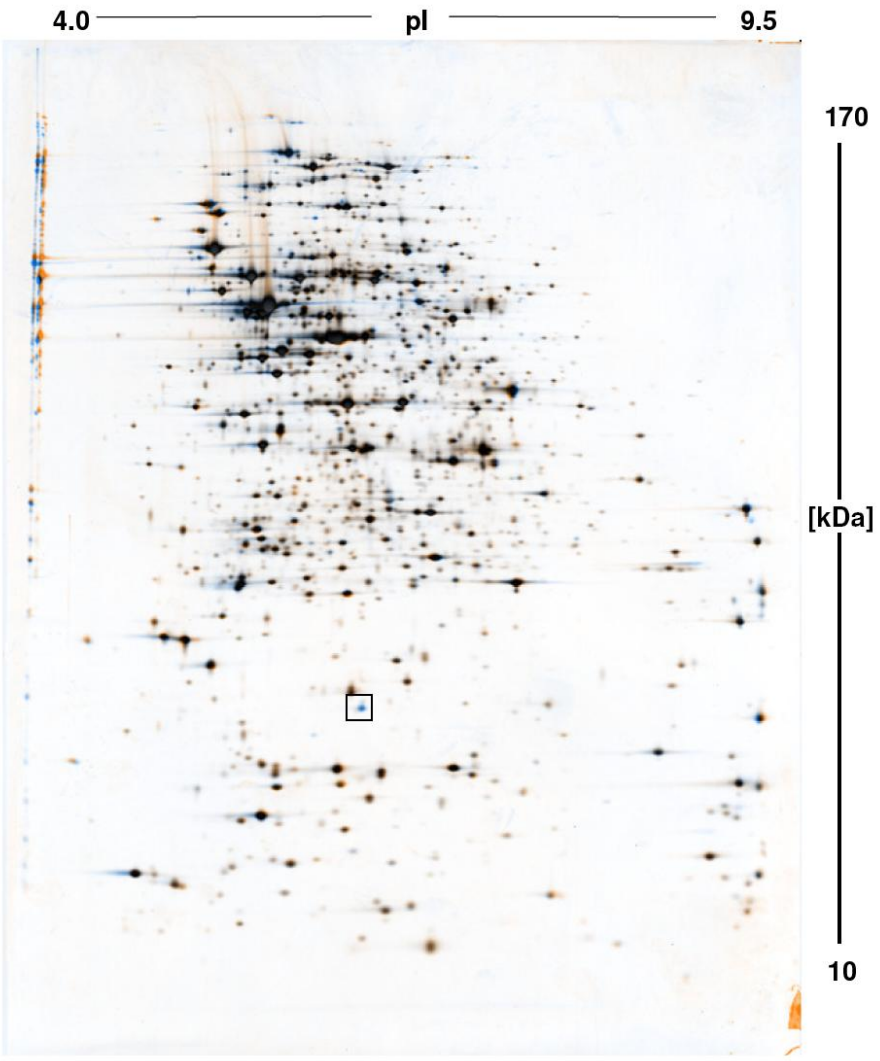

Figure A.8.: Overlay of false-color images of gels from protein samples from the fed-batch process (24h) and the fed-batch RMT experiment with pyruvate after 18 min. Unchanged spots appear black, whereas changes appear orange or blue.

A.10. Fluxes in batch RMT experiments

Table A.13.: Metabolic fluxes estimated with flux balance analysis v_{FBA} and stoichiometric metabolite balancing v_{MFA} (in mmol g_{DW}^{-1} h^{-1}) in the fed-batch process (FB) and batch RMT experiments.

Reaction	**Model**	**FB**	**GLC**	**PYR**	**SUC**	**AC**
Glycolysis						
PTS	v_{FBA}	1.21	5.45	0.00	0.00	0.00
	v_{MFA}	1.21	5.45	0.00	0.00	0.00
pgi	v_{FBA}	1.16	2.98	-0.05	-0.34	0.00
	v_{MFA}	1.04	4.65	-0.42	-0.16	0.00
pfk	v_{FBA}	1.08	4.00	0.00	0.00	0.00
	v_{MFA}	1.07	4.78	-0.35	-0.14	0.00
fbp	v_{FBA}	0.00	0.00	0.31	0.25	0.00
	v_{MFA}	-	-	-	-	
fba	v_{FBA}	1.08	4.00	-0.31	-0.25	0.00
	v_{MFA}	1.07	4.78	-0.35	-0.14	0.00
tpi	v_{FBA}	1.07	3.93	-0.36	-0.27	0.00
	v_{MFA}	-	-	-	-	
gapd	v_{FBA}	2.15	8.64	-0.78	-0.49	0.00
	v_{MFA}	2.12	9.48	-0.74	-0.29	0.00
pgk	v_{FBA}	2.15	8.64	-0.78	-0.49	0.00
	v_{MFA}	-	-	-	-	
pgm	v_{FBA}	1.98	7.66	-1.25	-0.72	0.00
	v_{MFA}	-	-	-	-	
eno	v_{FBA}	1.98	7.66	-1.25	-0.72	0.00
	v_{MFA}	1.98	8.81	-1.09	-0.43	0.00
pyk	v_{FBA}	0.51	0.73	0.00	2.49	0.00
	v_{MFA}	0.45	1.85	-1.88	2.98	0.00
pps	v_{FBA}	0.00	0.00	2.17	0.00	0.00
	v_{MFA}	-	-	-	-	
pdh	v_{FBA}	1.50	3.88	6.52	2.13	0.00
	v_{MFA}	1.39	4.81	6.83	2.72	0.00

Reaction	Model	FB	GLK	PYR	SUC	AC
Anapleurotic reactions						
ppc	v_{FBA}	0.19	1.07	0.69	0.00	0.00
	v_{MFA}	0.27	1.29	0.67	-3.45	0.00
ppck	v_{FBA}	0.00	0.00	0.00	3.33	0.00
	v_{MFA}	-	-	-	-	
TCA Cycle						
cs	v_{FBA}	1.25	2.77	4.25	1.71	4.50
	v_{MFA}	1.04	3.67	4.53	2.38	4.50
acont	v_{FBA}	1.25	2.77	4.25	1.71	4.50
	v_{MFA}	1.04	3.67	4.53	2.38	4.50
icdh	v_{FBA}	1.25	2.77	4.25	1.71	4.50
	v_{MFA}	1.04	3.67	4.53	2.38	4.50
akgdh	v_{FBA}	1.16	2.26	3.96	1.36	4.50
	v_{MFA}	0.94	3.18	4.27	2.08	4.50
sucoas	v_{FBA}	1.12	2.03	3.83	1.29	4.50
	v_{MFA}	0.94	3.18	4.27	2.08	4.50
sucd	v_{FBA}	1.19	2.43	3.97	5.45	4.50
	v_{MFA}	0.94	3.18	4.27	6.17	4.50
fum	v_{FBA}	1.24	2.74	4.23	5.42	35.42
	v_{MFA}	0.94	3.18	4.27	6.00	4.50
mdh	v_{FBA}	1.24	2.76	4.24	5.42	35.42
	v_{MFA}	0.94	3.18	4.27	6.00	4.50
Pentose Phosphate Pathway						
g6pdh	v_{FBA}	0.04	2.39	0.00	0.32	0.00
	v_{MFA}	0.16	0.76	0.39	0.16	0.00
gnd	v_{FBA}	0.04	2.39	0.00	0.32	0.00
	v_{MFA}	-	-	-	-	
rpi	v_{FBA}	0.10	1.30	0.23	0.21	0.00
	v_{MFA}	0.12	0.58	0.30	0.12	0.00
rpe	v_{FBA}	-0.07	1.06	-0.24	0.10	0.00
	v_{MFA}	0.04	0.18	0.09	0.04	0.00
tkt1	v_{FBA}	-0.02	0.63	-0.07	0.08	0.00
	v_{MFA}	0.04	0.18	0.09	0.04	0.00
tkt2	v_{FBA}	-0.05	0.43	-0.18	0.02	0.00
	v_{MFA}	-	-	-	-	
tala	v_{FBA}	-0.02	0.62	-0.07	0.08	0.00
	v_{MFA}	0.04	0.18	0.09	0.04	0.00
Oxidative Phosphorylation						
sucd4	v_{FBA}	1.19	2.43	3.97	5.45	4.50
nadh6	v_{FBA}	6.29	18.91	14.46	8.78	13.50
cytbd	v_{FBA}	7.51	21.34	18.52	14.29	0.00
thd	v_{FBA}	0.00	0.00	0.18	0.00	26.42
atps	v_{FBA}	10.01	28.42	23.35	16.23	7.60
NADP(H) oxidation	v_{MFA}	5.17	17.79	17.04	14.31	15.75
Biomass Flux						
Biomass	v_{MFA}	0.09	0.44	0.23	0.09	0.00

A.11. Fluxes in fed-batch RMT experiments

A.11.1. Glucose (aerobic)

Table A.14.: Metabolic fluxes estimated with flux balance analysis v_{FBA} and stoichiometric metabolite balancing v_{MFA} (in mmol g_{DW}^{-1} h^{-1}) in the fed-batch process (FB) and the aerobic fed-batch RMT experiment with three feeding rates of glucose A, B and C.

Reaction	**Model**	**FB**	**A**	**B**	**C**
Glycolysis					
pts	v_{FBA}	1.21	3.24	2.16	1.08
	v_{MFA}	1.21	3.24	2.16	1.08
pgi	v_{FBA}	1.16	2.21	1.61	1.07
	v_{MFA}	1.04	2.81	1.89	0.97
pfk	v_{FBA}	1.08	2.57	1.75	1.00
	v_{MFA}	1.07	2.88	1.93	0.99
fbp	v_{FBA}	0.00	0.00	0.00	0.00
	v_{MFA}	-	-	-	-
fba	v_{FBA}	1.08	2.57	1.75	1.00
	v_{MFA}	1.07	2.88	1.93	0.99
tpi	v_{FBA}	1.07	2.53	1.72	0.99
	v_{MFA}	-	-	-	-
gapd	v_{FBA}	2.15	5.39	3.62	1.97
	v_{MFA}	2.12	5.72	3.84	1.97
pgk	v_{FBA}	2.15	5.39	3.62	1.97
	v_{MFA}	-	-	-	-
pgm	v_{FBA}	1.98	4.88	3.27	1.85
	v_{MFA}	-	-	-	-
eno	v_{FBA}	1.98	4.88	3.27	1.85
	v_{MFA}	1.98	5.36	3.61	1.88
pyk	v_{FBA}	0.51	0.87	0.58	0.58
	v_{MFA}	0.45	1.31	0.94	0.60
pps	v_{FBA}	0.00	0.00	0.00	0.00
	v_{MFA}	-	-	-	-
pdh	v_{FBA}	1.50	2.99	2.11	1.25
	v_{MFA}	1.39	3.31	2.43	1.23

Reaction	Model	FB	A	B	C
Anapleurotic reactions					
ppc	v_{FBA}	0.19	0.56	0.38	0.14
	v_{MFA}	0.27	0.69	0.44	0.17
ppck	v_{FBA}	0.00	0.00	0.00	0.00
	v_{MFA}	-	-	-	-
TCA Cycle					
cs	v_{FBA}	1.25	1.96	1.65	1.14
	v_{MFA}	1.04	2.25	1.99	1.10
acont	v_{FBA}	1.25	1.96	1.65	1.14
	v_{MFA}	1.04	2.25	1.99	1.10
icdh	v_{FBA}	1.25	1.96	1.65	1.14
	v_{MFA}	1.04	2.25	1.99	1.10
akgdh	v_{FBA}	1.16	1.70	1.47	1.07
	v_{MFA}	0.94	1.99	1.83	1.03
sucoas	v_{FBA}	1.12	1.58	1.39	1.05
	v_{MFA}	0.94	1.99	1.83	1.03
sucd	v_{FBA}	1.19	1.71	1.47	1.07
	v_{MFA}	0.94	1.99	1.83	1.03
fum	v_{FBA}	1.24	1.95	1.64	1.13
	v_{MFA}	0.94	1.99	1.83	1.03
mdh	v_{FBA}	1.24	1.96	1.65	1.14
	v_{MFA}	0.94	1.99	1.83	1.03
Pentose Phosphate Pathway					
g6pdh	v_{FBA}	0.04	0.98	0.52	0.00
	v_{MFA}	0.16	0.40	0.26	0.10
gnd	v_{FBA}	0.04	0.98	0.52	0.00
	v_{MFA}	-	-	-	-
rpi	v_{FBA}	0.10	0.59	0.36	0.06
	v_{MFA}	0.12	0.31	0.20	0.08
rpe	v_{FBA}	-0.07	0.38	0.16	-0.07
	v_{MFA}	0.04	0.10	0.06	0.02
tkt1	v_{FBA}	-0.02	0.24	0.12	-0.02
	v_{MFA}	0.04	0.10	0.06	0.02
tkt2	v_{FBA}	-0.05	0.14	0.04	-0.05
	v_{MFA}	-	-	-	-
tala	v_{FBA}	-0.02	0.24	0.11	-0.02
	v_{MFA}	0.04	0.10	0.06	0.02
Oxidative Phosphorylation					
sucd4	v_{FBA}	1.19	1.71	1.47	1.07
nadh6	v_{FBA}	6.29	11.25	9.08	5.42
cytbd	v_{FBA}	7.51	13.04	10.61	6.51
thd	v_{FBA}	0.00	0.00	0.00	0.00
atps	v_{FBA}	10.01	17.44	14.14	8.64
NADP(H) oxidation	v_{MFA}	5.17	10.40	9.82	5.41
Biomass Flux					
Biomass	v_{MFA}	0.09	0.24	0.15	0.06

A.11.2. Pyruvate

Table A.15.: Metabolic fluxes estimated with flux balance analysis v_{FBA} and stoichiometric metabolite balancing v_{MFA} (in mmol g_{DW}^{-1} h^{-1}) in the fed-batch process (FB) and the fed-batch RMT experiment with three feeding rates of pyruvate A, B and C.

Reaction	**Model**	**FB**	**A**	**B**	**C**
		Glycolysis			
pts	v_{FBA}	1.21	0.00	0.00	0.00
	v_{MFA}	1.21	0.00	0.00	0.00
pgi	v_{FBA}	1.16	-0.03	-0.02	-0.01
	v_{MFA}	1.04	-0.38	-0.25	-0.10
pfk	v_{FBA}	1.08	0.00	0.00	0.00
	v_{MFA}	1.07	-0.32	-0.21	-0.09
fbp	v_{FBA}	0.00	0.18	0.12	0.04
	v_{MFA}	-	-	-	-
fba	v_{FBA}	1.08	-0.18	-0.12	-0.04
	v_{MFA}	1.07	-0.32	-0.21	-0.09
tpi	v_{FBA}	1.07	-0.21	-0.14	-0.04
	v_{MFA}	-	-	-	-
gapd	v_{FBA}	2.15	-0.49	-0.33	-0.10
	v_{MFA}	2.12	-0.68	-0.44	-0.18
pgk	v_{FBA}	2.15	-0.49	-0.33	-0.10
	v_{MFA}	-	-	-	-
pgm	v_{FBA}	1.98	-0.77	-0.52	-0.16
	v_{MFA}	-	-	-	-
eno	v_{FBA}	1.98	-0.77	-0.52	-0.16
	v_{MFA}	1.98	-1.00	-0.65	-0.27
pyk	v_{FBA}	0.51	0.00	0.00	0.00
	v_{MFA}	0.45	-1.72	-1.12	-0.47
pps	v_{FBA}	0.00	1.41	0.95	0.30
	v_{MFA}	-	-	-	-
pdh	v_{FBA}	1.50	3.83	3.04	1.63
	v_{MFA}	1.39	3.40	2.81	1.40

Reaction	Model	FB	A	B	C
Anapleurotic reactions					
ppc	v_{FBA}	0.19	0.49	0.33	0.10
	v_{MFA}	0.27	0.62	0.40	0.17
ppck	v_{FBA}	0.00	0.00	0.00	0.00
	v_{MFA}	-	-	-	-
TCA Cycle					
cs	v_{FBA}	1.25	3.49	2.69	1.52
	v_{MFA}	1.04	2.80	2.30	1.19
acont	v_{FBA}	1.25	3.49	2.69	1.52
	v_{MFA}	1.04	2.80	2.30	1.19
icdh	v_{FBA}	1.25	3.49	2.69	1.52
	v_{MFA}	1.04	2.80	2.30	1.19
akgdh	v_{FBA}	1.16	3.30	2.57	1.48
	v_{MFA}	0.94	2.57	2.14	1.12
sucoas	v_{FBA}	1.12	3.22	2.51	1.47
	v_{MFA}	0.94	2.57	2.14	1.12
sucd	v_{FBA}	1.19	3.31	2.57	1.50
	v_{MFA}	0.94	2.57	2.14	1.12
fum	v_{FBA}	1.24	3.48	2.69	1.52
	v_{MFA}	0.94	2.57	2.14	1.12
mdh	v_{FBA}	1.24	3.49	2.69	1.52
	v_{MFA}	0.94	2.57	2.14	1.12
Pentose Phosphate Pathway					
g6pdh	v_{FBA}	0.04	0.00	0.00	0.00
	v_{MFA}	0.16	0.36	0.24	0.10
gnd	v_{FBA}	0.04	0.00	0.00	0.00
	v_{MFA}	-	-	-	-
rpi	v_{FBA}	0.10	0.13	0.09	0.03
	v_{MFA}	0.12	0.28	0.18	0.08
rpe	v_{FBA}	-0.07	-0.14	-0.09	-0.03
	v_{MFA}	0.04	0.09	0.06	0.02
tkt1	v_{FBA}	-0.02	-0.03	-0.02	-0.01
	v_{MFA}	0.04	0.09	0.06	0.02
tkt2	v_{FBA}	-0.05	-0.11	-0.07	-0.02
	v_{MFA}	-	-	-	-
tala	v_{FBA}	-0.02	-0.04	-0.02	-0.01
	v_{MFA}	0.04	0.09	0.06	0.02
Oxidative Phosphorylation					
sucd4	v_{FBA}	1.19	3.31	2.57	1.50
nadh6	v_{FBA}	6.29	11.05	8.92	5.52
cytbd	v_{FBA}	7.51	14.42	11.53	7.02
thd	v_{FBA}	0.00	0.00	0.00	0.00
atps	v_{FBA}	10.01	18.06	14.73	9.13
NADP(H) oxidation	v_{MFA}	5.17	8.06	7.48	4.15
Biomass Flux					
Biomass	v_{MFA}	0.09	0.21	0.14	0.06

A.11.3. Succinate

Table A.16.: Metabolic fluxes estimated with flux balance analysis v_{FBA} and stoichiometric metabolite balancing v_{MFA} (in mmol g_{DW}^{-1} h^{-1}) in the fed-batch process (FB) and the fed-batch RMT experiment with three feeding rates of succinate A, B and C.

Reaction	**Model**	**FB**	**A**	**B**	**C**
		Glycolysis			
pts	v_{FBA}	1.21	0.00	0.00	0.00
	v_{MFA}	1.21	0.00	0.00	0.00
pgi	v_{FBA}	1.16	-0.03	-0.01	0.00
	v_{MFA}	1.04	-0.21	-0.15	-0.04
pfk	v_{FBA}	1.08	0.00	0.00	0.00
	v_{MFA}	1.07	-0.17	-0.12	-0.03
fbp	v_{FBA}	0.00	0.09	0.05	0.00
	v_{MFA}	-	-	-	-
fba	v_{FBA}	1.08	-0.09	-0.05	0.00
	v_{MFA}	1.07	-0.17	-0.12	-0.03
tpi	v_{FBA}	1.07	-0.11	-0.05	0.00
	v_{MFA}	-	-	-	-
gapd	v_{FBA}	2.15	-0.23	-0.13	-0.01
	v_{MFA}	2.12	-0.37	-0.26	-0.07
pgk	v_{FBA}	2.15	-0.23	-0.13	-0.01
	v_{MFA}	-	-	-	-
pgm	v_{FBA}	1.98	-0.37	-0.20	-0.02
	v_{MFA}	-	-	-	-
eno	v_{FBA}	1.98	-0.37	-0.20	-0.02
	v_{MFA}	1.98	-0.54	-0.39	-0.11
pyk	v_{FBA}	0.51	1.81	1.35	0.83
	v_{MFA}	0.45	1.54	1.05	0.67
pps	v_{FBA}	0.00	0.00	0.00	0.00
	v_{MFA}	-	-	-	-
pdh	v_{FBA}	1.50	1.59	1.23	0.82
	v_{MFA}	1.39	1.22	0.82	0.61

Reaction	Model	FB	A	B	C
Anapleurotic reactions					
ppc	v_{FBA}	0.19	0.00	0.00	0.00
	v_{MFA}	0.27	-2.14	-1.48	-0.79
ppck	v_{FBA}	0.00	2.25	1.59	0.85
	v_{MFA}	-	-	-	-
TCA Cycle					
cs	v_{FBA}	1.25	1.35	1.10	0.81
	v_{MFA}	1.04	0.79	0.52	0.53
acont	v_{FBA}	1.25	1.35	1.10	0.81
	v_{MFA}	1.04	0.79	0.52	0.53
icdh	v_{FBA}	1.25	1.35	1.10	0.81
	v_{MFA}	1.04	0.79	0.52	0.53
akgdh	v_{FBA}	1.16	1.26	1.05	0.80
	v_{MFA}	0.94	0.67	0.43	0.50
sucoas	v_{FBA}	1.12	1.22	1.03	0.80
	v_{MFA}	0.94	0.67	0.43	0.50
sucd	v_{FBA}	1.19	3.77	2.78	1.66
	v_{MFA}	0.94	3.15	2.15	1.36
fum	v_{FBA}	1.24	3.82	2.81	1.67
	v_{MFA}	0.94	3.15	2.15	1.36
mdh	v_{FBA}	1.24	3.82	2.81	1.67
	v_{MFA}	0.94	3.15	2.15	1.36
Pentose Phosphate Pathway					
g6pdh	v_{FBA}	0.04	0.02	0.00	0.00
	v_{MFA}	0.16	0.20	0.14	0.04
gnd	v_{FBA}	0.04	0.02	0.00	0.00
	v_{MFA}	-	-	-	-
rpi	v_{FBA}	0.10	0.07	0.03	0.00
	v_{MFA}	0.12	0.15	0.11	0.03
rpe	v_{FBA}	-0.07	-0.05	-0.04	0.00
	v_{MFA}	0.04	0.05	0.03	0.01
tkt1	v_{FBA}	-0.02	-0.01	-0.01	0.00
	v_{MFA}	0.04	0.05	0.03	0.01
tkt2	v_{FBA}	-0.05	-0.04	-0.03	0.00
	v_{MFA}	-	-	-	-
tala	v_{FBA}	-0.02	-0.01	-0.01	0.00
	v_{MFA}	0.04	0.05	0.03	0.01
Oxidative Phosphorylation					
sucd4	v_{FBA}	1.19	3.77	2.78	1.66
nadh6	v_{FBA}	6.29	6.65	5.42	4.03
cytbd	v_{FBA}	7.51	10.43	8.20	5.69
thd	v_{FBA}	0.00	0.00	0.00	0.00
atps	v_{FBA}	10.01	12.14	9.75	7.07
NADP(H) oxidation	v_{MFA}	5.17	4.91	3.22	3.19
Biomass Flux					
Biomass	v_{MFA}	0.09	0.12	0.08	0.02

A.11.4. Glucose (anaerobic)

Table A.17.: Metabolic fluxes estimated with flux balance analysis v_{FBA} and stoichiometric metabolite balancing v_{MFA} (in mmol g_{DW}^{-1} h^{-1}) in the fed-batch process (FB) and the anaerobic fed-batch RMT experiment with three feeding rates of glucose A, B and C.

Reaction	**Model**	**FB**	**A**	**B**	**C**
Glycolysis					
pts	v_{FBA}	1.21	3.01	1.94	0.96
	v_{MFA}	1.21	3.01	1.94	0.96
pgi	v_{FBA}	1.16	3.01	1.94	0.96
	v_{MFA}	1.04	2.89	1.87	0.94
pfk	v_{FBA}	1.08	3.00	1.93	0.96
	v_{MFA}	1.07	2.91	1.88	0.94
fbp	v_{FBA}	0.00	0.00	0.00	0.00
	v_{MFA}	-	-	-	-
fba	v_{FBA}	1.08	3.00	1.93	0.96
	v_{MFA}	1.07	2.91	1.88	0.94
tpi	v_{FBA}	1.07	3.00	1.93	0.96
	v_{MFA}	-	-	-	-
gapd	v_{FBA}	2.15	6.00	3.87	1.91
	v_{MFA}	2.12	5.80	3.75	1.88
pgk	v_{FBA}	2.15	6.00	3.87	1.91
	v_{MFA}	-	-	-	-
pgm	v_{FBA}	1.98	5.98	3.86	1.91
	v_{MFA}	-	-	-	-
eno	v_{FBA}	1.98	5.98	3.86	1.91
	v_{MFA}	1.98	5.70	3.69	1.87
pyk	v_{FBA}	0.51	2.95	1.90	0.94
	v_{MFA}	0.45	2.45	1.62	0.87
pps	v_{FBA}	0.00	0.00	0.00	0.00
	v_{MFA}	-	-	-	-
pdh	v_{FBA}	1.50	0.00	0.00	0.00
	v_{MFA}	1.39	0.16	0.24	0.24

Reaction	Model	FB	GLK	PYR	SUC	AC
Anapleurotic reactions						
ppc	v_{FBA}	0.19	0.02	0.01	0.01	
	v_{MFA}	0.27	0.20	0.11	0.03	
ppck	v_{FBA}	0.00	0.00	0.00	0.00	
	v_{MFA}	-	-	-	-	
TCA Cycle						
cs	v_{FBA}	1.25	0.01	0.01	0.00	
	v_{MFA}	1.04	0.00	-0.08	-0.11	
acont	v_{FBA}	1.25	0.01	0.01	0.00	
	v_{MFA}	1.04	0.00	-0.08	-0.11	
icdh	v_{FBA}	1.25	0.01	0.01	0.00	
	v_{MFA}	1.04	0.00	-0.08	-0.11	
akgdh	v_{FBA}	1.16	0.00	0.00	0.00	
	v_{MFA}	0.94	-0.08	-0.12	-0.12	
sucoas	v_{FBA}	1.12	0.00	0.00	0.00	
	v_{MFA}	0.94	-0.08	-0.12	-0.12	
sucd	v_{FBA}	1.19	0.00	0.00	0.00	
	v_{MFA}	0.94	-0.08	-0.12	-0.12	
fum	v_{FBA}	1.24	0.01	0.00	0.00	
	v_{MFA}	0.94	-0.08	-0.12	-0.12	
mdh	v_{FBA}	1.24	0.01	0.00	0.00	
	v_{MFA}	0.94	-0.08	-0.12	-0.12	
Pentose Phosphate Pathway						
g6pdh	v_{FBA}	0.04	0.00	0.00	0.00	
	v_{MFA}	0.16	0.12	0.07	0.02	
gnd	v_{FBA}	0.04	0.00	0.00	0.00	
	v_{MFA}	-	-	-	-	
rpi	v_{FBA}	0.10	0.01	0.00	0.00	
	v_{MFA}	0.12	0.09	0.05	0.02	
rpe	v_{FBA}	-0.07	-0.01	0.00	0.00	
	v_{MFA}	0.04	0.03	0.02	0.00	
tkt1	v_{FBA}	-0.02	0.00	0.00	0.00	
	v_{MFA}	0.04	0.03	0.02	0.00	
tkt2	v_{FBA}	-0.05	-0.01	0.00	0.00	
	v_{MFA}	-	-	-	-	
tala	v_{FBA}	-0.02	0.00	0.00	0.00	
	v_{MFA}	0.04	0.03	0.02	0.00	
Oxidative Phosphorylation						
sucd4	v_{FBA}	1.19	0.00	0.00	0.00	
nadh6	v_{FBA}	6.29	0.00	0.00	0.00	
cytbd	v_{FBA}	7.51	0.00	0.00	0.00	
thd	v_{FBA}	0.00	0.12	0.08	0.04	
atps	v_{FBA}	10.01	-0.82	-0.53	-0.26	
NADP(H) oxidation	v_{MFA}	5.17	-0.71	-0.42	-0.22	
Biomass Flux						
Biomass	v_{MFA}	0.09	0.07	0.04	0.01	

List of Tables

List of Figures